

OBSERVATIONS OF ADVECTION AND TURBULENT INTERFACIAL MIXING IN  
THE SAINT JOHN RIVER ESTUARY, NEW BRUNSWICK CANADA

by

Nicole Delpeche

B.Sc. Surveying and Land Information, University of the West Indies, 2001

A Thesis submitted in Partial Fulfilment of the Requirements for the Degree of  
Master of Science in Engineering  
in the Graduate Academic Unit of Geodesy and Geomatics Engineering

Supervisor: Dr. John Hughes Clarke, Ph.D., Geodesy and Geomatics Engineering

Examining Board: Dr. Susan Nichols, Ph.D., Geodesy and Geomatics Engineering  
Dr. Susan Haigh, Ph.D., Geodesy and Geomatics Engineering  
Dr. Katy Haralampides, Ph.D., Civil Engineering

This thesis is accepted

Dean of Graduate Studies

THE UNIVERSITY OF NEW BRUNSWICK

December, 2006

©Nicole Delpeche, 2007

## **ABSTRACT**

Theoretical studies, laboratory experiments, numerical simulations and field observations suggest that turbulent interfacial mixing in stratified environments initially takes the form of internal waves. Regardless of this suggestion, the generation and development of internal waves in the field is still not well observed. The main factor that limits the observations and as a result our understanding of internal waves in the field, is the spatial and temporal resolution of observations acquired.

Under highly stratified conditions oceanographic surveys are performed in Long Reach (part of the Saint John River Estuary) for the duration of a tidal cycle. Survey sensors such as an Acoustic Doppler Current Profiler (which measures current magnitude and direction), Conductivity Temperature Depth sensor (from which density is derived) and an echosounder (which indirectly measures density interfaces, turbulence, zooplankton and suspended sediments) are all implemented to map the main oceanographic processes occurring.

The results show that turbulent interfacial mixing occurs at a period of maximum velocity shear, within the vicinity of the lateral and vertical constrictions of Long Reach. The survey sensors and survey design used, allow the generation and evolution processes of internal waves to be captured. Different types of internal waves are observed before, during and after the turbulent mixing process. However at the exact moment of turbulent mixing, the pycnocline dips downward into the bottom salty layer. This latter observation, suggests that there may possibly be another mechanism, other than internal waves that contribute to turbulent interfacial mixing in Long Reach.

# TABLE OF CONTENTS

	page
Abstract.....	ii
Table of Contents.....	iii
List of Figures.....	vi
List of Tables.....	x
Acknowledgments.....	xi
1. INTRODUCTION.....	1
1.1 Objectives.....	6
1.1.1 Scientific Questions.....	6
2. STUDY AREA.....	7
2.1 Saint John River Estuary.....	7
2.2 Climate.....	9
2.2.1 Temperature, Rainfall and Snowfall Pattern.....	10
2.3 Tides and River Discharge.....	12
2.3.1 Bay of Fundy/Saint John Harbour: Tidal Range & Currents.....	12
2.3.2 Saint John River Estuary.....	15
2.3.3 Water Levels for Survey Dates.....	19
2.4 River Discharge.....	22
2.5 Geological Characteristics.....	24
2.5.1 Bedrock Geology of New Brunswick.....	24
2.5.2 Rock Types of Long Reach.....	25
2.5.3 The Three Sill of the Saint John River Estuary.....	32
2.6 Salinity Characteristics: Previous Research.....	41
2.6.1 Salinity Structure of Saint John River Estuary.....	42
2.6.2 Temperature Structure of Saint John River Estuary.....	44
2.7 Summary of Study Area.....	48
3. SALINITY CLASSIFICATION AND MIXING IN ESTUARIES.....	50
3.1 Estuarine Classification: Salinity Structure.....	50
3.1.1 Highly Stratified or Salt Wedge.....	51
3.1.2 Highly Stratified: Fjord.....	52
3.1.3 Partially Mixed.....	54
3.1.4 Well Mixed or Vertically Homogenous.....	55
3.2 Turbulent Mixing in Estuaries.....	57
3.2.1 Measurements of Turbulent Mixing.....	57
3.3 Sources of Turbulent Mixing.....	60
3.3.1 Turbulent Mixing at the Interface.....	61
3.3.2 Discussion on Methods of Determining Turbulent Mixing...	73
3.4 Field Examples of Interfacial Mixing in Estuaries.....	74

3.5	Summary on Mixing in Estuaries.....	78
4.	BACKSCATTER.....	79
4.1	Acoustic Wave.....	79
4.1.1	Frequency and Wavelength.....	80
4.1.2	Beamwidth.....	81
4.1.3	The Ensonified Area.....	81
4.1.4	Spherical Spreading.....	82
4.1.5	Noise.....	83
4.2	Backscatter.....	84
4.2.1	Target Strength.....	85
4.2.2	Targets.....	86
4.2.3	Volume Backscattering.....	87
4.2.4	Backscatter Intensity.....	88
4.2.5	Water Column Targets.....	89
4.3	Discussion on Backscatter.....	95
4.4	Currents.....	97
4.4.1	ADCP and the Doppler Effect.....	98
4.4.2	Range Gate and Depth Cell Size.....	100
4.4.3	Bottom Tracking.....	101
4.4.4	Discussion on ADCP.....	102
4.5	Summary on Acoustics.....	103
5.	SURVEY DESIGN.....	104
5.1	Survey Instruments.....	105
5.1.1	Survey Platform.....	105
5.1.2	Positioning.....	106
5.1.3	ADCP.....	107
5.1.4	Moving Vessel Profiler and CTD.....	108
5.1.5	Echosounder.....	111
5.1.6	Summary on Instruments.....	111
5.2	Processing of Data.....	112
5.2.1	Velocity.....	113
5.2.2	Salinity, Temperature and Density Longitudinal Profiles....	118
5.2.3	Echosounder.....	118
5.3	The 2003 Seasonal Surveys.....	120
5.3.1	The 2003 Survey Plan.....	121
5.3.2	The 2003 Results.....	121
5.3.3	Summary of 2003 Results.....	135
5.4	The 2004 Survey Plan.....	136
5.4.1	Procedure for Calc of the Gradient Richardson Number.....	138
5.5	Summary of Survey Plan.....	139
6.	ANALYSIS: SECTION ONE.....	141
6.1	Bathymetry of the Study Area.....	142



6.2	Descriptive Analysis: Section One.....	145
6.2.1	Density Structure: Section One.....	148
6.2.2	Velocity Structure: Section one.....	162
6.2.3	Summary of Density and Velocity Structure.....	169
6.2.4	The Acoustic Backscatter Images.....	170
6.2.5	Summary of Observations.....	179
6.3	Dynamical Investigation: Linear Stability Analysis.....	184
6.3.1	Interfacial Mixing and the Gradient Richardson Number....	185
6.3.2	Linear Stability Analysis.....	199
6.4	Summary of Section One.....	214
7.	ANALYSIS: SECTION TWO.....	216
7.1	Bathymetry.....	216
7.2	Density Structure.....	217
7.3	Velocity Structure.....	226
7.4	Acoustic Backscatter Images.....	231
7.5	Summary of Density and Velocity Observations.....	235
7.6	Spring Tidal Cycle.....	236
7.7	Summary on Neap and Spring Tidal Cycle.....	237
7.8	The Gradient Richardson Number.....	243
7.9	Linear Stability Analysis.....	245
7.10	Summary.....	248
8.0	CONCLUSIONS AND RECOMMENDATIONS.....	251
8.1	Internal waves and Mixing.....	251
8.2	Methodology.....	254
8.3	Observations of Section One.....	256
8.4	Observations of Section Two.....	260
8.5	Conclusions.....	264
8.6	Recommendations.....	266
	References.....	268
	Appendix I.....	273
	Appendix II.....	277
	Appendix III.....	282
	VITA	

## LIST OF FIGURES

	page
1.1	Map of the Saint John River watershed..... 5
2.1	Map of the Saint John River plume advancing into the Bay of Fundy..... 8
2.2	Map showing the delimitation of the Saint John River Estuary..... 9
2.3	Mean monthly air temperature at Saint John..... 10
2.4	Mean monthly rainfall at Saint John..... 11
2.5	Mean monthly snowfall at Saint John..... 11
2.6	Map of the Bay of Fundy showing the tidal range and the M2 amplitude... 13
2.7	Map of the Saint John River Estuary showing the locations of the tidal stations..... 17
2.8	Graphs of tidal cycle for the neap and spring tides survey dates..... 19
2.9	Graphs of the predicted and observed tides for the Saint John Harbour..... 20
2.10	Graphs of water level for the 14 <sup>th</sup> and 15 <sup>th</sup> September 2004..... 21
2.11	River discharge from 1966 to 1995 at Mactaquac dam..... 23
2.12	Mean daily discharge at Mactaquac for the survey dates..... 23
2.13	The different geological zones of New Brunswick..... 26
2.14	Rock types of the land masses surrounding Long Reach..... 27
2.15	Sediment results for Metcalfe et al [1976] and the OMG..... 30
2.16	Pictures of soil samples in Long Reach..... 31
2.17	Circulation pattern at the Reversing Falls sill..... 33
2.18	Longitudinal salinity profile of Saint John River Estuary..... 34
2.19	Site map showing the Boars Head Sill..... 36
2.20	Map showing the bathymetry of the Boars Head Sill..... 37
2.21	Salt water intrusion from the gorge into the West Field channel..... 38
2.22	Salt water Intrusion from Grand Bay into Kennebecasis..... 39
2.23	Bathymetry images of Long Reach..... 41
2.24	Seasonal variation of salinity and temperature of the Saint John River estuary..... 45
2.25	Seasonal variation of the density in the Saint John River estuary..... 46
2.26	Seasonal variation of salinity in the Saint John River estuary..... 47
3.1	Tidally averaged salinity and velocity structure of a highly stratified estuary..... 52
3.2	Tidally averaged salinity and velocity structure of a fjord..... 53
3.3	Tidally averaged salinity and velocity structure of a partially mixed estuary..... 55
3.4	Tidally averaged salinity and velocity structure of a well mixed estuary.... 56
3.5	Diagrams of the internal waves..... 62
3.6	Density and velocity profile of the KH and Holmboe wave..... 63

3.7	Density and velocity profile for the piecewise approx and smooth profile method.....	65
3.8	Procedure for piecewise approx. and the smooth profile method.....	68
3.9	Linear Stability diagrams at $\epsilon = 0$ and $\epsilon = 0.5$ .....	70
3.10	Profile view of a soliton wave packet.....	72
3.11	A soliton packet in the centre of Tarife Narrows in Gibralta.....	73
3.12	Kelvin- Helmholtz waves observed by acoustic imagery by Geyer et al. [1980].....	77
3.13	Holmboe waves observed by Yoshida et al. in Japan [1998].....	77
3.14	Soliton wave packets observed by Farmer et al [1980] in the Knight Inlet sill.....	77
4.1	Diagram showing a wavelength and a pulse length.....	80
4.2	The 3dB limit referred to as the beamwidth.....	81
4.3	The ensonified area of two different size targets.....	82
4.4	Coherent and incoherent scattering from a target.....	83
4.5	The different types of zooplankton.....	90
4.6	Sound at a fixed and changing frequency.....	98
4.7	The depth cell size and the range gate used in the ADCP.....	101
5.1	The research vessel (Heron).....	106
5.2	The survey sensors.....	107
5.3	Hardware components of the MVP and the stages of the MVP vertical profiles.....	109
5.4	The effect of irregular bathymetry on the actual depth off bottom of CTD casts.....	110
5.5	Example of locations of the CTD casts in section one.....	110
5.6	Procedure performed for the processing of the ADCP data.....	115
5.7	Conversion to the coordinate system of Long Reach.....	116
5.8	The ADCP 2D surface plot of the velocity magnitude data.....	117
5.9	Example of the acoustic backscatter profile sourced from the ADCP data.....	117
5.10	2D surface plot of the density overlaid with the velocity arrows.....	118
5.11	The original acoustic backscatter images.....	120
5.12	Longitudinal profile plots of the density for the year 2003.....	127
5.13	Longitudinal profile plots of salinity and temperature for the year 2003.....	128
5.14	Cross-sections of salinity, temperature and density surveyed in February 2004.....	129
5.15	Acoustic backscatter images for the year 2003.....	130
5.16	Zoomed in illustrations of the pycnocline for September 2003.....	131
5.17	Zoomed in image of a Kelvin-Helmholtz wave from the September 2003 survey.....	132
5.18	Zoomed in illustrations of the pycnocline for October 2003.....	133
5.19	Longitudinal profile of the echosounder images for November 2003.....	134

5.20	Map of Long Reach showing the survey areas of section one and section two.....	137
5.21	Procedure for averaging of the velocity and density data.....	139
6.1	Cross-sections and profiles in section one.....	143
6.2	Graph of the tidal cycle for the neap and spring tides.....	147
6.3	Density profile plots of all CTD dips.....	149
6.4	Longitudinal density and acoustic volume backscatter images for neap tide.....	150
6.5	Acoustic volume backscatter images overlaid with the density contours for neap.....	152
6.6	Displacement of the pycnocline from late falling to low tide at neap tide.....	154
6.7	Longitudinal density and acoustic backscatter profiles at late falling tide.....	155
6.8	Downward dip of the pycnocline from density images.....	156
6.9	Downward dip of the pycnocline from acoustic backscatter image.....	157
6.10	Individual density and velocity profiles of the longitudinal profiles.....	160
6.11	Density profiles for the tidal cycle at the three groups.....	161
6.12	Longitudinal density and velocity profiles overlay with velocity arrows.....	163
6.13	Longitudinal density and velocity profiles at falling tide.....	165
6.14	Longitudinal profiles of density and velocity at rising tide.....	167
6.15	Shape and form of the type 1, type 2 waves and the plunging pycnocline...	171
6.16	The type 1 waves and the plunging pycnocline.....	172
6.17	The acoustic backscatter images showing the type 2 wave.....	175
6.18	Type 2 wave from late falling tide to low tide.....	177
6.19	Depression of pycnocline.....	178
6.20	Longitudinal density and velocity profile for the spring tidal cycle.....	181
6.21	Acoustic volume backscatter images for the spring tidal cycle.....	182
6.22	Identification of type 1 and type 2 wave for the spring tidal cycle.....	183
6.23	Gradient Richardson number from rising into high tide at neap and spring tides.....	188
6.24	Ri for the three groups at neap tides.....	189
6.25	Ri for the three groups at spring tides.....	192
6.26	Echosounder images.....	197
6.27	Velocity and density profiles observed at rising tide.....	199
6.28	Stability diagrams of the wave amplitude derived from the piecewise approx.....	203
6.29	The interpolation of the J on the wave amplitude for the piecewise approx.....	206
6.30	Plunging of the pycnocline and Holmboe wave identification.....	207
7.1	Plan view map of bathymetry in section two.....	216
7.2	Individual density profiles.....	218
7.3	Longitudinal profiles of density and acoustic backscatter.....	220

7.4	Longitudinal profiles showing the displacement at the pycnocline.....	221
7.5	Individual density profiles at location A and location B.....	223
7.6	Acoustic volume backscatter profiles overlaid with density contours.....	224
7.7	The progression of an internal wave and the possible collapse.....	225
7.8	Long. profiles of the acoustic backscatter and velocity at neap tides.....	227
7.9	Type 1 waves at the interface just after high tide.....	233
7.10	Type 2 wave at low tide.....	234
7.11	Long. profiles of density and acoustic volume backscatter at spring tide....	239
7.12	Long. profiles of density and acoustic volume backscatter at spring tide....	240
7.13	Type 1 wave at the pycnocline at spring tide.....	241
7.14	Type 2 wave at the pycnocline at spring tide.....	242
7.15	Location of mixing events and location A and B.....	243
7.16	Graphs of the gradient Richardson number for locations A.....	244
7.17	Velocity profiles of the theory and the observed.....	245
7.18	Results of the linear stability analysis.....	247
8.1	The three types of interfacial waves.....	252
8.2	Map of Long Reach illustrating sections one and sections two.....	256
8.3	Density and acoustic backscatter for the different phases of the tide.....	258
8.4	The plunges observed in Long Reach and that referred to in Apel [2002]...	259
8.5	Profiles of density and acoustic volume backscatter for section two.....	263
I.1	Sediments graphs of Long Reach.....	274
II.1	Piecewise approximations for section one.....	278
II.2	Smooth profile approximations for section one.....	280
III.1	Piecewise approximation for section two.....	283

## LIST OF TABLES

	page
2.1	The main harmonic constituents for the Bay of Fundy.....14
2.2	The main harmonic constituents for the Saint John River..... 18
5.1	The resolution of the ADCP, MVP and echosounder..... 112
5.2	Dates and phase of the tides of the surveys performed.....135
6.1	The time periods for the different phases of the tides for neap and spring tides..... 147
6.2	Velocity magnitude, direction and velocity shear.....168
6.3	Results of the linear stability analysis using piece wise approximations..... 202
6.4	Results of the linear stability analysis using smooth profiles..... 213

## ACKNOWLEDGEMENTS

This research was funded by NSERC and the chair in Ocean Mapping Group funding, thus I wish to thank both groups for making this study possible. To my supervisor Dr. John Hughes Clarke thank you for giving me a beautiful project and for all your guidance and enthusiasm. A special thanks to Dr. Susan Haigh for, showing me the mathematical view of internal waves and for pointing out my grammatical errors. To Dr. Colm Caulfield thanks for your advice on the Holmboe waves. Dr. Katy Haralampiles, thank you for giving me access to the sediment lab at UNB. A special thanks to members of the ocean mapping group and GGE 3353 class of 2004 whom assisted with my tidal cycle surveys and multibeam surveys. Thank you.

David thanks for Paramaribo, let us go watch some waves now. To my mother, Marlon, Jay, Kurt, Artu, Azadeh and all my friends, you are the best and thank you all for your support and encouragement.

# CHAPTER 1

## INTRODUCTION: RESEARCH INTEREST

Stratified environments are of importance because of their association with the processes of mixing and advection. These processes are known to occur in nature (air, ocean, space, land (land slides, volcanoes, and plate tectonics)) and in industry (oil and gas). At the interface of stratified environments turbulent mixing is created by interfacial waves (which will be referred to as internal waves). The literature implies that the three main known internal waves that contribute to the mixing process are: (1) Kelvin-Helmholtz waves (KH), (2) Holmboe waves and (3) Solitons.

The basic understanding of internal waves is based on a combination of theoretical studies and laboratory experiments. The theory of internal waves has been studied by many. For example the KH has been studied theoretically by Hazel [1972]; Holmboe waves by Holmboe [1962]; and Solitons by Korteweg et al. [1895]. Laboratory experiments have been performed by Thorpe [1973, 1985] for the KH wave and by Browand and Winant [1973] and Lawrence et al. [1991] for Holmboe waves. Solitons were first sighted in the field by J. Scott Russell [1838, 1844] in the Scottish canal and this initiated further studies. These theories and experiments are used as a guide to understand turbulent mixing in stratified environments.

Laboratory experiments and computer numerical simulations are a good method used to understand mixing in stratified environments. However application of the theory to field observations has its limitations. This is partly due to the fact that in laboratory experiments controlled conditions exist, whilst in the environment these exact controlled



conditions are not always present. Thus in particular cases, field observations do not always agree with the theory. This emphasises that there is still much more to be known of the processes that occur in stratified environments. However of utmost importance for field observations with respect to identifying mixing events and internal waves, is the resolution of the data collected (horizontally, vertically and time).

The implementation of acoustics in mapping of the oceans, allows the mixing processes to be efficiently remotely imaged more accurately than in other stratified environments. In other environments these processes may not be so easily remotely imaged. Thus the observations made in the ocean can aid in the understanding of the mixing processes in other stratified environments.

Turbulent mixing tends to be a major concern in estuaries because of its influence on: (1) the distribution of polluted water sourced from the land or open sea, (2) biological activity production, (3) sedimentation, (4) recreation and (5) commercial activity.

This research investigates the dominant processes occurring in a section of the Saint John River estuary, N.B known as Long Reach (see Figure 1.1). The Saint John River originates in Maine, USA and flows in a south easterly direction into New Brunswick, Canada where it empties into the Bay of Fundy. Studies performed in Long Reach by Trites [1959] and Metcalfe et al. [1976] concentrated on the seasonal variation of the stratification structure. From these surveys it was observed that during the summer months (when the River discharge was low) mixing or/and advection appear to be taking place in Long Reach. These surveys were performed with sensors of a lower resolution than that which is now available. Yet the processes were hinted at. However to confirm

the presence of mixing, advection or internal waves from the data collected would have been an almost impossible task.

This research seeks to investigate the processes of turbulent mixing and lateral advection occurring in Long Reach. To accomplish this, the seasonal stratification of Long Reach is remapped, using modern survey sensors and for the duration of a tidal cycle the dominant oceanographic processes are monitored.

Chapter 2 examines the study area, with respect to the physical and geological characteristics. The previous oceanographic studies performed in Long Reach by Trites [1959] and Metcalfe et al. [1976] are also described.

Chapter 3 presents the classification of the different types of estuaries that exists based on their salinity and velocity profiles; an introduction to mixing and how it is determined theoretically using the Reynolds number ( $Re$ ), Gradient Richardson number ( $Ri$ ), Bulk Richardson number ( $J$ ) and the Froude number ( $Fi$ ); and the methodology of using a linear stability analysis to differentiate between Holmboe waves and Kelvin-Helmholtz waves.

The introduction of acoustics in the oceans allows measurements to be made more accurately than was previously performed by Trites [1959] and Metcalfe et al. [1976]. Chapter 4 presents the background theory of acoustics with respect to the backscatter from targets in the water column and the measurement of velocity magnitude and direction using acoustics.

Chapter 5 describes:

1. The survey sensors: the Acoustic Doppler Current Profiler (ADCP) which is used in this study for the measurement of velocity magnitude and direction; a

Conductivity Temperature Depth Sensor (CTD) which measures conductivity, temperature and pressure and an echosounder which measures acoustic backscatter (this was used to identify the pycnocline and internal waves).

2. The procedure used for the processing of the data
3. A description of the 2003 seasonal distribution of stratification
4. The survey design for 2004 tidal cycle surveys. To observe in detail the processes occurring in Long Reach only a section of Long Reach is investigated.

Chapter 6 and Chapter 7 present the results and analysis of Long Reach. These results are first presented descriptively with respect to longitudinal profiles of the density, along velocity and acoustic backscatter. A dynamical analysis using the available theory is then performed to confirm the observations made.

Chapter 8 summaries the observations made in Long Reach

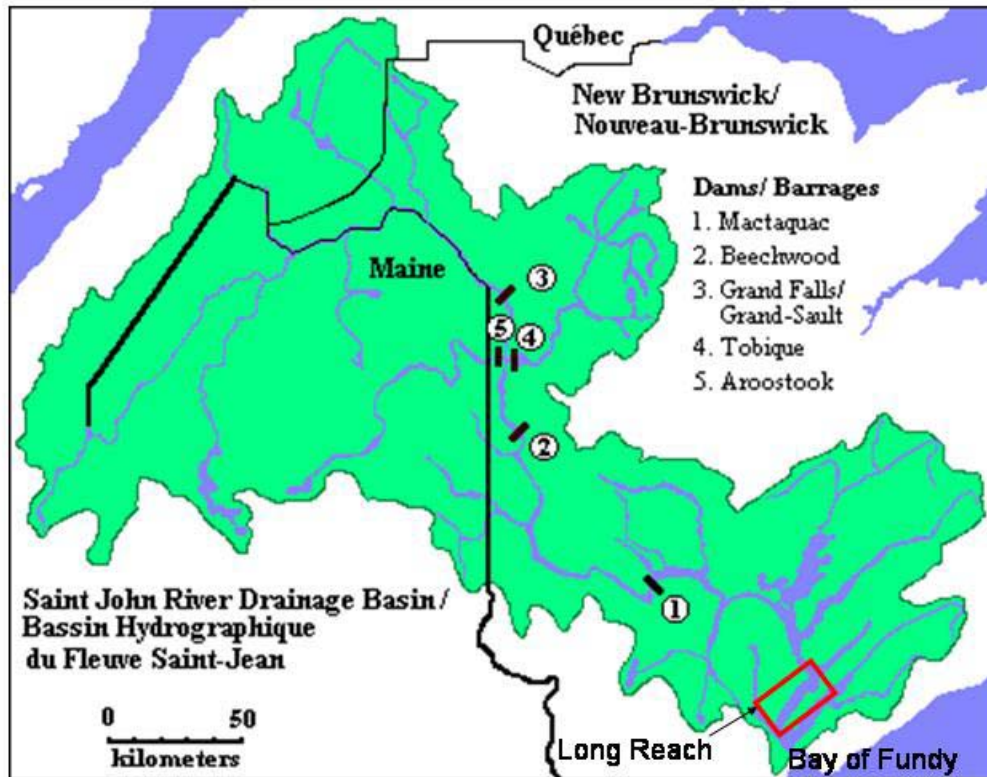


Figure 1.1: Map of the Saint John River watershed (purple colour). The red rectangle identifies Long Reach, the survey area for this research. This diagram was referenced from Fisheries and Oceans Canada [2002].

## **1.1 Research Objectives**

- To describe the seasonal variation of stratification within Long Reach
- To identify the processes occurring in a section of Long Reach during summer conditions for the duration of a tidal cycle
- To describe and explain the influence of the bathymetry and geometry on the stratified flow in Long Reach

### **1.1.1 Scientific Questions**

- What are the dominant oceanographic processes occurring in a section of Long Reach that are characterized as possessing irregular bathymetry and stratified flow?
- What are the dominant oceanographic processes occurring in a section of Long Reach that are characterized as possessing almost uniform bathymetry and stratified flow?
- Do variations in the tides influence the dominant oceanographic processes occurring in a section of Long Reach?

## **CHAPTER 2**

### **THE STUDY AREA**

This section describes the physical and geological features of Long Reach. Section 2.1 to 2.4 explains the climate, tides and River discharge. Section 2.5 describes the geology of the area and Section 2.6 summarizes the previous research performed in the Saint John River Estuary.

#### **2.1 Saint John River Estuary**

The salt water (salinity of ~32‰) of the Bay of Fundy and the fresh water (salinity of 0‰) of the Saint John River are two strongly contrasting water masses. As a result of these two contrasting water masses being in proximity to one another, density currents are produced.

In the Bay of Fundy the fresh water from the Saint John River spreads as a plume over the salty water (see Figure 2.1). Whilst in the Saint John River the salt water of the Bay of Fundy percolates beneath the fresh water. This salt water can move as far upstream as Gagetown which is ~60km upstream from the Saint John Harbour (see Figure 2.2).

This research concentrates on the area in the Saint John River where saline water percolates up the River. This area is referred to as the Saint John River Estuary. The demarcation of the estuary is defined by Trites [1959] and Metcalfe et al. [1976] as the seaward limit being that of the Reversing Falls (a sill located at the mouth of the River) and the landward limit being that of Gagetown (60km from mouth) (see Figure 2.2). The

focus area of this research is a portion of the upper section of the Saint John River Estuary known as Long Reach (see Figure 2.2).

There are two main sources of fresh water that enter Long Reach: the Nerepis River that enters at the western end of Long Reach (see Figure 2.2) and the Saint John River. The water supply from the Nerepis River is negligible compared to that produced by the Saint John River.

The main characteristics of the estuary that affect the density distribution and as a result the stratification, of the Saint John River estuary are: (1) the climate, (2) the tides, (3) the river discharge and (4) the bathymetry of the area. The following sections now describe in detail these characteristics of the estuary. It is noted that detailed surveys were performed in September 2004 at neap (5<sup>th</sup> and 7<sup>th</sup> September) and spring (14<sup>th</sup> and 15<sup>th</sup> September) tides. Thus reference is made with respect to the conditions of the climate, the tides and the river discharge at this period.

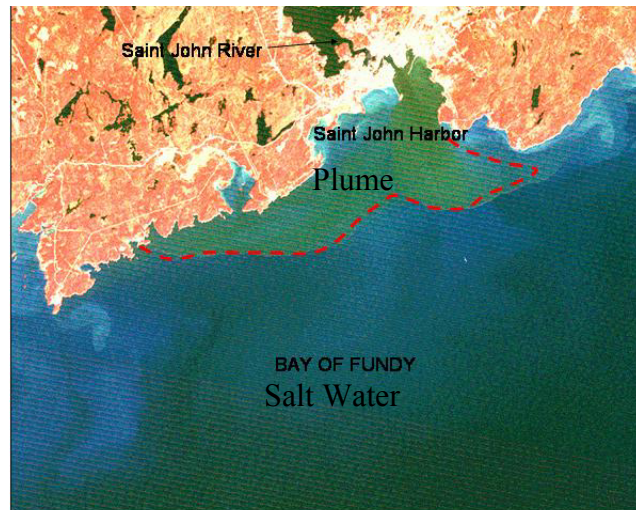


Figure 2.1: Map of Saint John River plume (salinity of ~27‰ to 29‰) advancing into the Bay of Fundy. This LANDSAT T.M image was generated by John Hughes Clarke [2002].

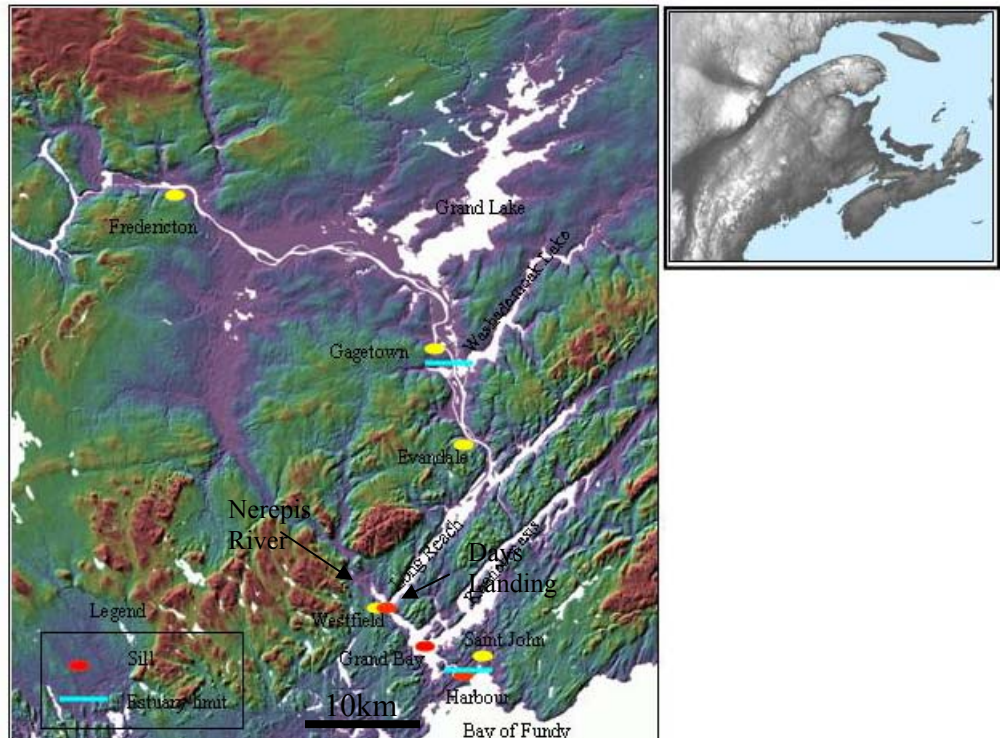


Figure 2.2: Map showing the delimitation of the Saint John River Estuary and the survey site of Long Reach. Topographic image using Service New Brunswick aerial photo spot height generated by John Hughes Clarke [2002].

## 2.2 Climate

To illustrate the temperature, rainfall and snowfall conditions that exist for Long Reach, data were acquired for the City of Saint John which is within close proximity of Long Reach (see Figure 2.2). The data were acquired from Environment Canada [2005] and illustrates the mean conditions from the years 1971 to 2000 and the year 2004. It should be noted that the data set from January 2004 to March 2004 was not available.



## 2.2.1 Temperature, Rainfall and Snowfall Pattern

The study area experiences four main seasons: spring (March to June), summer (June to September), autumn (October to November) and winter (December to March). The highest mean air temperature occurs in the summer months ( $\sim 17^{\circ}\text{C}$ ), whilst the lowest mean air temperature occurs in the winter months ( $\sim -8^{\circ}\text{C}$ ) (see Figure 2.3). The highest amount of rainfall occurs in spring and in autumn. The autumn rainfall tends to be the higher of the two seasons (see Figure 2.4). The highest amount of snowfall occurs in January (see Figure 5).

A comparison of the 2004 data with the norm shows that: (1) the temperature patterns are similar, (2) the snowfall for December 2004 was less than expected, (3) an increase in rainfall for August 2004 and (4) a decrease in rainfall for September 2004 and October 2004. These results indicate that for the September 2004 surveys the rainfall was low which was expected for summer conditions.

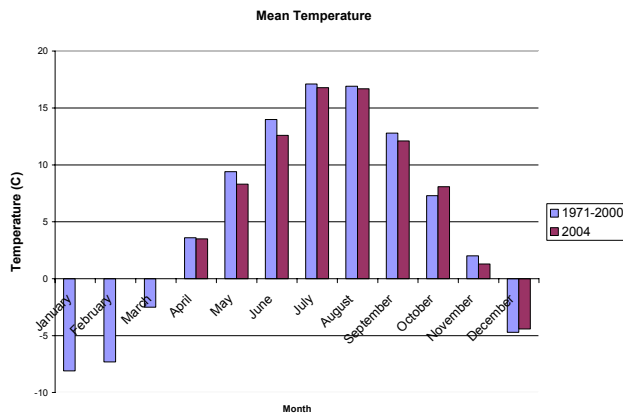


Figure 2.3: Mean monthly air temperature at Saint John. In 2004 data were not available from January to March.

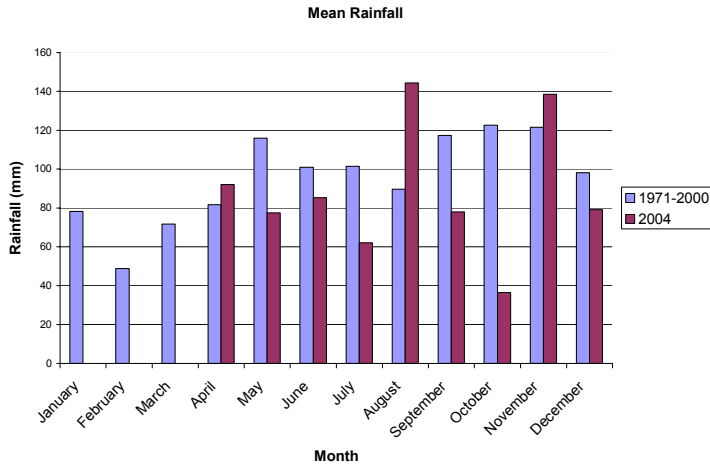


Figure 2.4: Mean monthly rainfall at Saint John. In 2004 data were not available from January to March.

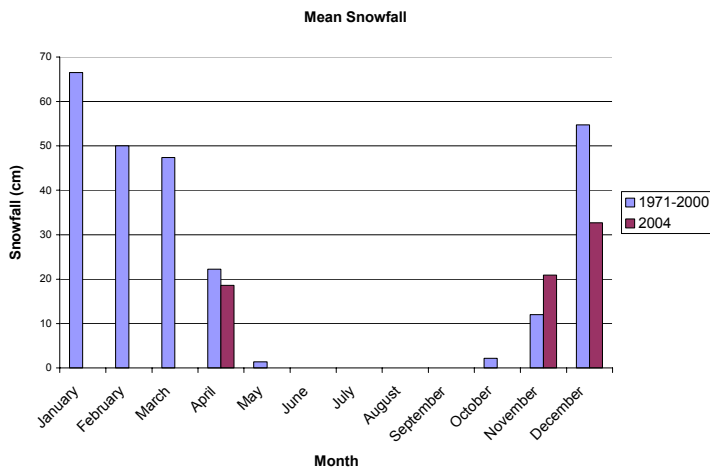


Figure 2.5: Mean monthly snowfall at Saint John. In 2004 data were not available from January to March.

## **2.3 TIDES AND RIVER DISCHARGE**

### **2.3.1 Bay of Fundy/Saint John Harbour: Tidal Range & Currents**

The Bay of Fundy is characterized as having semi-diurnal tides with huge tidal ranges. The tidal range is enhanced due to: the length of the coast; the V shape configuration of the coast; and the depth change of the Atlantic Ocean into the Bay of Fundy. The tidal range increases due to the horizontal limitation of the coastline and due to a resonance effect that takes place.

This resonance affects the tidal range in that the time it takes the water to move back and forth within the Bay coincides with high tide and low tide of the Atlantic Ocean. According to Godin [1991] one resonance takes between 12.5 and 12.7 hrs, which lies close to the N2 (12.66h) tidal constituent and the M2 (12.42h) tidal constituent. Thus the resonance is in synchrony with the period of the tides. This causes the tides to be amplified.

The range of the tide increases the further inland that it progresses into the Bay of Fundy. At Saint John harbour a range of 8m exists whilst at Minas Basin it is 15m (see Figure 2.6). Table 2.1 displays the main semi-diurnal harmonic constituents and their constants for the Bay of Fundy region which were obtained from the Canadian Hydrographic Service [2005]. From the table it is observed that the main harmonic constituent is that of the M2.

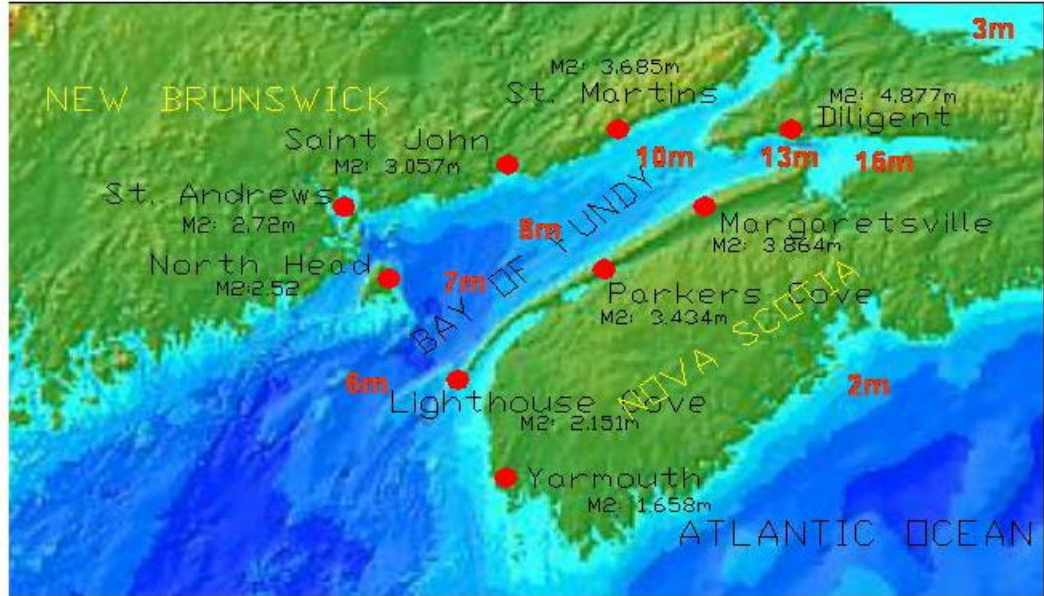


Figure 2.6: Map of the Bay of Fundy showing the different tidal range (in red) and the M2 amplitude (in black) that is observed at different locations.

Table 2.1: The main harmonic constituents for the Bay of Fundy

Station	M2		N2		S2	
	Phase	Amplitude (m)	Phase	Amplitude	Phase	Amplitude (m)
<b>North Head</b>	338.6	2.52	314.4	0.356	9.8	0.427
<b>St Andrews</b>	350.6	2.722	324.6	0.547	30.9	0.406
<b>Saint John</b>	342.54	3.0577	312.2	0.6549	17.75	0.4799
<b>St Martins</b>	345.7	3.685	314.6	0.903	28.2	0.585
<b>Diligent River</b>	356.5	4.877	327.9	1.032	36.3	0.719
<b>Margaretsville</b>	337	3.864	305.8	1.069	22.8	0.417
<b>Parkers Cove</b>	333.9	3.434	307.2	0.658	8.8	0.516
<b>Lighthouse</b>	325	2.151	297	0.451	357	0.341
<b>Yarmouth</b>	307.14	1.658	27871.	0.3727	337.63	0.2653

### **2.3.2 Saint John River Estuary**

The tides of rivers are not only influenced by the astronomical effects of the sun and moon on the earth but also by: friction, wind, ice and fresh water discharge. In the Saint John River Estuary there exists a sill situated at the mouth of the Saint John River. This sill is referred to as the Reversing Falls and it hinders the advancement of the huge tides of the Bay of Fundy up into the River. However the effects of the tidal wave can still be felt as far up as Fredericton.

According to Trites [1959] the tidal range decreases from about 0.7m near the mouth, 0.4m in Long Reach and 0.15m at Fredericton (see Figure 2.7). A phase lag also exists between the tides at the Saint John Harbour and those upstream. At the Reversing Falls there is a 1.5 hour delay, at Long Reach a 3 hour delay and at Fredericton there is a 10 hour delay.

Studies performed by Hansen [1977] on the Saint John River Estuary confirm that river discharge plays a major role in affecting the tides. Hansen [1977] results were based on the construction of a physical model of the Reversing Falls and environment and concluded that high river discharge caused the level of the River to increase. It should be noted that Hansen's [1977] published results were based on the modelling of only high outflows through the Reversing Falls. Thus a single fluid model with only fresh water was used. Density currents were ignored. Hansen [1977] results are of importance because they show that, in the case where the River discharge varies daily, the variation in the River discharge can now be superimposed on the daily tidal variation.

Godin [1985] with field observations in the Fraser River, Saint Lawrence River and the Saint John River took into consideration density currents. The observations show

that, for increasing discharges at the upstream section of the River (where the currents don't reverse), the tidal range is reduced by an increased discharge; the time of arrival of low water is accelerated, and high water is retarded. In the downstream section (where the currents reverse) an increased discharge causes a decrease in the effective friction during flood (different direction of currents) and an increase in it during ebb (currents moving in the same direction). This causes the timing of low water to be retarded and high water to be accelerated. Godin's [1985] results show that density currents affect the duration of the phases of the tide. Whilst in the absence of a density current, both the tidal range and duration of the phases of the tide are affected.

Table 2.2 shows the main harmonic constituents for the Saint John River and Figure 2.7 shows the locations of the stations used. Public Landing is the only station located in Long Reach. From the table it is shown that for most stations the M2 and M4 are the main constituents dominating the tides. This emphasises the fact that the tides in Long Reach are not only affected by the astronomical effect of the moon but also by the bottom friction in the estuary. Thus it is expected that the natural M2 component will be distorted by the effects of the M4 component.

Figure 2.8 shows graphs of the tidal cycles for the dates surveys were performed at neap (5<sup>th</sup> and 7<sup>th</sup> September 2004) and spring tides (14<sup>th</sup> and 15<sup>th</sup> September 2004). The tidal data were collected from a tide gauge located at Days Landing (see Figure 2.2).

The maximum tidal range at Long Reach for both neap and spring tides is 0.4m. It is observed that for the spring tidal cycle (14<sup>th</sup> and 15<sup>th</sup> September 2004) there was an increase in the tidal height. This coincides with the increase in River discharge that was observed in Figure 2.12. It is also observed that falling tide occurs for a longer duration

(~7.5 hours) than rising tide (~4 hours). This confirms the conclusions made by Godin [1985] that when a density current exists in a river high tide is accelerated whilst low tide is retarded (see Section 2.3.2). This emphasises the effects of bottom friction on the tides.

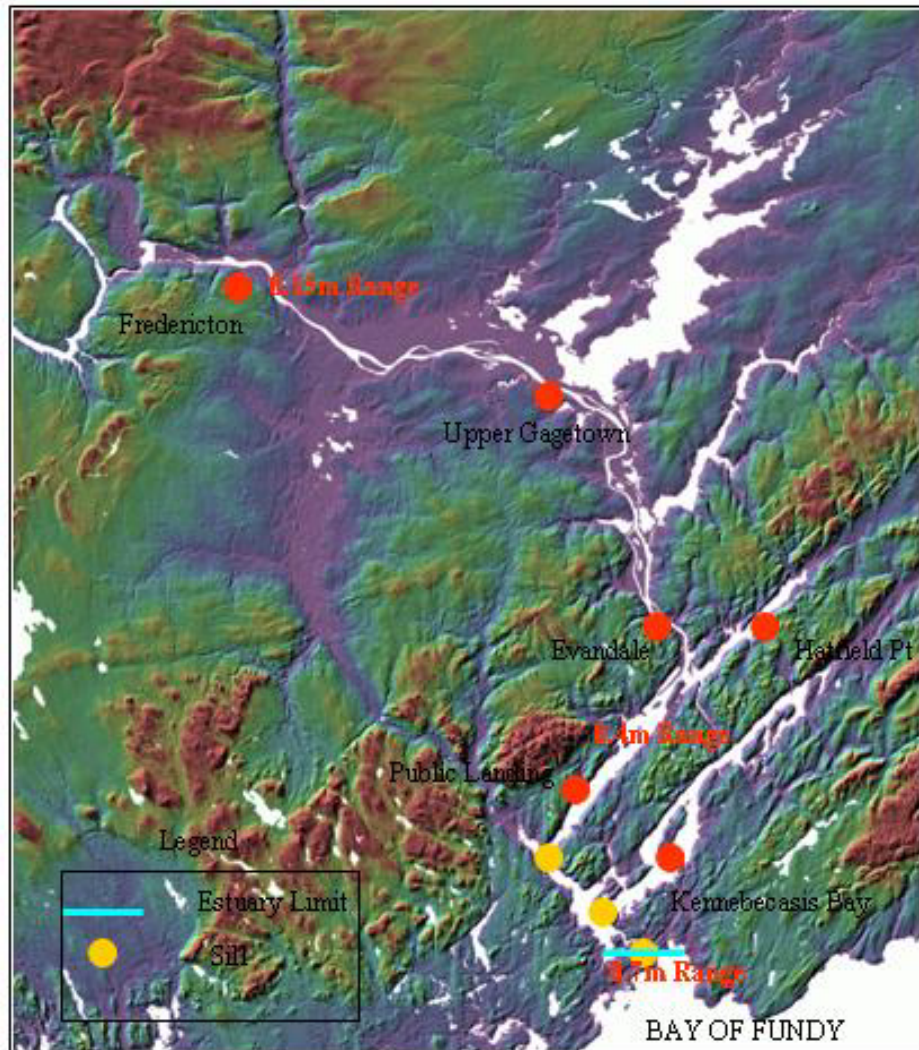


Figure 2.7: Map of the Saint John River Estuary showing the locations of the tidal stations.



Table 2.2: The main harmonic constituents for the Saint John River

	<b>M2</b>		<b>N2</b>		<b>S2</b>		<b>M4</b>	
<b>Station</b>	<b>Phase</b>	<b>Amp</b>	<b>Phase</b>	<b>Amp</b>	<b>Phase</b>	<b>Amp</b>	<b>Phase</b>	<b>Amp</b>
<b>Kennebecasis</b>	72	0.194	13.8	0.035	76.6	0.027	19	0.034
<b>P. Landing</b>	12.61	0.135	NA	NA	152.02	0.0303	316.02	0.0546
<b>Hatfield Pt</b>	93.9	0.138	59.8	0.025	120	0.021	130.5	0.036
<b>Evandale</b>	95.1	0.131	63.9	0.021	128.5	0.018	126	0.03
<b>Upper Gagetown</b>	171.6	0.062	141.9	0.012	194.3	0.008	259.4	0.012
<b>Fredericton</b>	251.1	0.038	220.2	0.008	296.4	0.007	49.3	0.008

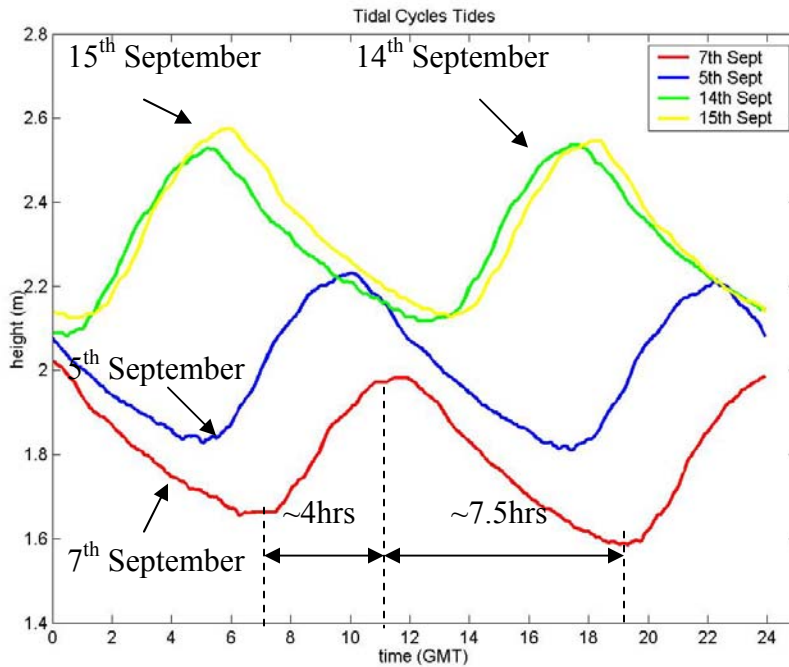


Figure 2.8: Graphs of tidal cycle for the neap (5<sup>th</sup> and 7<sup>th</sup> September 2004) and spring tides (14<sup>th</sup> and 15<sup>th</sup> September 2004) survey dates.

### 2.3.3 Water Levels for Survey Dates

Water level data were collected for three main areas within the Saint John River estuary to emphasise the variation in height and phase lag that exists. These areas are the Saint John Harbour, Indiantown (above the Reversing Falls) and at Oak Point. The data were obtained from Environment Canada [2005] and Canadian Hydrographic Service [2005]. The water levels displayed are for the 14<sup>th</sup> and 15<sup>th</sup> September 2004 (spring tides).

There was a malfunctioning of the tide gauge at the Saint John Harbour for the month of September. Data were retrieved for the 1<sup>st</sup> September, thus a comparison is

made of the predicted (also obtained from the Canadian Hydrographic Service) and observed tides of that exact station (see Figure 2.9). The results show that the predicted and observed phases of the tides for the Saint John harbour are similar, however there was a 0.3m difference in tidal amplitude. Nevertheless, for the Saint John harbour area, predicted tides are employed to represent the data for the survey dates (see Figure 2.10).

From the graphs of the 14<sup>th</sup> and 15<sup>th</sup> September (see Figure 2.10) it is observed that that high tide first occurs in the Saint John Harbour, next 1.5 hours later above the Reversing Falls and then three hours later at Oak Point. The amplitude of the tide also decreases from ~6.5m at the Saint John Harbour to ~0.4m at Oak Point.

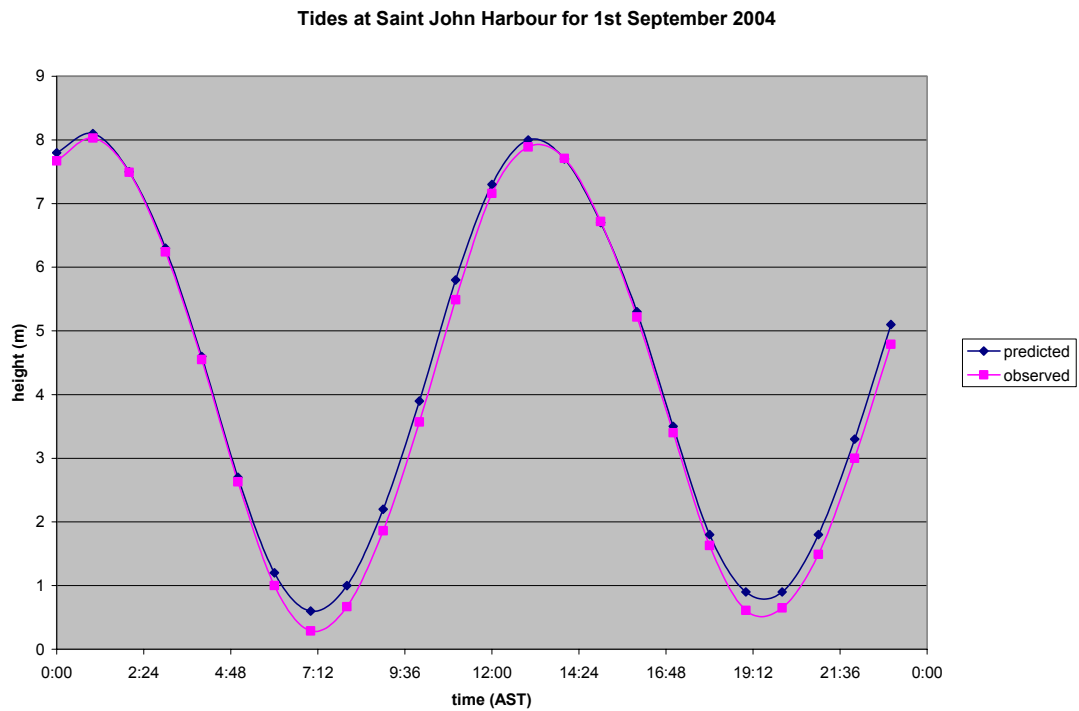
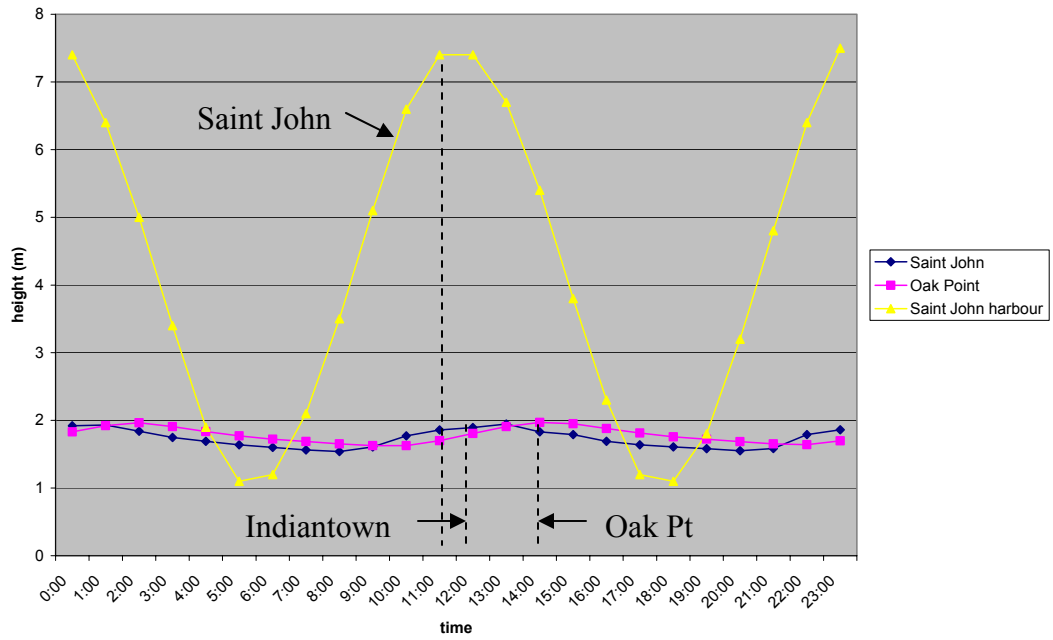


Figure 2.9: Graphs of the predicted (blue) and observed (red) tides for the 1<sup>st</sup> September 2004 for the Saint John Harbour.

Water Level for Saint John River Estuary 14th September 2004



Water Levels for the Saint John River Estuary on 15th Sept 2004

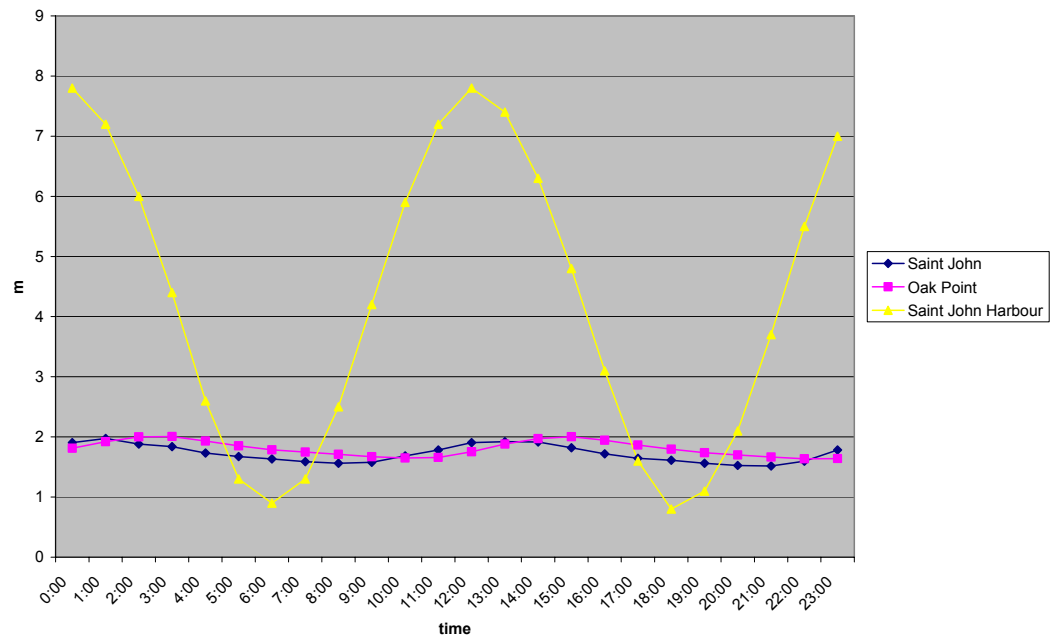


Figure 2.10: Graphs of water level for the 14<sup>th</sup> and 15<sup>th</sup> September 2004.

## 2.4 River Discharge

The discharge from the Saint John River varies widely both seasonally and from year to year. River discharge data were collected from Water Survey of Canada [2004] from 1966 to 1995. This data were collected at a station located just below the Mactaquac Dam (see Section 1.1 Figure 1 for location of Mactaquac Dam), however data for the year 2004 was collected from New Brunswick Power whose station was at the Mactaquac dam.

In general two yearly discharge peaks occur. One is in the autumn and related to heavy autumn rains the second and the larger of the two occur in the latter half of April or first half of May and are associated with the melting of ice (see Figure 2.11). For the year 2004 it was observed that the autumn peak occurred earlier than normal. It peaked in August/September 2004 when normally it peaks in October/November.

The River discharge for the survey dates are illustrated in Figure 2.12. It is observed that on the 14<sup>th</sup> and 15<sup>th</sup> September (spring tides) there is an increase in the river discharge. For the surveys, the increase in River discharge caused an increase in water level from neap to spring tides (see Figure 2.8).

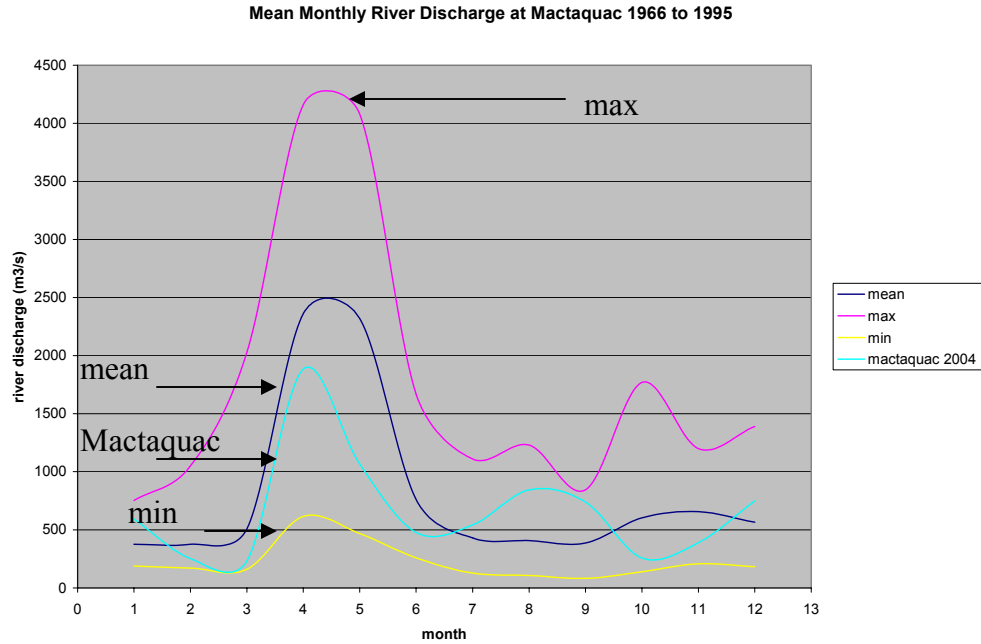


Figure 2.11: River discharge from 1966 to 1995 at Mactaquac dam.

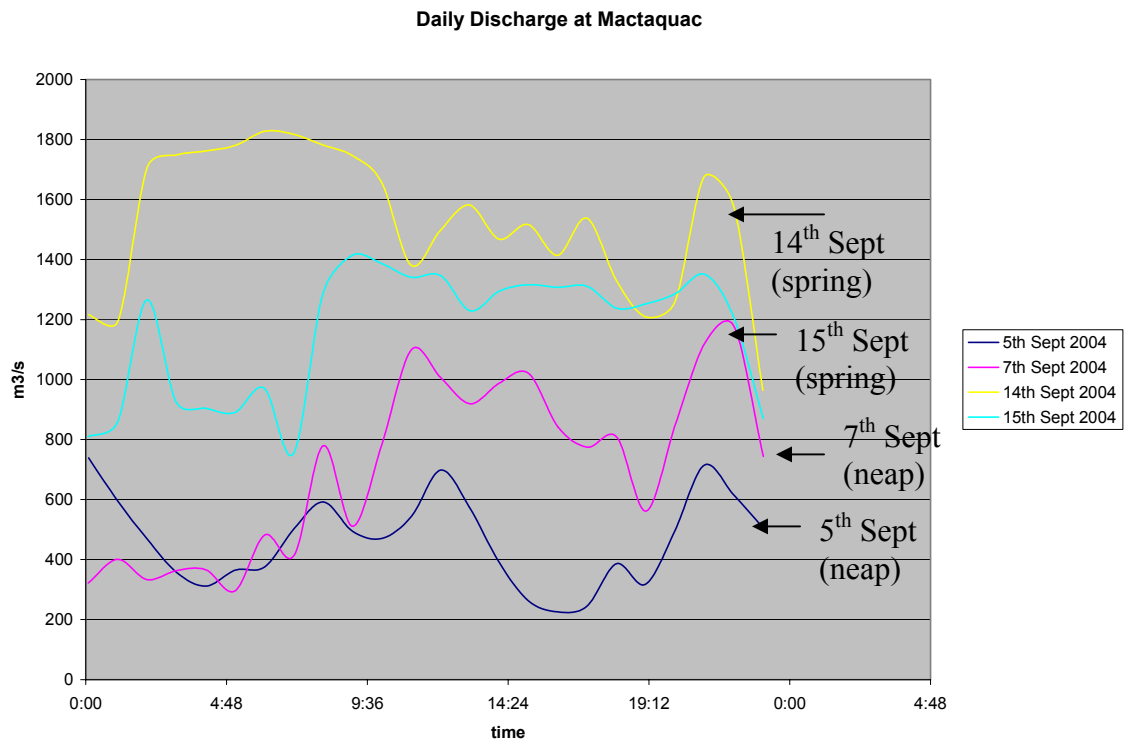


Figure 2.12: Mean daily discharge at Mactaquac for the 5<sup>th</sup> and 7<sup>th</sup> September (neap tides), 14 and 15<sup>th</sup> September (spring tides).

## **2.5 Geological Characteristics**

Previous studies performed by Trites [1959], Metcalfe et al. [1976] and Hughes Clarke et al. [2005] have observed that the geological features of the Saint John River estuary influence the oceanographic characteristics. Therefore a brief overview of the geology of New Brunswick with particular attention to Long Reach is now described.

### **2.5.1 Bedrock Geology of New Brunswick**

The last ice age is referred to as the Wisconsinan and this occurred from ~1.6 million years ago to 10,000 years ago. During this period a continental ice sheet known as the Laurentide ice covered most of Canada. It is suggested in Seaman [2004] that New Brunswick was influenced by regional ice sheets rather than the Laurentide ice. It was also suggested that these regional ice sheets may have been followed by local ice caps and this occurred during the late Wisconsinan period.

The movement of glaciers causes the bedrock to be eroded, thus carving it. Remnants of this are recognized by sills, gorges and eroded sediment (till), that are now present in the landscape of New Brunswick. An example of the remnants created by the glaciers that can be visually observed in the Saint John River is the three sills located in a north-south direction from the entrance of Long Reach into the Bay of Fundy. These sills are described in detail in section 2.6.3.

In New Brunswick it is observed, in most locations, that a single till sheet covers the underlying bedrock rather than multiple till sheets. Multiple sheets were observed in the Nova Scotia and Quebec regions. The observation of a single sheet existing may have

been the result of: (1) nunatak zones existing, (2) the area was influenced by only one major stage of glaciation.

In New Brunswick the bedrock geology consists of two contrasting regions: the New Brunswick Lowlands and the New Brunswick Highlands. The New Brunswick Lowlands are flanked to the south and the west by the New Brunswick Highlands. The Lowlands are an extensive flat surface that slopes gently towards the Gulf of Saint Lawrence, this region consists mostly of sandstone of Carboniferous age (360 to 280 million years ago). The Lowlands control the features observed at Grand Lake, Washdemoak and the Saint John River up to Gagetown (see Figure 2.13).

The Highlands are divided into three sub units: the Miramichi Highlands; the St. Croix Highland and the Caledonia Highlands. Long Reach is located in the Caledonia Highlands. The Caledonian Highlands have rocks of the Upper Precambrian (544 millions of years ago to beginning of earth) and Cambrian (544 to 505 million years ago) group which are overlain by Carboniferous sediments (360 to 280 million years ago).

## **2.5.2 Rock Types of Long Reach**

Figure 2.14 shows that Long Reach is oriented in the same South - West to North-East direction as the Silurian fault. This indicates that Long Reach is fault controlled.

To the immediate south of Long Reach the rock is from the Palaeozoic era (544 to 248 million years ago), whilst to the north of Long Reach the rock type consists of both Pre-Cambrian era (beginning of earth to 544 million years ago) and Palaeozoic era. Palaeozoic rocks are observed at Craig's Pt, Public Landing, Beulah Camp and Devils' Back.



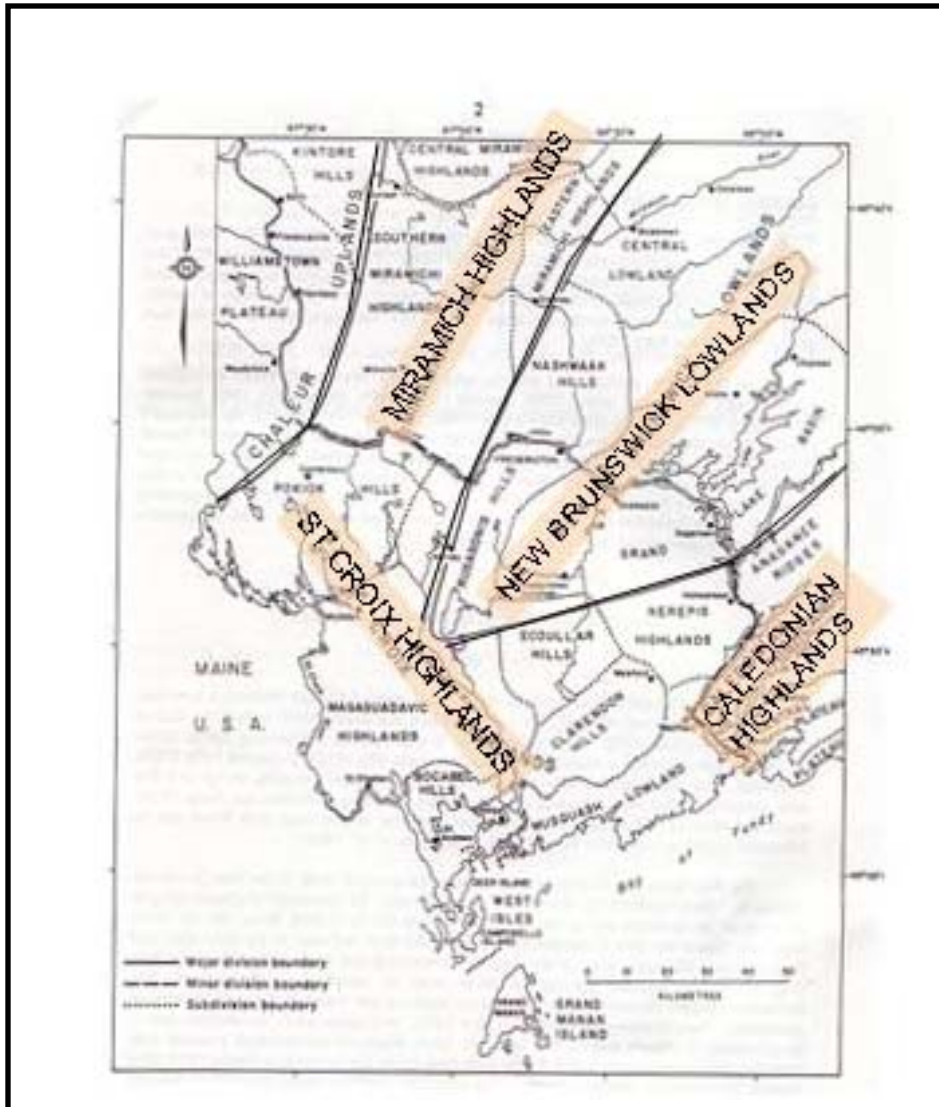


Figure 2.13: The different geological zones of New Brunswick.

To the north and south of Long Reach there exist some differences in the rock types such as: the thin strip of Palaeozoic rocks that exist to the south of Long Reach and evidence of the Palaeozoic rock existing at Devils Back. These observations suggests that the Palaeozoic rock (softer) was eroded either glacially or fluvial.

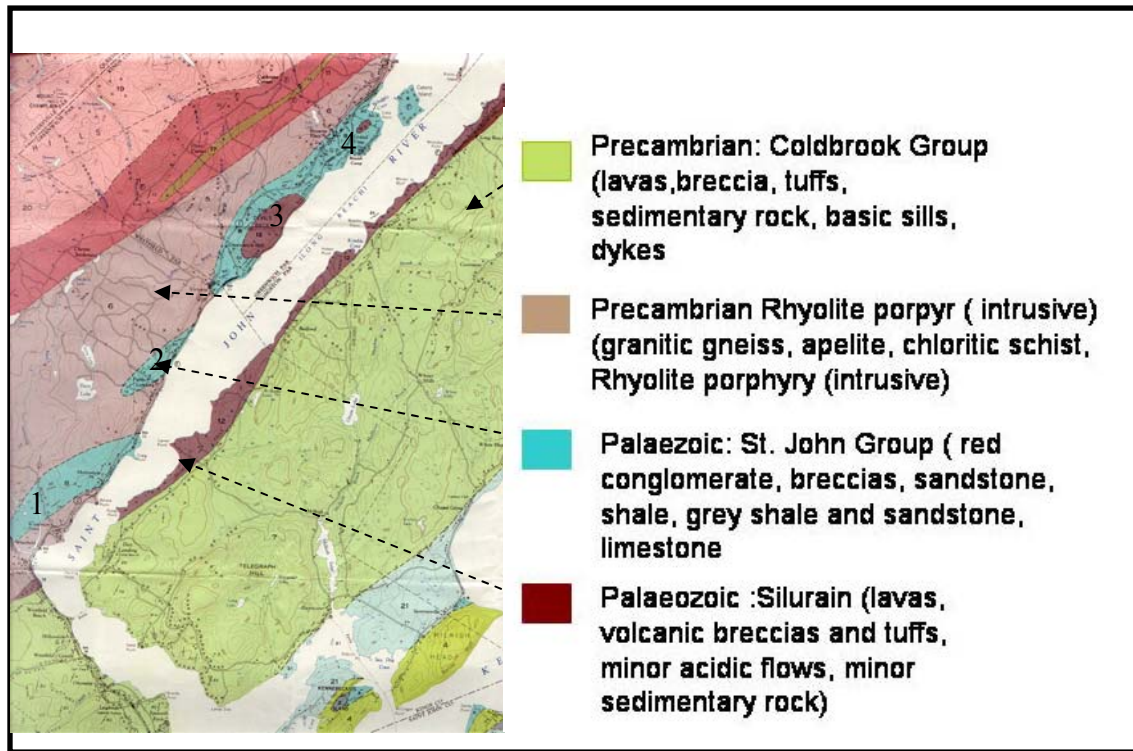


Figure 2.14: Rock types of the land masses surrounding Long Reach. The Palaeozoic era on the northern side of Long Reach consists of outcrop at (1) Craig Pt, (2) Public landing, (3) Devils Back and (4) Beulahs Camp.

An investigation on the modern sediments that exist on the seabed of Long Reach was performed by Metcalfe et al. [1976] (see Figure 2.15). The method of sediment size analysis used was the hydrometer method (distinguishes between the silt and clay particles). The results found that: clay particles exist from the southern entrance of Long Reach to Beulah camp; silt particles from the entrance of Long Reach to Public Landing; sand particles from the south of Beulah camp to Belleisle Bay and at the entrance of Long Reach; and gravel particles at Westfield channel.

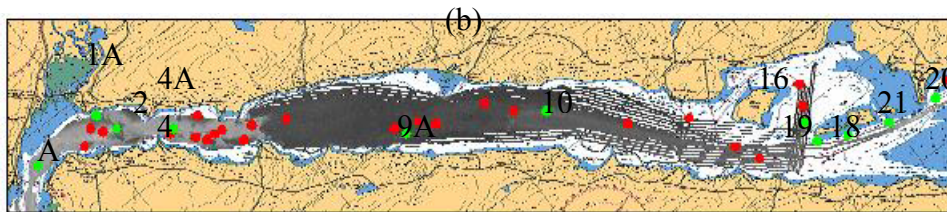
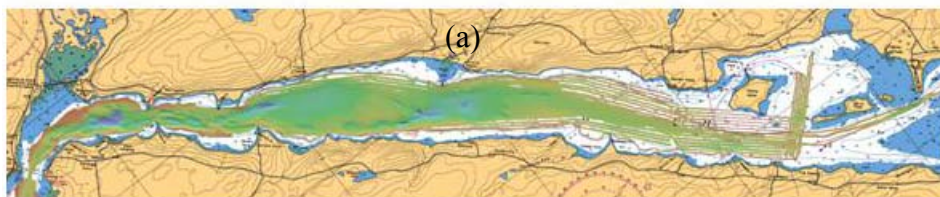
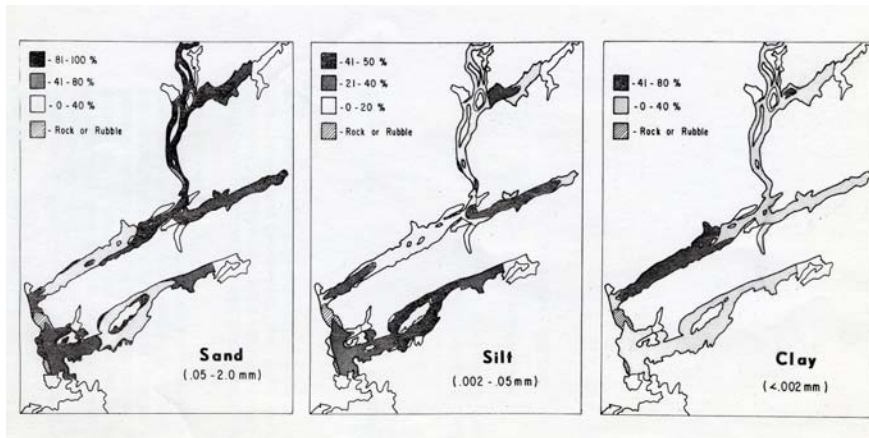
From Metcalfe et al. [1976] observations it appears that the sediment grain sizes decreases upstream with the exception of the sand particles at Belleisle Bay. It is suggested in Seaman [2004] that the Saint John River may have been: (1) an iced dammed lake referred to as Lake Acadia and (2) a glacial lake followed by an estuary or vice versa. These suggestions were inferred from evidence of varves (layers of alluvium sediment deposited in glacial lakes) and the grey in the overlying silt suggest the existence of a brackish environment. Thus the sand particles observed at Belleisle Bay may have been sourced from this period.

As was mentioned in section 2.1 a density current can exist in Long Reach that brings with it salt water and fine grained suspended sediments from the Bay of Fundy. Based on this process and the suggested geological history of the Saint John River the observations made by Metcalfe et al [1976] studies may be influenced by: (1) the density current that contains suspended sediments which are deposited into Long Reach; (2) the Nerepis River that may have eroded its bedrock upstream thus depositing sand at the entrance of Long Reach and (3) the Grassy Island Region that may have previously been a delta, thus a potential source of sand particles.

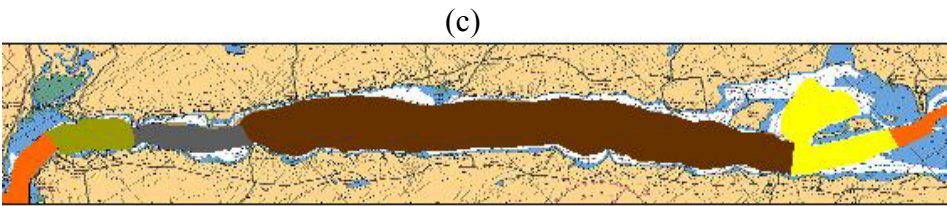
A sediment sampling survey was performed by the OMG in June 2004 to reconfirm the results of Metcalfe et al. [1976]. It should be noted that the procedure used by the OMG was that of sieving (cannot distinguish between the silt and clay particles), thus Metcalfe et al. [1976] results are still more detailed in the classifying the grain size. Not all of the samples were analysed (see Figure 2.15). The samples chosen to be analysed were based on their location on the multibeam backscatter and bathymetry images and on their visual difference from the other samples (see Appendix I for detail graphs of analysed samples).

The samples obtained in June 2004 (see Figure 2.15) show similar results to that of Metcalfe et al [1976]. However there appears to be evidence of gravel particles present with the silt and clay between Purdy's Pt to Carters Pt and at Oak Pt. Figure 2.16 shows the pictures of the soil samples taken in Long Reach.

The presence of gravel particles at the entrance of Long Reach indicate that the particles may have been deposited from glacial till and that the bottom velocities at the centre of Long Reach are weaker than that at Purdys Pt to Carters Pt and at Oak Point. Thus the deposition of silt and clay particles is much greater at the centre of Long Reach than at Oak Point and at Purdys Pt. to Carters Pt.



● analyzed  
● not analyzed



■ sand  
■ silt and clay  
■ gravel, silt, clay  
■ gravel, sand  
■ sand, silt, clay

Figure 2.15: Sediment results for Metcalfe et al [1976] and the OMG. (a) bathymetry image, (b) Multibeam backscatter and (c) inferred sediment distribution.





Figure 2.16: Pictures of soil samples in Long Reach.

### **2.5.3 The Three Sills of the Saint John River Estuary**

The three main sills of the Saint John River estuary are situated in a sequential alignment along the lower axis of the river (see Figure 2.2). These sills influence the oceanographic dynamics of the estuary, in that they hinder the movement and amount of saltwater that advects upstream and the amount of fresh water that advects downstream.

#### **2.5.3.1 Reversing Falls Sill**

At the mouth of the Saint John River there exists a 5m deep rock known as the Reversing Falls. The depth of this sill restricts the amount of fresh water that can pass from the Saint John River into the Bay of Fundy and the amount of saline waters from the Bay of Fundy into the Saint John River.

Trites [1959] and Metcalfe et al. [1976] observed that due to the depth of the Reversing Falls sill, the pycnocline of the Saint John Harbour is always just at or below the sill. Within the vicinity of the sill extreme turbulence occurs.

Whether the flow of water is upstream or downstream is determined by the water level on either side of the Reversing Falls Sill. When normal water level conditions occur and the River is close to high tide, the water level on the seaward side of the Sill tends to be higher than that of the river. As a result seawater is able to flow upstream into the river. In contrast, when low tide occurs the water level on the landward side of the sill is greater than that of the seaward side. Thus the flow is predominantly downstream into the Bay of Fundy (see Figure 2.17). When extreme high river discharge occurs the flow for the whole tidal cycle is always seaward (see Figure 2.17).

Salinity observations performed by Trites [1959] in May 1957 under conditions of high river discharge shows that salt water can be present in the estuary. In contrast observations made by Metcalfe et al. [1976] shows that, in April and May 1976, salt water is not present in the main estuary (see Figure 2.18), however in the Kennebecasis Bay salt water is always present.

These two contrasting observations made by Trites [1959] and Metcalfe et al. [1976] show the influence of the river discharge and, possibly the time of measurements have on the observation of salt water penetration up the estuary.

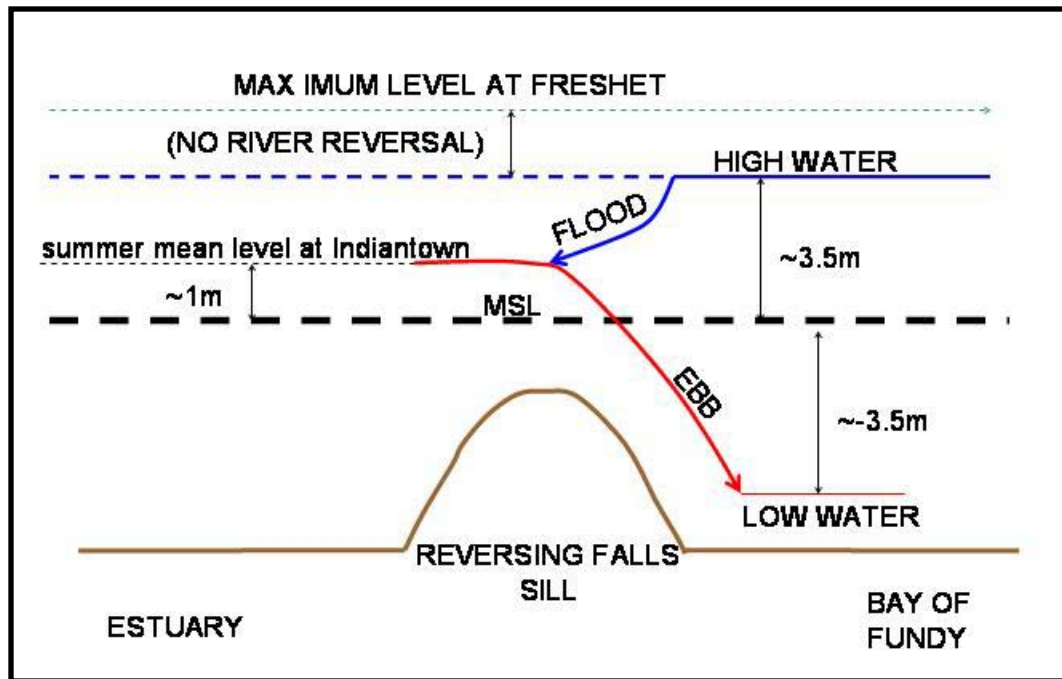


Figure 2.17: Circulation pattern at the Reversing Falls sill at high tide, low tide and high river discharge.



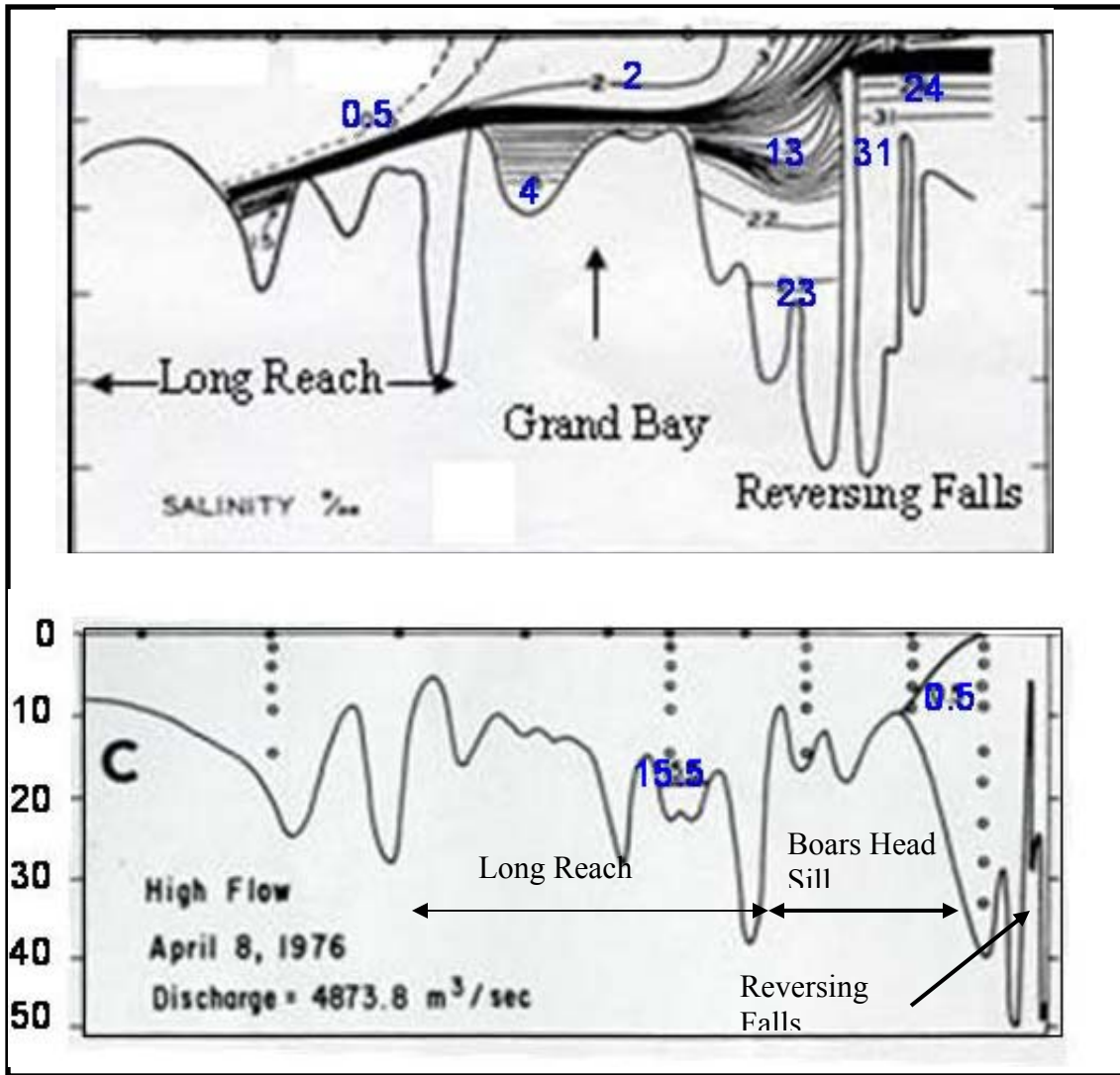


Figure 2.18: Longitudinal salinity profile of Saint John River Estuary. The profile shows the salinity at high River discharge for (top) Trites [1957] and (bottom) Metcalfe et al [1976] results.

### **2.5.3.2 Boars Head Sill**

Approximately 6km upstream of the Reversing Falls there exists another sill known as the Boars Head Sill (see Figure 2.19). Multibeam and oceanographic surveys performed during the period 2000 to 2004 by the OMG shows that the shallowest depth of the sill varies from between 6m to 8.4m Hughes Clarke and Haigh [2005] (see Figure 20).

The surveys found that:

- The Boars Head Sill lies at or above the mean level of the pycnocline (which would vary seasonally and tidally).
- During the summer and winter months (which experience low river discharge) at flood tide the pycnocline rises over the top of the sill.
- During high periods of river discharge the sill top is never exposed to saline waters

The bathymetry image shows that the Boars Head sill lies mostly to the east side of the river channel and several channels exist (see Figure 2.20). Two scenarios occur with respect to the advancement of water from the Gorge: scenario one refers to water penetrating from the Gorge across the Boars Head Sill and into the Westfield Channel and scenario two refers to water penetrating from the gorge across the Boars Head Sill and into Kennebecasis Bay.

At flood tide salt water is able to penetrate over the Sill and into the Westfield channel (see Figure 2.21). Channel E is the path taken by the salt water from the Gorge into Westfield Channel (scenario 1) (see Figure 2.20).

The second scenario considers salt water penetrating into the Kennebecasis Bay. Observations found that two intrusions occur around high tide. At early flood tide, slightly brackish water (6‰ to 8‰) is observed to flow along the fjord and this is not the same waters as channel E. It appears to be the waters of channel A. Channel A waters is sourced from slightly mixed waters at the south of Grand Bay that is pushed back over the Boars Head sill. Thus at high tide this water flows through channel A and into Kennebecasis Bay. This water is slightly denser than the main upper fresh water layer in the Kennebecasis thus it flows as a subsurface layer (see Figure 2.22).

After high tide a second intrusion in the form a bore is observed and it occurs in the mixed water (~10‰ to 16‰) along the halocline. This bore propagates several hours after the flow up the bypass channel has terminated. This bore tends to be the carrier of the more saline waters into the Kennebecasis Bay.

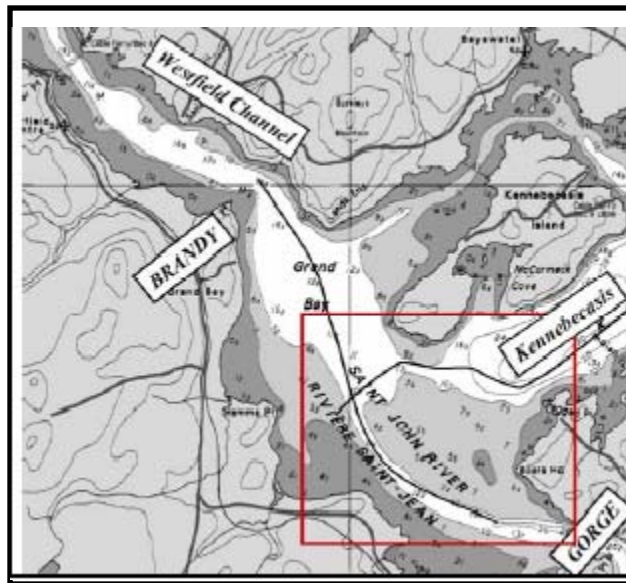


Figure 2.19: Site map showing the Boars Head Sill. Reference from Hughes Clarke and Haigh [2005].

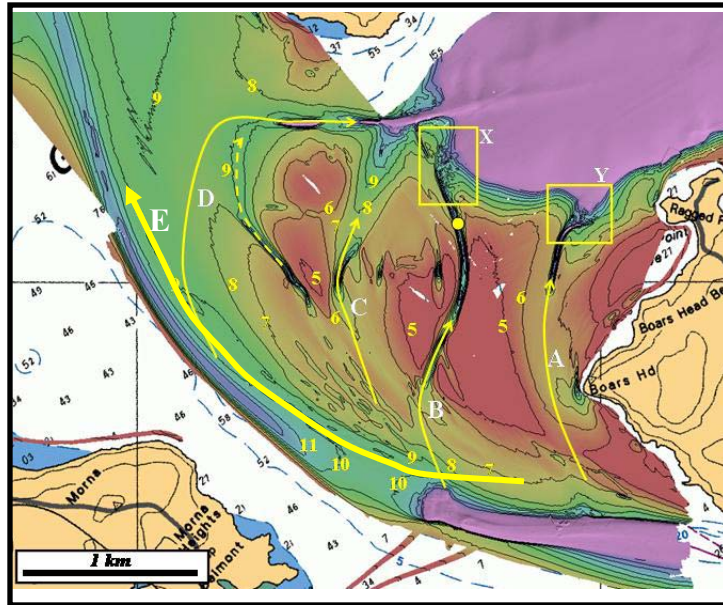


Figure 2.20: Map showing the bathymetry of the Boars Head Sill. Reference from Hughes Clarke and Haigh [2005].

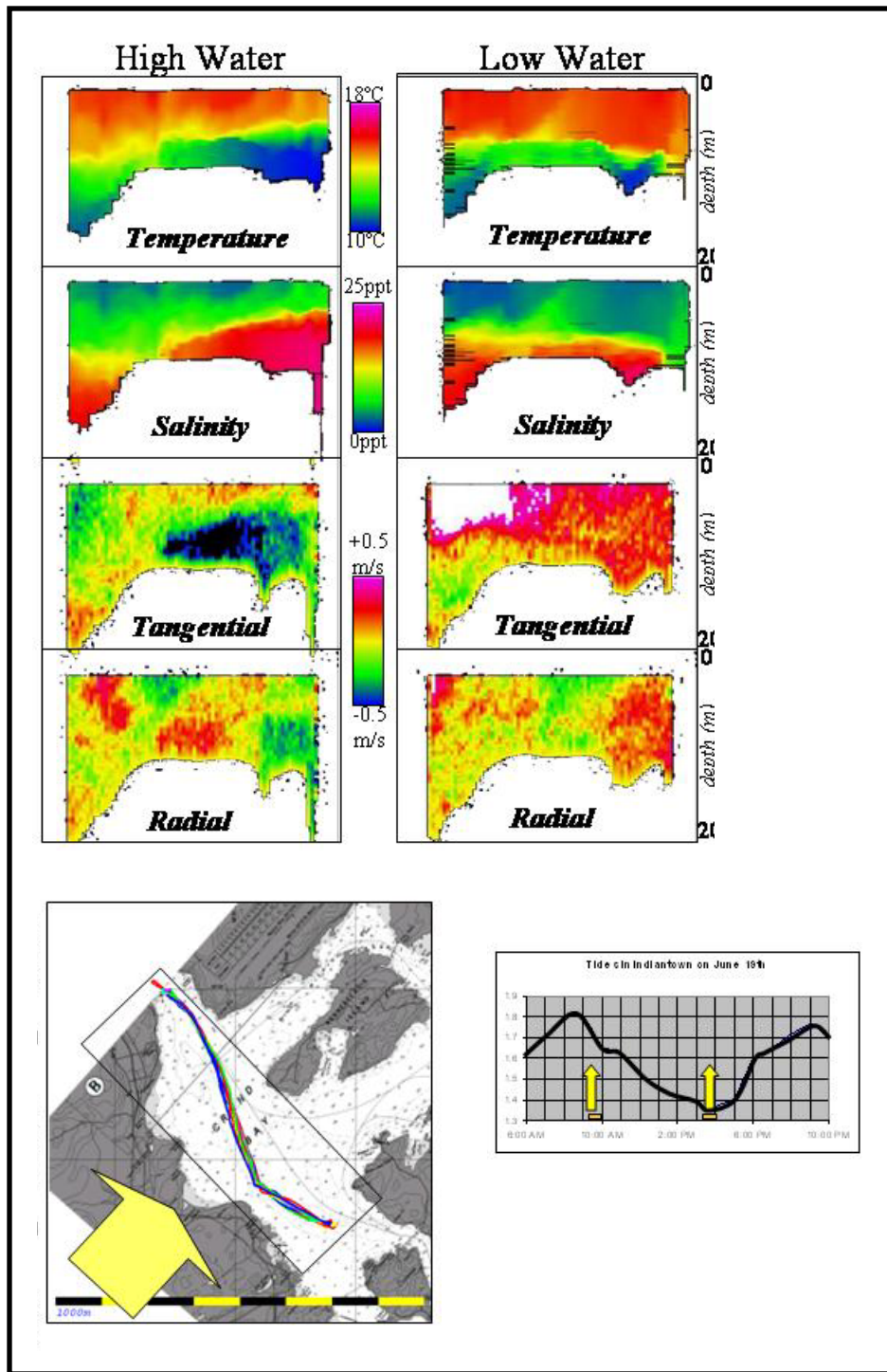


Figure 2.21: Salt water intrusion from the gorge into the West Field channel (Scenario 1) at High and Low Tide. Reference from Hughes Clarke and Haigh [2005].



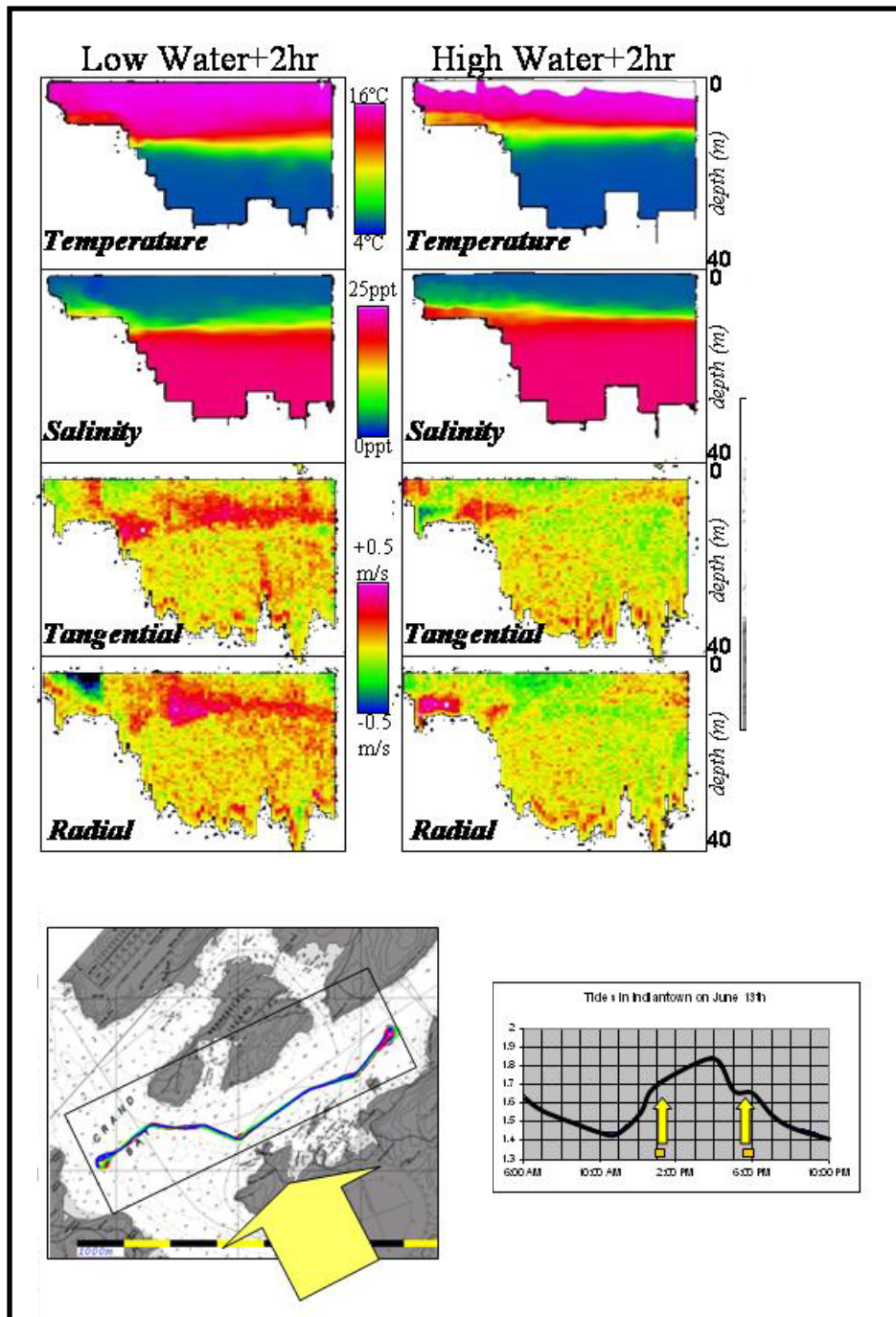


Figure 2.22: Salt water Intrusion from Grand Bay into Kennebecasis (Scenario 2) at high and low tide. Reference from Hughes Clarke and Haigh [2005].

### **2.5.3.3 Long Reach Sill**

Multibeam surveys for Long Reach were performed in May 2004 by students of UNB Geodesy and Geomatics Engineering (GGE) 5083 class of 2004. Figure 2.23 shows the results of these surveys. It is observed that from Westfield channel to the entrance of Long Reach the river makes a right angle turn. When this occurs the depth of the thalweg decreases from 17m to 11m whilst the banks of the River shoals to ~6m (see Figure 2.23). On entering Long Reach within the vicinity of Woodsman Pt the depth of the thalweg increases to 17m.

Oceanographic measurements at the sill have been restricted by the West Field ferry service that operates just immediately downstream of the Long Reach sill. A towed CTD is normally used by the Ocean Mapping Group and the continuous operations of the ferry service made the CTD measurements hazardous. This research concentrates on the area from the entrance of Long Reach at Woodsman's Pt to Oak Pt. However it is expected that, similar to the Reversing Falls Sill and the Boars Head Sill, the sill located at the entrance of Long Reach will influence the flow of fresh and salt water.

The multibeam images show that, on entering Long Reach, a deep hole area with a depth of 42m exists followed by an irregular area where several shoals exist. Upstream of Carter's Pt the bathymetry is basically homogenous with a depth between 22m to 25m. However, west of Victoria Shoals, a 15m shoal exists and to the north and south of this shoal 25m to 30m channels exists.

Upstream of Victoria Shoals there exist several islands and the depth in this area varies between 8m to 11m. At Oak Point the bathymetry shoals to a depth between 7m to 10m.

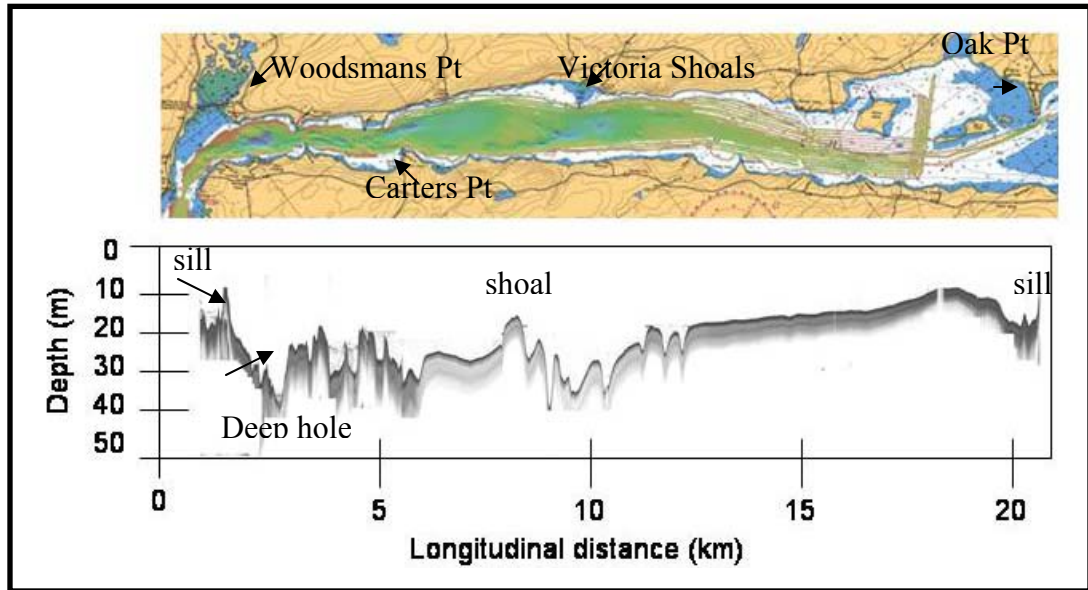


Figure 2.23: Bathymetry image of Long Reach.

## 2.6 Salinity Characteristics: Previous Research

Detailed observations of the salinity characteristics of the Saint John River Estuary have been performed by Trites [1959], Metcalfe et al. [1976], and Hughes Clarke and Haigh [2005]. Trites [1959] and Metcalfe et al. [1976] have investigated the seasonal distribution of salinity, temperature and density within the whole Saint John River estuary. The studies performed by Hughes Clarke and Haigh [2005] have concentrated on the oceanographic characteristics of the Boars Head Sill whose results were mentioned in Section 2.4.3.2. Therefore Trites [1959] and Metcalfe et al. [1976] studies are the most recent results on the salinity characteristics of Long Reach.

Trites [1959] observations are for the period of 1957 to 1958 whereas Metcalfe et al. [1976] observations are for the period 1972 to 1976. The data collection by Trites [1959] and Metcalfe et al. [1976] were performed in the 1950's and 1970's. However the results obtained and the interpretation of these results serve as a base for understanding



the oceanographic characteristics of the Saint John River estuary. Summarized below is a description of the salinity and temperature structure of the Saint John River Estuary which is sourced from Trites [1959] and Metcalfe et al. [1976].

### **2.6.1 Salinity Structure of Saint John River Estuary**

Salinity observations made by both Trites [1959] and Metcalfe et al. [1976] show that for the different seasons of the year (spring, summer, autumn and winter) the position of the salinity front varies (see Figures 2.24 & 2.26). Comparison of Trites's [1959] spring salinity profile with the salinity profiles for summer, autumn and winter shows that in spring the saline front ends in Long Reach (just before Oak Point) whilst for the other seasons, the saline front appears to advance further upstream (see Figure 2.24).

A comparison of Trites [1959] and Metcalfe et al. [1976] results also shows that the stratification pattern is not always constant from year to year. For example Trites's [1959] spring salinity profile shows salt water present in the estuary whilst in Metcalfe et al. [1976] salinity profile for spring, salt water is almost absent (the exception being the deep holes). This absence of salt water from Metcalfe et al. [1976] spring profile is due to the fact that in spring the ice that had accumulated over the winter melts. As a result the River discharge increases. Thus in Metcalfe et al. [1976] studies, the river discharge may have been greater than for Trites [1959] studies. Thus whether salt water is present in spring depends on the magnitude of the river discharge and the time of the survey.

During the summer and winter months the river discharge is usually at its lowest, due to low rainfall. It's observed that for summer the surface and bottom salinity is the greatest compared to that of spring, autumn and winter.

Trites [1959] summer salinity profile shows that the surface salinity varies from 4‰ to 10‰. For the spring, autumn and winter the surface salinity is within the 0‰ to 3‰ range (see Figure 2.24). In Long Reach in the summer, the surface salinity is ~4‰ and, in autumn and winter, the surface salinity is 0‰. The halocline is also much thicker in the summer than it is in the autumn and winter. The increase in surface salinity at summer indicates that possibly mixing or advection processes are more dominant in the summer.

Both Trites [1959] and Metcalfe et al. [1976] studies show that, as the saline front progresses upstream, the salinity decreases. The greatest change in bottom salinity occurs from the Gorge to the entrance of Long Reach. The concentration of salt water that advances to Long Reach depends on the height of the halocline at the Boars Head Sill (see autumn and winter). Studies performed by Hughes Clarke and Haigh [2005] show that the Boars Head sill contains a channel deep enough for the salt water from the Gorge to be able to discontinuously penetrate into the Westfield channel and thus into Long Reach (see section 2.5.3.2). These observations indicate that the Boars Head sill limits the amount of salt water that penetrates into Long Reach.

In Metcalfe et al.'s [1976] spring profile, the saline front doesn't advance into the estuary due to the high river discharge. However pockets of salt water remained in the deep holes of Long Reach. These pockets of salt water appear to be trapped. In Trites's [1959] autumn and winter profiles more saline waters are also trapped in the deep holes.

## **2.6.2 Temperature Structure of the Saint John River Estuary**

Trites's [1959] temperature profiles for the autumn and winter months show that: the bottom waters are warmer than the surface water; the salinity profiles show that the salinity of the bottom waters is greater than the surface waters salinity and the density profiles show that the density of the bottom waters is greater than that of the surface. These observations indicate that the density structure of Long Reach is influenced mainly by the salinity concentration rather than the temperature (see Figure 2.25).

It's also observed that in the deep holes in Long Reach in autumn and winter, the temperature is much warmer than in the remainder of the estuary. These deep holes also coincide with the area that saline waters are trapped. This result indicates that the deep waters in Long Reach are old water that was deposited in the deep hole in the summer or autumn when the Bay of Fundy waters were warmer. When the air temperature decreases it causes the river water to also chill but the waters that were deposited in the deep hole took longer to cool down.

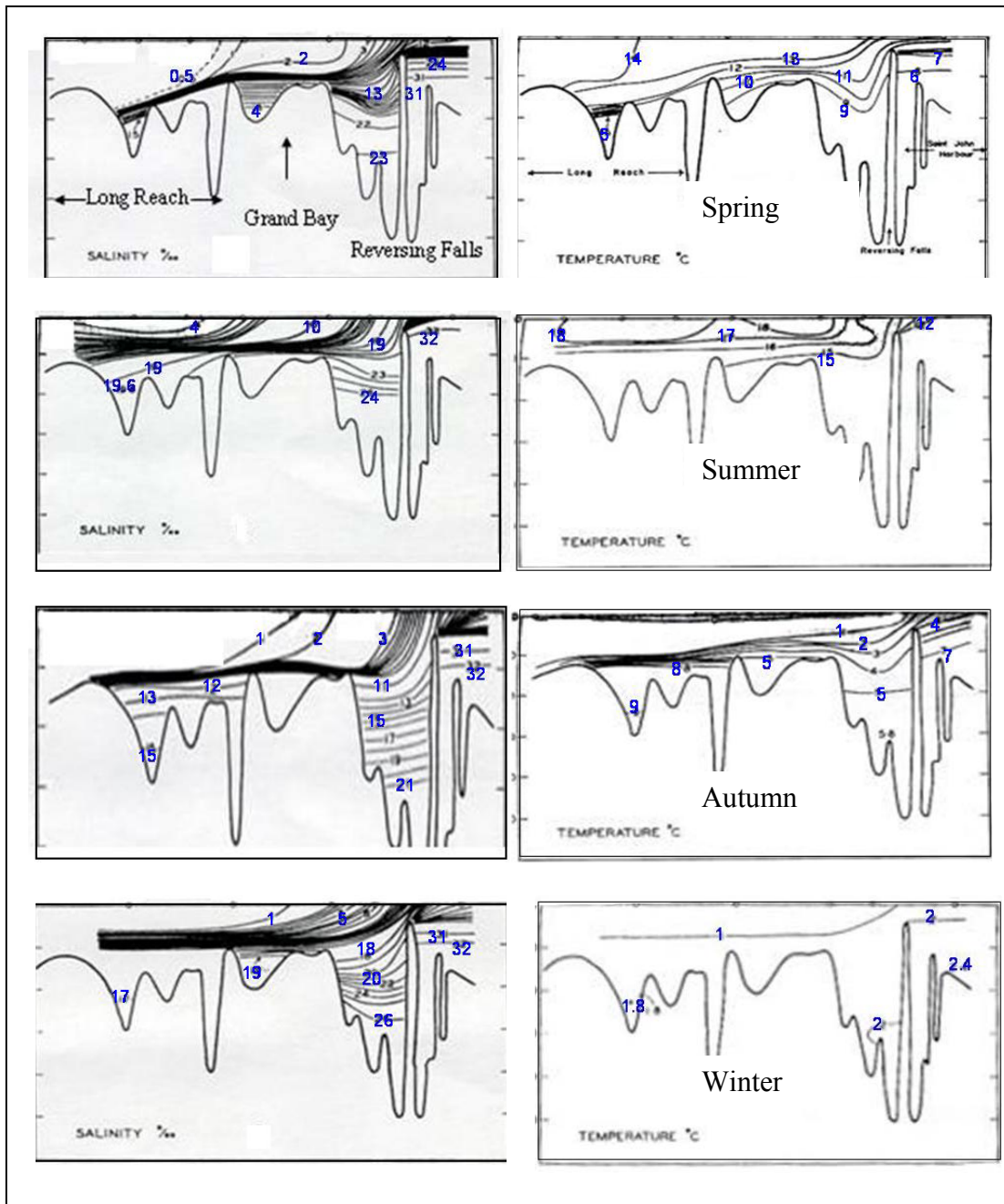


Figure 2.24: Seasonal variation of salinity (left) and temperature (right) of the Saint John River estuary. Diagrams referenced and edited from Trites [1959].

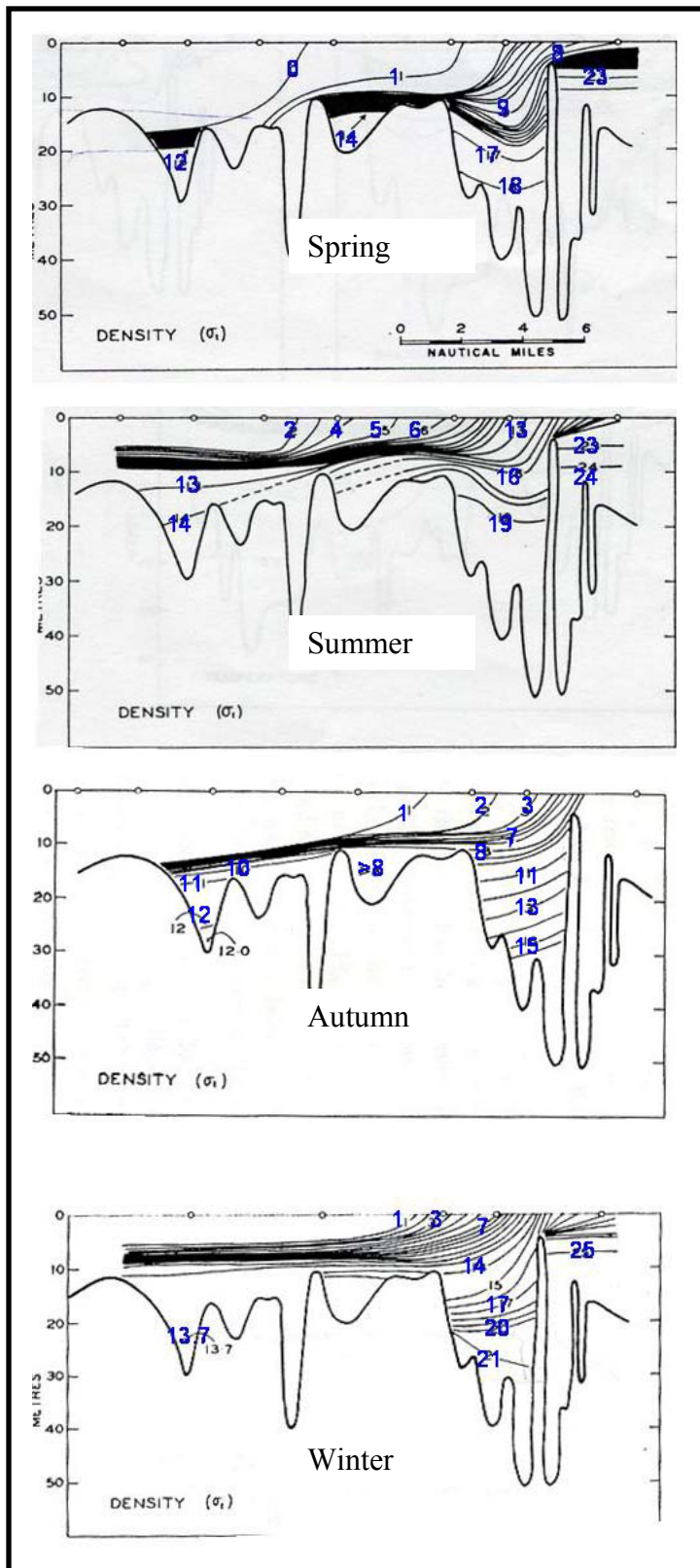


Figure 2.25: Seasonal variation of the density. Referenced and edited from Trites [1959].  
 The -o- indicates the location of the CTD profiles.

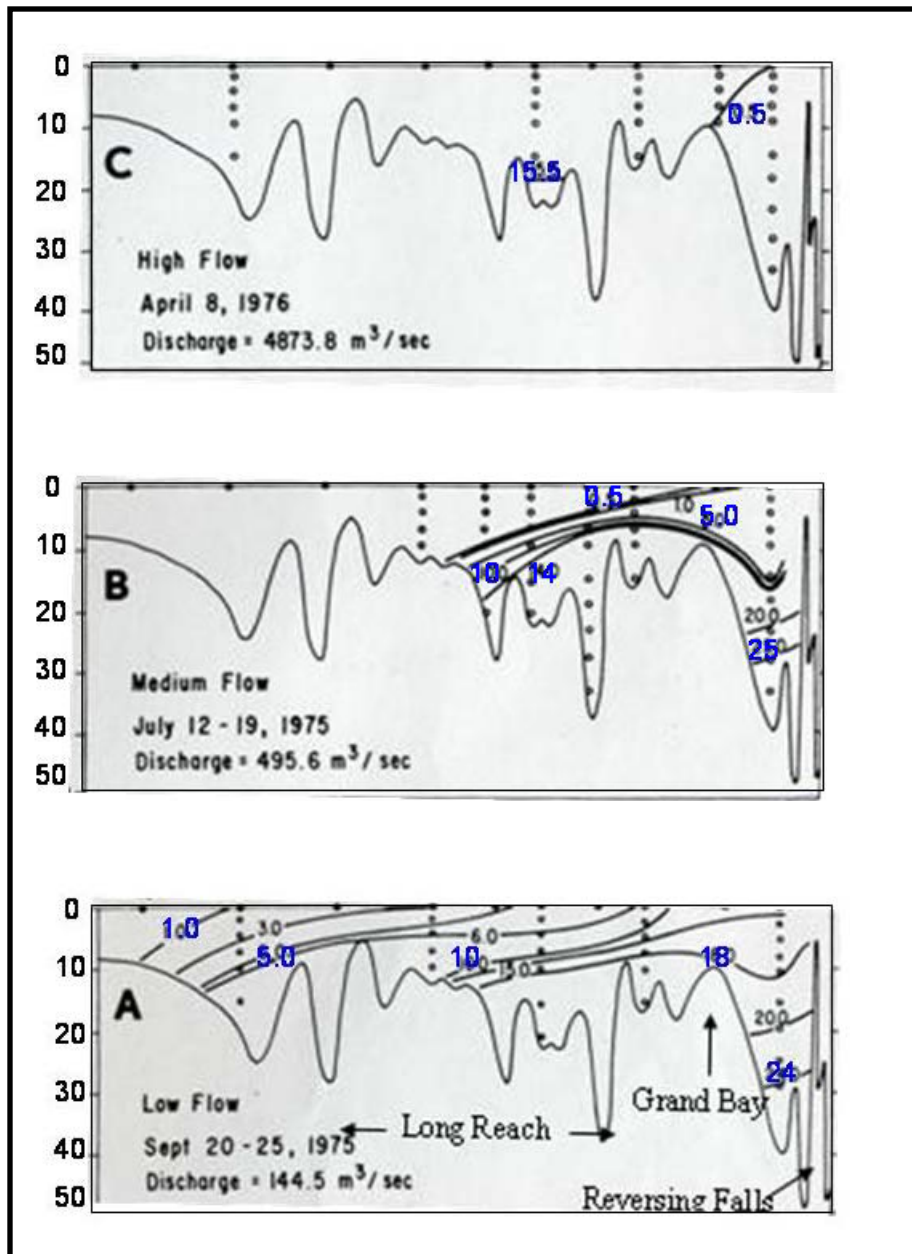


Figure 2.26: Seasonal variation of salinity in the Saint John River estuary. Referenced and edited from Metcalfe et al. [1976]. The -o- indicates the location of the CTD profiles.

## 2.7 Summary of Study Area

The advancement of salt water from the Bay of Fundy into the Saint John River Estuary varies seasonally and yearly. The main factor influencing the salt water advancement is the river discharge.

The river discharge is influenced by the amount of snow melt and rainfall. There are normally two yearly peaks, one in spring and the other in autumn. At extremely high river discharge all of the salt water can be flushed out of the estuary, the exception being, the deep holes of Long Reach which may contain remnants of salt water.

During the summer the greatest increase in surface salinity occurs and the halocline thickness increases. These characteristics indicate that possible mixing or advection processes may be occurring in the summer.

The studies of the Saint John River Estuary performed by Trites [1959] and Metcalfe et al. [1976] are based on the seasonal estuarine circulation pattern. In these studies the mapping of the seasonal stratification of the estuary was dependent on the spatial resolution of the CTD profiles. It is known that the processes of advection and mixing occur at smaller temporal and spatial resolution. The more detailed the spatial resolution the greater the chance of capturing these processes. Therefore to monitor the processes occurring in Long Reach in more detail the observations need to be performed at higher temporal and spatial resolution.

There exist three sills in the Saint John River estuary that can hinder the advancement of salt water into Long Reach. The greatest decrease in bottom salinity occurs within the vicinity of the three sills of the Saint John River estuary. This observation also indicates that mixing may be taking place within the vicinity of the sills.

There exist several shoals and deep hole areas in Long Reach which also may have similar characteristics to the three main sills of the Saint John River Estuary.

To investigate the dominant oceanographic processes occurring in Long Reach the River discharge, bathymetry of the area, tides and the season of survey were all considered in the design of the survey.



## CHAPTER 3

### SALINITY CLASSIFICATION AND MIXING IN ESTUARIES

Estuaries can be classified based on their tidal, topographic and salinity properties Dyer [1973, 1997]. In chapter two an overview of previous research performed in Long Reach showed that a seasonal variation in the salinity structure exists. Section 3.1 of this chapter describes the different classifications of estuaries based on their salinity and velocity structure. These descriptions were referenced from Dyer [1973, 1997].

In Chapter 2 it was also illustrated that, during the summer, the waters were the least stratified in Long Reach. It was hinted from this observation that possible mixing or advection processes may be taking place. Section 3.2 of this chapter presents the theory that is used to determine if mixing is occurring.

In stratified environments, internal waves play a major role in the mixing process. Section 3.2.1 describes the three known internal waves (Kelvin-Helmholtz, Holmboe and Solitons) that are known to exist in stratified environments and that contribute to the turbulent mixing process. A brief mathematical overview of one of the methods used to differentiate between the Kelvin- Helmholtz waves (KH) and the Holmboe waves is also presented.

#### **3.1 Estuarine Classification: Salinity Structure**

“Pritchard (1955) and Cameron and Pritchard (1963) have classified estuaries by their stratification and the characteristics of their salinity distribution” (Dyer, 1997). These classifications are based on tidally averaged conditions of salinity and velocity profiles.

Listed below are the four main estuary types identified based on their salinity structure whose descriptions were referenced from Dyer [1973, 1997]:

- Highly Stratified or Salt Wedge
- Fjord
- Partially mixed
- Well Mixed or Vertically Homogenous

### **3.1.1 Highly Stratified or Salt Wedge**

In this estuary the fresh water flow is greater than the tidal flow. The tidally averaged freshwater flows seaward in the upper layer of the water column and the seawater flows landward in the bottom layer. There is a marked distinction at the interface of the fresh and salt water.

At the interface, shear can be created due to the different velocities of the upper and lower layer. The upper surface layer tends to have a greater velocity than the lower layer. Shear at the interface can cause a thin layer of the top of the halocline to be swept seaward. This process is referred to as entrainment. This is strictly a one-way process where entrainment increases the volume of water in the surface layer.

Typical velocity and salinity profiles are shown in Figure 3.1. Observe that the halocline is well defined and the velocity falls to near 0 below the halocline. In this type of estuary, salinity will be almost homogenous in both surface and bottom layers. The exception occurs in the case where the halocline meets the surface at the tip of the wedge. Examples of highly stratified estuaries are the Mississippi River USA and the Vellar Estuary, India. With respect to Long Reach the autumn and winter surveys performed by

Trites [1959] and Metcalfe et al. [1976] resembled that of a highly stratified estuary (see Section 2.6.1 Figures 24, 26).

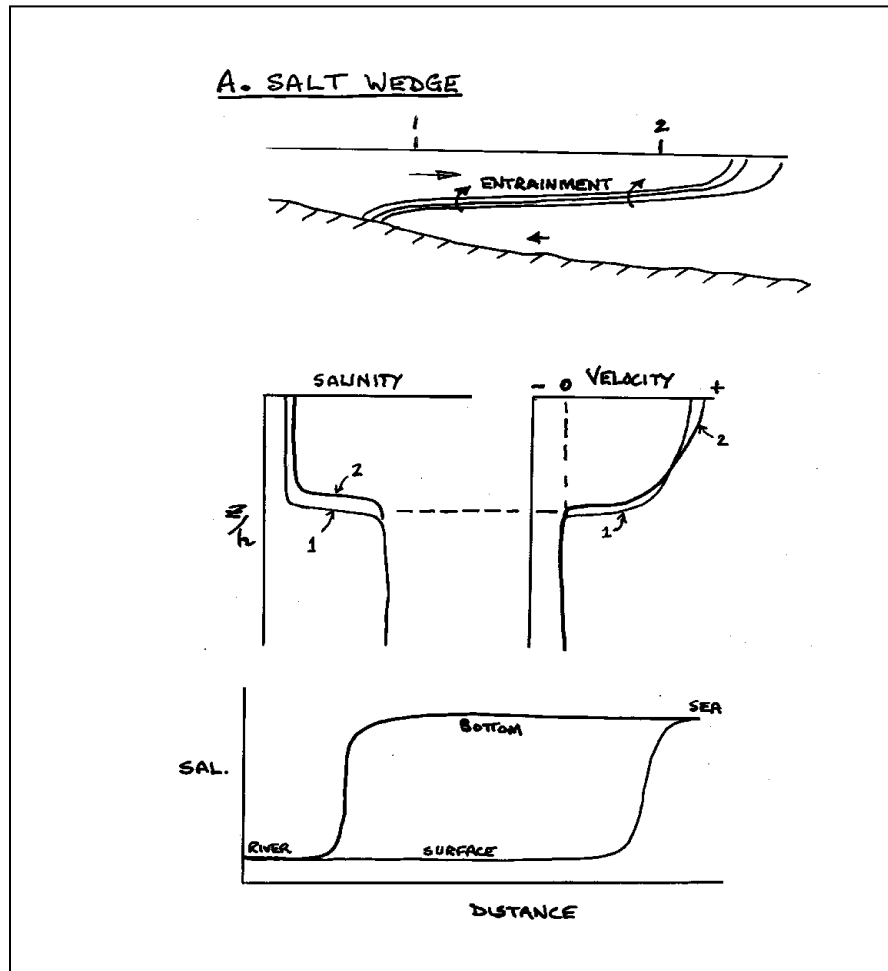


Figure 3.1: Tidally averaged salinity and velocity structure of a highly stratified estuary. This figure was referenced from Dyer (1973).

### 3.1.2 Highly Stratified: Fjord type

An estuary with a sill at its mouth is known as a fjord. The stratification of a fjord resembles that of the highly stratified estuary where the river flow dominates and a

noticeable distinction can be made between the fresh and the salt water. However at the sill, mixing of the fresh and salt waters may occur which cause the waters to be diluted in the estuary. The depth of the sill may deter the flow and the intrusion of salt water may only occur intermittently.

The intrusion of the salt water will vary depending on the river discharge, the phase of the tide and the phase of the moon. This causes a layered stratification to exist within the estuary based on the previous intrusion of salinity (see Figure 3.2). There may be cases when the deep waters may not be replenished and anoxic conditions may exist. Examples of this estuary are the Alberni Inlet, British Columbia and Silver Bay, Alaska. The Kennebecasis Bay in the Saint John River Estuary can also be considered to be a fjord (see section 2.1 Figure 2.2).

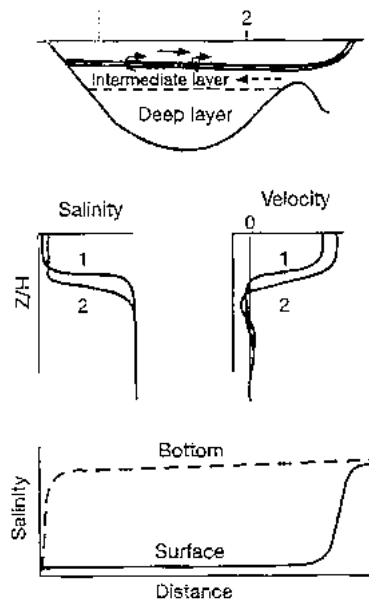


Figure 3.2: Tidally averaged salinity and velocity structure of a fjord. This figure was referenced from Dyer [1997].

### **3.1.3 Partially Mixed**

In this estuary both the river flow and the tidal flow are turbulent. Shear is generated at the interface and/or at the seabed. Shear at the interface encourages waves to develop. These waves may break which causes mixing to take place. Thus mixing can take place both at the interface and at the seabed.

The efficient exchange of salt and fresh water between both layers causes the salinity structure of this estuary to be different from that of a salt wedge type. The surface salinity increases much more steadily down the estuary and undiluted fresh water only occurs very near the head of the estuary.

Figure 3.3 shows the salinity and velocity structure, where the surface salinity increases more steadily down the estuary and undiluted fresh water only occurs very near the head of the estuary. Examples of this estuary are the James River, the Mersey and Southampton Waters. In Long Reach this was observed for the summer months by Trites [1959] and Metcalfe et al. [1976] (see section 2.6.1, Figure 2.24, 2.26). This is the season that the most mixing and/or advection is hypothesized to be occurring in Long Reach.

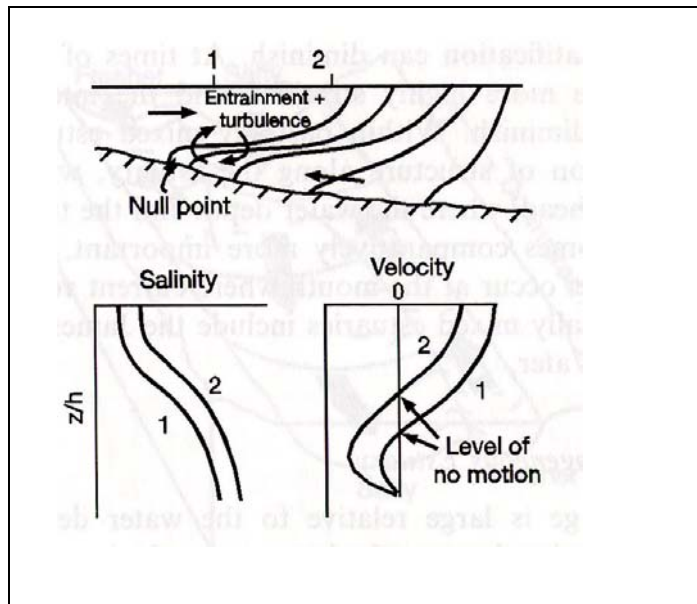


Figure 3.3: Tidally averaged salinity and velocity structure of a partially mixed estuary. This figure was referenced from Dyer [1973].

### 3.1.4 Well Mixed or Vertically Homogenous

When the tidal range is large enough relative to the water depth the turbulence produced by the velocity shear at the bottom may be large enough to mix the water column completely Dyer [1997]. An increase in fresh water discharge can also cause an estuary to become well mixed or just flushed out.

Dyer [1997] has further classified a well mixed estuary into lateral inhomogeneous and laterally homogenous estuaries. In the lateral inhomogeneous case, the estuary is wide and the Coriolis and centrifugal forces cause a horizontal separation of flow. The seaward net flow occurs at all depths on the right hand side in the northern hemisphere and the compensating landward flow on the left.

In the laterally homogenous section case the width is smaller and lateral shear may be sufficiently intense to create laterally homogenous conditions. Salinity increases

evenly towards the mouth and the mean flow is seaward throughout the cross-sections, which tends to drive the salt out of the estuary. Figure 3.4 shows the salinity and velocity profiles of a well mixed estuary. Examples are the Delaware and Raritan estuary.

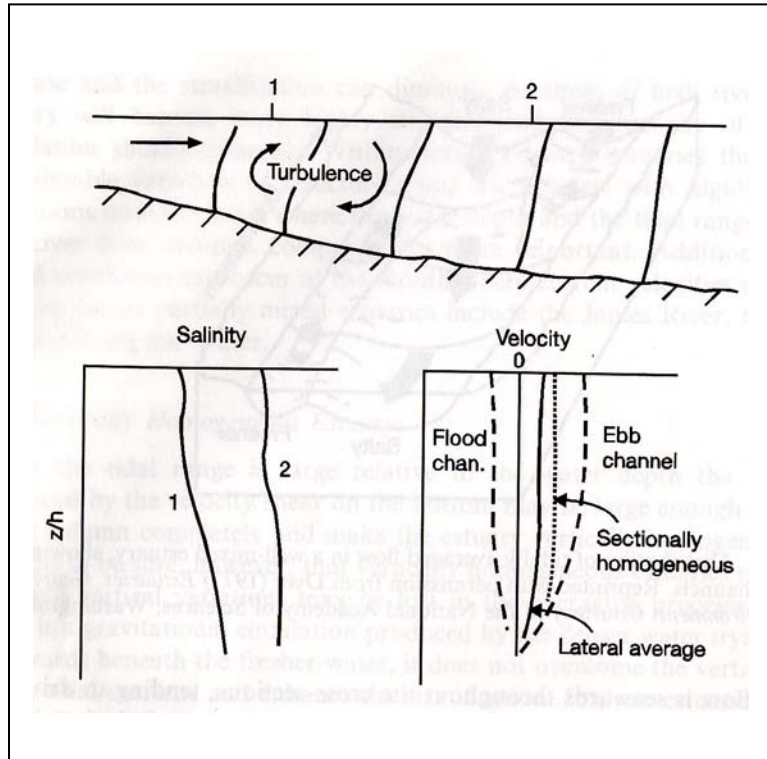


Figure 3.4: Tidally averaged salinity and velocity structure of a well mixed estuary. This figure was referenced from Dyer [1973].

## 3.2 Turbulent Mixing in Estuaries

In Section 3.1.1 and 3.1.3 it was stated that at the interface of the salt and fresh water, a velocity shear may exist which causes mixing. This section presents the theory most commonly used to determine if mixing is occurring and the sources of the mixing process.

### 3.2.1 Measurements of Turbulent Mixing

Turbulent mixing can occur with fluids of different densities, or with fluids of homogenous densities. The relationship of the density and velocity profiles with respect to each other are the main factor used to determine turbulent mixing. Based on laboratory experiments the Reynolds number (Re), Richardson number (Ri) and Froude number (Fi) are all used to determine if turbulent mixing is occurring in estuaries. Whilst the Prandtl number (Pr) and the Schmidt number (Sc) are used to give an indication of the state of a flow by comparing its viscosity and diffusivity, they do not actually determine if turbulent mixing occurs.

#### Reynolds number (Re)

This number is used in homogenous waters to determine if a fluid is laminar or turbulent. It is the ratio of the inertial force to the viscous force acting on the body of interest (see equation 3.1). The inertial force is the force that was necessary to accelerate the body to the velocity it now possesses.

$$\text{Re} = \frac{u * d}{\nu} \quad (3.1)$$

u = typical velocity scale; d=typical length scale;  $\nu$ =kinematic viscosity.



It was noted by Reynold that when Re is approximately 2000 or less the flow is laminar, whilst when it is greater than  $10^5$  the flow is fully turbulent. Between these two ranges the flow is considered transitional, Dyer [1997].

### **Richardson number (Ri)**

This number is used in stratified environments to determine if mixing is occurring at the interface. Dyer [1997] states the gradient Richardson number (Ri) as “The comparison of the stabilizing forces of the density stratification to the destabilizing influences of the velocity shear” (see equation 3.2). The stratification of a fluid may be quantified by the Brunt-Vaisala frequency (N). N represents the natural frequency of the vertical oscillation of fluid particles.

$$N^2 = -\frac{g}{\rho} \frac{\partial \rho}{\partial z}$$

$$Ri = \frac{N^2}{(\partial u / \partial z)^2}$$

$$Ri = -\frac{\frac{g}{\rho} \frac{\partial \rho}{\partial z}}{(\partial u / \partial z)^2} \quad (3.2)$$

g=gravitational acceleration ( $9.81\text{m/s}^2$ );  $\rho$ =average density; u=velocity

The general stability of the flow may be determined by the Ri. The three general cases are:

- Ri>0 indicates that the stratification is stable (less dense fluid overlays more dense fluid)
- Ri=0 it is neutral and no stratification exists

- $Ri < 0$  indicates that the flow is unstable (more dense fluid overlays the less dense)

Dyer [1997] states that the transition from laminar to turbulent occurs when  $Ri = 0.25$ .

Computing  $Ri$  for a given flow requires the gradients of the velocity and density data to be calculated. This is not always possible. Thus a bulk Richardson number ( $J$ ) was derived which investigates the velocity and density difference of the upper and lower layer (see equation (3.3)).

$$J = \frac{g((\rho_2 - \rho_1)/\rho_2)h}{|U_2 - U_1|^2} \quad (3.3)$$

$g$ = gravitational acceleration ( $9.81\text{m/s}^2$ );  $\rho_1$ =density of upper layer;  $\rho_2$ =density of lower layer;  $h$ = thickness of the shear layer;  $U_1$ =upper layer velocity;  $U_2$ =lower layer velocity;

### **Froude number (Fi)**

The Froude number ( $Fi$ ) compares the velocity of the flow with that of a progressive wave that travels at the density interface. The propagation of the speed of a long wave at the interface is given by:  $c = (\Delta\rho/\rho * gh)^{1/2}$ . Thus the interfacial Froude number is defined in equation 3.4 as:

$$Fi = \frac{u}{((\Delta\rho/\rho) * gh)^{1/2}} = \sqrt{\frac{1}{J}} \quad (3.4)$$

In equation 3.4 the  $Fi$  is calculated with respect to a thin surface layer flowing over a dense stationary lower layer. In reality both layers may be moving hence an adjustment of a two layer Froude number that can be used (see equation 3.5)

$$Fi = \sqrt{(U_1^2(g'H_1) + U_2^2(g'H_2))} \quad (3.5)$$

Where  $U_1$  and  $U_2$ , are the upper and lower velocities;  $H_1$  and  $H_2$  are the upper and lower layer depths and  $g'$  is reduced gravity ( $g\Delta\rho/\rho$ ). When  $Fi$  approaches unity it indicates that supercritical conditions are present and mixing occurs. When it is less than unity it indicates that the flow is sub critical and that mixing is not occurring.

### **Prandtl number (Pr) and Schmidt number(Sc)**

The Prandtl number (Pr) is the ratio of kinematic viscosity ( $\nu$ ) to thermal diffusivity ( $k_t$ ) (see equation 3.6).

$$Pr = \frac{\nu}{k_t} \quad (3.6)$$

The Schmidt number (Sc) is the ratio of kinematic viscosity to the coefficient of mass diffusivity (diffusion of salt)(see equation 3.7).

$$Sc = \frac{\nu}{k_s} \quad (3.7)$$

The Pr and Sc are used to measure how quickly a system evolves from a critical state.

## **3.3 Sources of Turbulent Mixing**

Turbulent mixing occurs due to turbulence which can be initiated in an estuary due to winds interacting with the surface waters, shear at the seabed and shear at the halocline [Dyer, 1997].

### **3.3.1 Turbulent Mixing at the Interface**

At the interface of stratified fluids waves may be generated. The waves that travel within the interior of a fluid are called internal waves (Apel [2002]). The three known internal waves that contribute to mixing in stratified environments are Kelvin-Helmholtz (KH), Holmboe and Solitons. These three waves are now described.

#### **3.3.1.1 Kelvin-Helmholtz waves (KH) and Holmboe waves**

Shear at the interface of stratified fluids are known to create KH and Holmboe waves. The interface influenced by shear can cause the two different densities to roll into each other. The rolling up of the two densities creates a cat's eye feature known as the KH. The KH eventually breaks in a turbulent manner and mixing occurs. The KH is known to be stationary with respect to the mean flow for the duration of its life cycle. Laboratory experiments for the KH were first performed by Thorpe [1973, 1985] and Koop et al. [1979].

Holmboe waves can also be created at the interface when shear and stratification is present. These waves consist of two trains of interfacial waves of equal strength that travel at the same speed but in opposite direction with respect to the mean flow Lawrence et al. [1991](see Figure 3.5). The mixing process of the Holmboe instability occurs in the form of fluid from the crest of the wave being ejected into the more turbulent layer as the wave propagates along the density interface. It should be noted that the two trains of interfacial waves can be either symmetric or non symmetric with respect to each other.

Laboratory experiments of the Holmboe were first performed by Browand et al. [1973] and reproduced by Lawrence et al. [1991].

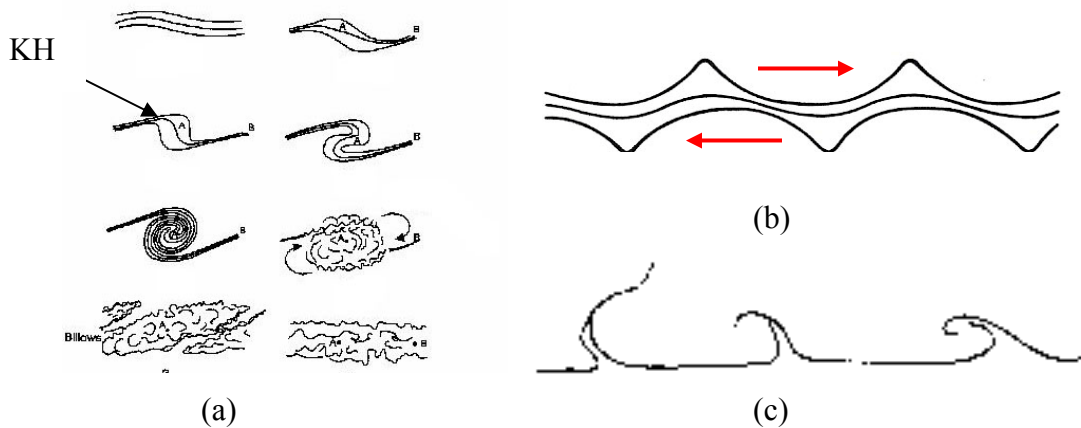


Figure 3.5: Diagram of the internal waves. KH wave (a), (b) the symmetric Holmboe wave (c) non symmetric Holmboe wave breaking. KH and Holmboe wave referenced from Dyer [1997] and non symmetric Holmboe wave from Lawrence et al. [1991].

The identification of mixing events at the interface can be determined by the use of the gradient Richardson number ( $Ri$ ). Richardson [1920] suggests that the critical value at which mixing can occur in stratified fluid is  $0 < Ri < 1$ . Theoretical investigations by Miles [1961] and Miles et al. [1964] have placed the critical value to be  $0 < Ri < 0.25$ , for the fastest growing instability, which is that of the KH. Dyer [1997] places a critical value of  $0 < Ri < 0.25$  for the KH wave and  $Ri > 0.4$  for the Holmboe wave.

Comparison of the velocity and density profiles allows one to intuitively identify between that of the KH wave and the Holmboe wave (see Figure 3.6). For a given density profile the difference between the density interface thickness distinguishes the KH wave from the Holmboe wave. This difference is described using two scenarios:

- Scenario 1: A thin density interface exists
- Scenario 2: A thick density interface exists

In scenario 1 both the KH and Holmboe wave can be present whilst in scenario 2 only the KH wave is present. In a highly stratified environment, to distinguish between the KH and Holmboe wave, a linear stability analysis using a normal mode approach may be employed.

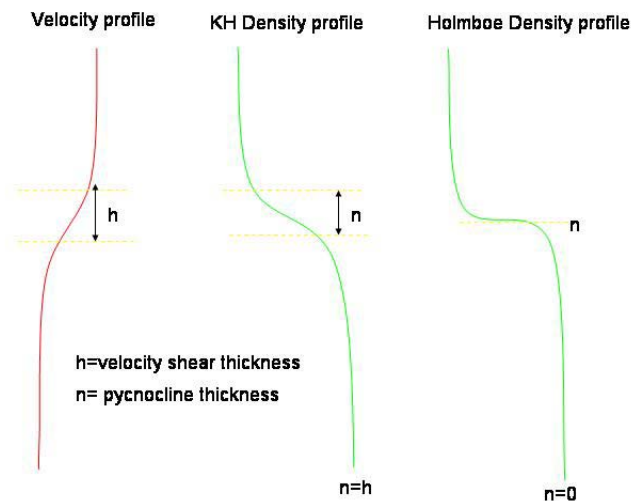


Figure 3.6: Density and velocity profiles of the KH and Holmboe waves.

### 3.3.1.1 Distinguishing between the KH and Holmboe waves

A normal mode approach investigates the effects of a perturbation on a background flow. The background flow is defined by the characteristics of the velocity and density profiles. This approach assumes that the perturbation is caused by random noise in the flow and it is this random noise that is modelled as an instability (Haigh, 1995). This instability initially grows exponentially Miles [1961]. The following theory of the linear stability analysis is summarized from Haigh [1995] and Lawrence et al. [1991].

## Background Flow

The background flow is defined by the mean density and velocity profiles. There are two popular methods used in a linear stability analysis:

- piecewise approximations
- smooth profile approximations

Piecewise approximations are used for velocity and density profiles that fit the profile of Figure 3.7a. In using this profile it is assumed that the thickness of the density interface ( $n$ ) can be approximated as an abrupt step. This profile may not always be suitable due to the shape of the observed density and velocity profiles. In order to accommodate these shapes a smooth profile is usually used. This smooth profile can be represented by any valid algorithm that fits the profile (see Figure 3.7b).

Holmboe [1962], who first studied the case where  $h > n$  and  $n = 0$  characterized the background flow using the bulk Richardson,  $J = 2(\rho_2 - \rho_1)gh / (\rho_2 + \rho_1)(U_1 - U_2)$ . In Lawrence et al. [1991] the non-dimensional parameter of the bulk Richardson number and the asymmetry  $\varepsilon = 2d/h$  was used for the piecewise approximation of the linear stability analysis to define the background flow. In the smooth profile cases  $J$ ,  $\varepsilon$ , Reynolds number ( $Re$ ), Prandtl number ( $Pr$ ) and the ratio of the shear layer thickness to that of the pycnocline thickness  $R = h/n$  are all used in this study to define the background flow.

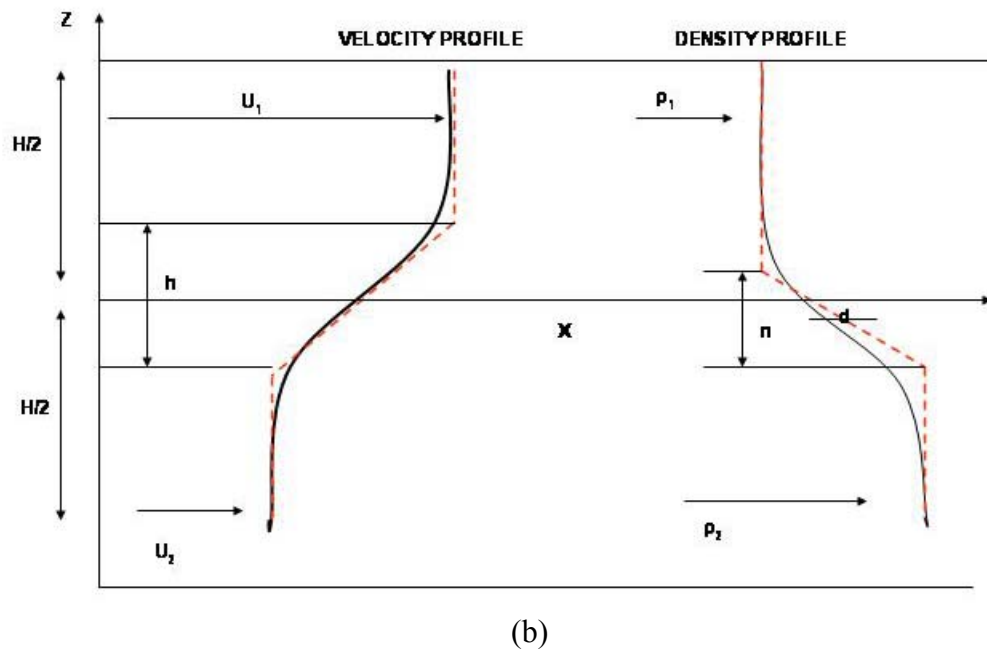
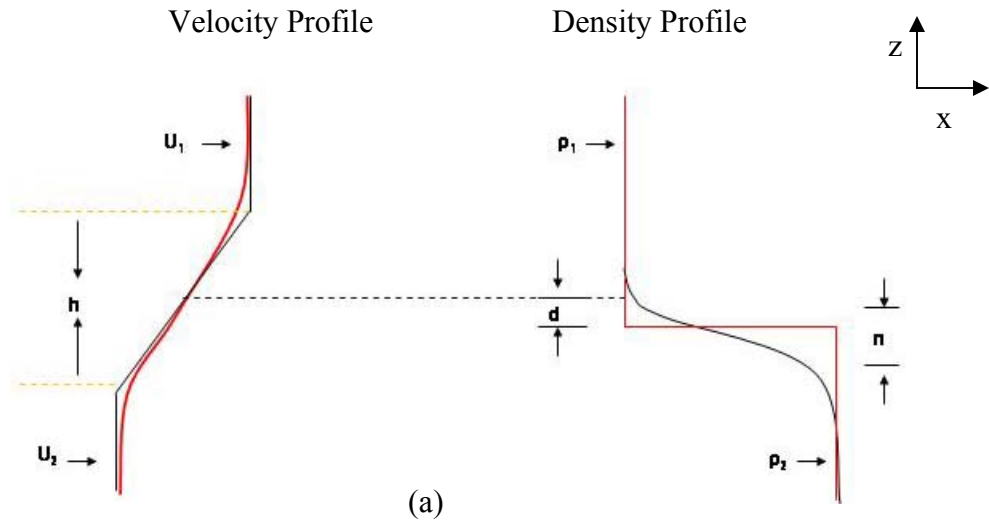


Figure 3.7: Density and velocity profiles for the piecewise approximation method (a) and the smooth profile method (b).  $U_1$  and  $U_2$  represent the upper and lower layer velocities,  $\rho_1$  and  $\rho_2$  the upper and lower layer densities,  $h$  the shear layer thickness,  $H$  the total depth,  $n$  the density interface thickness and  $d$  the displacement at the centre of the density interface with respect to the centre of the shear layer.



## The Perturbation and the Eigen-Problem

Once the background flow has been defined (either using the piecewise approximation or the smooth profiles) it is perturbed and it is assumed that these perturbations are two dimensional with respect to the horizontal (x) and vertical (z) and proportion to  $\exp [i\alpha(x-ct)]$ , where  $\alpha$  is the non dimensional wave number and c is the complex wave speed. This results in an eigen –problem of the form:

$$(U-c)(\emptyset_{zz}-\alpha^2\emptyset)-U_{zz}\emptyset=J\rho-i/(\alpha Re)(\emptyset_{zzzz}-2\alpha^2\emptyset_{zz}+\alpha^4\emptyset) \quad (3.8)$$

$$(U-c)\rho-\rho_{az}\emptyset=-i/(\alpha Re) Pr(\rho_{zz}-\alpha^2\rho)$$

$\emptyset_z$  is the vertically varying amplitude of the stream function perturbation,  $\rho(x,z,t) = \rho_a(z) + \rho'(x,z,t)$  and  $\rho_a(z) = p(z,0)$  which was used from initial mean profiles. For more background on the derivation of the eigen problem the reader is recommended to reference Haigh (1995) Sec 2.2 to 3.2.

For the inviscid case equation 3.8 reduces to the Taylor-Goldstein equation which for the piecewise approximation background flow (see equation 3.9) is of the form:

$$(U-c)(\emptyset_{zz} - \alpha^2\emptyset) - U_{zz}\emptyset + 2J\rho\delta(z+\epsilon) \emptyset / (U-c) = 0 \quad (3.9)$$

$\delta(z)$  is the delta function

Equation 3.9 models the behaviour of an instability given its wave number, wave speed, and the conditions of the background flow. Equation 3.9 when solved for the piecewise profiles of figure 3.6a results in a dispersion relation, which takes the form of:

$c^4+a_1c^3+a_2c^2+a_3c+a_4=0$ . The coefficients of  $a_1, a_2, a_3, a_4$  are all functions of  $J, \varepsilon$  and the wave number (see Lawrence et al.[1991] for calculation of coefficients). The eigen values results are the wave speeds which are defined as complex numbers  $c=c_r \pm i c_i$ . The real part depicts the speed of the wave whilst the imaginary part depicts growth rate of the wave. The dispersion relation result in four solutions and it is fastest growing growth rate that is taken as the most unstable. The procedure for determining the wave number is illustrated in Figure 3.8.

For the smooth profile case any function that can fit the profile may be used. The hyperbolic tangent function is commonly used to define the background flow in the smooth profile method. Using the hyperbolic tangent function the density and velocity profiles are defined as:

$$U(z) = (U_1 - U_2)/2 * \tanh(2z/h) + (U_1 + U_2)/2 \quad (3.10)$$

$$\rho_a(z) = -((\rho_2 - \rho_1)/2 * \tanh(2z/n) * (z+d) + (\rho_1 + \rho_2)/2) \quad (3.11)$$

Equations 3.10 and 3.11 are then non-dimensionalised and substituted in the eigen-problem. Using the smooth profile method the eigen-problem equation is solved numerically (see Haigh (1995) section 3.3.31 on the procedure used to solve this equation numerically). See Figure 3.8 for smooth profile method.

Both the piecewise approximation and the smooth profiles method can be used to determine the wavelength and wave speed. The piecewise approximation tends to be simpler to calculate and results in exact solutions. However the density and velocity profiles of the piecewise method may not always be observed in the field. When this

occurs the smooth profile case is more suitable. However the smooth profile case is solved numerically.

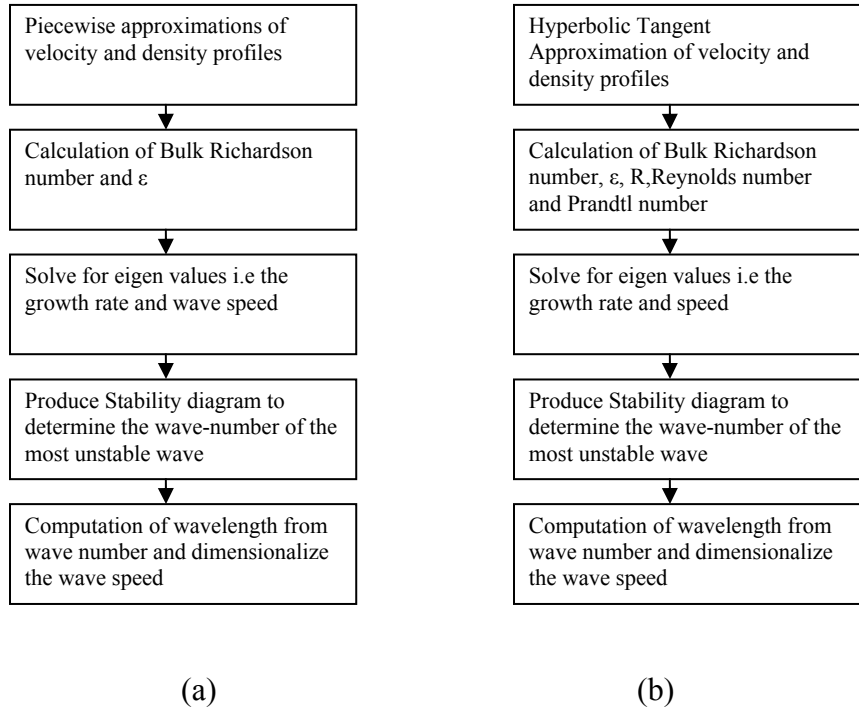


Figure 3.8: Procedure for the piecewise approximation method (left) and the smooth profile method (right).

### Determination of Possible Instability

Two cases are known to occur based on the results of the asymmetry  $\varepsilon$ . Case 1: When  $\varepsilon=0$  three results are possible, the flow is stable and no instabilities exist, KH waves are possible, or symmetric Holmboe waves are possible. It has been found that for  $J$  greater than 0 Holmboe instabilities are present and when  $J$  is less than 0.07 KH instabilities dominate Lawrence et al. [1991] (see Figure 3.9).

Case 2: When  $\varepsilon \neq 0$ . For  $\varepsilon > 0$  (shear above pycnocline) non symmetric Holmboe waves are present. Two unstable waves are known to occur one moving to the right and the other moving to the left (assuming that the upper layer shears to the right). The right wave is known to protrude into the upper layer and move to the right with respect to the mean flow whilst the left wave protrudes into the bottom layer and moves to the left with respect to the mean flow. The right moving wave tends to dominate. In a stability diagram the right moving solution is the branch that is closer to the J axis whilst the left moving solution is closer to the wave number axis (Lawrence et al. 1991).

For  $\varepsilon < 0$ , (shear below the pycnocline) non symmetric Holmboe waves are present. The left moving wave (in the lower layer) dominates and is the fastest growing wave, thus the left moving wave is closer to the J axis and the right moving mode is closer to the wave-number axis.

In the smooth profiles case there exist a relationship between  $R$  ( $h/n$ ) and the presence of KH and Holmboe waves. For  $R=1$  only KH waves are present and for  $R>2.4$  both KH and Holmboe waves are present (Smyth et al., 1989). Recent studies performed by Alexakis [2005] have shown that Holmboe instabilities can exist within the range of  $2.4 < R < 2$ .

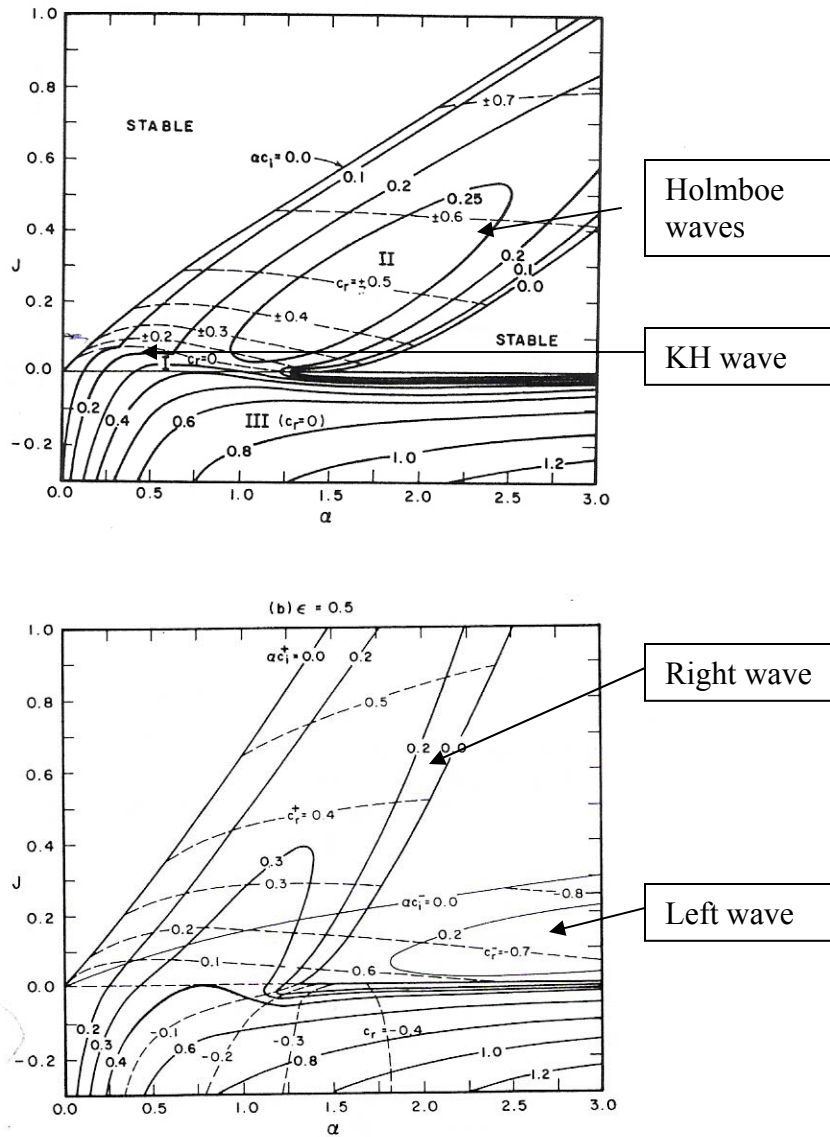


Figure 3.9: Linear Stability diagrams at  $\epsilon = 0$  (top) and  $\epsilon = 0.5$  (bottom) from Lawrence et al. [1991]. — represent contours of constant amplification rate ( $\alpha c_i$ ); ---- represent contours of constant phase speed ( $c_r$ ).

### 3.3.1.2 Solitons

As a stratified flow passes over irregular bathymetry it creates a disturbance as the stratification tries to conform to the shape of the seabed. This disturbance creates a series

of interfacial waves known as lee waves. Dyer [1997] states that: (1) the phase velocity of these waves almost equals the velocity of the flow, thus the waves are stationary in stable flow, (2) with increasing current velocities the waves with shorter wavelengths are gradually displaced by larger wavelengths and amplitude. Dyer [1997] refers to these waves as internal waves however based on the literature by Apel [2002] these waves have been classified as a type of internal wave referred to as solitons. In this study the terminology used by Apel [2002] is employed.

Dyer [1997] also states that on approaching critical conditions the solitons grow and eventually a hydraulic jump occurs and mixing ensues. If critical conditions are not reached the phase velocity of the waves causes them to propagate upstream as the mean flow diminishes. Critical conditions are encountered if depth change occurs, stratification decreases or layer thickness decreases. These waves when interacting with shear at the interface can cause mixing to occur. When this occurs the critical  $Ri$  value is reached.

Solitons can be formed both on ebb and flood tide. However they are mostly formed on the ebb due to increasing water depth downstream. Mixing tends to occur around areas of rough topography or sudden depth changes. Solitons can be observed at the surface as patches of smooth and rippled waters as they propagate along the estuary. The rippled water coincides with the crest of the internal waves.

The conditions that favour soliton development are strong tides, stratification and irregular topography. From Apel [2002], solitons may be identified from the following characteristics:

- The individual oscillations are non-sinusoidal, with mostly a downward displacement.

- The amplitudes are rank-ordered with the largest at the front of the packet and the smallest at its rear
- The wavelengths are rank ordered with the longest waves at the front of the group
- The number of individual oscillations within the packet increases as its age increases
- They are dissipated by radial spreading, bottom interactions, instability and fluid turbulence
- The leading oscillation appears to be related to the magnitude of the downward displacement of the pycnocline

Figure 3.10 shows a profile view of a soliton. To identify these waves mathematically a numerical analysis is performed. For more background on the theory of solving these waves mathematically the reader is directed to Apel [2002]

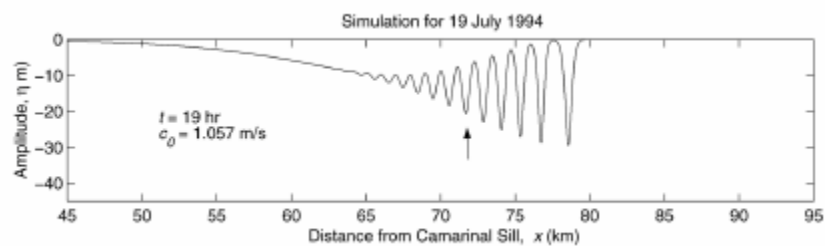


Figure 310: Profile view of a soliton wave packet. Referenced from Apel [2002].

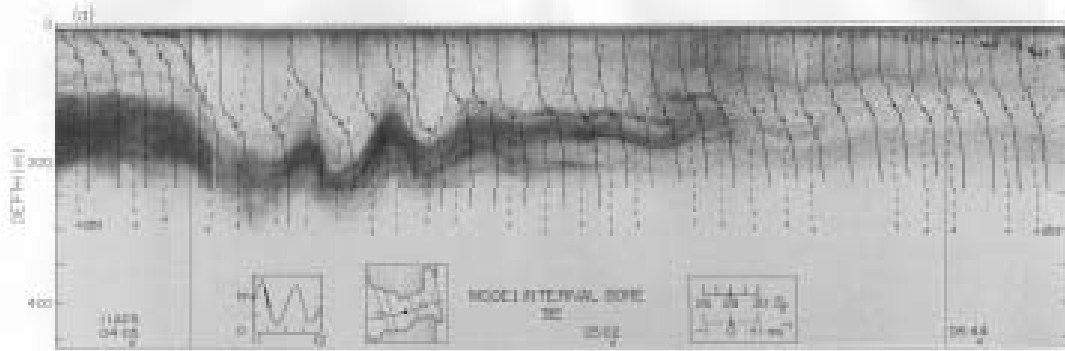


Figure 3.11: A soliton packet in the centre of Tarife Narrows in Gibraltar. Referenced from Apel (2002).

### 3.3.2 Discussion on Methods of Determining Turbulent Mixing

The  $Re$  is used in non stratified flows to determine if it is turbulent or laminar. In an estuary where stratification exists, this can only be implemented if the surface and bottom layers are considered separately. The implementation of  $Re$  in estuaries does not determine if mixing is occurring between the two different layers. Thus this is not an effective method to be used to determine mixing between two different densities in estuaries.

The  $Ri$  is a very effective method for determining interfacial mixing. It is based on calculations of the gradients of the density and velocity profiles. To apply the theory of the  $Ri$  requires a fine scale resolution of the velocity and density profile. Thus the data collected must be of a small scale resolution vertically.

The theory of the  $Ri$  states a critical value of  $0 < Ri < 0.25$  for KH waves to exist and  $Ri > 0.4$  for Holmboe waves. However the theory does not mention the resolution at which the data should be collected at to obtain these critical values. The lower the



resolution of the data can create an underestimate of the gradients, thus the less accurate the calculations will be in obtaining the critical values.

The bulk Richardson number ( $J$ ) was derived as a result of not being able to measure the velocity and density gradients and considers instead the relationship of the upper and lower layers only. Thus it considers the conditions of the flow. However mixing is known to occur at small scales. The averaging of the upper and lower layer density and velocity smoothes out these small scale events.

The interfacial Froude number is also a good parameter used to determine mixing events. However it is very similar to the bulk Richardson number in that the conditions of the whole flow are considered. Thus the small scale processes of mixing may not be determined from this calculation. The  $Fi$  cannot distinguish the source of the mixing whilst the  $Ri$  can.

### **3.4 Field Examples of Interfacial Mixing in Estuaries**

Interfacial mixing occurs when a density gradient and shear exist. This section refers to field observations from studies performed in the Hudson River, USA; the Fraser River, Canada; the Columbia River, USA and the Ishikari River, Japan.

The phase of the tide plays a major role when mixing occurs in estuaries. For example, in the Columbia River, Jay and Smith [1990] observed that turbulent mixing mainly occurs at high tide. In contrast, studies performed by Geyer and Farmer [1989] in the Fraser River observed turbulent mixing to occur predominantly during the ebb tide.

In the Jay and Smith [1990] studies, the greatest shear was observed to occur when the surface and bottom layers flowed in opposite directions which occurred at high

tide. In contrast, in the Geyer et al. [1989] studies, where the lower layer was very thin, increasing velocities at ebb tide caused velocities of the surface layer to increase whilst in the bottom layer the bottom friction also increased. This caused the lower layer velocities to decrease. Thus the maximum shear occurred at ebb tide.

Using acoustic imagery in the Fraser River, Geyer and Farmer [1989] observed that mixing does not occur everywhere simultaneously. The mixing was first initiated where lateral constrictions existed. This was then followed by the collapse of the whole salt wedge.

The importance of constrictions in encouraging mixing was also observed by Chant et al. [2000] in the Hudson River estuary where the halocline became depressed in the constricted region and shoaled in the expansion region. Using the Froude number ( $Fi$ ) they found that during maximum ebb the flow is supercritical whilst sub-critical during the flood tide. Thus most of the mixing occurred at the ebb tide.

The phase of the moon also influences when mixing occurs. Increased tidal velocities may increase the shear at the interface which encourages mixing. In a straight section of the Hudson River estuary, Peters [1996] observed that at neap tides mixing occurs during the flood tide whilst at spring tide mixing occurs during the ebb tide.

These studies have shown that different conditions exist in each estuary and that the relative importance of the phases of the tide and the moon and the location at which mixing occurs varies for each estuary. The type of internal waves that may have initiated the mixing will also similarly vary.

The identification of the type of internal waves that may have initiated the mixing process was performed for the Fraser River by Geyer and Farmer [1989]. Using the Ri

and acoustic imagery, confirmation of the KH as a possible source of mixing was made (see Figure 3.12). In the Ishikari River, Yoshida et al [1998] confirmed the presence of the Holmboe waves by the use of a linear stability analysis and acoustic imagery (see Figure 3.13). In the Knight Inlet Sill, British Columbia Canada, Farmer et al. [1980] observed solitons with the use of acoustic imagery (see Figure 3.14).

From the studies mentioned above it can be concluded that the following factors either occurring independently, or in a combination with each other, influence interfacial mixing in an estuary:

- The phase of the tide
- The phase of the moon
- The river discharge
- The geomorphology of the area
- The shear
- The density structure

To identify the type of instability that may initiate mixing processes in estuaries various dynamical approaches have been employed based on the conditions of a particular estuary. Most of the field examples mentioned above have made use of acoustic imagery which allows one to descriptively visualize and confirm the instabilities.

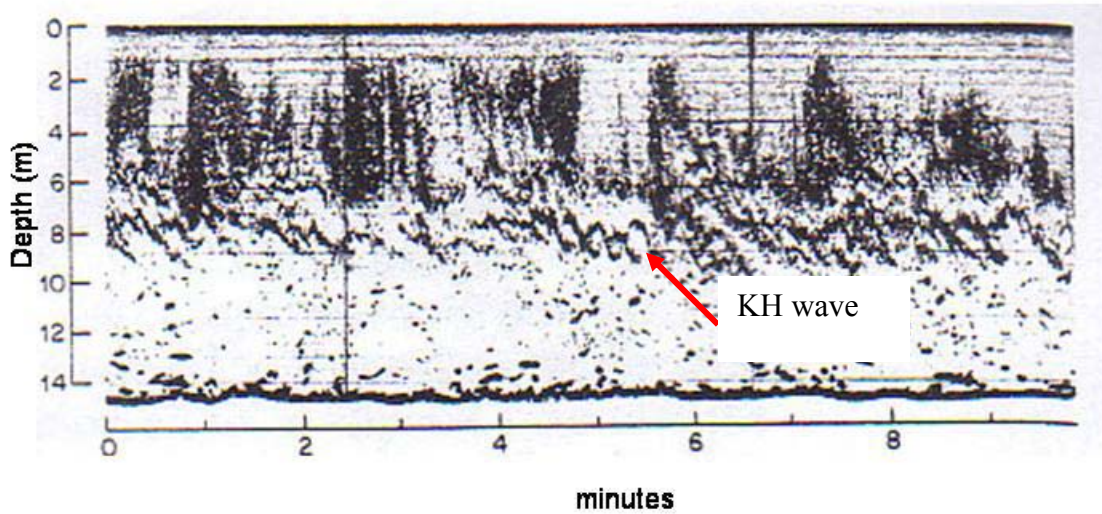


Figure 3.12: Kelvin- Helmholtz waves observed by acoustic imagery by Geyer and Farmer [1980].

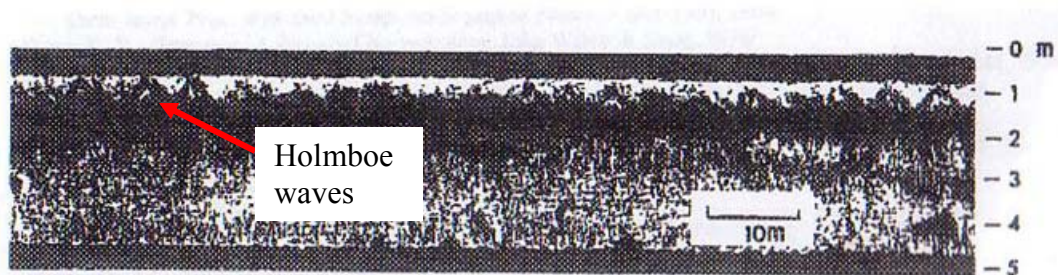


Figure 3.13: Holmboe waves observed by Yoshida et al. in Japan [1998].

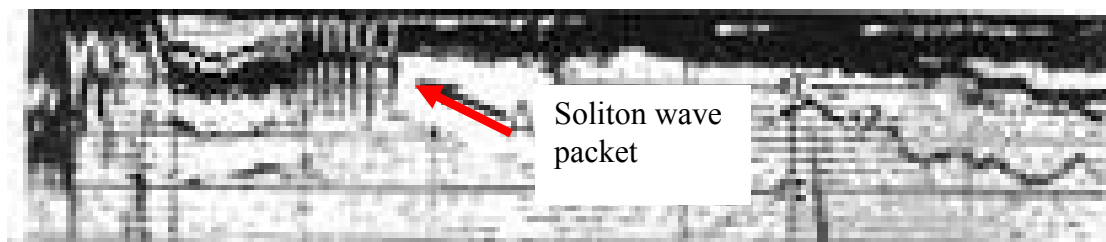


Figure 3.14: Soliton wave packets observed by Farmer et al [1980] in the Knight Inlet sill.

### 3.5 Summary on Mixing in Estuaries

Estuaries can be classified into highly stratified, fjord, partially mixed and well mixed. The classification is determined by the salinity structure of the estuary. The salinity structure of an estuary is determined by the mixing and advection process that occur.

To confirm that mixing occurs the Reynolds number ( $Re$ ), Richardson number ( $Ri$ ), Bulk Richardson number ( $J$ ) and Froude number ( $Fi$ ) may be employed. These theories were derived from laboratory and theoretical studies.

The  $Ri$  investigates, in a localised discrete scale, the gradients in the velocity and density profile to determine if mixing is occurring. However  $J$  and  $Fi$  investigate the conditions of the whole flow with respect to the upper and lower layer. The  $Ri$  results tend to be more accurate with respect to identify where turbulent mixing is occurring. This is due to the fact that the resolution at which the  $Ri$  results are presented are more accurate at identifying the smallest scale of mixing.

To identify the type of internal wave that may be present in a highly stratified environment a linear stability analysis may be employed. However this analysis only distinguishes between the KH and Holmboe wave.

The theory for identifying the internal wave has been used with success in the field. The implementation of acoustic imagery has allowed these theories to be confirmed and the internal wave to be visualized. The following chapter now explains the use of acoustics for visualization in the water column.

## **CHAPTER 4**

### **BACKSCATTER**

Chapter 3 illustrated that, in previous estuarine studies, acoustic sensors were used to visualize the processes that were taking place in the water column. In this chapter, section 4.1 introduces the reader to the basic background information on the acoustic wave which was sourced from Ingham [1994] and Lurton [2002]. This is followed by section 4.2 which presents the backscatter theory with respect to the water column. The use of acoustics for the measurements of currents in the ocean is discussed in Section 4.4.

#### **4.1 Acoustic Wave**

An acoustic wave originates from the propagation of a mechanical perturbation. This perturbation can be configured to be constant. The medium used to convert electrical power into sound power by vibrations and vice versa is referred to as a transducer.

For surveying purposes transducers are designed to produce beams of sound power of various shapes normally concentrating the energy along an axis orthogonal to the radiating surface. For example a long narrow surface produces a narrow beam in the plane orthogonal to the along direction whilst a circular transducer will produce a cone shaped beam.

A system that performs targets and obstacle detection/location using acoustic signals are called sonars (Lurton, 2002). The following main characteristics of the acoustic wave shall now be described with respect to the propagation of wave through water column.

- The frequency and wavelength
- The beamwidth
- The ensonified area
- Spherical Spreading
- Noise

### 4.1.1 Frequency and Wavelength

The frequency is the number of cycles per second, expressed in Hertz (Hz). The frequencies used in acoustics normally range from 10Hz to 1MHz. The wavelength is the distance travelled by one of the cycles (see Figure 4.1). The higher the frequency the shorter the wavelength. The pulse length for a narrow band pulse (see Figure 4.1) is the length of the cycles and it is calculated using the pulse duration, the wavelength and the frequency. The pulse length determines the resolution of identifying an object (vertically). For example if two object are separated less than half a pulse length apart they will be identified as one object whereas if they are more than half the pulse length they will be identified as two separate objects.

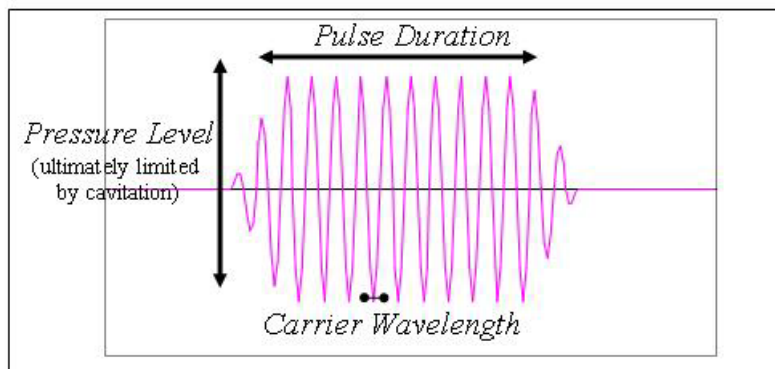


Figure 4.1: Diagram showing a wavelength and a pulse length.

### 4.1.2 Beamwidth

When an acoustic pulse is transmitted there is an azimuth at which the energy will be at a maximum (usually the centre). Away from this azimuth the energy will tend to decrease. The angle at which the energy is half of the maximum is referred to as the -3dB limit which is known as the beamwidth (see Figure 4.2). The smaller the angle the more concentrated the beam is within a particular area. Therefore the identification of target increases with narrower beamwidth.

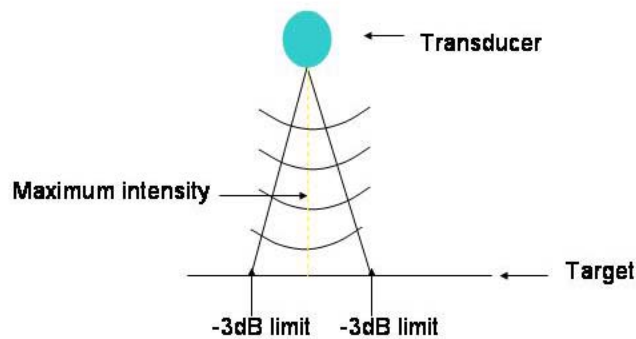


Figure 4.2: The -3dB limit referred to as the beamwidth.

### 4.1.3 The Ensonified area

The ensonified area is the area on the target that the beam width illuminates. The actual dimensions of the area covered depend on the depth of the target and the beam width. The strength of echoes returned from an object will be determined by the size of the object with respect to the ensonified area and the type of object.

If the target is greater than the solid angle cross-section of the beam at the range of the target then there will be many hits on the target assuming that it has good



reflection. If the target is smaller than the ensonified area then it may not be identified due to the strength of the return echo not being strong enough (see Figure 4.3). The ensonified area is referred to the area that the backscatter energy actually reflects back to the source.

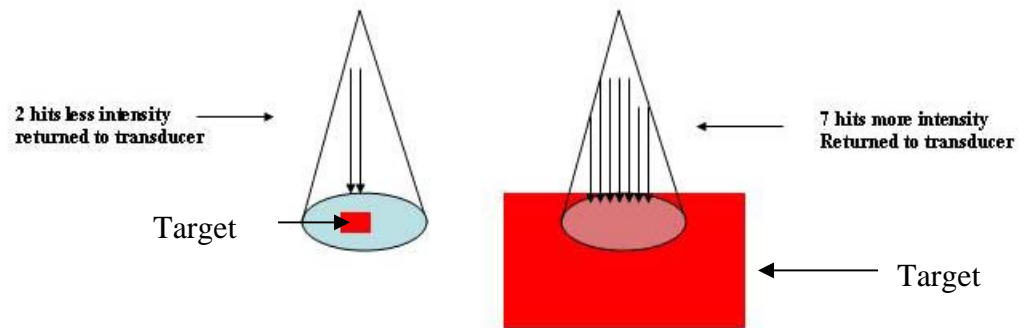


Figure 4.3: The ensonified area of two different size targets.

#### 4.1.4 Spherical spreading

As an acoustic wave propagates energy is lost. Energy is lost on its path to the target and on its way back to the transducer. This energy decays at a rate of  $1/R^2$ , where  $R$  is the distance travelled by the wave from the transducer. On interaction with the target the dispersion of the energy back to the transducer can occur in two different methods: a coherent reflection case or an incoherent scatterer case. The former tends to occur on smooth targets whilst the latter occurs on rough targets (see Figure 4.4).

Coherent Reflection case:

$$\text{Energy is coherently reflected so: } 1/(2R)^2 = -20 \log 2R \quad (4.1)$$

Incoherent Scatterer case:

Target scatters and re-radiates energy spherically

$$1/R^2 * 1/R^2 = 1/R^4 = -40 \log R \quad (4.2)$$

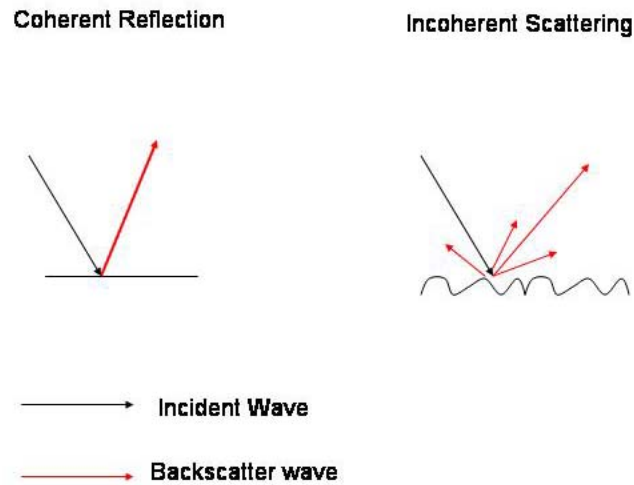


Figure 4.4: Coherent and incoherent scattering from a target.

### 4.1.5 Noise

Lurton [2002] has grouped the causes of noise into 4 main categories:

1. Ambient Noise- This noise originates from the natural environment (e.g. wind, waves, rain) or man made (shipping, industrial activity)
2. Self Noise- This is the noise caused by the underwater acoustics (electronics)
3. Reverberation- This is caused by the multiple echoes of the sonar. This can originate from the water column, the seabed and the sea surface.
4. Acoustic Interference- This is caused by other acoustic systems working in the same vicinity either onboard the same ship or underwater platforms

There exist different models that are used to model the noise (NL). Equation 4.3 is commonly used

$$NL = N_c + 10 \log W \quad (4.3)$$

W= receiver bandwidth

N<sub>c</sub>= noise spectral density at centre frequency

## 4.2 Backscatter

A sonar, given a particular amount of power, creates an acoustic wave that sends out a pulse which travels through the water column. This wave, whilst travelling through the water, will collide/interact with:

- Obstacles in the water column (zooplankton, turbulence, suspended sediment, density interfaces)
- Objects at the limits of the water (sea surface, seabed)
- The subsurface of the seabed

The wave begins to lose energy the further it advances from the sonar. When the wave interacts with obstacles in the water some of the signal is scattered back to the sonar. The remainder of energy continues on its journey through the water column until it reaches the seabed where it is also reflected back towards the sonar. The reflection of energy towards the sonar is referred to as backscatter.

The wave that is reflected from these obstacles obtains its energy on initial collision. However on collision, energy is now scattered in all directions and only a portion makes it back to the sonar. It is the task of most sonars to recognize this backscattered energy. The energy received by the sonar depends on the following:

- The amount of power that was initially sent out by the sonar
- The directivity of the energy sent out (beamwidth)

- The loss of energy as the wave travels through the water column, which increases with distance from the sonar
- The target strength which depends on the properties of the target and the incident angle
- Noise

The sonar equation which takes into consideration all of the above factors is used to represent the intensity of power received by the sonar. This equation is listed below.

$$EL = SL - 2TL + TS - NL + DI \quad (4.4)$$

EL – echo received by the sonar

SL – Energy initially transmitted by the source

TL – Transmission loss which decreases with distance from the target

TS – the target strength obtained from when the wave collides with the obstacle

NL – Noise level

DI – Directivity index

### 4.2.1 Target Strength

The target strength (TS) depends on: the type of target, the angle at which the wave collides with the target and the angle at which energy is scattered. The general equation for the target strength is defined as the ratio (in db) of the backscattered (I<sub>bs</sub>) and incident waves (I<sub>i</sub>).

$$TS = 10 \log (I_{bs}/I_i) \quad (4.5)$$

To obtain the backscattered energy from the target (TS) it is important to know the amount of energy that actually interacted with the target and the amount of energy that was backscattered. To obtain these values, information on the angle of incidence, the angle of the scattered wave, the cross-sectional area of the incident wave, and the cross-sectional area of the backscattered wave are needed.

#### **4.2.2 Targets**

An acoustic wave can encounter two types of targets:

1. **Small Targets:** Targets small enough to be completely ensonified by the sonar beam and signal. Their backscatter strength is an intrinsic strength independent of the distance to the sonar or its characteristics (beam width, pulse length).
2. **Large Targets:** Other targets will be too large to be ensonified completely at once by the same beam. The strength of these targets will depend on their geometric intersection with the sound beam. The target strength is no longer a point value but uses the insonified space (surface or volume) associated with a surface or volume backscattering coefficient. The latter is therefore an expression of the amount of energy scattered by a unit scattering element

Most applications would require either that: the target be of the same size as the beam footprint (ensonified area); or that it be bigger than the ensonified area Hughes Clarke [1996]. With respect to the latter occurring this ensures that the target is detected and that there are enough “hits” to identify it.

When the target is smaller than the ensonified area it may not be identified and if it is identified there is the possibility that it will not be strong enough to be heard over the background noise, or it may be regarded as an outlier in processing. The potential backscatter received by the sonar can either be from a point target or a surface target.

### **4.2.3 Volume Backscattering**

Volume backscattering occurs when the size of the object is greater than the ensonified area or the ensonified area contains a number of small objects. These targets are delimited by the sonar characteristics (beam width and pulse length) rather than by their own dimensions. The backscattering cross-section can then be decomposed into two contributors:

- The size of the target portion(surface or volume) effectively ensonified by the sonar
- The corresponding backscatter strength

The volume backscattering of a distribution of targets can be analysed as the sum of the contributions from each target present in an average cubic metre of water. However, for a given frequency, each contribution will depend on: the size, the shape (the shape being less important if its dimensions is much smaller than the signal wavelength) and on the nature of each member (structure, density and sound velocity of the targets).

The difference between volume backscatter and point backscatter targets is that in the volume backscatter the whole surface/volume insonified by the beam is taken into

consideration. Whereas the point backscatter mostly considers the object itself and the relationship to its backscatter strength.

To identify the source of backscatter or to determine if the backscatter originated from a point or surface/volume source is not that easily performed. Section 4.2.5 shall illustrate that the backscatter of one object can have the same intensity as that of a number of small objects collectively.

#### **4.2.4 Backscatter Intensity**

As was illustrated in the previous sections the backscatter from a target depends on the characteristics of the sonar (beamwidth, pulse length), the environment (depth, noise) and the target (size, shape orientation). Targets in the water column are, in general, weak backscatters. To increase the strength of the backscatter the following may be performed:

- Increasing the power
- Amplifying the return signal which indicates using a higher gain for the backscatter received by the echosounder.

Increasing the power to identify a target has its limitations. For example when a speaker is cranked up to its highest volume it is not possible to hear anything useful as it is too loud. The same occurs with a sonar when the power is too high. The sonar targets legitimate targets as well as noise, such as reverberation which is power dependant and ambient noise which is independent. This indicates that the noise level is increased and the data may not be very useful.

Most sonars are equipped with an amplifier that increases the intensity of the return echo. In most systems this is taken to be  $40\log R$  which would correspond to the amount

that was lost by the signal in travelling and being scattered incoherently. Amplification of the return signal may be preferred to increasing the power. Amplification assumes that the target has been identified and all that is required is an extra “boost” so that the signal can be visualized more clearly. Thus this method does not add additional noise to the return signal but amplifies the existing return signal and ambient noise.

It is the decision of the user to decide whether the target to be detected is reverberated noise or ambient noise. This is necessary to determine whether to increase the power or to increase the gain.

#### **4.2.5 Water Column Targets**

Historically echosounders were used mainly for bottom detection. However it was soon found that the backscatter from obstacles in the water column allowed scientists and fishermen to visually map the water column. The main targets found in the water column are zooplankton, density interfaces, turbulence and suspended sediments.

The backscatter and possible identification of these four targets will depend on two factors: the sonar (the beamwidth, the wavelength and the pulse length) and the characteristics of the targets. This research is mainly concerned with the backscatter from the pycnocline. Therefore the backscatter from targets in the water column is emphasized. This section now discusses the characteristics of the backscatter from zooplankton, density interfaces, turbulence and suspended sediments.



#### 4.2.5.1 Zooplankton

Zooplanktons are microscopic animals that vary in sizes from about 1mm to 20mm. There are different types of zooplankton such as siphonophores (gas bearing), euphausiids (fluid like) and pteropods (hard elastic-shelled) (see Figure 4.5). Zooplanktons have been found to often produce good backscatter. Thus scientists have used the backscatter to mainly calculate the amount of zooplankton present in an area.

To acquire the relationship of the strength of the backscatter with the amount of zooplankton present in an area has proven to be a difficult task. This difficulty mainly occurs due to the variation of size, type and shape of zooplankton that exist. Listed below are these characteristics.

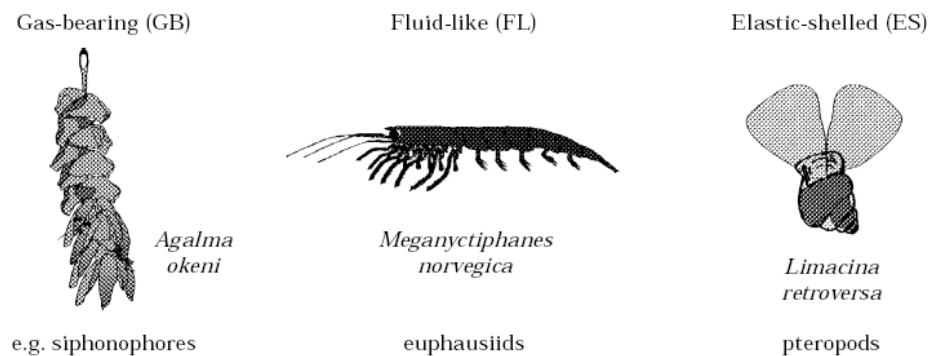


Figure 4.5: The different types of zooplankton. Referenced from Martin et al. [1996, pp.218].

##### 4.2.5.1.1 Size

Variation in size of zooplankton was illustrated by Greenlaw [1979] who showed that the volume scattered from a 22mm fish was the same as that of 260 zooplankton of

smaller sizes. Thus it has proven to be a difficult task to determine if the source of the backscatter is one fish or many fish.

This limitation is partly due to the characteristics of the sonar with respect to the target. If the target is large enough and falls within the ensonified area then it will be recorded as one object. If there are many targets that falls within the ensonified area and they are less than half the pulse length apart then these targets will also be represented as one target. However if these targets were within the ensonified area and they were greater than the half the pulse length apart they would be recorded as individual objects.

#### **4.2.5.1.2 Type**

The type of zooplankton influences the strength of the return echo. Martin et al. [1996] performed laboratory experiments using different sonar frequencies on individual zooplankton such as gas bearing (siphonophores), fluid like(euphausiids) and hard elastic shelled (pteropods). The results found that the gas bearing zooplankton had a stronger return echo than the others. Warren et al. [1999] using field experiments, has confirmed these results using different frequency sonars and a camera which were all attached to a ROV. These results also confirmed that the gas bearing zooplankton had a higher intensity than that of the other zooplankton types.

#### **4.2.5.1.3 Orientation**

Laboratory experiments performed by Traykovski et al. [1998] on *Euphausia superba* (Atlantic Krill) using a 500 kHz echosounder and a video recorder observed that the echo intensity varied based on the zooplankton orientation with respect to the incidence angle

of the pulse. These results showed that the echo intensity was greatest when the zooplankton was broadsided (perpendicular to the beam) than off broadsided. Similar results based on laboratory experiments were also found by Martin et al. [1996] for fluid like (euphausiids) and hard elastic shelled pteropods. Field experiments by Warren et al. [1999] have also confirmed that the orientation affected the echo intensity for gas bearing Siphonophores.

Most of the studies performed on zooplankton intensity were carried out using a variety of different frequency sonars. For example Stanton et al.[1998], working in 60m depth, observed zooplankton on the high frequency sonars but not on the low frequency sonars. Thus the type of frequency used also influences whether zooplanktons is detected.

#### **4.2.5.2 Density Interface**

An acoustic wave colliding with a density interface in the water column causes the speed of the wave to change and some of the energy is backscattered towards the sonar. When this occurs the remainder of the wave is refracted and continues through the new medium. Seim et al. [1995] and Goodman et al. [1992] have illustrated, both in the laboratory and in the field, that backscatter is observed at a density interface.

The strength of the backscatter from the interface will normally tend to be weaker than that of the seabed, since the interface has similar properties to that of the surrounding waters.

The backscatter from density interfaces will depend greatly on the frequency of the sonar being used. It has been found that the density interface tends to be identified for high frequencies whilst when using low frequency sonars it is not easily identified. The

scale of turbulence is always smaller than the ensonified area, thus the backscatter tends to be that of volume backscattering.

As was mentioned in section 3.1, acoustics have been used to identify density interfaces by Geyer and Farmer [1989] in the Fraser River where a 200kHz echosounder was used to map the advancement and break down of the salt wedge; in the Knight inlet sill in British Columbia, Farmer and Smith [1979] observed the plunging of the pycnocline using a 100-200kHz echosounder; and Klymak et al. [2002] used the echosounder to show the development of stratified flow and waves in the vicinity of a sill.

Studies performed by Mann [1991] on three different types of zooplankton, *spisula solidissima*, *mulinia lateralis* and *rangia cuneata*, has found that the *mulinia lateralis* and *rangia cuneata* had a preference for preferentially settle either above the pycnocline or just below it. It was also observed that the *spisula solidissima* preferred the seawater and preferred to swim across the pycnocline. These observations indicated that the different types of zooplankton actually preferred a particular salinity range to inhabit and thus can usefully act as a useful proxy for the density structure.

The above studies show that a relationship exists between the location of the pycnocline and the zone where zooplankton tend to swim. In Klymak et al.'s [2003] studies it was found that high backscatters of zooplankton tended to accumulate on the pycnocline. The fact that the zooplankton swim on the pycnocline indicates that if the zooplankton existed at the pycnocline it should increase the strength of the backscatter.

Thus conditions that affect the backscatter from density interface are:

- The degree of stratification present

- The prevalence of zooplankton on the pycnocline
- The distance of the pycnocline from the sonar. This is related to the amount of gain that the system would need to be set at
- The background noise in the field
- The frequency of the system being used

#### **4.2.5.3 Turbulence**

As was mentioned in Section 3.2 mixing in the water column can be generated by winds at the surface, at density gradients and at the seabed. Density gradients influenced by velocity shear may produce internal waves. These waves may break in a turbulent manner causing mixing to occur. Thus density gradients, internal waves and turbulence are related.

The backscatter from turbulence depends on the frequency used, the size of the target and the depth of the waters. Studies performed by Stanton et al. [1998] in the Gulf of Maine using echosounder frequencies of 43kHz, 120kHz and 200kHz, 420kHz and 1MHz has found that in a depth of 25m, to 30m the scattering was highest at the lower frequencies whilst it was hardly detectable at frequencies higher than 420kHz. In the Admiralty Inlet, Seim et al. [1995] in the Admiralty Inlet using an echosounder, advance microstructure profile and an ADCP, observed a 20 m high dissipative billow that was formed at the pycnocline. It was shown that the billow efficiently mixed fluid across a strong density gradient producing large temperature and salinity structures.

#### **4.2.5.4 Suspended Sediments**

Suspended sediments (usually sand, silt or clay) are also potential volume scatterers. High frequency sonars are normally used to map these targets. However in deep waters high frequency sonars may not operate well.

In a study performed in the Taw Estuary UK, Betteridge et al. [2003] in 7m depth employed a triple frequency acoustic backscatter system with a beamwidth of 1-2° and a frequency range of 1MHZ to 5MHz. These sonars were used to obtain mean concentration profiles where an on site sample measurement was made for calibration purposes. The results of this study showed that the strength of the backscatter signal depended on the concentration, the composition size and shape of the scatters. In estuarine environments, the suspended sediment level is often strongly correlated with salinity and this acts as a proxy for water mass boundary identification.

### **4.3 Discussion on Backscatter**

Backscatter from the water column is sourced from 4 main targets: zooplankton, density contrast, turbulence and suspended sediments. The strength of the backscatter from these depends on the characteristics of the sonar (beamwidth, pulse length), the environment, and the target. Two of the main limitations of using acoustics to identify objects in the water column are as follows:

- The backscatter indicates to the user that a target exists but it does not identify the type of target (zooplankton, density interface, turbulence or suspended sediments).

- The identification of whether the backscatter is sourced from a point target (point) or many targets (volume) is not easily distinguished. As was discussed in Section 4.2.5.1.1, the backscatter from one large fish can be the same as that for many small fishes.

To remedy the above limitations of the sonar the following has been employed:

- Scientists now look at the backscatter from one fish in a lab and compare this backscatter to that observed in the field. Such a method, in concept, appears reasonable however different environmental conditions exist in the lab than in the field. Warren et al. [1999] has compared the limitations of observations in the lab with those in the field due to depth differences and temperature. These comparisons indicate that there is the need for making controlled measurements of target strength in the natural environment. One method of overcoming this limitation is the calibration of the same target in the lab as in the field. This will then verify the differences in the environment that have taken place. An example of this can be by placing a brick or obstacle in the lab and observing its backscatter and then placing this same obstacle in the field and observing its backscatter.
- For the identification of the source of the backscatter, scientists now employ the use of multiple frequency sonars and complimentary measuring tools. This assists in the identification between the different types of scatterers. This was the case with the BIOMAPPER used by Stanton et al. [1998] and Seim et al. [1995] whom employed salinity and temperature data to verify the acoustic images.

Acoustics can be a very useful tool in detecting targets of the water column. The spatial sampling of the backscatter intensity represents the highest vertical and horizontal resolution of any oceanographic equipment. Thus even given problems in interpolation it still provides good data that compliments conventional density data. However, due to its limitations in identifying the type of targets, it is advisable that additional measurements be made to compliment the observations made with the sonar. This can be done by collecting samples of the water column for organism, salinity and temperature measurements or by the use of different frequency echosounders.

In this study a 200 kHz, 28 kHz and 600 KHz were used; best results were obtained from the 200 kHz echosounder. Complementary measuring tools in this study include a MVP-30 with a CTD and optical backscatter.

#### **4.4 Currents**

Currents are used to describe the movement of water with reference to a particular magnitude and direction. In an enclosed area currents may be due to winds, tides, topography, density gradients and upwelling.

Previously, currents were measured by current meters which required that they be placed in the location of the measurement. However, with recent advances in acoustics, there has been the introduction of the Acoustic Doppler Current Profiler (ADCP) and Reciprocal Transmission. For this research the ADCP was used. The background knowledge of the ADCP is described in the following section.



#### 4.4.1 ADCP and the Doppler Effect

With a transducer sound radiates with a narrow fixed range of frequencies. The Doppler effect is the shift in frequency which can vary depending on:

- a source moving with respect to a medium
- receiver moving with respect to the medium
- the movement of the medium itself

Figure 4.6a shows, on the left hand side, a source (the red dot) propagating sound at a fixed frequency (constant wave length). When the source begins to move to the right the frequency increases to the right (wavelength decreases) (see Figure 4.6b). The difference in frequency when the source is stationary to that when it was moving is referred to as the Doppler effect. The same effect can take place when the observer is moving and the source remains stationary.

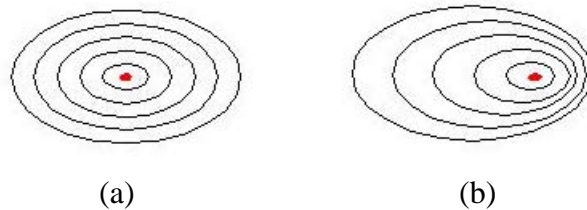


Figure 4.6: (a) Sound at a fixed frequency and (b) changing frequency, as the source moves to the right.

The ADCP uses the Doppler effect to measure velocity in the following way:

An acoustic pulse is sent out at a fixed frequency (which can vary from 40kHz to 3MHz).

The transducer listens for backscatter from small particles or plankton from the water (it

is assumed that these creatures flow with the same velocity as that of the surrounding water). These scatters are all moving thus the echo received by the scatters is Doppler shifted and the return echo to the transducer will be Doppler shifted. In some cases both the transducer and the water particle will be moving whilst in another case the transducer can be stationary and the water particle moves. On receiving the return echo from scatters the component of the velocity vector projected along the axis of the beam can be calculated with the aid of the transmit times of the pulses, the return echo time/phase and the speed of sound.

The description above is for one velocity measurement parallel to the transducer. However velocity is a vector and thus there are 3 components to a velocity (one in each x,y,z directions). Thus the ADCP is equipped with 3 to 4 beams that allow for the calculation of these components.

The ADCP is equipped with a magnetic compass which is used to acquire the velocity direction. However the compass tends to be in error. These errors are:

- The ADCP when deployed on a moving platform, tends to be in close vicinity of the ships hull which is made of steel. This affects the earth's magnetic field readings and thus the compass gives inaccurate readings.
- The compass needs to be level. There is no certainty that it is level, as the ADCP may be tilted.

Since the ADCP employs the use of acoustics and broad band technology in addition to the phase difference of the return signal, the transducer also measures the strength of the return echo. Thus, as was explained in section 4.2.5, the detection of targets such as turbulence, zooplankton, density interface and suspended sediments can

also be determined. The backscatter strength of such targets will depend on the frequency of the ADCP and the water depth of the area. The following section now describes the resolution of the ADCP.

#### **4.4.2 Range Gate and Depth Cell Size**

The transducer sends out a pulse, which interacts with scatters and return an echo. There will be backscatter from the water column. To have order and pattern of the return echo, the user has the option of deciding how often they would like a record of the velocity measurement at a particular depth interval through the water column. This depth interval decided by the user, is referred to as the depth cell size.

The range gate determines the time period at which echoes will be recorded. This is determined by the depth cell size. The centre of the gate is sampled most and the top and bottom of the gate sampled the least. An average is then made for all the hits within this range gate to produce one value which is then assigned the velocity for that particular depth cell (see Figure 4.7)

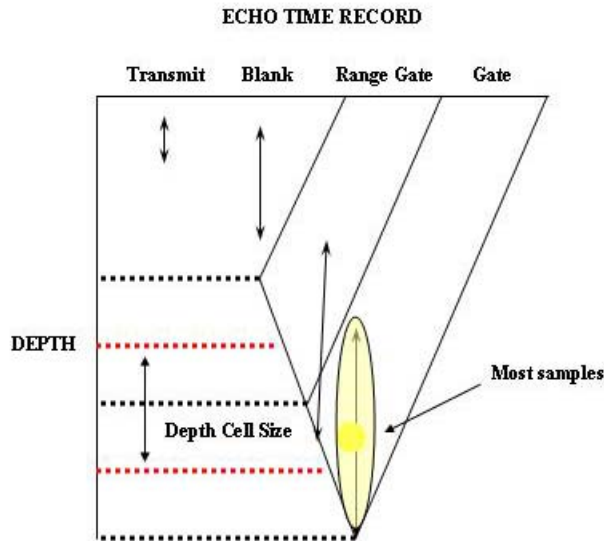


Figure 4.7: The depth cell size and the range gate used in the ADCP. Referenced from RD Instruments manual.

#### 4.4.3 Bottom Tracking

The bottom tracking capability measures the frequency difference of the transmitted pulse to that of the returned echo from the seabed. From this, the velocity of the vessel with respect to the sea bed (assumed stationary) is derived.

In the cases where the ADCP is deployed on a moving platform and acquires data as the vessel moves, it is necessary to correct the observed velocities for the vessel speed. This is performed in post processing or before if no bottom tracking is used. GPS and gyro compass derived speed and heading can be substituted.

#### 4.4.4 Discussion on ADCP

The ADCP is a bit more complex than the conventional current meter used for measuring currents. However, because of its accuracy, resolution and ease of use, it is a very popular method. Some advantages of the ADCP over that of the current meter are:

- The resolution (horizontal) of the ADCP can be acquired more easily. The horizontal resolution of the ADCP depends on the boat speed, depth, beam separation angle and ensonified area.
- The vertical resolution of the ADCP depends on the bin size and pulse length chosen by the user. The accuracy of the bin size is better than the current meter as the ADCP measures the average current within this bin size whereas the current meter measured that of the current at that particular point. It should be noted that, if needed, the current meter spacing is decided upon by the user. Thus its resolution can be greater than 0.5m.
- The ADCP is capable of measuring the strength of the return echo which can aid in the determination of targets in the water column. The strength of the return echo will depend on the frequency, depth of the area, pulse length and type of target in the water column.
- By using the graphic interface available, on site visualization of the currents can be performed. This allows the user to have a basic idea of what is taking place as the data re collected.

Some of the disadvantages of the ADCP are:

- Limitation of the vertical resolution of the ADCP which for the system used was 0.5m. This is the smallest that the bin size is allowed to be.

- The processing of the data can be complex.
- Due to the blanking period and the draft of the ADCP the surface currents are not measured. The bottom currents are also, at times, not measured since the bottom currents echoes tend to be inferred by the side lobes of the acoustic beam and thus the signal strength may not be great enough.
- Compass errors.
- Noisy estimates of single pings. This requires the user to perform ensemble averaging.

As was mentioned, the compass of the ADCP is likely to have errors associated with it due to its position on the ship and due to tilting errors. To compensate for these errors requires comparing observations made with the compass with that of a sensor which does not use the same compass. This can be performed using DGPS system or a Gyro.

## **4.5 Summary on Acoustics**

This chapter has shown that acoustics allow: (1) the mapping of the water column in order to visualize the density interface, zooplankton, internal waves and suspended sediments; and (2) the observations of the current magnitude and direction with a better accuracy. In this research acoustics are used for the identification of the pycnocline and internal waves and to determine the current magnitude and direction. Thus consideration is made of the sonars frequency, beam width, pulse length and pulse duration with respect to the water depth and the type of target required. Chapter 5 now illustrates the methodology that was employed.

## **CHAPTER 5**

### **SURVEY DESIGN**

Previous studies performed in Long Reach by Trites [1959] and Metcalfe et al. [1976] concentrated on the estuarine circulation pattern with respect to regional scale measurements of salinity, temperature and density. These studies showed that in Long Reach: (1) a seasonal variation in the stratification structure existed and (2) there appeared to be mixing or possibly advection processes taking place in the summer months.

To confirm that mixing/advection are actually occurring in Long Reach requires that density and velocity be of a particular resolution both spatially and temporally. In the previous studies performed in Long Reach, using the equipment available, this would have been an almost impossible and certainly uneconomical task to perform.

Since the 1950's to 1970's (when the previous surveys were performed) there has been great advancement in the technology available. The introduction of digital acoustics (the echosounder, ADCP) and new improvements in the measurement of salinity and temperature now makes it possible to remap Long Reach and to investigate in detail the "hinted" processes that may be occurring.

The remapping of the seasonal stratification and circulation characteristics were performed in May 2003 to October 2004. Based on the 2003 results it was observed that dynamic processes were occurring at the pycnocline at particular locations in Long Reach. It was decided that an oceanographic survey should be performed to investigate these processes.

This chapter describes (1) the instrumentation that that was used in the surveys, (2) the method employed in processing the data, (3) a description of the 2003 seasonal surveys, (4) the survey design for 2004 tidal cycles and (5) summary on the methodology used.

## **5.1 Survey Instruments**

It was mentioned in chapter 4 that the implementation of acoustics as a tool for oceanographic surveying has increased our understanding of the processes that occur in the oceans. The water column can now be mapped with a better spatial resolution and accuracy (both horizontally and vertically) and targets in the water column can now be visualized at a resolution that allows useful interpretation. This section describes in detail the sensors used in this research, such as the Acoustic Doppler Current Profiler (ADCP), Conductivity Temperature Depth sensor (CTD) and acoustic imaging from echosounder.

### **5.1.1 Survey Platform**

The research vessel used in these surveys was the CSL Heron which has been loaned for a ten year period to the OMG group of UNB by the Canadian Hydrographic Service. It is approximately 10m in length and 2.5 m in width (see Figure 5.1). The Heron has a draft of 1.15m and is capable of operating at 6m/s at 2100rpm and 4m/s at 1800rpm. For this research the vessel speed used was approximately that of 3.5m/s at 1500rpm.





Figure 5.1: The research vessel (Heron).

### 5.1.2 Positioning

A Differential Global Positioning System (DGPS) with a positioning accuracy of 0.5m to 1m was used. The positioning was sourced to the ADCP, Moving Vessel Profiler (MVP) and the echosounder (see Figure 5.2). The MVP which had a CTD attached to it was linked to a multibeam system which provided the depth to the system.

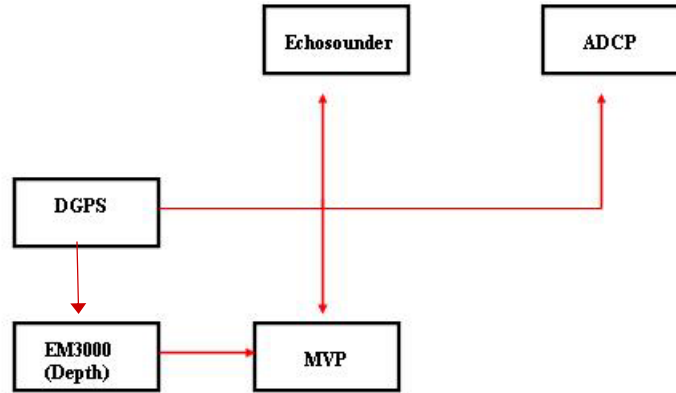


Figure 5.2: The survey sensors.

### 5.1.3 ADCP

To obtain velocity magnitude, direction and acoustic backscatter a RDI 600 kHz workhorse ADCP was used. This model ADCP consists of four beams, each with a beam width of  $20^\circ$ . The ADCP was mounted on a pole with a lever that was located on the port side of the vessel (see Figure 5.1). As the vessel moves the ADCP pings away. The ping rate of the ADCP was  $\sim 1\text{Hz}$ , thus with a boat speed of  $4\text{m/s}$  there was a horizontal resolution of  $4\text{m}$  whilst a vertical depth cell size of  $0.5\text{m}$  was used.

The ADCP was equipped with bottom tracking capabilities which takes into consideration the correction of the boat velocity in the measurements made. The ADCP had a draft of approximately  $1.2\text{m}$  and a blanking size of  $0.5\text{m}$  was used. Due to the blanking size and the draft of the boat the first measurement of velocity would be  $\sim 2\text{m}$  below the surface.

#### **5.1.4 Moving Vessel Profiler and CTD**

The CTD measures conductivity, temperature and pressure of the water column. Conventional methods of CTD profiles require either the vessel be stationary whilst a profile is made or a mooring be placed at discrete locations. These methods tend to be time consuming and the measurements are spatially restricted to the number of moorings available.

The Moving Vessel Profiler (MVP) is an autonomous profiler that acquires vertical profiles of CTD data as the vessel travels. The MVP consists of a controller box; a winch and a housing for the CT(which was shaped like a fish) (see Figure 5.3a). Attached to the fish were a CTD and an optical backscatter sensor. The winch is computer controlled and thus a free fall system takes place where the system takes vertical dips to the required depth as the vessel moves (see Figure 5.3b). A profile is made approximately every 60 seconds in less than 10m of water. However in 30m of water it will takes a dip approximately every 80seconds.

The vertical resolutions of the CTD measurements were 0.1m throughout the water column. In most of the surveys performed, the MVP was programmed to autonomously acquire vertical profiles up to 2m off the bottom of the seabed. When this was not performed mention will be made in the text.

One limitation of the MVP is that in an area with irregular bathymetry the MVP uses the shallowest depth whilst falling. As a result the actual depth off the bottom may be more/less than the programmed depth off bottom (see Figure 5.4).The horizontal resolution between profiles depended on boat speed and depth of the area. Thus for a boat

speed of 4m/s and an average depth of 15m a CTD profile was made approximately every 400m (see Figure 5.5).

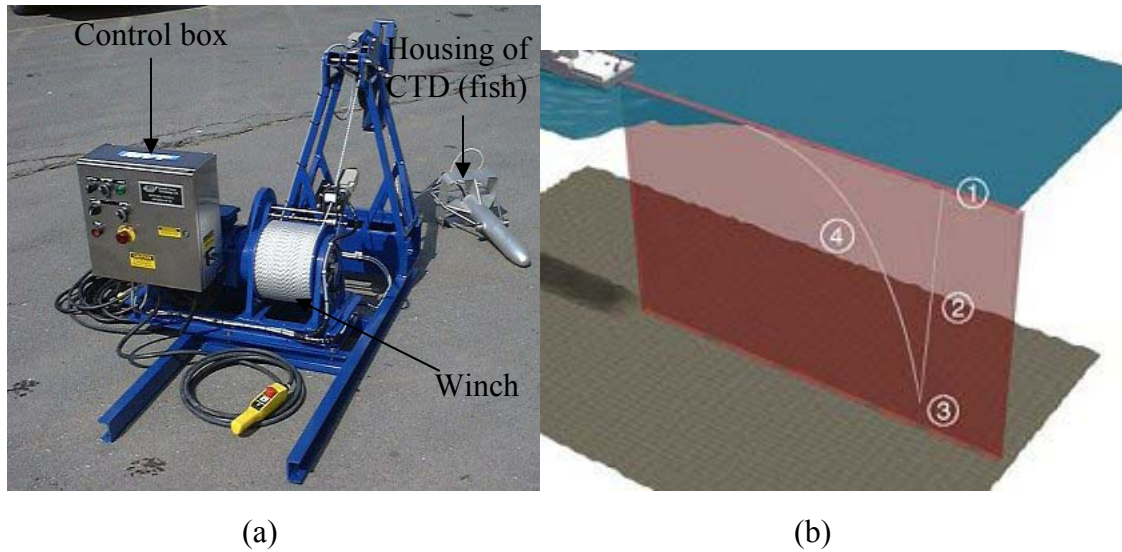


Figure 5.3: (a) hardware components of the MVP and (b) the stages of the MVP vertical profiles.

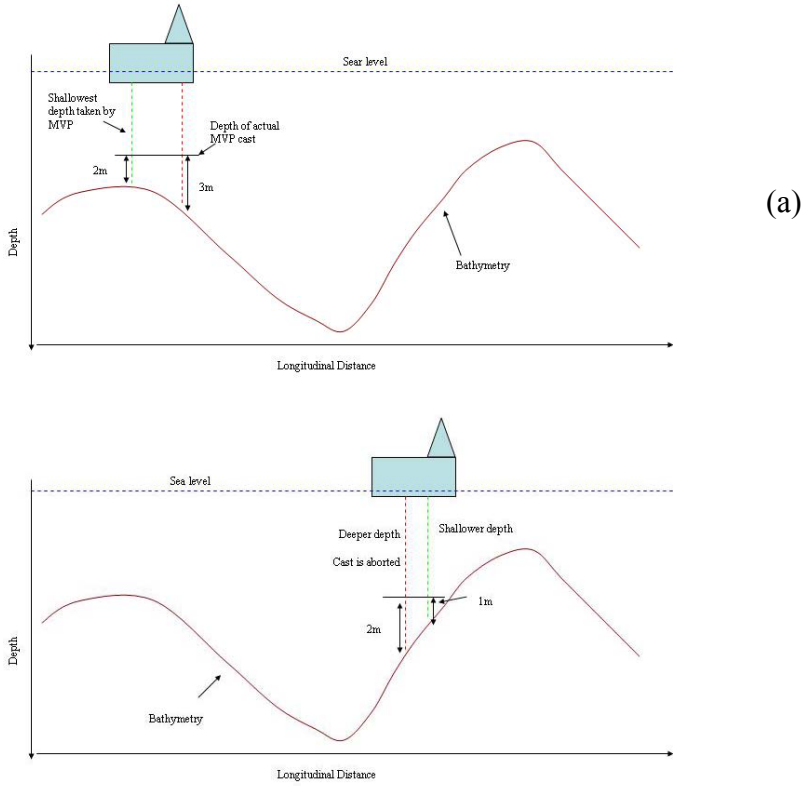


Figure 5.4: The effect of irregular bathymetry on the actual depth off bottom of CTD casts. It should be noted that in (a) the actual depth off bottom is 3m whilst the MVP was programmed to dip to 2m off bottom and in (b) the MVP cast is aborted.

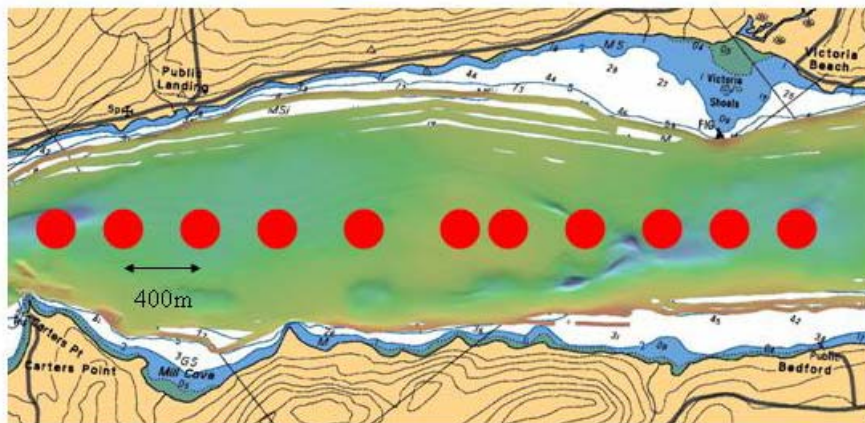


Figure 5.5: Example of locations of the CTD casts in section one.

### **5.1.5 Echosounder**

A Knudsen 320 B/P 200 kHz echo sounder with a beam width of  $6^\circ$  and a pulse duration of 0.1m/s was used. Thus the echosounder had a pulse length of 0.15m and an effective range resolution of 0.075m. The echosounder was attached to the hull of the boat. For most of the surveys the gain was set to its highest (100) whilst the power was set to its lowest (1).

The echosounder was used to detect the pycnocline and internal waves in the water column. The range of the echosounder was set to measure depth of up to 50m. The horizontal resolution of data collected was 0.5 to 1.5m and the vertical resolution was 0.07m.

### **5.1.6 Summary on Instruments**

The sensors used to collect data in Long Reach were the CTD, ADCP and echosounder. Table 5.1 illustrates the differences between the horizontal and vertical resolution of each sensor. Inspection of the resolution of each sensor showed that the echosounder has the greatest resolution. For the purposes of this study, the images from the echosounder were used to visualize the pycnocline and internal waves in the water column. CTD and ADCP both represent quantitative measurements. It is intended that the CTD data will confirm if the acoustic backscatter from the echosounder is the pycnocline.

Even though the horizontal and vertical resolution of the CTD and ADCP are much less than those of the echosounder, the data collected from these instruments should, when collectively combined, assist in understanding the processes occurring. The ADCP and the echosounder both measure the acoustic backscatter strength; however the

resolution of the echosounder is better than that of the ADCP. Thus the images of the echosounder showed more detail than those of the ADCP. For this research the ADCP backscatter images were processed but were not used. The time used to correlate all the different data types was that of the GPS time.

Table 5.1: The resolution of the ADCP, MVP and echosounder

<b>Sensor</b>	<b>Frequency(kHz)</b>	<b>H. Resolution(m)</b>	<b>V.Resolution (m)</b>
<b>ADCP</b>	600	4	0.5
<b>MVP(CTD)</b>	N/A	400	0.1
<b>Echosounder</b>	200	0.5-1.5	0.07

## 5.2 Processing of Data

To describe the seasonal variation of circulation and stratification in Long Reach, a 2-D vertically oriented profile map (depth(y axis) and distance along (x axis)) was made of each of the survey lines along the axis of the estuary. The orientation of this longitudinal map was in a southwest to northeast direction. The user defines the boundaries of this profile. Thus the display of the salinity, temperature, density, velocity and acoustic backscatter data are all presented re-projected in this common format. The processing of the velocity, echosounder and CTD raw data into the 2D image are now described.

## **5.2.1 Velocity**

The ADCP data represents that of the current magnitude, direction and acoustic backscatter. The procedure used by the OMG to process the raw data into the 2D profile map is now described with reference to Figure 5.6.

### **5.2.1.1 Magnitude**

The raw data file was initially in a binary format however the WinRiver software converts these data into a text file. These text file data consisted of the depth, velocity magnitude, the east velocity component and the north velocity component, vertical velocity, velocity direction, backscatter for the 4 beams, velocity error and river discharge. The data were recorded for each ping.

The OMG software recalculates the resultant velocity magnitude data using the east and north component and then each ping is projected into an array with respect to time and depth. This is performed in the sequence that the data were collected.

Each ping has a specific position assigned and each bin is depth referenced to them. Thus the position along the estuary is calculated and plotted along the 2D map.

The user has the choice of defining the distance each pixel represents on the map. This option is available both in the x direction and in the y direction. However in deciding the resolution of the map, consideration was taken into the actual resolution of the data collected.

The ADCP had an observation approximately every 4m however using 1 pixel to represent 4m was found to be visually noisy. Thus in this study 1 pixel was used to



represent 10m resulting in at least two to three pings being averaged to represent one pixel. This is performed horizontally.

The ADCP also has a vertical resolution of 0.5m which indicates that when projected on the profile there will be only one velocity at that particular depth. For our representation we require a velocity profile image extending to the surface vertically. Thus the shallowest velocity measurement is interpolated up to the surface. Also the deepest good velocity is linearly interpolated to zero at the bottom depth.

#### **5.2.1.2 Direction**

It was mentioned in Section 4.4.1 that the ADCP magnetic compass possesses particular errors. Thus the ADCP velocity direction which was obtained from the magnetic compass also has an error associated with it. To determine the magnetic compass error of the ADCP a comparison is made between that of the boat course made good derived from the GPS position to that of the bottom tracking heading (which uses the magnetic compass). The difference between these two calculated headings is deduced to be the ADCP compass error. This difference is then applied to velocity direction.

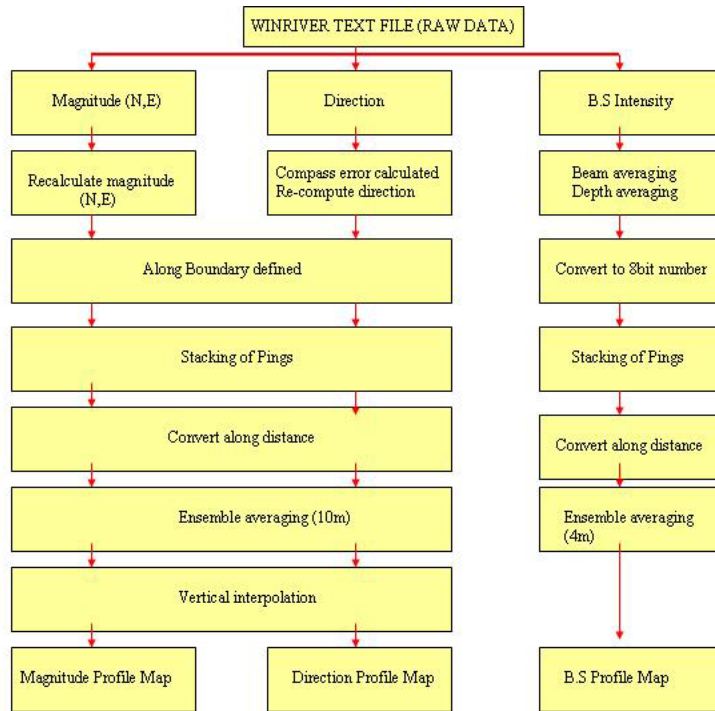


Figure 5.6: Procedure performed for the processing of the ADCP data.

### 5.2.1.3 The Along and Across Velocity

The calculations of the velocity magnitude and direction are performed with respect to a Cartesian coordinate system (see Figure 5.7a). Long Reach is oriented at a 35° bearing. To visualize more effectively the direction and magnitude of the velocity with respect to the orientation of Long Reach the along and across channel velocity magnitude were calculated (see Figure 5.7b, 5.7c). Thus, in this study, the along estuary velocity are visualized in the 2D profile plots.

To further emphasise the magnitude and direction of the velocities arrows, these arrows were overlaid on the 2D surface plots (see Figure 5.8). The arrows were created in Matlab. The direction of the arrows indicated whether the flow of water was upstream (-) or downstream (+).

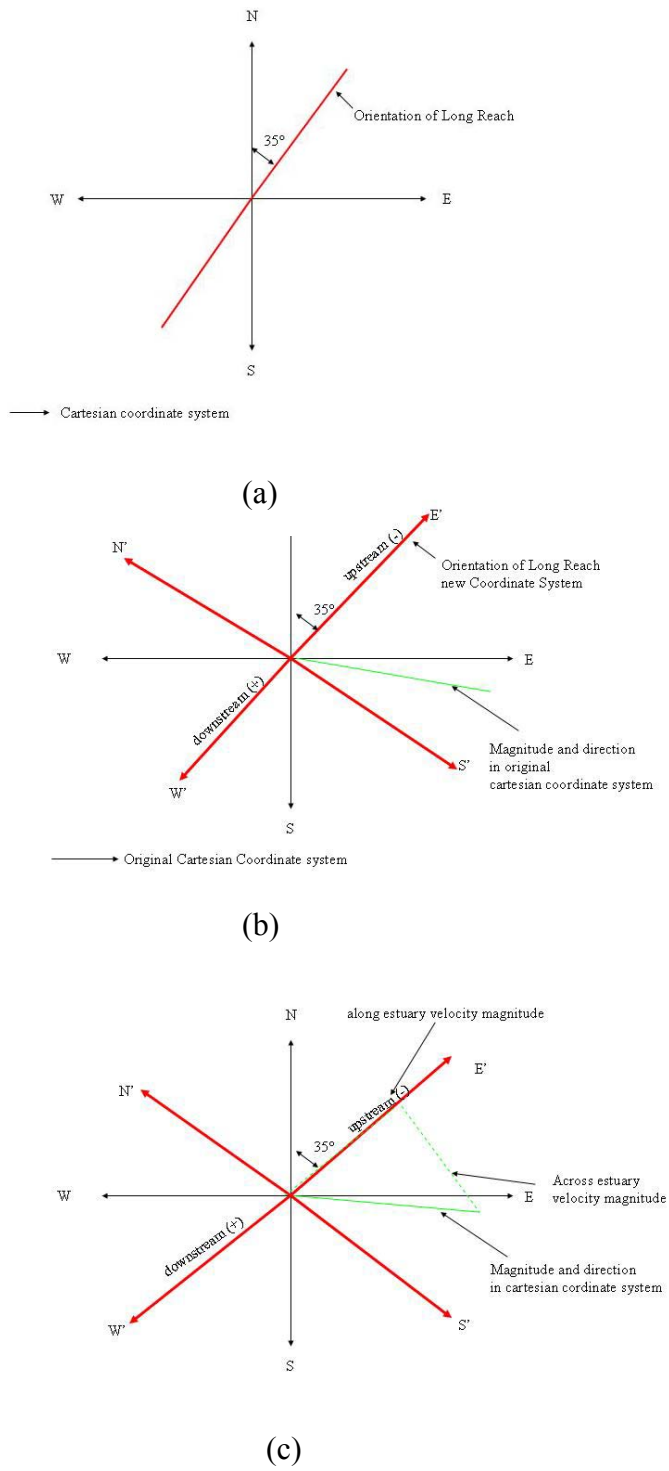


Figure 5.7: Conversion to the orientation of the axis of Long Reach.

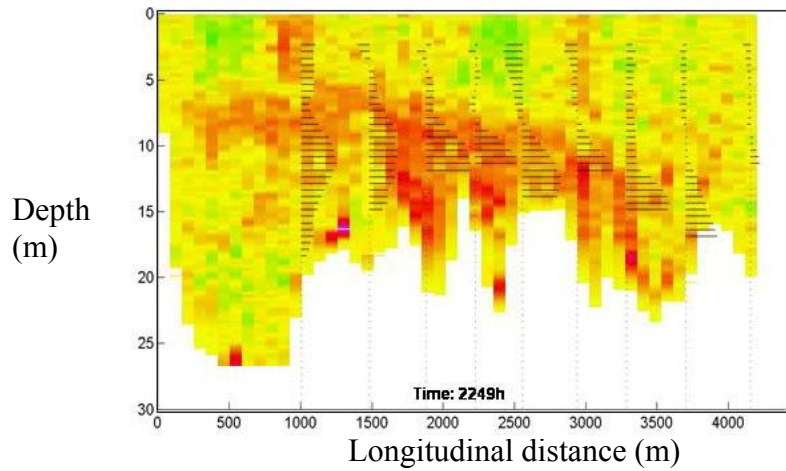


Figure 5.8: The ADCP 2D surface plot of the along channel velocity magnitude data overlaid with the velocity arrows

#### 5.2.1.4 Backscatter

Backscatter data are available for all four beams. Thus this data are averaged to represent the average backscatter. The depth of each beam is also averaged. The value of the backscatter is then converted to represent an 8 bit value and then plotted in the same manner as that of the velocity magnitude and direction.

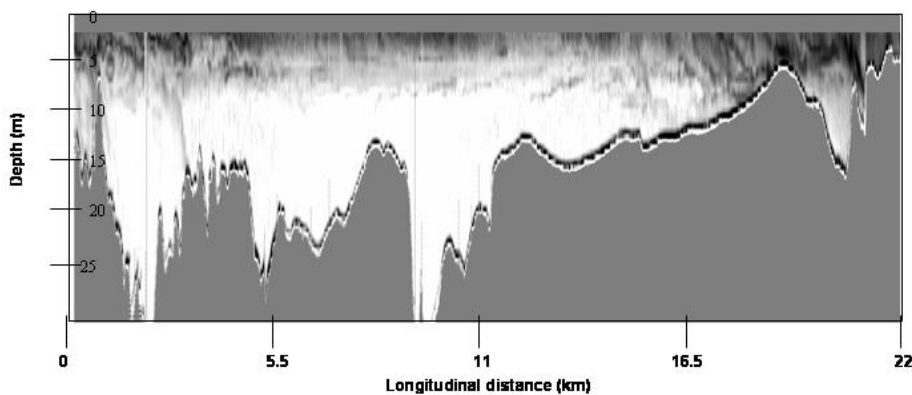


Figure 5.9: Example of the 600 kHz acoustic backscatter profile sourced from the ADCP data

## 5.2.2 Salinity, Temperature and Density Longitudinal Profiles

The CTD measures conductivity, temperature and pressure. From these measurements the density is derived. It should be noted that the CTD quantifies salinity using the Practical Salinity scale of 1978(PSS-78) which is represented by psu.

The OMG software called plotSVP reads the data from the file and projects the information in a 2D surface profile map. Only the CTD casts that fall within the region of the boundary are plotted.

The horizontal resolution of the MVP is ~400m whilst the vertical resolution is 0.1m. To produce a surface image, the data are interpolated to fill the gaps. To emphasise the direction of the flow, the velocity arrows overlay the density plots (see Figure 5.10b).

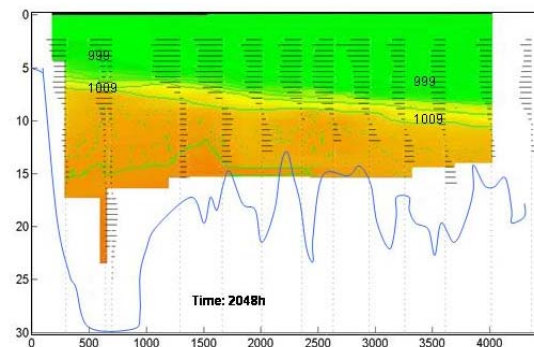


Figure 5.10: 2D surface plot of the density overlaid with the velocity arrows.

## 5.2.3 Echosounder

The echosounder was used in this study to identify the pycnocline and internal waves. The data from the echosounder are in binary format. The OMG software (called knud2glo) reads the raw data file (.keb file) and converts it into an OMG format (.merged file).

Conversion to the OMG format includes: calculation of the depth and reading the time, echo strength, gain, power level and pulse length. It should be noted that the echo strength is corrected by the echosounder by  $40\log R$  for the spherical spreading loss assuming incoherent scattering.

Another OMG software called MakeSeisPlot reads the information from the .merged file and creates a seismic plot of the echo intensity. The y axis of the seismic plot represents the depth whilst the x axis represents the distance along. The user defines the horizontal and vertical resolution of the plot. For the seismic plot the original echo strength data are logged as a linear intensity in 16bit. The data are converted to a logarithmic display in 8 bit. Figure 5.11a shows an illustration of the acoustic backscatter images.

The acoustic backscatter images are overlaid with the density contours (which were produced in matlab) to confirm that the acoustic backscatter strength was that of the pycnocline and not zooplankton or suspended sediments (see Figure 5.11b).

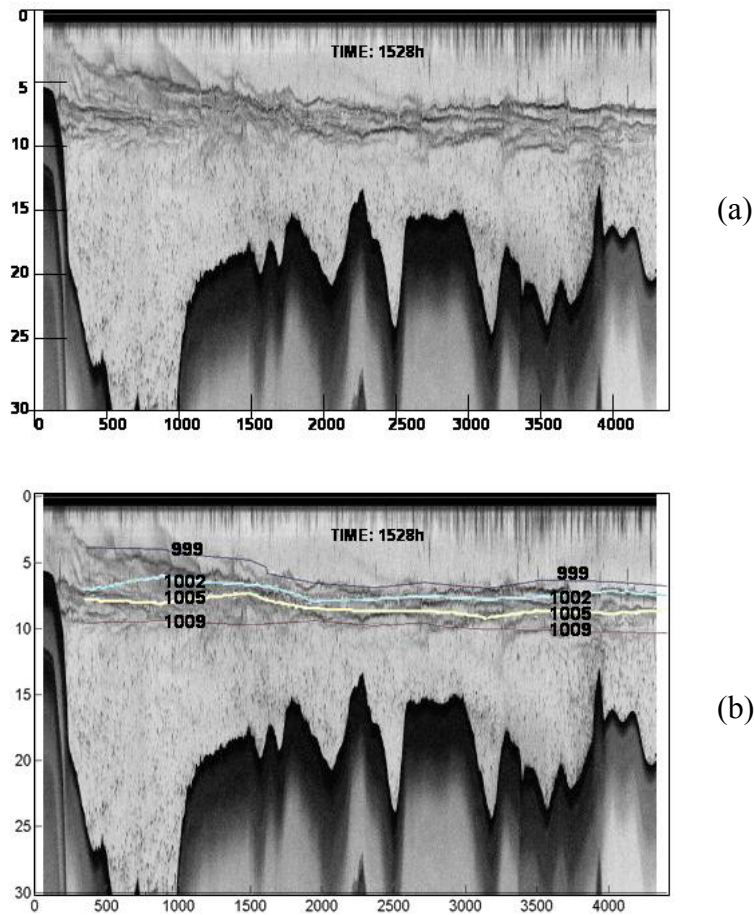


Figure 5.11: The original acoustic backscatter images (a) and the images overlaid with the density contours (b).

### 5.3 The 2003 Seasonal Surveys

The purpose of the 2003 surveys was to remap the seasonal stratification of Long Reach using instruments with improved resolution. The previous research performed in Long Reach by Trites [1959 and Metcalfe et al. [1976] hint at the possibility of mixing or advection processes occurring in the summer (see Section 2.5). Since then there have been improvements of survey sensors and the introduction of new survey sensors such as the ADCP, echosounder and the MVP. These sensors now allow the characteristics of the

water column to be mapped with a greater resolution (horizontally and vertically and with respect to time).

It is intended that the 2003 surveys shall reconfirm Trites [1959] and Metcalfe et al. [1976] results and that the observations made may result in a better understanding of the processes taking place in Long Reach.

### **5.3.1 The 2003 Survey Plan**

Surveys were performed in Long Reach for May 2003, September 2003, October 2003, November 2003 and February 2004. The survey sensors used were the ADCP, MVP and an echosounder. Survey lines were performed along the axis of the estuary from Woodmans Pt to Oak Pt (22km distance), the exception was in February 2004 when Long Reach was covered by ice and a cross-sectional survey within the vicinity of Public Landing was made using bore holes. The results of these surveys are illustrated with respect to longitudinal profiles of the salinity, temperature, density and the acoustic backscatter. For February 2004 only a cross-section of the CTD data is displayed.

### **5.3.2 The 2003 Results**

The salinity and temperature for September 2003 (see Figure 5.13) showed a strong correlation to the density profiles (less dense, warmer, fresh water overlay more dense colder, salty water) (see Figure 5.12). For the months of May, October, November 2003 and February 2004 (see Figure 5.12, 5.13, 5.14) fresh water overlays salty water but the surface fresh layer is colder than the bottom salty layer (warmer). However the density profiles still maintain statically stable conditions (less dense overlay more dense



waters). This observation verifies that the salinity is the major component affecting the density structure in Long Reach. These observations were similar to that observed by Trites [1959] and Metcalfe et al. [1976]. The density structure is now used to describe the 2003 results.

### **5.3.2.1 Density Structure**

The density structure for the month of May resembled that of a vertically homogenous estuary. The surface and bottom layer consisted of fresh water (density of  $998\text{kg/m}^3$ ; salinity of 0‰ to 0.5‰). However at the bottom of the deep hole hot saline waters were present (see Figure 5.12). This survey is similar to the results of Trites [1959] and Metcalfe et al. [1976] for spring (see Section 2.5). It can now be hypothesized from these results that the warm salty water that was present in the deep holes originates from the previous summer months.

For the month of September, at various locations in Long Reach, the stratification varied from resembling a partially mixed estuary to a highly stratified estuary. This survey was performed one day after spring tides at approximately low tide. Overall the surface layer consisted of fresh water (density of  $1000\text{kg/m}^3$ ; salinity of 2.5 psu; temperature of  $18^\circ\text{C}$ ) whilst the bottom layer basically consisted of salty water (density of  $1013\text{kg/m}^3$ ; salinity of 19.0 psu; temperature of  $15^\circ\text{C}$ ). These two layers were separated by a well defined pycnocline (see Figure 5.12) of  $\sim 3.5\text{m}$  thickness. The salinity structure resembled the observations made by Trites [1959] and Metcalfe et al. [1976] for the summer (see Section 2.5).

There exists a difference in bottom density (due to salinity) from the entrance of Long Reach to Carter's Pt. Within this area the bottom waters were more dense than the remainder of the estuary (salinity of 21.0 psu; temperature of 15°C; density of 1015kg/m<sup>3</sup>). This observation indicated that either saltier water from downstream is advected into Long Reach or that mixing events were occurring in the remainder of the estuary.

The density and acoustic backscatter profiles at the pycnocline suggest that mixing and/or advection processes possibly occur at two specific regions in Long Reach: within the vicinity of Woodsman's Pt to Craig Pt, where there exists irregular bathymetry (referred to as Area 1) and Kimble Cove to Oak Pt, where the bathymetry shoals to ~8m (referred to as Area 2) (see Figure 5.12, 5.15(a)).

Zoomed in illustrations of the acoustic backscatter images, showed the presence of two types of internal waves in Long Reach. (see Figure 5.16). Within the vicinity of Area 1 small amplitude periodic waves with a wavelength varying between 15m to 30m are observed. Within Area 2 the waves take a different shape and resembled that of the KH waves described by Dyer [1997] and observed by Geyer et al. [1989] (see Section 3.3). The KH waves appeared to the right of the sill and the wavelengths varied from 15m to 30m (see Figure 5.17). The amplitude of the KH waves also varied.

At the Oak Pt sill the small amplitude periodic waves observed in Area 1 were present (see Figure 5.16(7)). However the amplitude of the wave appears to have increased and the plunging of the pycnocline at the sill occurred. A decrease in density in the layer of water below the pycnocline takes place in both Area 1 and Area 2. In the area between Area 1 and Area 2 the density is constant in both the surface and bottom layer,

thus a sharp interface exists between the fresh and salt water. Thus the pycnocline is flat in this section of the estuary (see Figure 5.12, 5.13, 5.16(3, 4, and 5)).

For the month of October Long Reach resembles that of a highly stratified estuary. This survey was performed 5 days before spring tides at approximately rising tide. The stratification of the estuary was similar to the density structure observed by Trites [1959] and Metcalfe et al. [1976] for autumn. The main differences between the observations of September 2003 and October 2003 were:

- The surface and bottom waters were both less dense (surface: salinity of 1.0 psu; temperature of 12.5C; density of 1000kg/m<sup>3</sup>, bottom: salinity of 18.0 psu; temperature of 14.5° C, density of 1013kg/m<sup>3</sup>) in October than those of September 2003
- The saltier water observed entering at the entrance of Long Reach in September was no longer present
- The pycnocline thickness had decreased to ~2m in October. This implies a stronger vertical density gradient
- The bottom temperature in Long Reach shows that the upstream section is warmer than the downstream section (see Figure 5.13). The decrease in temperature in the downstream section occurs because the salt water in the Bay of Fundy is getting colder due to the decrease in air temperature. Thus the salt water that now advects upstream in Long Reach is colder than that from the summer months. This implies that the hotter water originated from the summer months, whilst in the downstream section the waters originate from the autumn months

Similar to the September 2003 survey, observations in October at the pycnocline, appear to indicate where mixing processes were taking place. However these processes were now observed to occur all the way from Woodsman's Pt to Victoria Shoals (see Figure 5.12, 5.15(b)). The sinusoidal interfacial waves observed in Area 1 in September 2003 now also exist from Woodsman's Pt to Victoria Shoals. These waves have a wavelength of 15m to 30m and are concentrated around the areas of undulating bathymetry. At Oak Point KH waves were observed in September 2003. However for October 2003 the KH waves are not present (see Figure 5.18).

The survey in November occurred two days before spring tides at approximately rising tide. For the month of November the MVP was programmed specifically to dip 1m from the seabed. The stratification structure resembles that of the well mixed estuary observed in May 2003. A salinity content of 0.05 psu, temperature of 8° C and density of 999kg/m<sup>3</sup> exists (see Figure 5.12, 5.13). However specific effort was made to traverse within the deep hole areas. Within these deep hole areas salty water is present (salinity of 17.0 psu, temperature of 13°C and density 1012kg/m<sup>3</sup>).

The acoustic backscatter images also show the salty water of the deep holes. There also appears to be evidence of mixing and/or advection taking place in the layer above the salty water (see Figure 5.19). The

For February 2004 the survey was performed three days before spring tides. The stratification resembles that of a highly stratified estuary at this location. The surface fresh, cold surface water (salinity of 0 psu, temperature of -8° C and density 998.5kg/m<sup>3</sup>) lies over by salty, warmer water (salinity of 19.0 psu, temperature of 1° C and density

1015kgm<sup>3</sup>) (see Figure 5.14). From the cross-section there appears to be a slight upward tilt of the pycnocline towards the south of Long Reach.

Assuming that the surface in February was level and the flow was upstream, indicates that the Coriolis force would be acting towards the right of the flow (because we are in the northern hemisphere) and this the compensating pressure force would be acting towards the north of Long Reach.

Calculation of the velocity of the upper and lower layer flow (using the pressure gradient force ( $1/\rho * dp/dx$ )) results a velocity shear of 0.15. This geostrophic calculation has the advantage over instantaneous ADCP results in that the regional tilt represents a channel width estimate of the velocity shear.

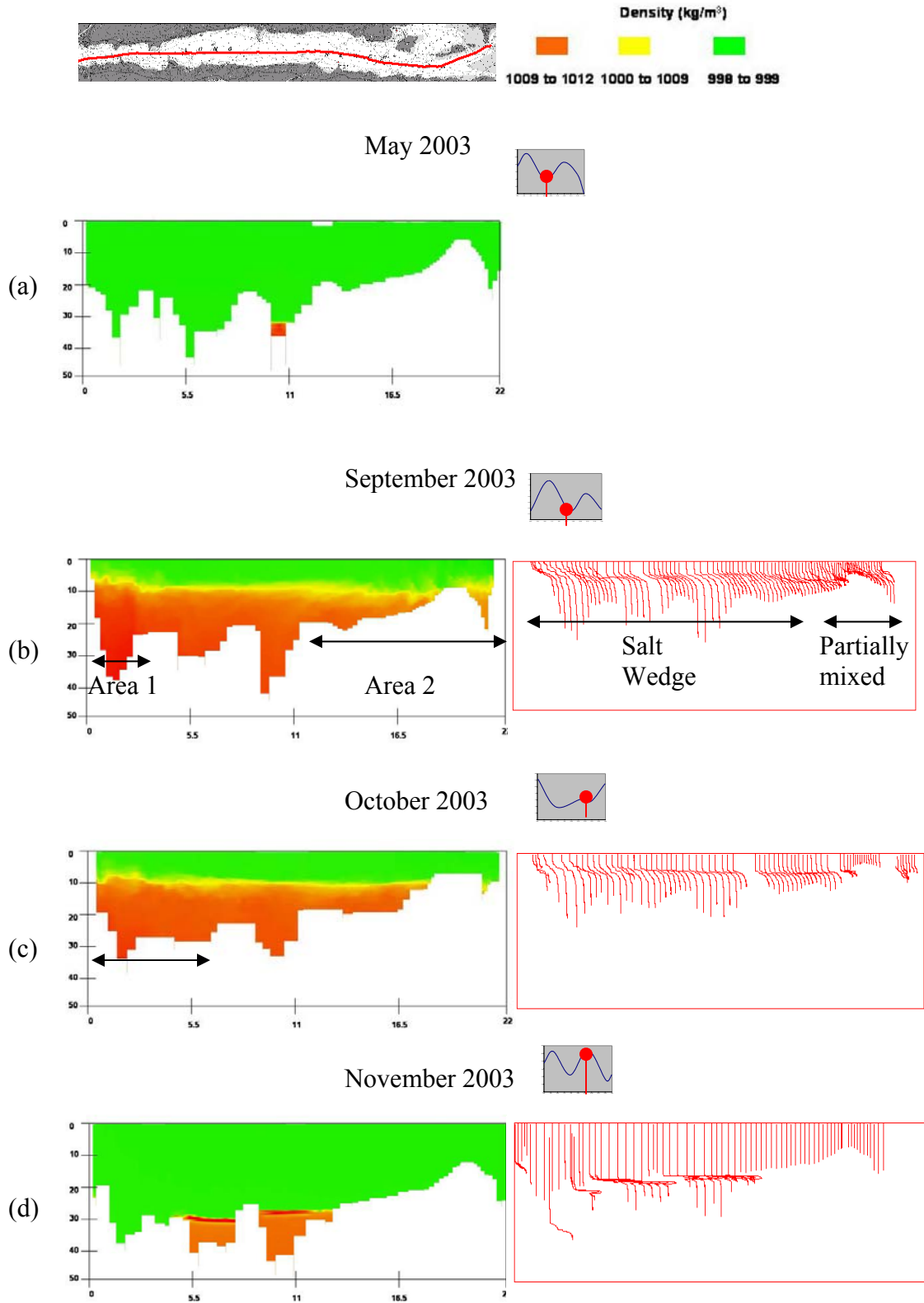


Figure 5.12: Longitudinal profile plots (left) and individual density profiles of the density for the year 2003.

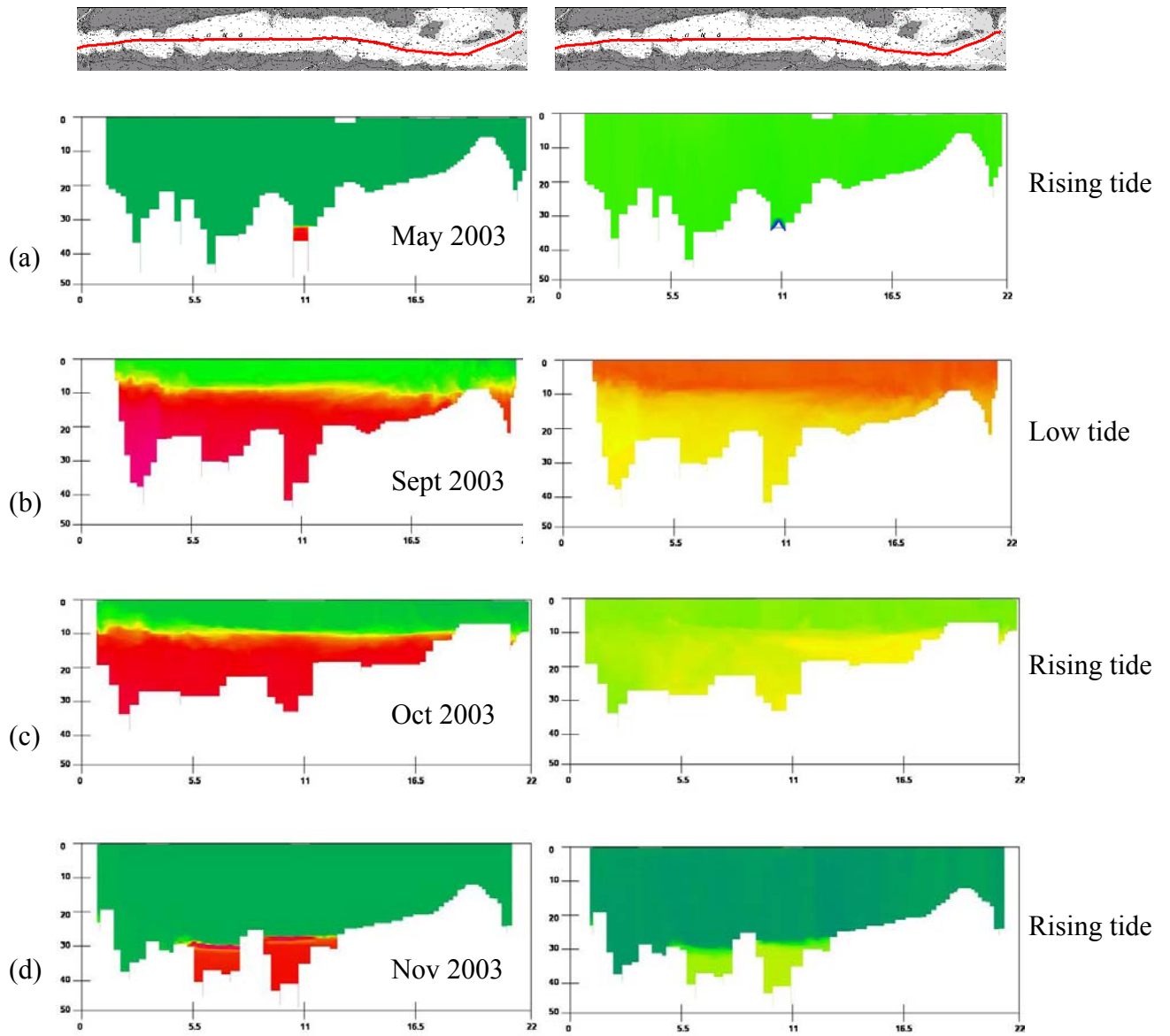


Figure 5.13: Longitudinal surface profile plots of salinity (left) and temperature (right) for the year 2003.

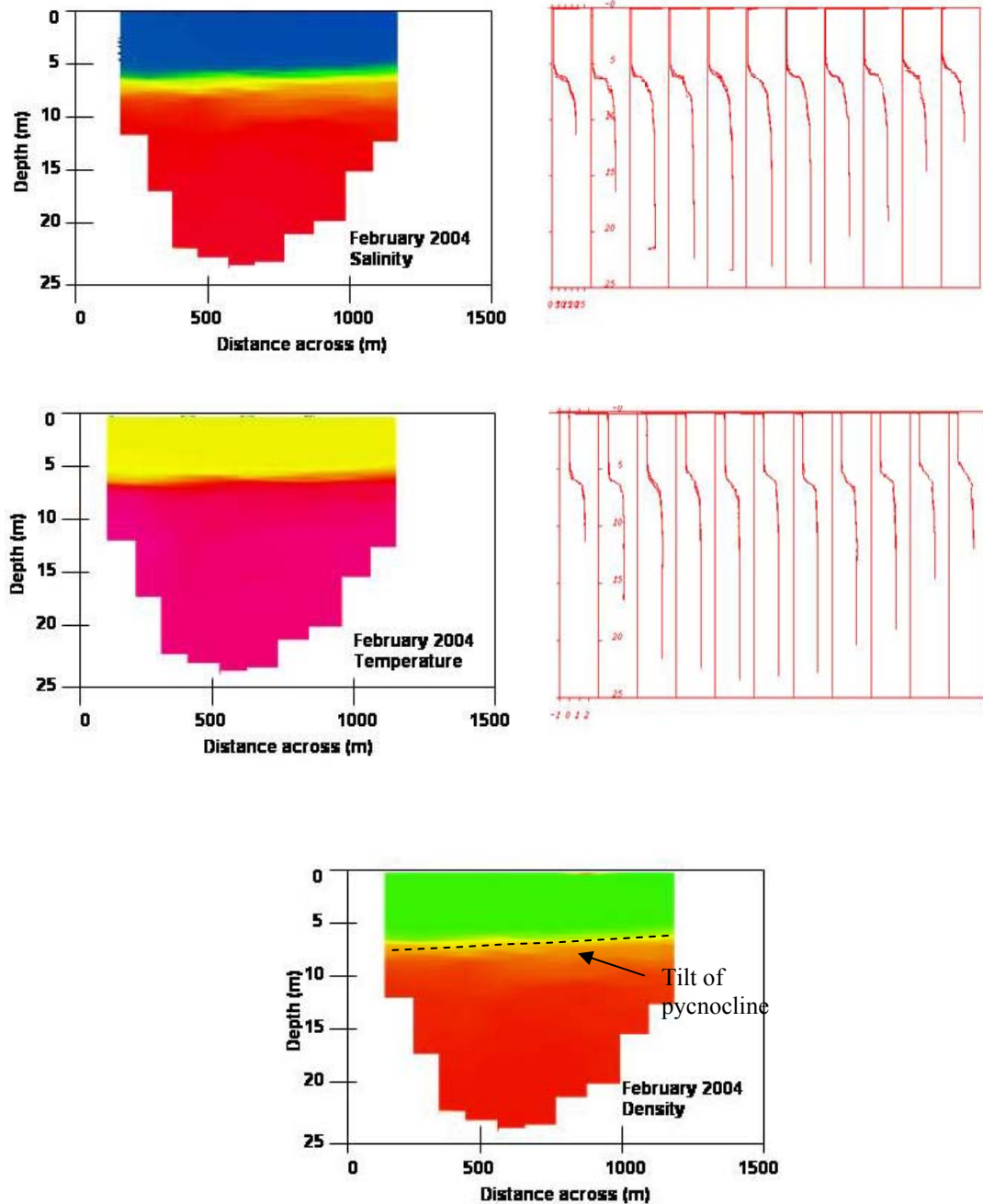
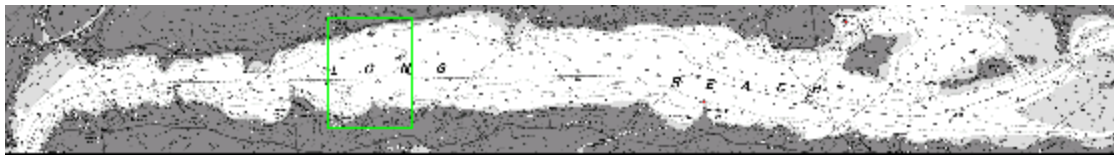


Figure 5.14: Cross-sections of salinity, temperature and density surveyed in February 2004.



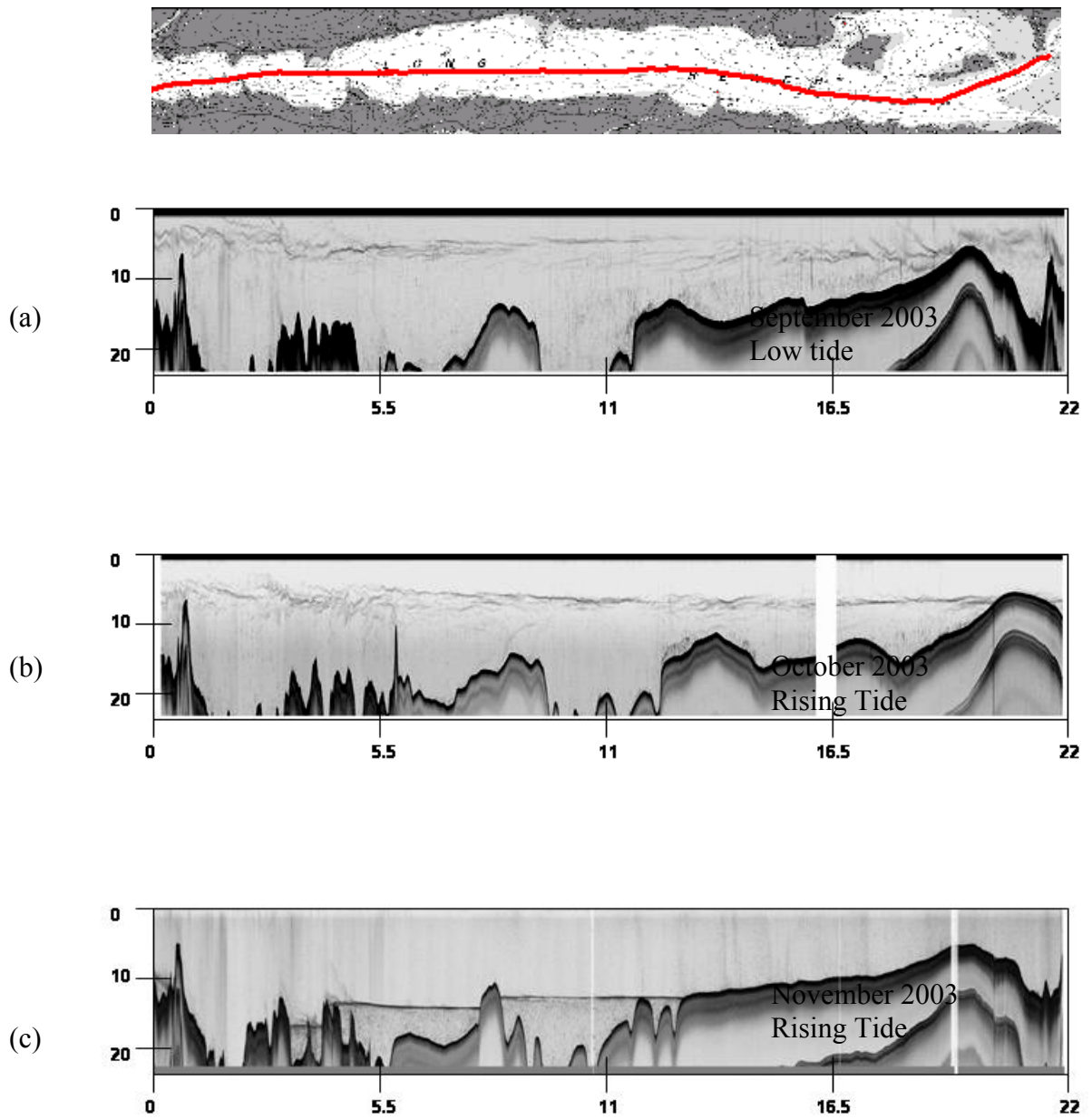


Figure 5.15: Acoustic backscatter images for the year 2003.

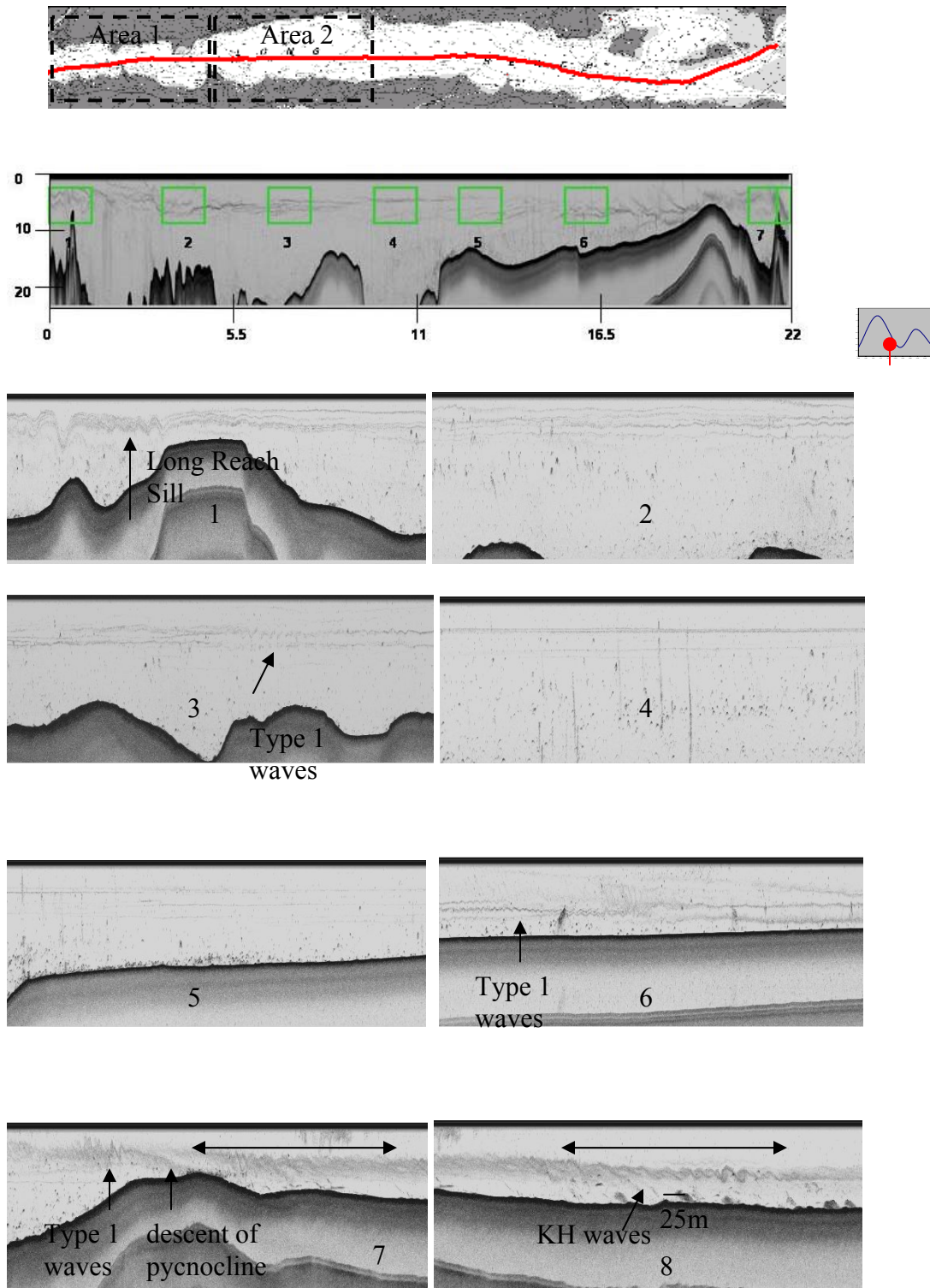


Figure 5.16: Zoomed in illustrations of the pycnocline for September 2003.

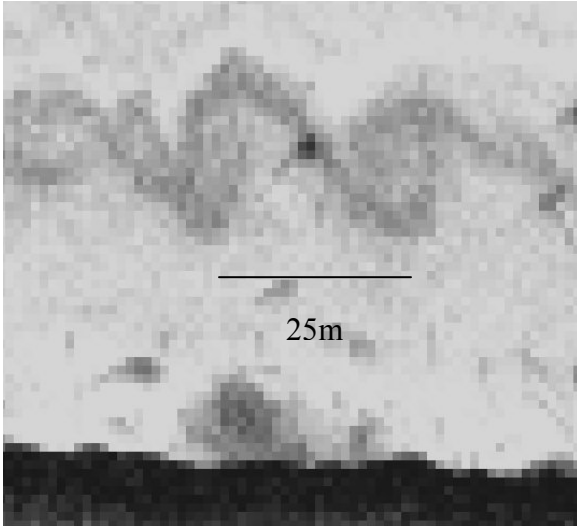


Figure 5.17: Zoomed in image of a Kelvin-Helmholtz wave from the September 2003 survey. The waves are located on the lee side of the Oak Point sill. Zoomed in from Figure 5.14 (8).

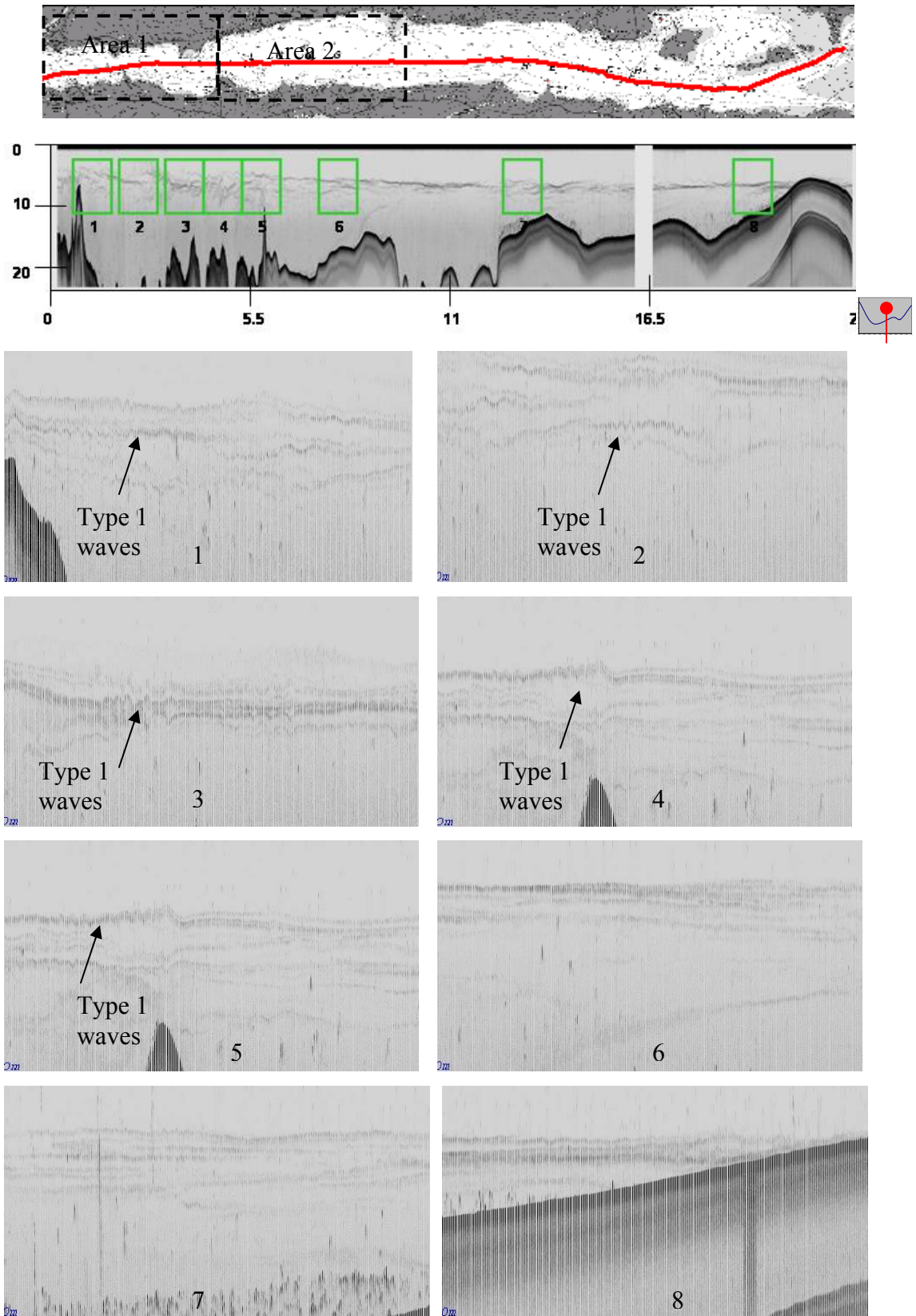


Figure 5.18: Zoomed in illustrations of the pycnocline for October 2003.



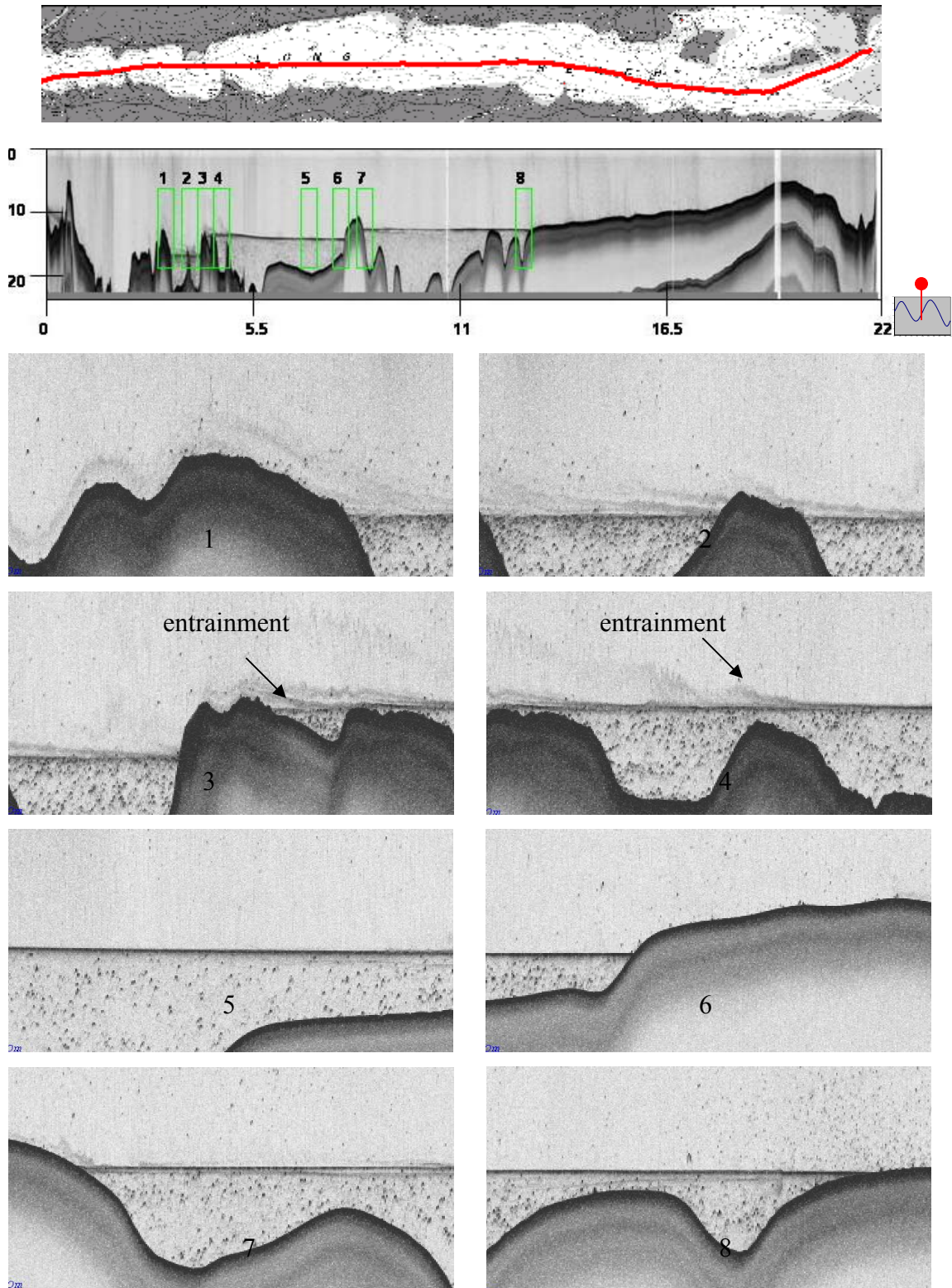


Figure 5.19: Longitudinal profile of the echosounder images for November 2003.

### **5.3.3 Summary of 2003 Results**

The 2003 surveys verify the observations of Trites [1959] and Metcalfe et al. [1976] that a seasonal variation of the stratification pattern in Long Reach exists. In the Trites [1959] and Metcalfe et al. [1976] studies, mixing and/or advection processes were only implied from lateral density gradients. The acoustic imagery taken in the 2003 surveys has confirmed that interfacial turbulent mixing does indeed exist in Long Reach.

There appears to be processes taking place at the pycnocline for the month of September and October when the River discharge is low or moderate. Inspection of the acoustic backscatter images shows two types of interfacial waves. In the September 2003 survey KH waves are identified within the vicinity of the Oak Pt Sill and small amplitude periodic waves at various locations. In October 2003 the KH wave is not present at the interface at Oak Point. The internal waves observed appear to be influenced by the bathymetry and flow conditions of Long Reach mainly occur in the lower section and get weaker as the geometry of the area widens by Public Landing.

It should be noted that these surveys were performed along the axis of the estuary at arbitrary phases of the tide. To accurately understand and describe the changes occurring in Long Reach requires observations for the duration of a tidal cycle. These observations should also be performed under different flow conditions. The 2004 survey plan takes into consideration the observations obtained seasonally, the bathymetry of the area and the processes occurring at the interface.

## 5.4 The 2004 Survey Plan

Based on the along-estuary oceanographic surveys performed in 2003 the decision was taken to investigate the processes occurring from Woodman's Point to Victoria Shoals (see Figure 5.20). This area was decided upon based on the variation in bathymetry that existed and the processes that were observed to be taking place at the pycnocline.

The area (Woodmans to Victoria Shoals) was surveyed at both neap and spring tides. This was performed to observe the effects that varying tidal velocities might have on stratification and mixing. The survey was designed to occur in the summer when the river discharge was expected to be near its lowest.

The section to be surveyed was ~9km in length and a vessel speed of 4m/s was used. It was calculated that using a 9km survey line would take ~45 minutes to complete. It was assumed that this repeated interval would hinder upon the resolution of observations (with respect to time) of the mixing events. If mixing is taking place it was important to capture these events.

Thus the section from Woodmans Point to Victoria Shoals was split into two sections: section 1 from Woodman's Point to Carters Point and section 2 from Carters Point to Victoria Shoals (see Figure 5.20). A survey line at each section was estimated to take approximately 20mins. The consequence of dividing the survey area into two sections was that only one of the sections will be surveyed exactly at neap and spring tides.

For each of these sections, a survey line was traversed back and forth over the duration of a tidal cycle for both neap and spring tides occurring in the month of

September 2004. Table 5.2 shows the sections and the amount of survey lines in a tidal cycle.

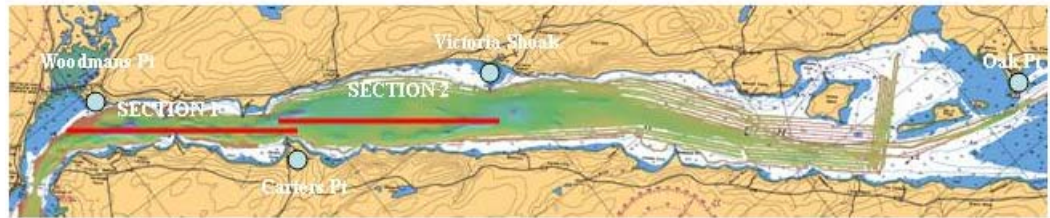


Figure 5.20: Map of Long Reach showing the survey areas of section one and section two.

Table 5.2: Dates and phase of the tides of the surveys performed. The asterisk indicates the exact dates of neap and spring tides.

Section	Date	Moon Phase	Number of S.lines
Section 1	7 <sup>th</sup> Sept 2004	*Neap	38
Section 2	5 <sup>th</sup> Sept 2004	Neap	37
Section 1	14 <sup>th</sup> Sept 2004	*Spring	36
Section 2	15 <sup>th</sup> Sept 2004	Spring	38



### **5.4.1 Procedure for Calculation of Gradient Richardson Number**

Obtaining the gradient Richardson number requires calculating the density gradient and velocity gradient. The ADCP data have a vertical resolution of 0.5m whilst the CTD profiles have a vertical resolution of 0.1m. The horizontal resolution of the ADCP is ~4m whilst the CTD casts are ~400m.

To calculate the Richardson number required that the velocity and density data be at the same horizontal position. Based on the position of the CTD casts a depth average was made of all the pings that were within a 200m radius of the MVP profile (see Figure 5.21). This was performed using the OMG software. The final velocity for a particular depth represented the average of all pings within a 200 m radius of that area. This vector was then converted to the along and across stream velocity of the estuary. The along stream velocity component was used for the calculation of the Richardson number.

To calculate the density gradient also required the averaging of the CTD data vertically. The CTD data had a vertical resolution of 0.1m whereas the ADCP data had a vertical resolution of 0.5m. Thus taking the depth of the ADCP all the CTD data is averaged to coincide with that of the ADCP depth.

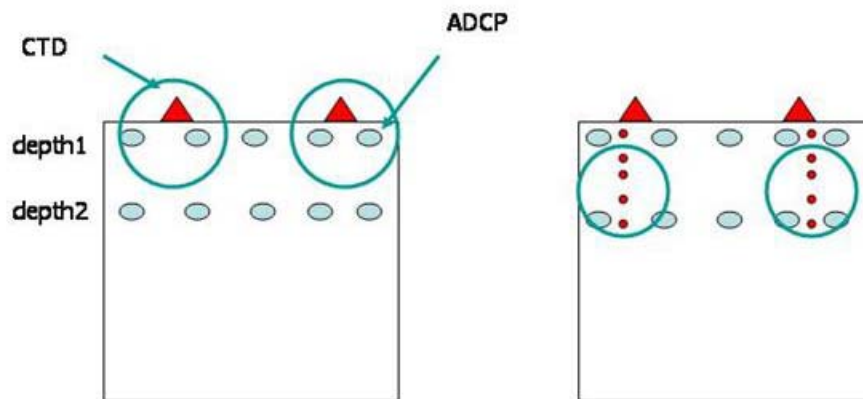


Figure 5.21: Procedure for averaging of the velocity and density data.

## 5.5 Summary on Survey Plan

Reconnaissance surveys (using ADCP, CTD and an echosounder) performed in Long Reach found that during the summer and autumn months, interfacial mixing processes appeared to be taking place at two locations in Long Reach: Woodsman's Pt to Victoria Shoal and Kimble Cove to Oak Pt. The in between region appears to be less active even though the velocity shear still existed.

To investigate in detail the mixing processes taking place from Woodsman's Pt to Victoria Shoal, surveys were designed for implementation in the summer of 2004. These surveys were designed to:

- Investigate the dominant mixing process occurring in Long Reach for the duration of a tidal cycle.
- Observe the dominant processes present at neap and spring tides

- Determine the influence of bathymetry and stratified flow on the dominant processes in Long Reach.

To visualize the observations made in the 2004 tidal cycle surveys, longitudinal profiles of density, along stream channel velocity and acoustic backscatter were used. To determine if mixing process are occurring in Long Reach the gradient Richardson number is employed along with a linear stability analysis.

## CHAPTER 6

### ANALYSIS: SECTION ONE

In stratified environments, variations in density, velocity and acoustic volume backscatter can occur both temporally and spatially. Observations of these variations tend to aid in understanding the processes of advection and turbulent mixing. Field studies that have used these observations include Geyer and Farmer [1989] (Fraser River Estuary), that monitored the collapse of a salt wedge at ebb tide and Farmer and Smith [1980] (Knight Inlet Sill in British Columbia), that monitored the dynamics over a sill in Knight Inlet.

These observations may be analysed both descriptively (visual inspection) and dynamically (mathematically). A descriptive analysis approach tends to serve as a general understanding of the possible processes that may be occurring. The dynamical analysis identifies these processes.

Studies that have used a descriptive analysis approach include Trites [1959] and Hughes Clarke and Haigh [2005] (Saint John River Estuary, N.B). The dynamical approach has been employed by Kay et al. [2003] (Columbia River Estuary) and Zhu and Lawrence [1996] (the Strait of Gibraltar and Hamilton Harbour) who combined a dynamical approach with laboratory experiments.

This research in Long Reach first employs a descriptive analysis approach, where variations in the longitudinal profiles of velocity, density and acoustic volume backscattering are inspected. Observations of the profiles indicate that Long Reach is statically stable at the time of survey. However particular processes appear to be

occurring at the interface, at specific locations and at specific times. These observations are presented in Section 6.2.

Based on the results of the descriptive analysis, a dynamical analysis approach is implemented. The dynamical approach used in this study takes the following steps: (1) The gradient Richardson number is employed to determine whether the processes observed at the interface could be a result of mixing; (2) in the event that mixing is occurring, a linear stability analysis using the normal mode approach is performed in an attempt to identify the type(s) of instability(s) that may possibly have initiated the mixing process. These results are presented in section 6.3.

This chapter analyses both descriptively and dynamically the processes occurring in section one of Long Reach. The results of section two are presented in Chapter 7.

## **6.1 Bathymetry of the Study Area: Section One**

The survey area is ~4.5km in length with the width varying from 300m to 800m and a depth range of 5m to 42m (see Figure 6.1 a). Four of the main observations made of the survey area are:

- The thalweg isn't always at the centre of the channel
- Several scours and possible channels exist
- At various locations the width of the estuary contracts and there is a decrease in the bathymetry
- When the width expands the depth increases

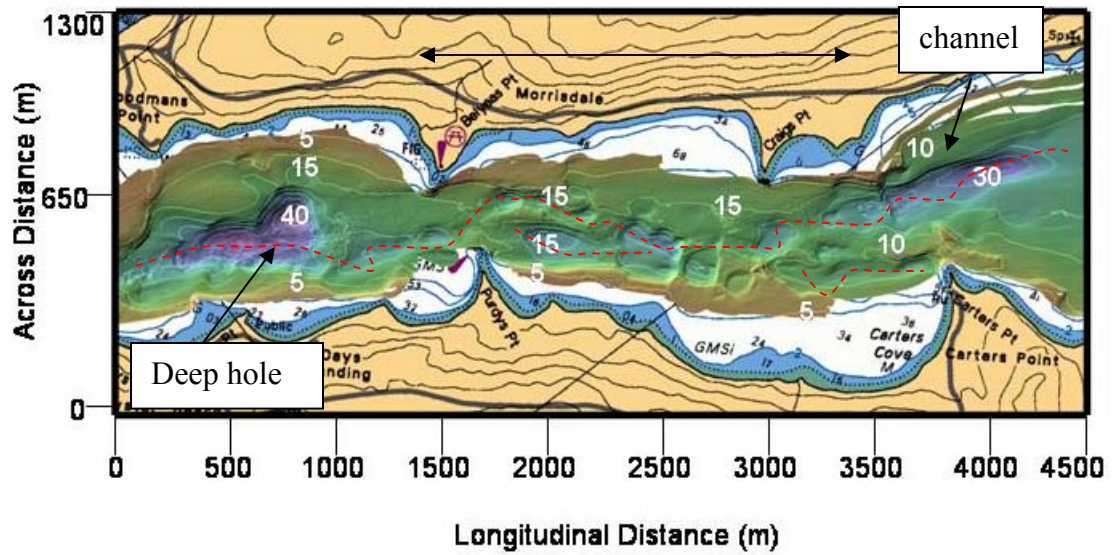


Figure 6.1 (a): Plan map of section one. The red dotted line shows the path of the deep areas.

At the entrance to the survey area the width is ~800m and the depth of the thalweg is on average 17m. This is soon followed (500m upstream) by an increase in depth to 42m where a deep hole area exists (see Figure 6.1b).

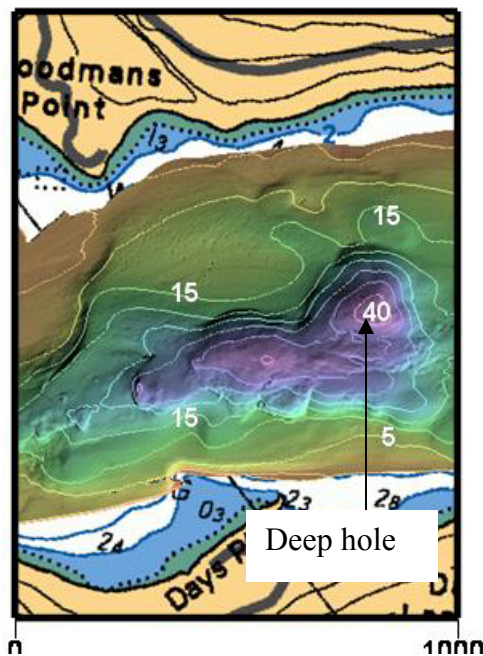


Figure 6.1(b): Plan view map of the 42m deep hole.

At 1700m upstream, within the vicinity of Belyeas Pt. and Purdy Pt. the width decreases to 300m and the depth varies from 13m to 25m. Upstream of these two constrictions the bathymetry is irregular (see Figure 6.1c). At Craig Pt (3000m upstream) another constriction exists with the estuary width of 600m and a thalweg depth of 25m. The average width of the irregular section is 700m and the depth varies from 13m to 25m.

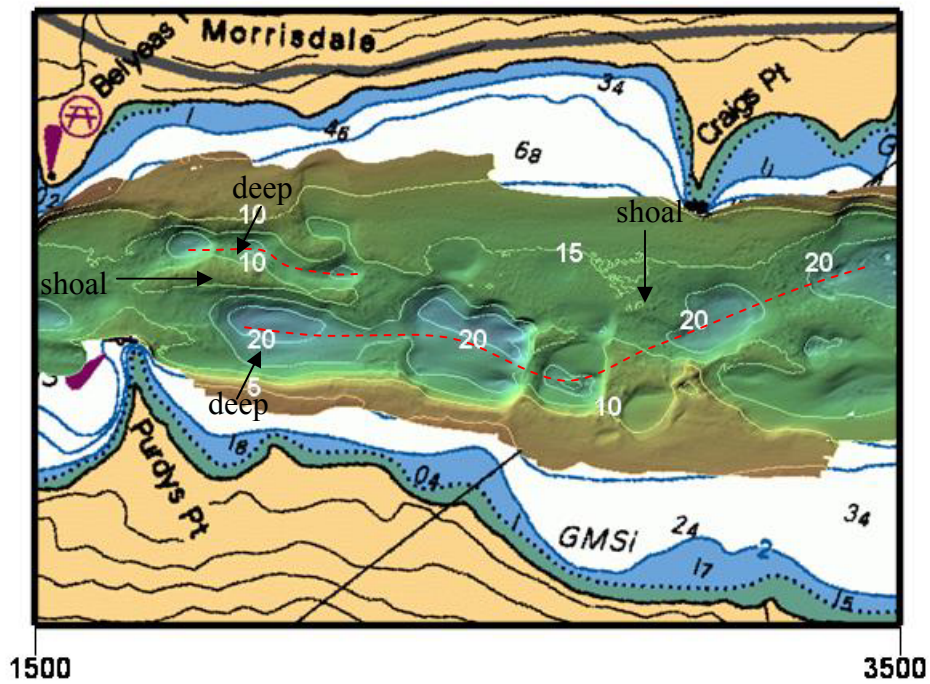


Figure 6.1(c): Plan view map of the area that constrictions exist both laterally and vertically.

At Carters point (4000m upstream) another constriction exists with a width of 600m. To the north of Carters Pt a deep channel of ~30m exists.

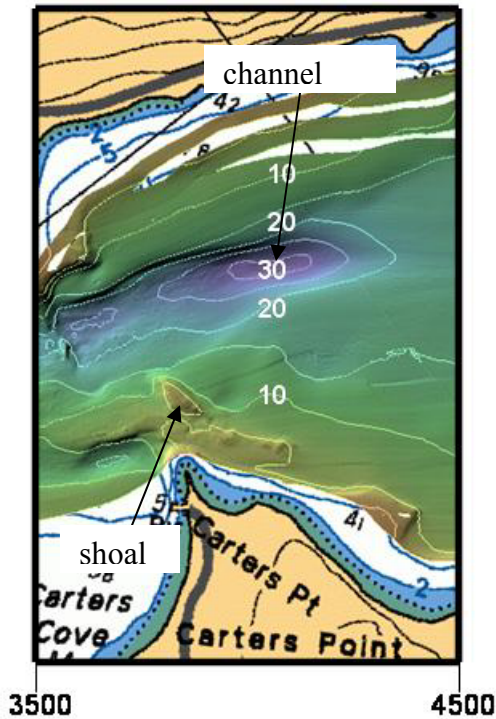


Figure 6.1(d): Plan view map at Carters Pt showing shoal and possible channel.

## 6.2 Descriptive Analysis: Section One

This section describes the density, along channel velocity and acoustic volume backscatter images. The main purpose of performing this is to compare the similarities and differences that occur both spatially and temporally with the various properties of the flow. This comparison may allow us to better understand the processes that are occurring.

The surface and bottom waters are referred to as the 0m to 3m and 12m to 42m depth ranges respectively. It should be cautioned that the current velocity data for the



surface two metres were not measured due to the blanking distance and the draft of the ADCP. The CTD casts were also programmed to dip 2m off the bottom, thus it is assumed that the bottom 2m of the waters are homogenous with the temporal set of the bottom most measured values.

The neap tidal cycle (7<sup>th</sup> September 2004) is described completely, followed by a brief overview of the spring tidal cycle (14<sup>th</sup> September 2004). The observations made in Long Reach shall be referenced with respect to the different phases of the tide (high, falling, low and rising) which are based on the data collected from the tide gauge at Days Landing (see Figure 2.2). Table 6.1 shows the duration of the different phases of the tide. A variety of characteristics were observed during the falling and rising phases of the tide. As a result, the observations for these two phases were further subdivided into early falling/rising tide, mid falling/rising tide and late falling/rising tide.

Table 6.1 shows that high/low tide periods are ~1.5 to 2.0 hours long. In this study of Long Reach the terminology exact low tide is used, this time is referred to as the peak point of low tide.

In this section, observations of the density and velocity structure are first presented followed by the acoustic volume backscatter.

### 5<sup>th</sup> and 7<sup>th</sup> September 2004 Tidal Cycle Graphs

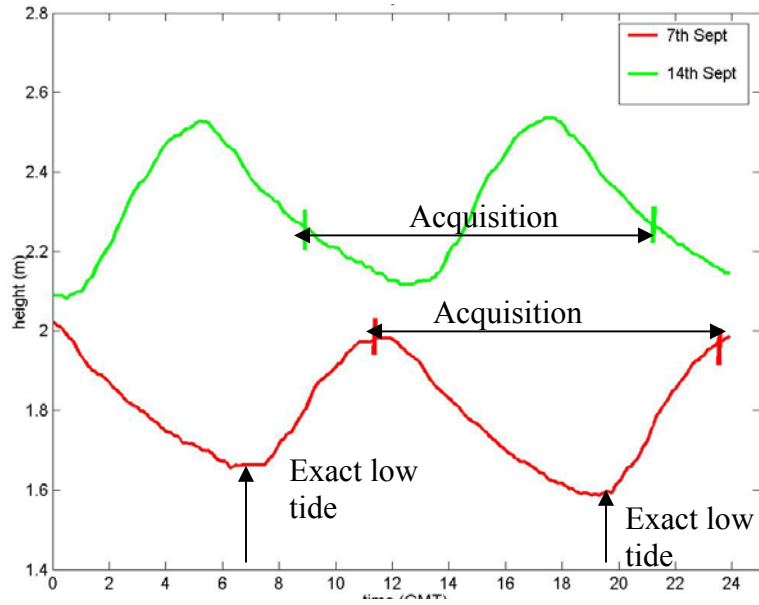


Figure 6.2: Graph of the tidal cycle for the neap (7<sup>th</sup> September 2004) and spring tides (14<sup>th</sup> September 2004). Tidal data was collected at Days Landing.

Table 6.1: The time periods for the different phases of the tides for 7<sup>th</sup> September 2004 (Neap) and 14<sup>th</sup> September 2004 (spring)

Tidal Phase	Time(h): 7 <sup>th</sup> Sept. 2004	Time(h): 14 <sup>th</sup> Sept. 2004
	Neap	Spring
<b>High</b>	1100 to 1235 (1.58h)	1700 to 1900 (2h)
<b>Falling</b>	1235 to 1820 (5.75h)	0930 to 1200 (2.5h) & 1900 to 2035 (0.58h)
<b>Low</b>	1820 to 2010 (1.83h)	1200 to 1400 (2h)
<b>Rising</b>	2010 to 2355 (3.75h)	1400 to 1700 (3h)

### **6.2.1 Density Structure: Section One**

The oceanographic surveys performed in September 2004 found section one to be highly stratified. The density observations show that the surface (fresh water with density of  $998 \text{ kg/m}^3$ , salinity 0.2 psu and temperature of  $19^\circ\text{C}$ ) and bottom waters (salty water with density of  $1011 \text{ kg/m}^3$  to  $1012 \text{ kg/m}^3$ , salinity 15.0 psu to 17.0 psu, temperature of  $16^\circ\text{C}$ ) are separated by a well defined pycnocline which has an average thickness of 2m. This stratification of the estuary is observed throughout the tidal cycle (see Figure 6.3).

Observations of the longitudinal profiles of the density structure shows that throughout most of the tidal cycle the surface and bottom densities remain constant (see Figure 6.4). However two exceptions are observed: (1) in the 'deep hole' area, located  $\sim 700\text{m}$ , the density of the bottom water ( $1012\text{kg/m}^3$ ) is greater than the remainder of the bottom waters in the section ( $1011\text{kg/m}^3$ ); and (2) at 3700m upstream in the 10m to 15m depth range a decrease in the density is observed from  $1010\text{kg/m}^3$  at falling and low tide to  $1009\text{kg/m}^3$  at rising and high tide.

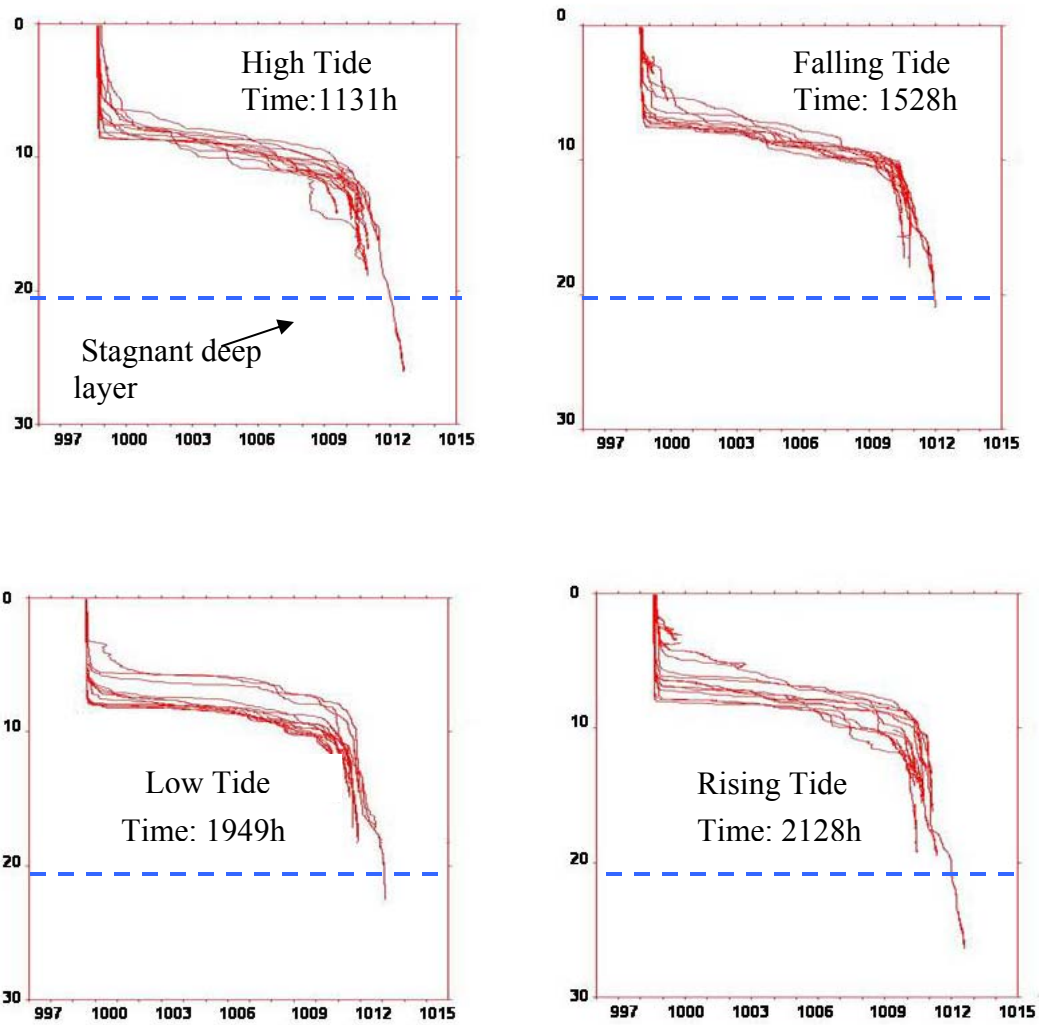


Figure 6.3: Density profile plots of all CTD dips at high tide, falling tide, low tide and rising tide.

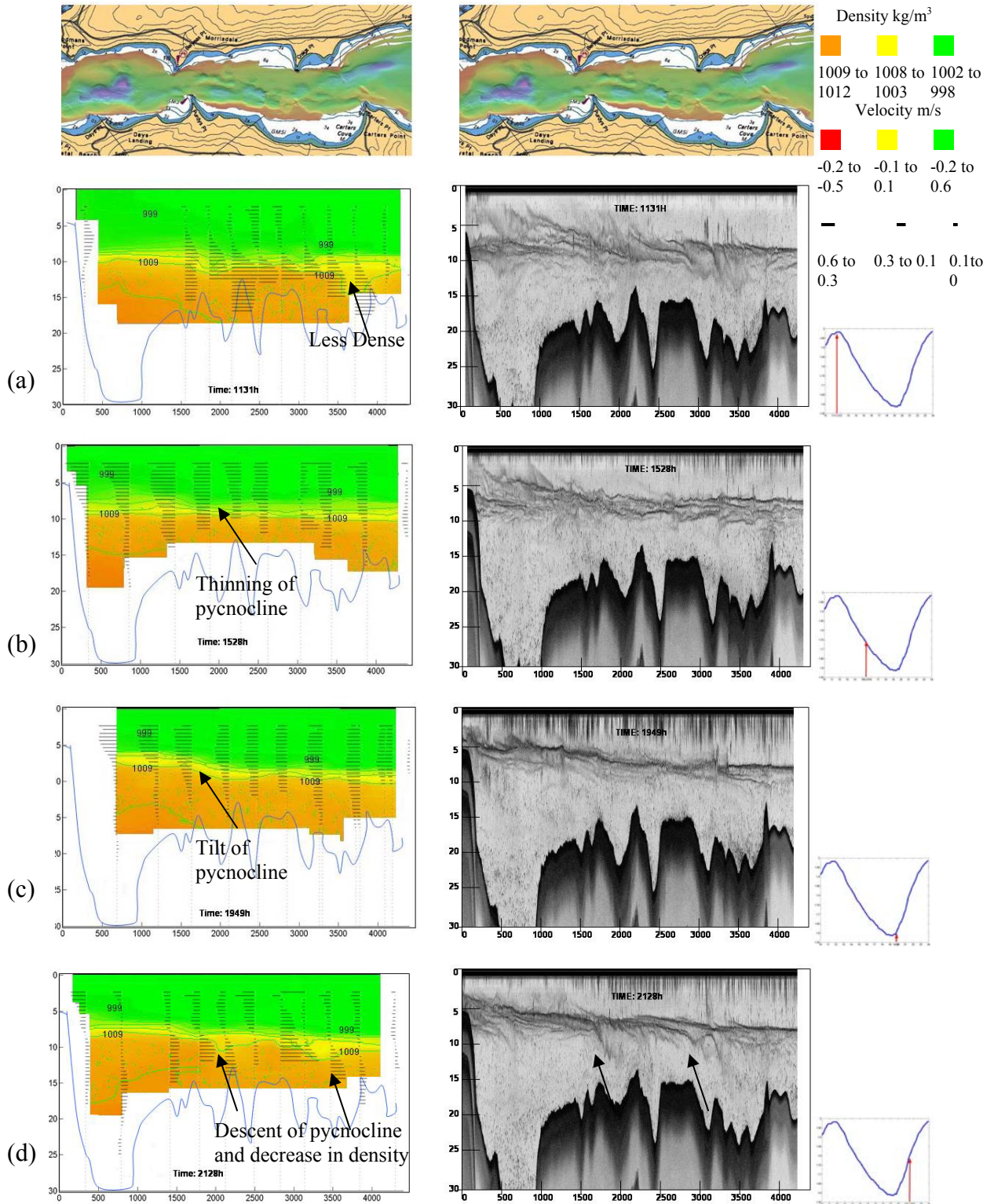


Figure 6.4: Longitudinal density (left) and acoustic volume backscatter images (middle) at the different phases of the neap tide (right).

### **6.2.1.1 Density Structure: The pycnocline region**

From the 4 to 10m depth range the transition is made from fresh water (0.2 psu) to salt water (10.0 psu). Within this range various characteristics are observed to occur throughout the tidal cycle. The overall characteristics at particular locations are:

- During the period of late falling tide, there is a periodic oscillation of the pycnocline
- At low tide, there is a thinning and horizontal tilt of the pycnocline
- From early rising to high tide the downward dip of the pycnocline occurs
- From rising tide to early falling tide, there is a thickening of the pycnocline

The acoustic volume backscatter images are overlaid with the density contour images and this verifies that the high intensity backscatter signal observed at the interface is that of the pycnocline (see Figure 6.5). The backscatter images can be used to infer higher resolution horizontal variability in the density structure. Therefore the tilts, thinning and thickening of the pycnocline is reconfirmed from these images.

The characteristics of the pycnocline mentioned above are all illustrated by the density and acoustic backscatter longitudinal profiles (see Figure 6.4). It should be noted that the horizontal and vertical resolution of the data used to produce the acoustic backscatter longitudinal profiles is greater than that used to produce the longitudinal density profiles. In this study the resolution of the data used to produce the density profile is ~400m. The echosounder, which collects the acoustic backscatter data, has a horizontal resolution of ~1m. In this section unless stated otherwise, the acoustic backscatter longitudinal profiles have been produced to represent a horizontal resolution of 10m. This indicates the backscatter had been averaged over 10m.

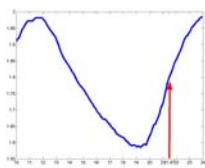
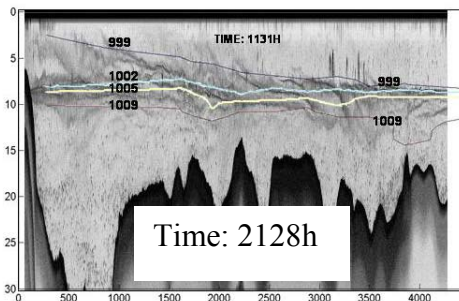
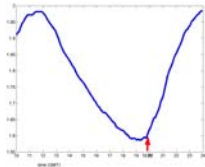
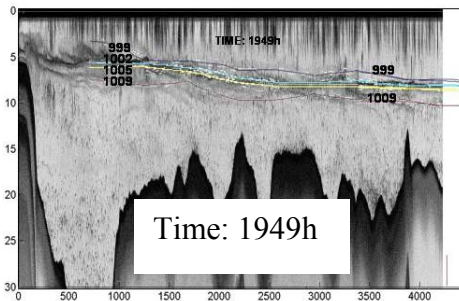
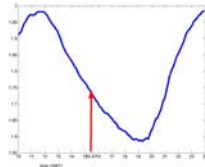
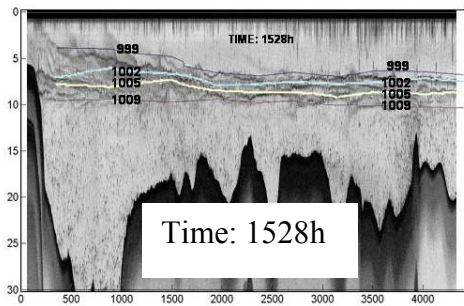
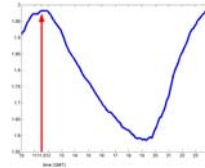
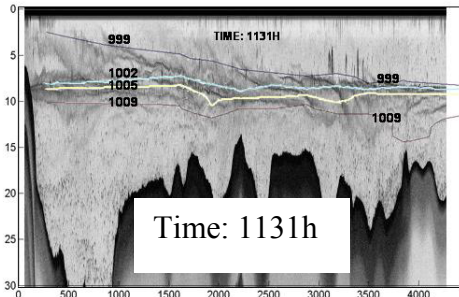
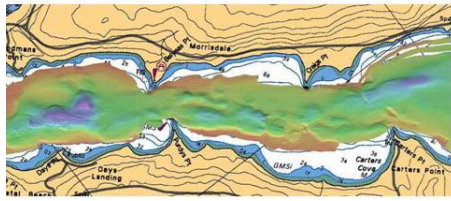


Figure 6.5: Acoustic backscatter images overlaid with the density contours for neap tides.



The detail of the acoustic backscatter images is better than the longitudinal density profiles, therefore it is expected that more features will be observed from these profiles.

This section describes in detail these observations of the pycnocline using the density and acoustic backscatter profiles.

### **Shape and Tilt of the Pycnocline**

At late falling tide, the pycnocline appears to be attempting to conform to the shape of the irregular bathymetry of the area (see Figure 6.6). The acoustic backscatter images also show at particular locations for this period, evidence of the periodic oscillations at the interface (see Figure 6.7). The periodic oscillation of the pycnocline from the acoustic backscatter images are first observed to occur at 1608h (~2.5 hours before exact low tide) and disappear at 2048h (~2hours after exact low tide). The periodic oscillation of the pycnocline from the acoustic backscatter images are described in more detail in section 6.2.4.

At late falling tide a thinning of the pycnocline (see Figure 6.6a) occurs and at low tide a tilt of the pycnocline develops within the vicinity of the lateral constrictions at Belyeas Pt and Purdys Pt (see Figure 6.6b).

Within the vicinity of the ~1700m and ~2700m markers the bathymetry shoals. During the period of early rising tide to high tide (see Figure 6.8) at these markers a downward dip of the pycnocline occurs (see Figure 6.8). To the immediate eastern side of the shoals the bathymetry deepens and the 1009 isopycnal descends to ~1.5m into the bottom salty layer (see Figure 6.8). The acoustic backscatter images also show the



descent of the pycnocline into deeper bottom salty layer during this time period (see Figure 6.9).

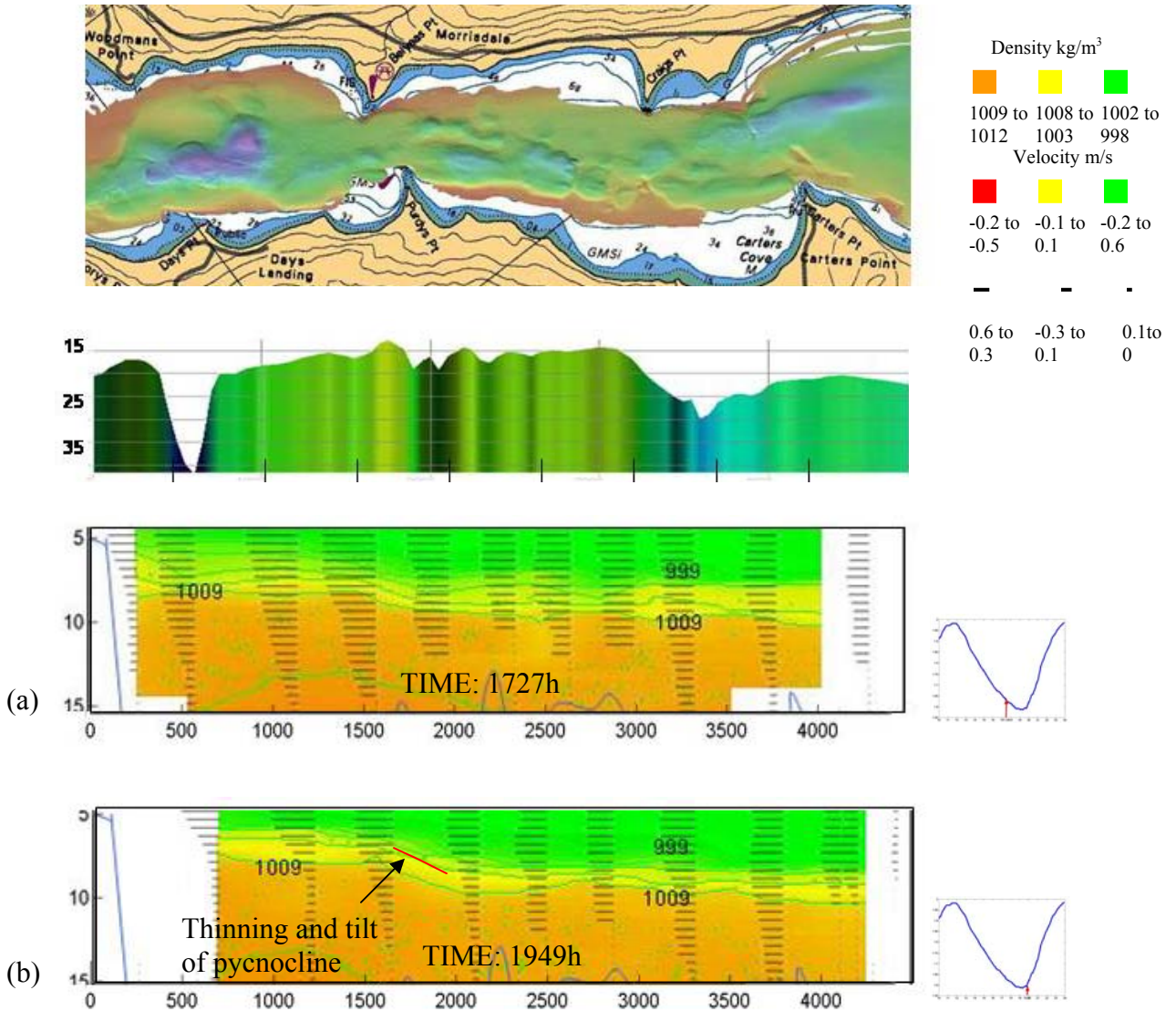


Figure 6.6: Displacement of the pycnocline from late falling to low tide at neap tide. (a) shows the periodic oscillation of the pycnocline as the pycnocline attempts to conform to the shape of the bathymetry and (b) shows the thinning and tilt of the pycnocline.

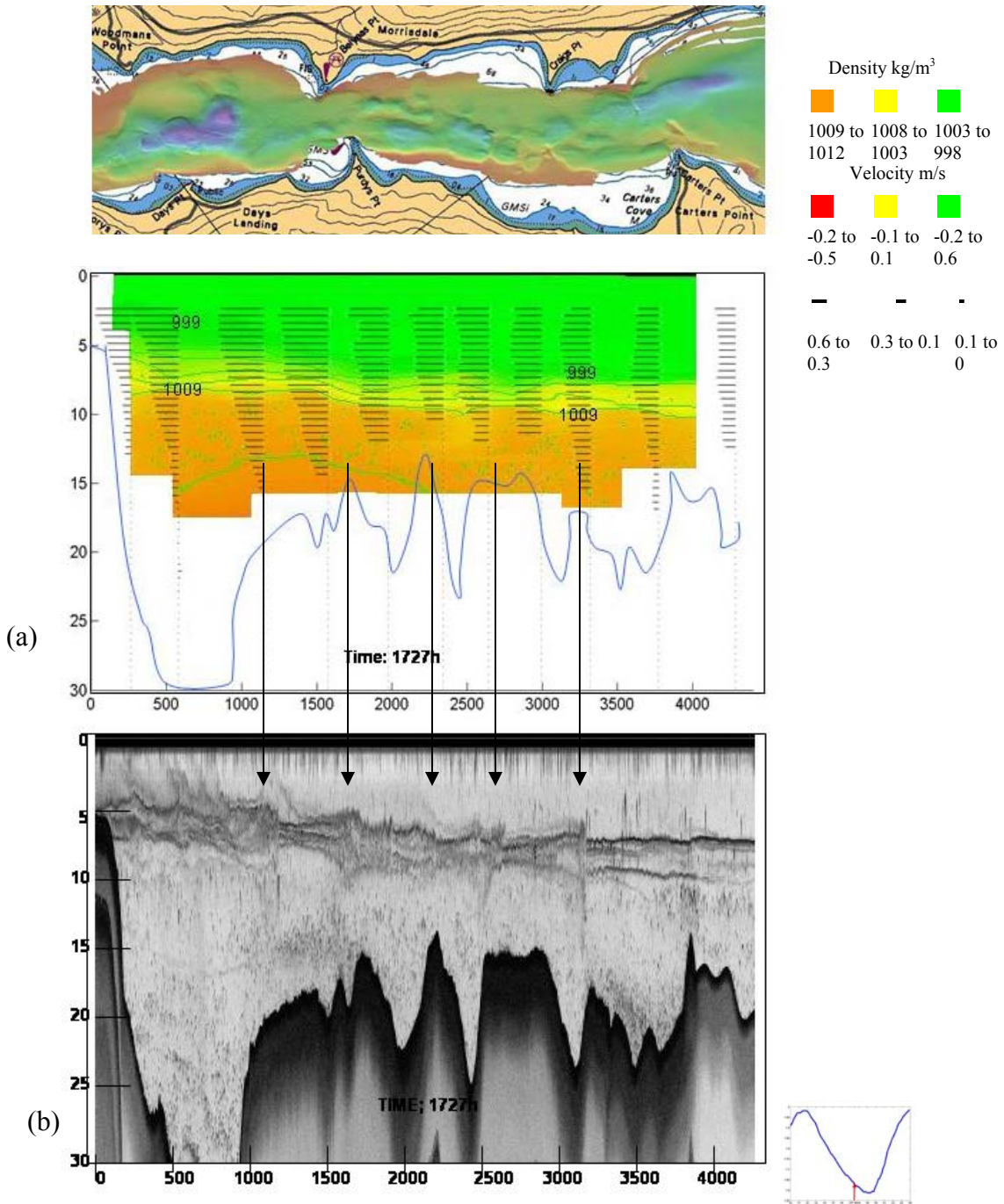


Figure 6.7: (a) Longitudinal density profiles and (b) acoustic backscatter profiles at late falling tide. The arrows indicate the locations that the periodic oscillations of the pycnocline was observed.

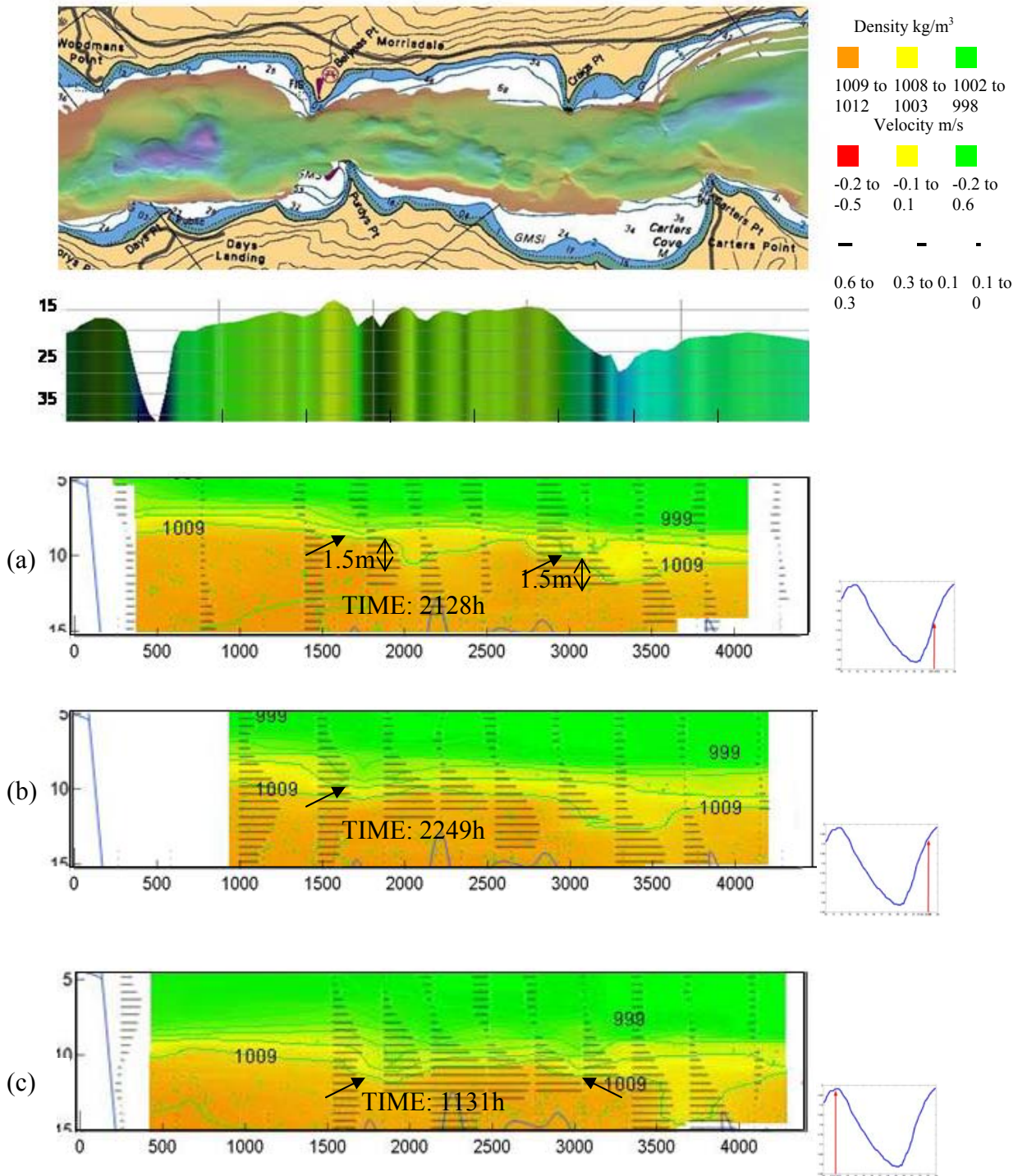


Figure 6.8: Downward dip of the pycnocline. The black arrows represent occurrences of the downward dip of the pycnocline.



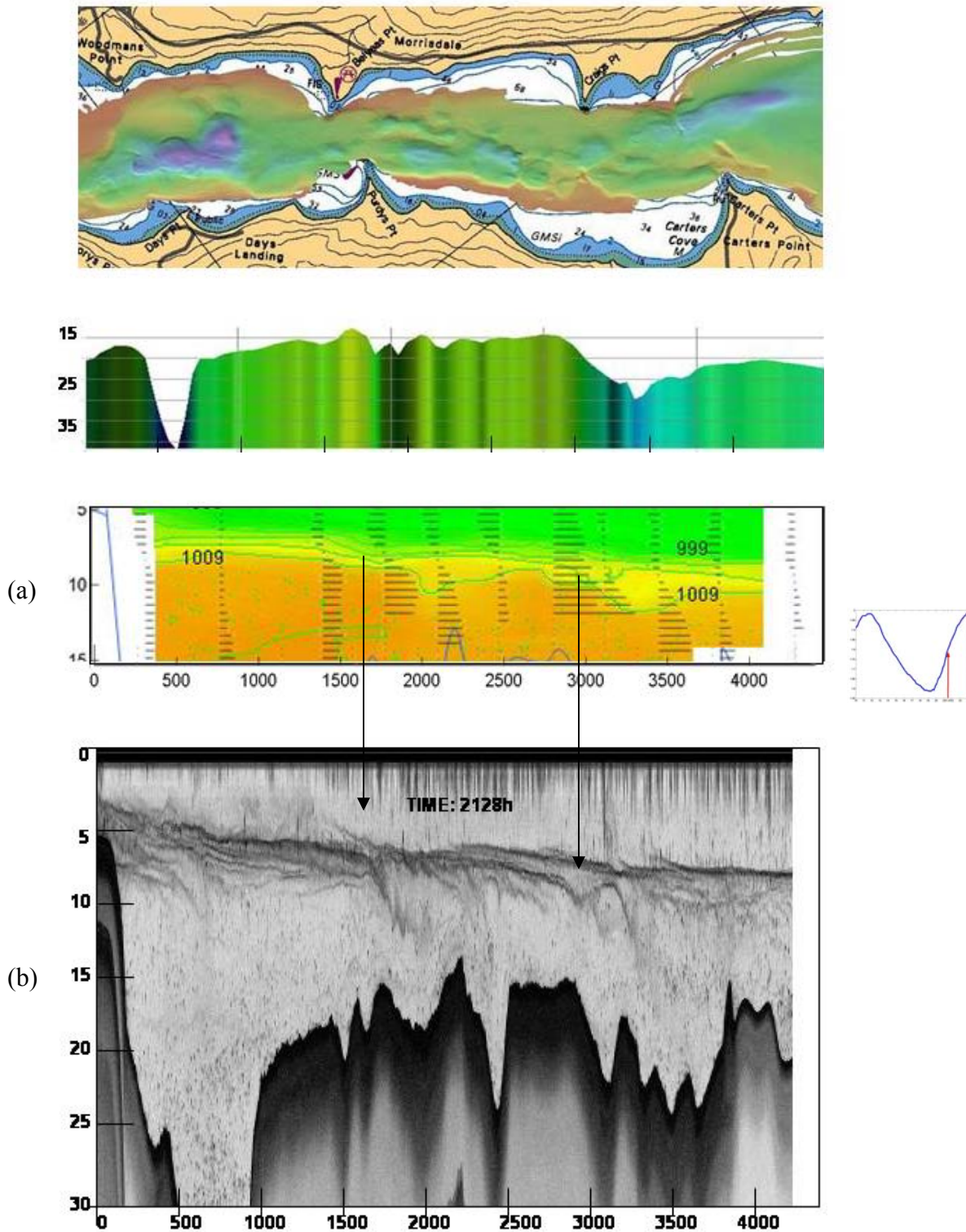


Figure 6.9: the downward dip of the pycnocline observed from the density profile (a) and (b) the acoustic backscatter image.

The descent of the 1009 isopycnal at the eastern side of the shoals appears to grow deeper into high tide.

It may be argued that at the locations where the downward dip of the pycnocline occurs (from rising tide) there will reactively be an upward displacement on either side. Thus intuitively it may appear that by comparing the density profiles there is no difference between the periodic oscillations of the pycnocline observed at late falling tide with that of the downward dip at early rising tide (see Figure 6.6 and 6.8).

For this study the periodic oscillations of the pycnocline that occur at late falling tide and the downward dip of the pycnocline that occur at rising tide have been interpreted to be two different features of the pycnocline. This was decided upon based on two factors: (1) the increased degree of downward dip that occurred at rising tide compared to that at late falling tide (compare Figure 6.6 and Figure 6.8) and (2) due to the fact that at early rising tide the echosounder images show the descent of the pycnocline whilst at late falling tide this is not observed. These characteristics of the pycnocline observed from the acoustic backscatter images are discussed in more detail in section 6.2.4.

### **Thickening of the Pycnocline**

Figure 6.8 and Figure 6.10 show that from rising tide into falling tide a thickening of the pycnocline occurs particularly within the vicinity of the 1700m and 2700m markers where the bathymetry shoals and then deepens. The thickening of the pycnocline occurs towards the bottom salty layer.

Figure 6.10 shows the density plotted along the stretch of the area for the different phases of the tide. The graph illustrates that the density profiles are not constant over the section especially within the vicinity of the 1500m to 4000m marker. The decrease in density at the pycnocline and the layer below the pycnocline is observed to occur within the 1500m to 4000m distance. However within this region the density profiles vary amongst each other. Thus this section is further divided into three sections (group 1, group 2 and group 3). These groups illustrate the overall characteristic of the density (see Figure 6.10).

Density profiles for group 1, group 2 and group 3 show that from rising tide into early falling tide a thickening of the pycnocline occurs (see Figure 6.11). The pycnocline thickness changes from 2m to 4m.

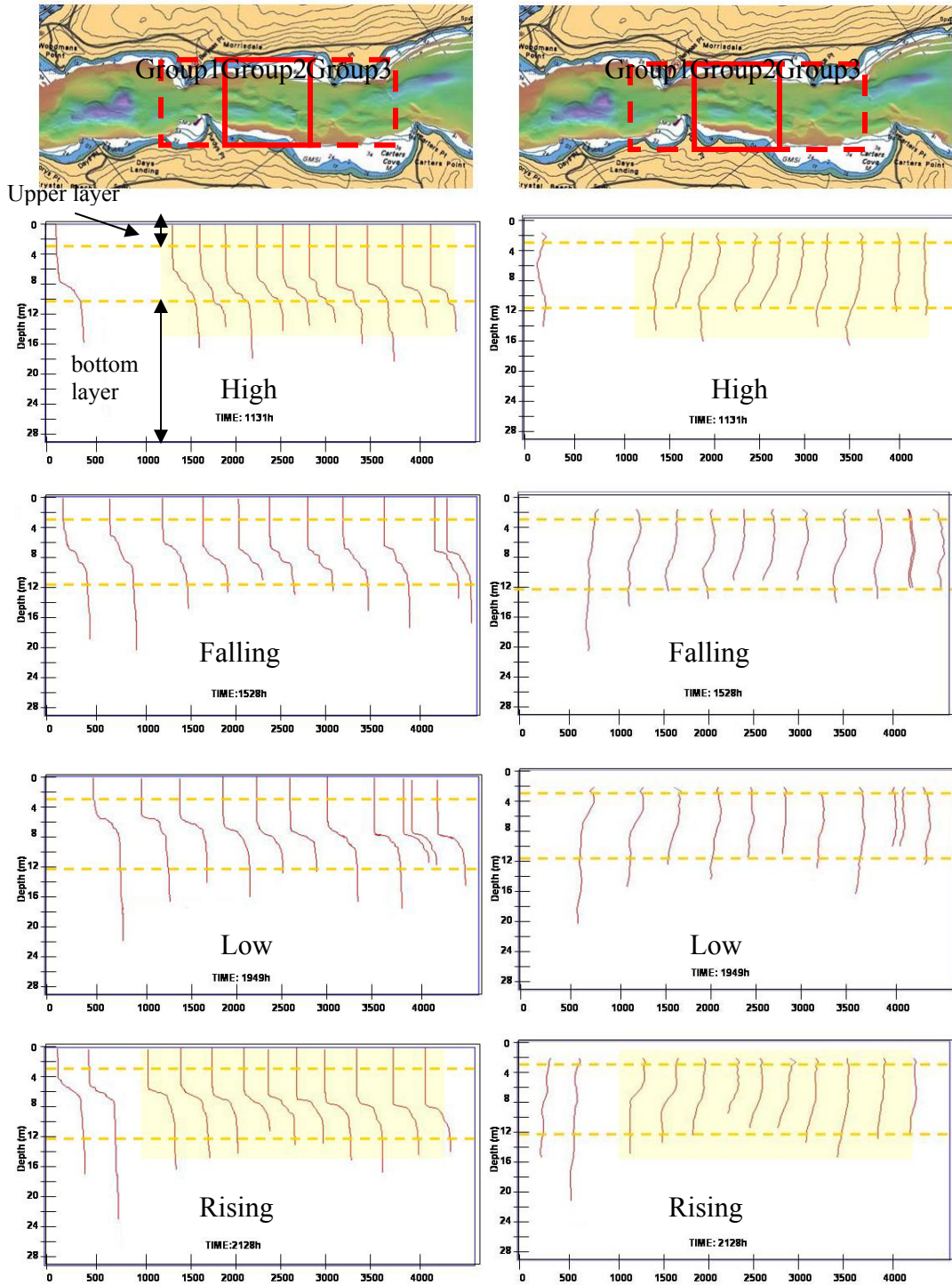


Figure 6.10: Individual density (left) and velocity (right) profiles of the longitudinal profiles. The tidal phases are the same as those depicted in Figure 6.4 and 6.5.

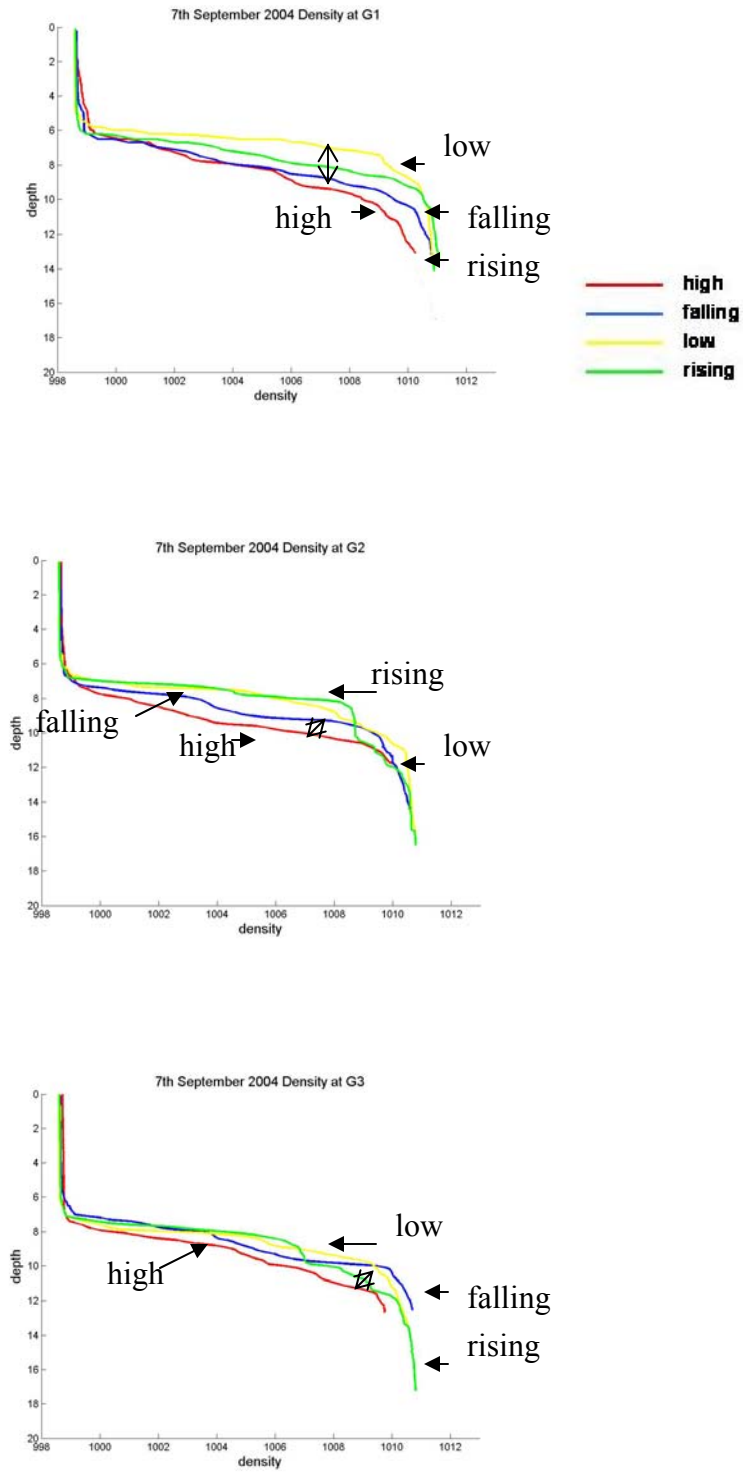


Figure 6.11: Density profiles for the tidal cycle at the three groups.



## 6.2.2 Velocity Structure: Section one

In contrast to the density structure the velocity structure of the surface and bottom layers are observed to change throughout the tidal cycle. Negative values represent flow upstream whilst positive values represent flow downstream.

### 6.2.2.1 High Tide

At high tide (see Figure 6.12, 1131h) the surface flow is almost stationary with velocities between 0m/s to 0.05m/s. However at the ~2700m marker (within the vicinity of Craig's Pt) the surface layer ebbs at 0.1m/s. The pycnocline velocities from the 0 to 3500m distance floods at -0.3m/s. The greatest velocity magnitude occurs within the 1500m to 4000m limit. Upstream of 4000m marker the flood velocities are ~-0.1m/s.

The bottom flow floods with a magnitude of -0.4m/s. However, within the vicinity of the 42m deep, hole the bottom velocities are basically stationary with a velocity of 0.05m/s at the 15m to 30m depth.

These observations at high tide show that the greatest flood velocity occurs between the limits of 1500m to 4000m upstream. This coincides with the area that constrictions exist both laterally and vertically (see Figure 6.1, pg 141). This limit is also where the descent of the pycnocline and a decrease in density was observed to occur. These observations of the velocity and density suggest that either mixing or advection processes are taking place within the 1500m to 4000m region.

It is also observed that, on entrance to the survey area, the flood velocities are the greatest at the pycnocline whilst the bottom layers are almost stationary. This area is also

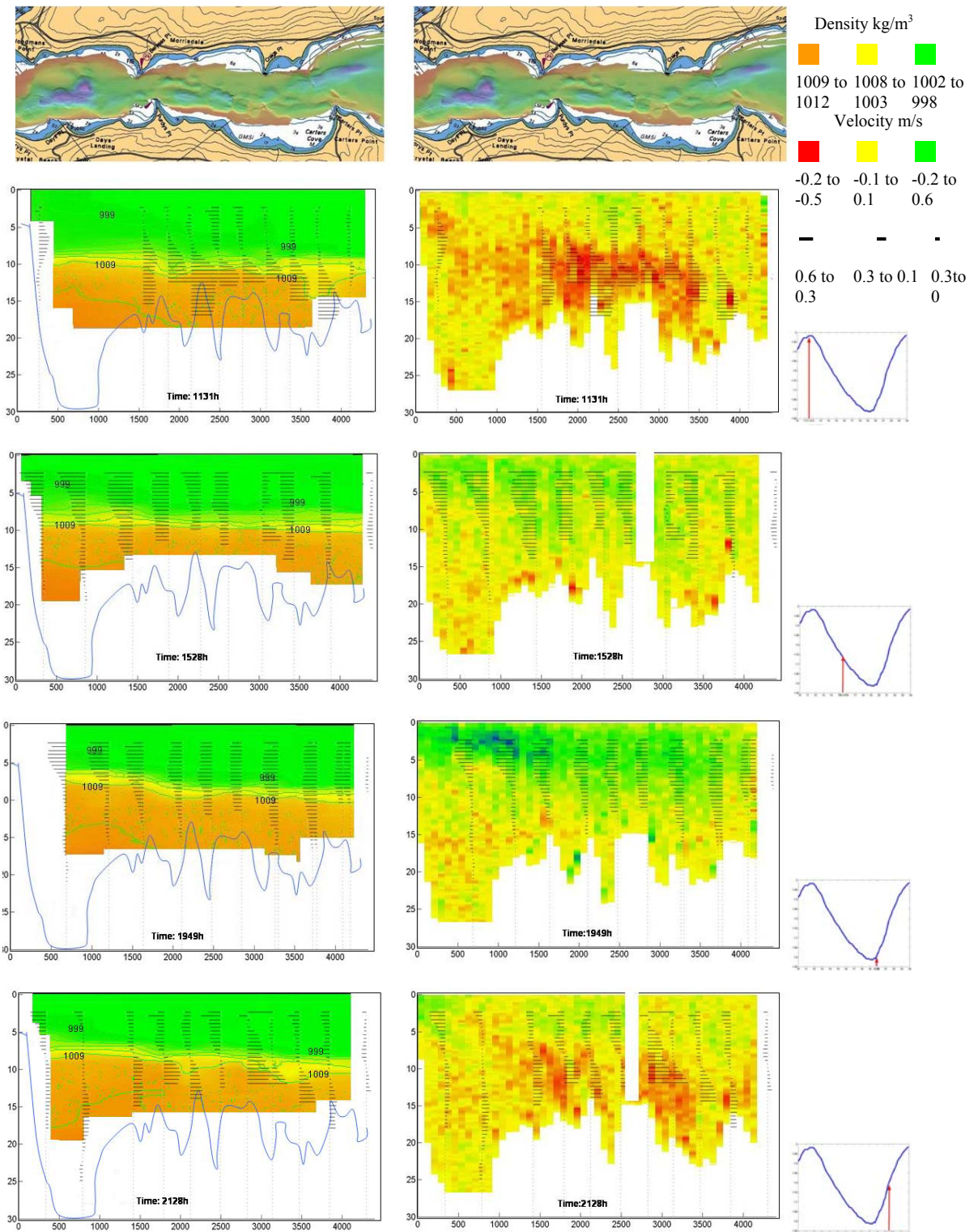


Figure 6.12: Longitudinal density (left) and velocity (right) profiles overlay with velocity arrows at different phases of neap tide.

where the most dense bottom waters are observed. These observations may imply that the waters in the deep hole are not replenished during the tidal cycle and are basically stagnant.

### **6.2.2.2 Falling Tide**

Figure 6.13 illustrates the different phases of falling tide. At early falling tide (1310h) the surface and bottom velocities are flowing in opposite directions. The surface flow ebbs at 0.1 to 0.2m/s, whilst the bottom flow has decreased, but is still flooding upstream at -0.2m/s. 1408h represents the period that the bottom flow has basically stopped flooding upstream and it is about to ebb downstream. At mid falling tide (1528h) both surface and bottom flows are ebbing downstream with a surface flow of 0.5m/s and a bottom flow of 0.3m/s. At late falling tide (1727h) the flow in both layers has increased to 0.6m/s at the surface and 0.4m/s at the bottom.

At early falling tide the waters within the pycnocline continues to flood at  $\sim$  0.2m/s however by mid falling tide and late falling tide the pycnocline now ebbs at  $\sim$ 0.2m/s.

### **6.2.2.3 Low Tide**

Low tide velocities (see Figure 6.12,time1949h) are similar to late falling tide, with surface velocity of 0.65m/s and bottom velocity of 0.4m/s. The greatest surface velocities occur at low tide within the deep hole area (500m to 1000m upstream).

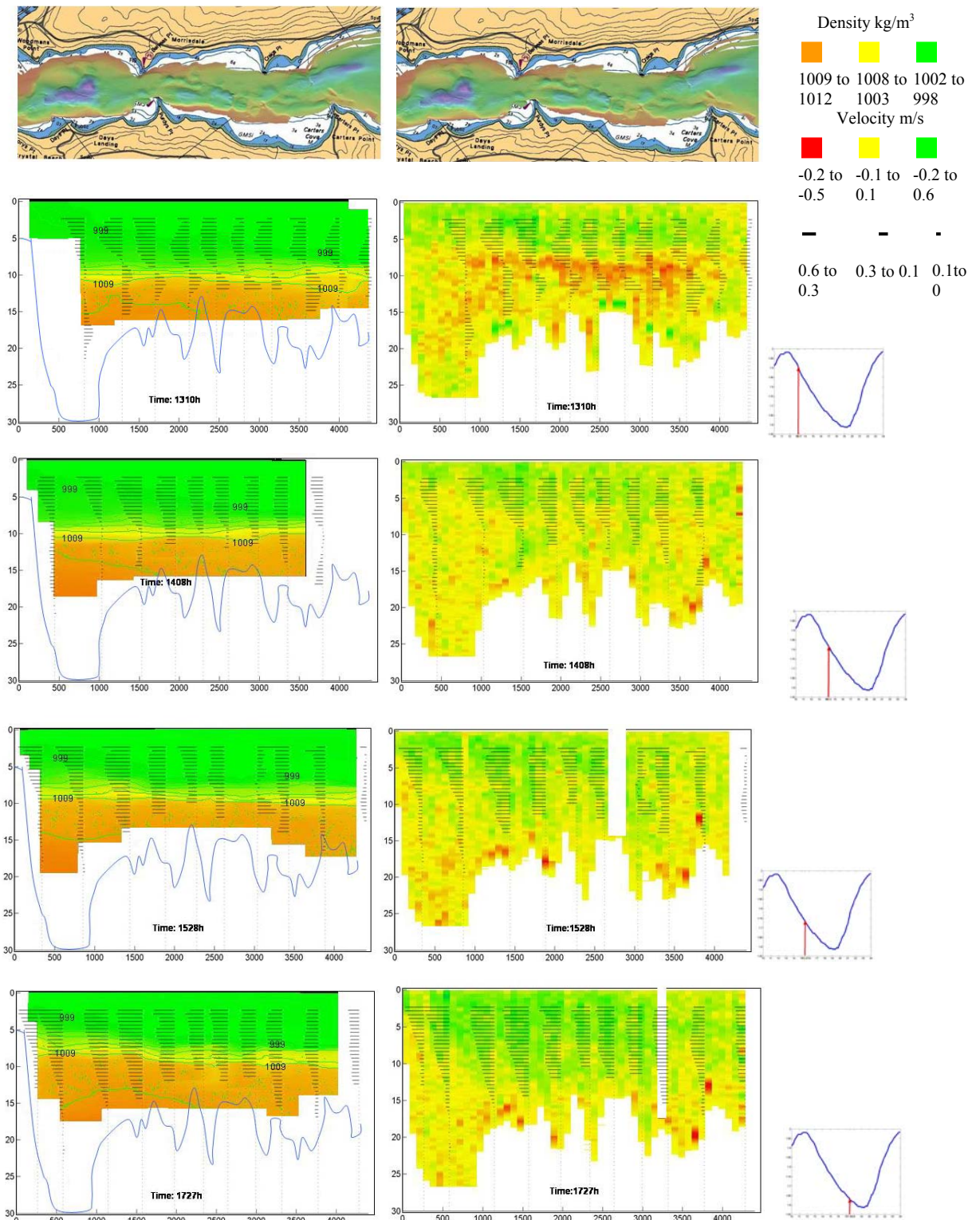


Figure 6.13: Longitudinal density (left) and velocity profiles for the different phases of falling neap tide (far right).

#### **6.2.2.4 Rising Tide**

Observations of rising tide (see Figure 6.14) are similar to the observations made at early falling tide, where both bottom and surface waters are flowing in opposite direction. Early rising tide represents the period where the bottom ebb waters have begun to change direction from flowing downstream to flowing upstream. Thus for early rising tide (2048h) the surface flow has decreased but ebbs at 0.4m/s, whilst the bottom flow has begun to flood at -0.1m/s. This period is the initial time of change in direction of the bottom waters. The greatest bottom flow occurs between the 1500m to 4000m upstream which is similar to the observations made at high tide for the bottom flow. At mid rising tide (2128h), the surface flow has decreased in magnitude to 0.25m/s whilst the bottom flow is flooding at -0.3m/s. At late rising tide (2249h) the surface flow are ebbing at 0.1m/s whilst the bottom flow are flooding upstream at -0.4m/s. These observations of the different phases show that the surface layer decreases in thickness with time whilst the bottom layer increases in thickness.

#### **6.2.2.5 Velocity Shear**

The maximum ebb flow occurs in the surface waters at late falling and low tide with a velocity between 0.6m/s to 0.65m/s. The maximum flood flow occurs in the bottom layer at high tide with maximum velocity of -0.4m/s (see Table 6.2). At maximum ebb flow the whole water column flows downstream at all depths, except for the waters in the 20m to 42 m deep hole area. At maximum flood flow the surface layer is basically stationary whilst the bottom layer flows upstream. The greatest flood velocity occurs 1500m to 4000m upstream.



Observations from rising tide into early falling tide represent the period of the greatest shear. This shear is mostly concentrated within the 1500m to 4000m distance upstream and was the greatest at rising tide (see Table 6.2).

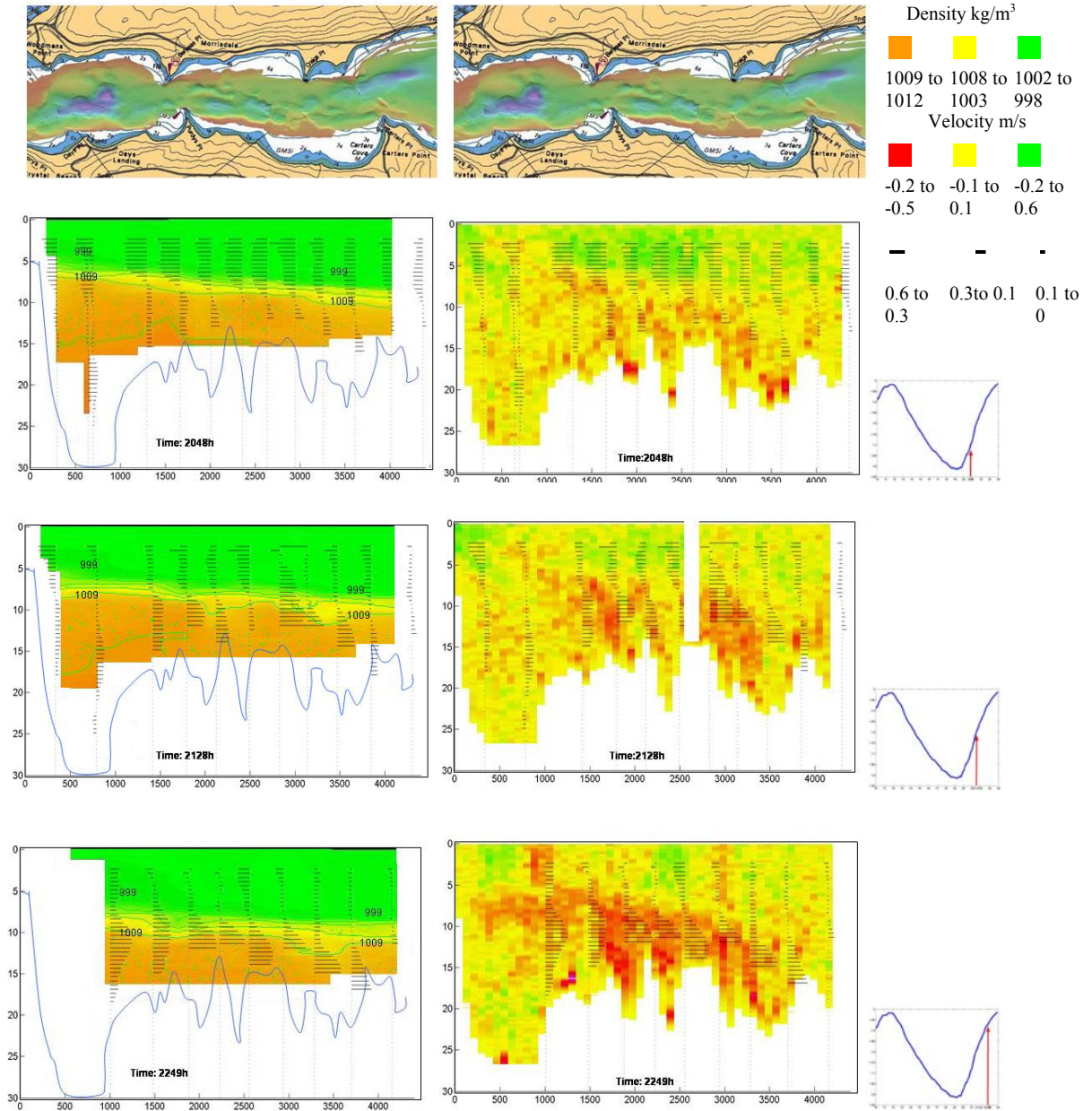


Figure 6.14: Longitudinal profiles of density (left) and velocity (right) at the different phases of rising neap tide.

Table 6.2: Velocity magnitude, direction and velocity shear for the different phases of the tide

<b>Phase of Tide</b>	<b>Surface Velocity</b>	<b>Bottom Velocity</b>	<b>Difference (Shear)</b>
<b>High</b>	0.05	-0.4	0.45
<b>Early Falling</b>	0.1	-0.2	0.3
<b>Mid Falling</b>	0.5	0.3	0.2
<b>Late Falling</b>	0.6	0.4	0.2
<b>Low</b>	0.65	0.4	0.25
<b>Early Rising</b>	0.4	-0.1	0.5
<b>Mid Rising</b>	0.25	-0.3	0.55
<b>Late Rising</b>	0.1	-0.4	0.5

### 6.2.3 Summary of Density and Velocity Structure

Surface and bottom layer densities remain basically homogenous for most of the tidal cycle. Two exceptions are observed with the bottom layer. First the deep hole area has the most dense bottom waters in the whole section. The velocities in this area appear to be stagnant throughout the tidal cycle. Secondly at high tide a decrease in bottom density occurs at ~3700m (Carters Pt). At this point in time the velocities are flooding at -0.4m/s. This decrease in density indicates that either mixing (molecular or turbulent) or the advection of water is taking place within this area.

The major changes in density occur in the pycnocline region 1500m to 4000m upstream. These changes include:

- From late falling to low tide a periodic oscillation of the pycnocline occurs
- At low tide a horizontal tilt of the pycnocline occurs within the vicinity of the two lateral constrictions (Belyeas Pt and Craig Pt)
- From rising to high tide there is the dip of the pycnocline within the vicinity of the lateral and vertical constrictions
- At rising tide into high tide a thickening of the pycnocline towards the bottom salty layer

The latter two observations of the pycnocline listed above occur when: (1) maximum velocity shear is observed and within the 1500m to 4000m marker where lateral and vertical constrictions exist. These results imply that there is the possibility of turbulent mixing occurring at the interface within the 1500m to 4000m marker.

Based on the observations made of the density and velocity structures, it can be hypothesized that, at rising tide, turbulent mixing events are possibly occurring within the



pycnocline region and/or within the vicinity of Carters Point where a decrease in density of the bottom waters is observed. Further observations of the pycnocline are now made using the acoustic volume backscatter which has a greater resolution both horizontally and vertically.

#### **6.2.4 The Acoustic Backscatter Images**

Observations at the interface of the longitudinal density profiles and the acoustic backscatter images illustrated two major features:

1. From 1608h (late falling tide) a periodic oscillation of the pycnocline occurs. The pycnocline appears to be attempting to conform to the shape of the bathymetry. Figure 6.7 illustrates that at time 1727 (~1.33h after it was first observed) the periodic oscillation of the pycnocline from the density and the acoustic backscatter images. These periodic oscillations of the pycnocline disappear at 2048h (~2 hours after exact low tide) when the bottom flow has begun to flow upstream.
2. From 2048h (early rising tide) to high tide within the vicinity of the lateral and vertical constrictions, the longitudinal density profiles show a descent of the pycnocline. The acoustic backscatter images also shows the dip of the pycnocline at these locations for this time period (see Figure 6.9)

The observations listed above were made with the longitudinal profiles of the acoustic backscatter images which had a horizontal resolution of 10m. To identify in more detail

the features observed the resolution of the acoustic backscatter images is increased to display the observations at 1m horizontally.

Inspection of the acoustic backscatter images at the interface shows the possible existence of two types of internal waves. The first wave is referred to as type 1 and takes the form of small amplitude periodic waves (see Figure 6.15). The second possible wave is referred to as type 2 and takes the form of groups of waves with varying wavelength and amplitudes (see Figure 6.15).

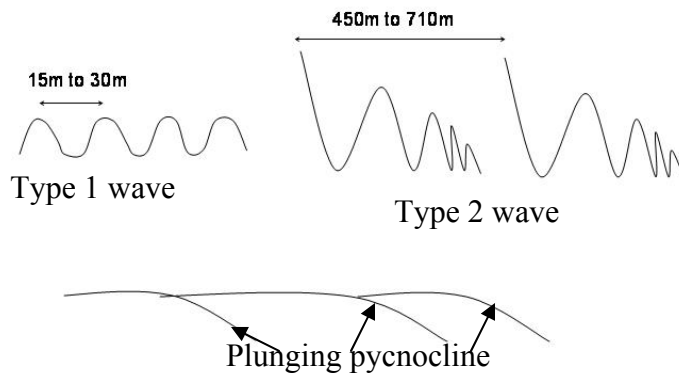


Figure 6.15: Shape and form of the type 1, type 2 waves and the plunging pycnocline

Figure 6.16(2, 3) illustrates type 1 waves at the pycnocline with the wavelengths that vary between 15m to 30m. Figure 6.16(1, 4, 5) illustrates areas of the pycnocline where type 1 waves are not present.

Type 2 waves are present within the vicinity of the 1500m to 4000m section. These waves are characterized as possessing a train of waves whose amplitude and wavelength vary. Out of each group of waves there is a leading wave that has the greatest amplitude. The distances between leading waves vary between 450m to 710m.

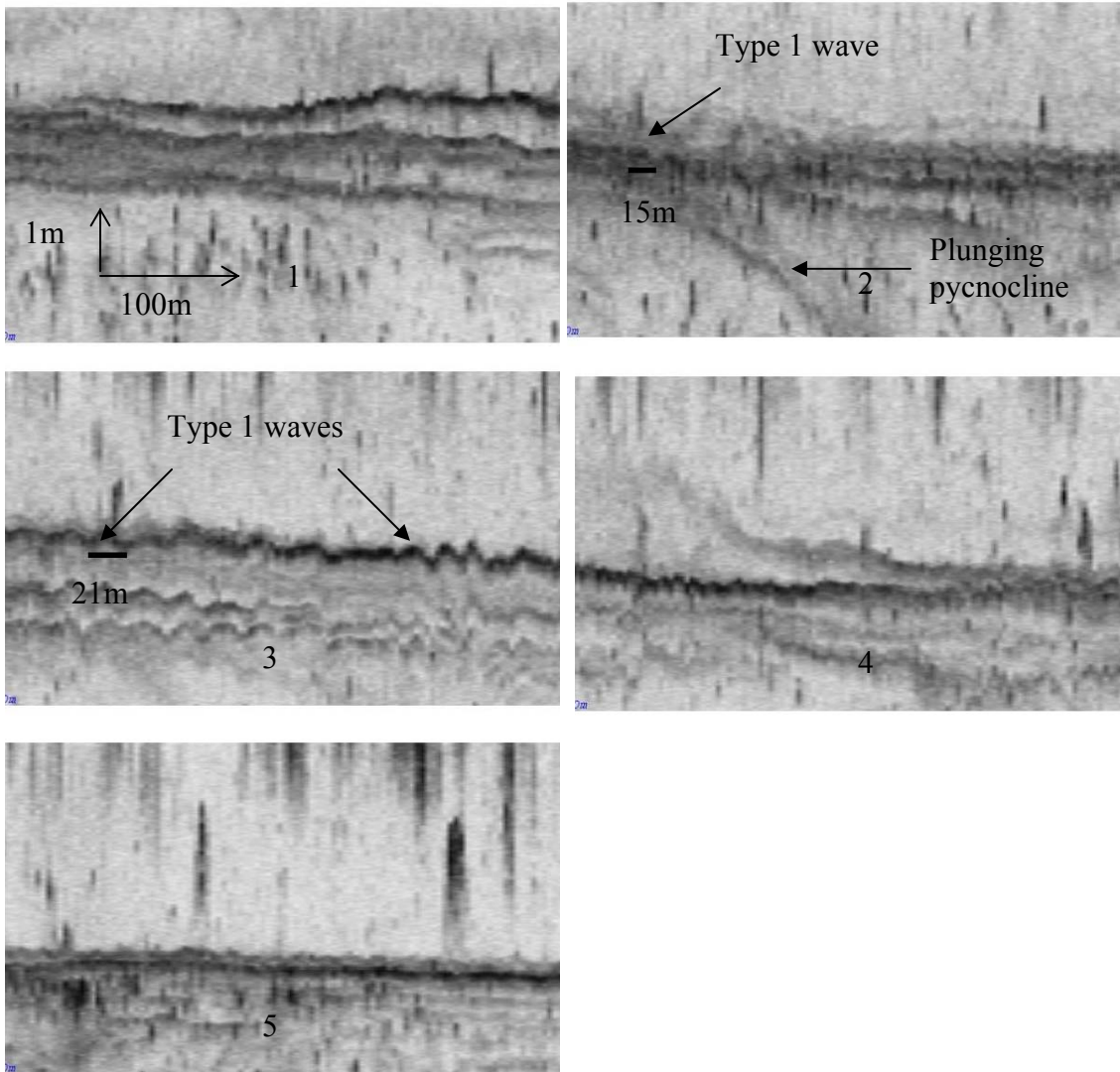
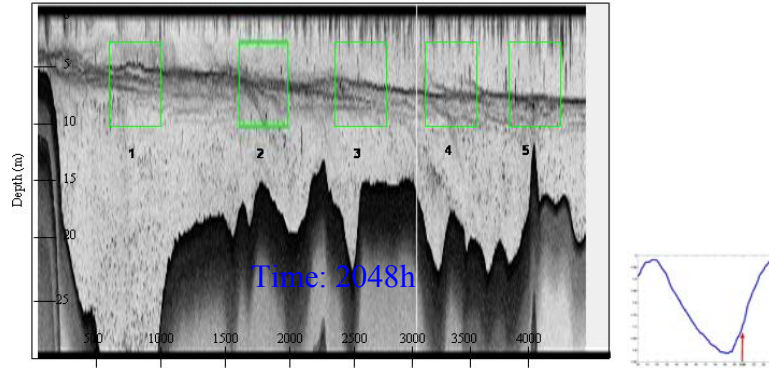


Figure 6.16: Type 1 waves (2, 3) and the plunging pycnocline (2). 1, 4, 5 shows the pycnocline where the type 1 waves are not present.

The acoustic volume backscatter images have a horizontal resolution of 1m. A manual estimate is used to actually measure the crest/trough to crest/trough spacing of waves. This manual estimate will have an error of greater than 1m. Therefore to confirm that the wavelengths are varying would be subject to many manual errors. However visual observations of the waves suggest that the wavelength varies.

At time 1608h type 2 waves are observed at the pycnocline at particular locations. However at time 1630h the leading edge of the type 2 wave that was at the 2400m marker at time 1608h is now observed at the 2100m marker. Thus this type 2 wave moves downstream with a speed of  $\sim 0.2\text{m/s}$ . However for all other sightings of the type 2 wave, the waves appear to remain almost stationary.

The type two waves life span began at 1608h (late falling tide) and disappeared at 2048h ( $\sim 2$  hours after exact low tide) (see Figure 6.17, 6.18). Figure 6.17 (3, 4, 5) illustrates the type 2 waves at the pycnocline, whilst 6.17 (1, 2, 6) illustrates the pycnocline where the type 2 waves are not present.

At 2048h the transition is made from the bottom waters flowing downstream to flowing upstream. These observations suggest that the type 2 waves develop at the period that both the upper and lower layer flow downstream. It appears that under these flow conditions the pycnocline is attempting to conform to the shape of the bathymetry.

The type 2 waves resemble the solitary wave packets described in section 3.3.1.2. These waves tend to be generated at locations where shoals, stratification and tides are present (Apel [2002]). Studies performed by Farmer and Armi [1999] suggest that shoals, stratification and shear may also generate these solitary wave packets. The characteristics

described by both studies are all present in Long Reach. However, in Long Reach, the solitary wave packets are observed to diminish at the period of maximum shear.

Solitary wave packets are characterized by a leading wave followed by waves that have decreasing wavelengths and amplitudes. This was observed for the type 2 waves. Solitary wave packets are known to encourage mixing at the interface and in areas of downwellings/upwellings. Thus these waves may be a possible source of mixing in Long Reach.

At early rising tide the type 2 waves disappear and a downward dip of the pycnocline isopycnals occurs at the areas where the bathymetry shoals then deepens (see Figure 6.18). In contrast, type 1 waves remain present when the downward dip of the pycnocline occurs at high tide.

It should be noted that the longitudinal density profiles show the periodic oscillation of the pycnocline from late falling to early rising tide. It is at this time that the acoustic backscatter images show the appearance of the type 2 waves. Yet the acoustic backscatter images only show the downward dip of the pycnocline occurring from early rising tide to high tide. At early rising tide the type 2 waves disappears. Thus these observations indicate that either: (1) the downward dip of the pycnocline is associated with the disappearance of the type 2 waves or (2) the occurrence of the downward dip of the pycnocline is a different phenomenon.

Apel [2002] reports observations performed by various authors in the New York Bight, Georges Bank, Knight Inlet Sill and in the Strait of Gibraltar (see Figure 6.19) that suggest that the descent of the pycnocline was associated with either: (1) a lee wave

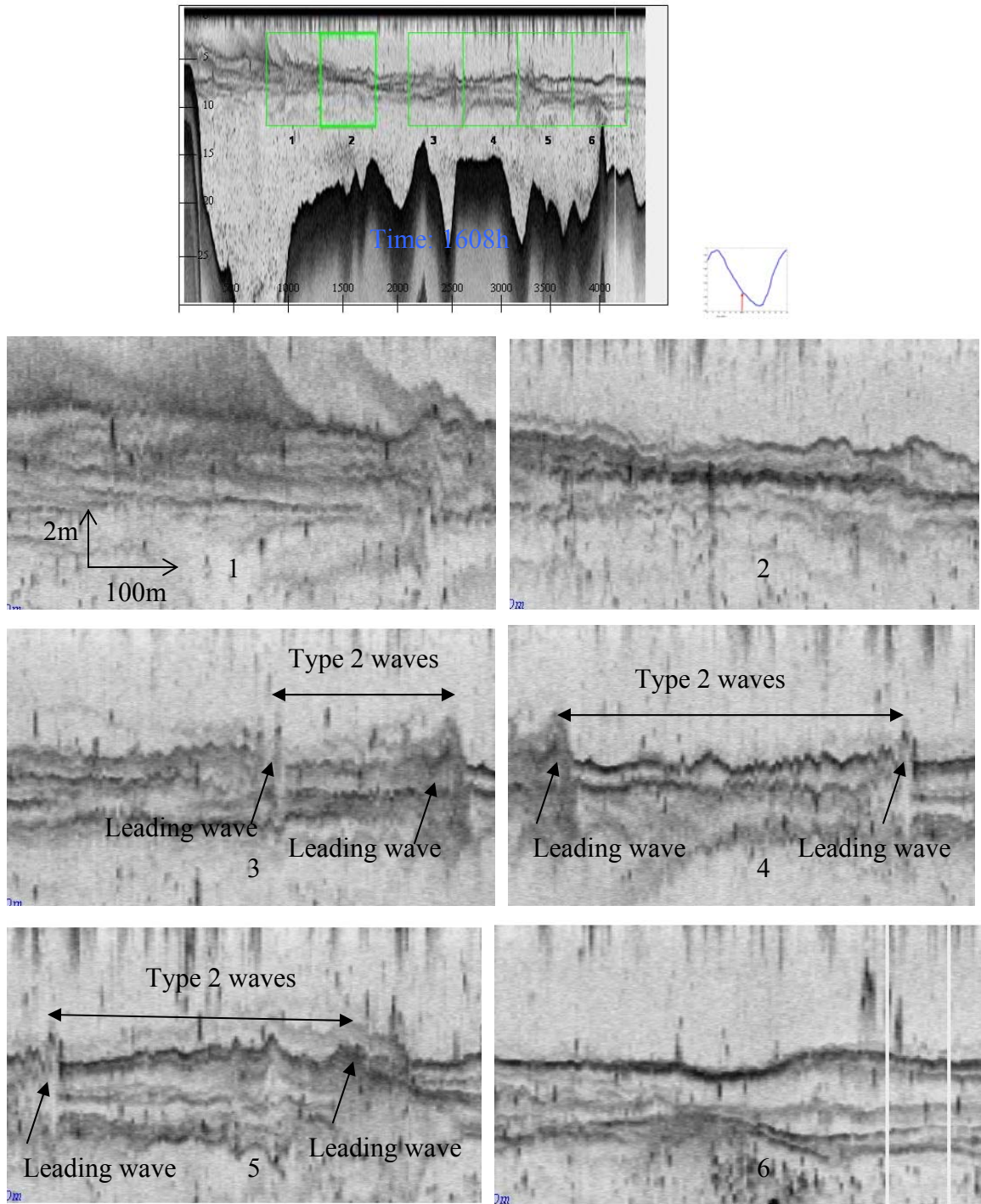


Figure 6.17: The acoustic backscatter images showing the type 2 wave (3, 4, and 5). 1, 2 6 shows the pycnocline where type 2 waves are not present.

down current caused by the sharp change in bathymetry or (2) internal solitary waves which are the leading edge of an undulatory bore. An undulatory bore is known to propagate. The density and acoustic backscatter images show that on most occurrences the soliton wave packets and the descent of the pycnocline are stationary. In Apel [2002] this descent of the pycnocline is referred to as the plunging of the pycnocline (see Figure 6.15, 6.16, 6.18).

It should be noted that the plunges described by Apel [2002] are at the rear of the periodic oscillation of the pycnocline. In Long Reach the periodic oscillation is not observed within the vicinity of the plunges. This observation may indicate that the plunges observed in Long Reach are due to a different phenomena occurring.

With respect to the geometry and bathymetry of the survey area, the type 2 waves and the plunging of the pycnocline occur only within the vicinity of the lateral constrictions (at Belyeas Point and Craig Point) and where the bathymetry shoals and then deepens (see Figure 6.18).

The plunging of the pycnocline also coincides with:

1. Observations made of the density profile within the 1500m to 4000m distance where a thickening of the pycnocline occurs.
2. With respect to the velocity, the plunging occurs at the areas where maximum shear is observed.

Based on these observations and the suggestions made by various authors cited by Apel [2002] it is possible that the plunges are related to one or more of the following: (1) a mixing process created by the solitary wave packets, (2) mixing process created by the type 1 waves or, (3) the stratification, under the influence of the flow patterns



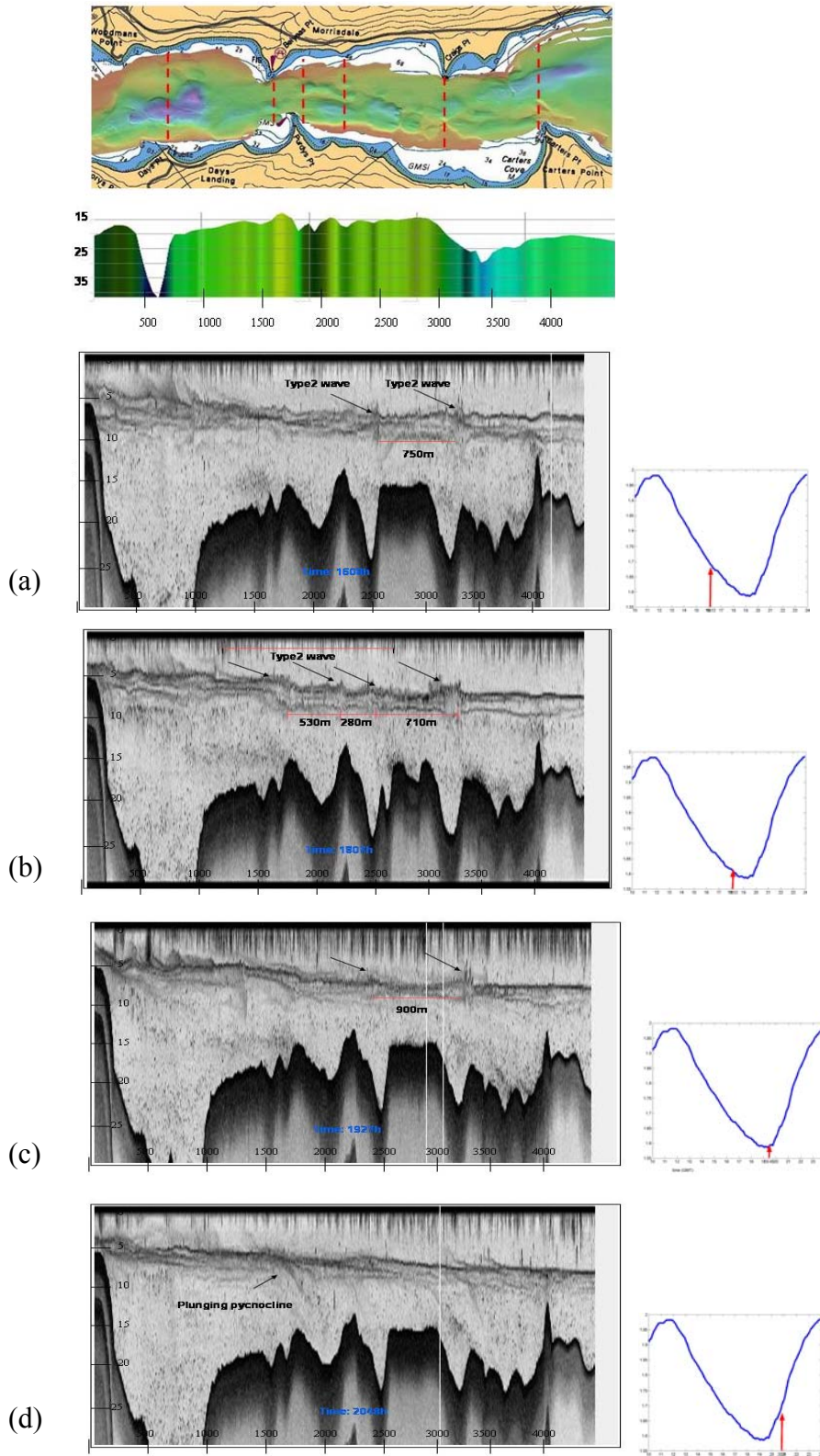


Figure 6.18: Type 2 waves from late falling tide to low tide (a, b, c). The plunging of the pycnocline occurs at rising tide (d).



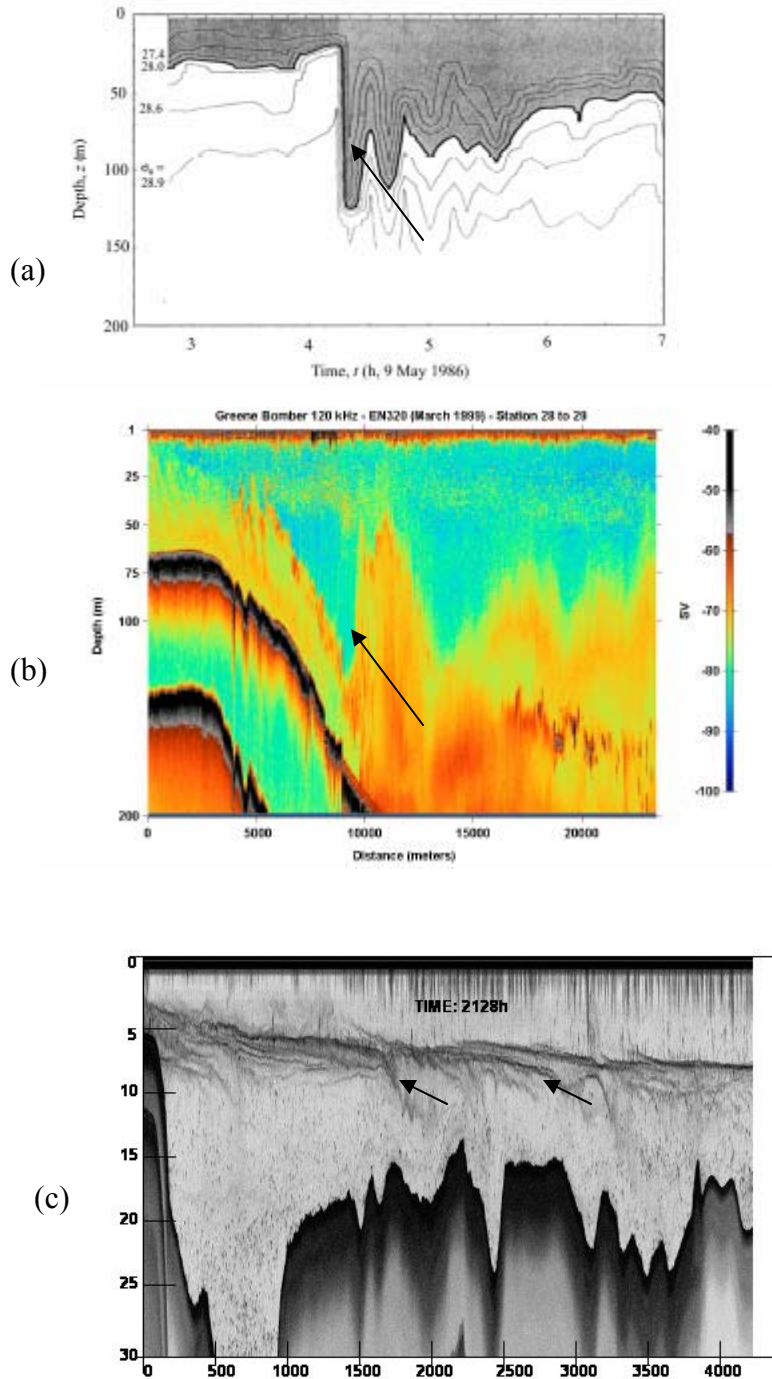


Figure 6.19: (a) Depression of pycnocline at Tarife Narrows in the Strait of Gibraltar, (b) plunging of pycnocline at Georges Bank with lee waves visible at the plunges and (c) the plunges observed in Long Reach. Illustrations of (a) and (b) are referenced from Apel [2002].

of the surface and bottom layers at rising tide (which flow in opposite directions to each other) as it passes over the shoals in the study area, plunging downwards.

### **6.2.5 Summary of Observations**

The density profiles show that at rising tide to high tide an increase in pycnocline thickness occurs. When this occurs a decrease in density gradient takes place. This observation was made at group1, group2 and group3 locations. The areas where the thickening of the pycnocline occur coincide with the areas that maximum shear occurs. These observations suggest that turbulent mixing may be occurring at the interface at rising tide. At this phase of the tide the surface layer flows downstream whilst the bottom layer flows upstream.

The acoustic backscatter images show the presence of two types of waves (type 1 and type 2) at the interface. The type 2 wave first appears at late falling tide. At this time the density profile shows the pycnocline attempting to conform to the shape of the bathymetry. The type 2 waves resembles the soliton wave packets described in section 3.3.1.2 which are characterized as having a leading wave where the wavelength and amplitude of the waves in the packets decreases away from the leading wave.

At early rising tide the type 2 wave disappears and the longitudinal density and acoustic backscatter images shows a downward dip of the pycnocline. Apel [2002] referred to this downward dip as the plunging of the pycnocline and suggests that this was associated with a lee wave down current caused by either a sharp change in bathymetry or internal solitons that are the leading edge of an undulatory bore.

The appearance of the solitary wave packets and the plunging of the pycnocline seem to have a relationship with the geometry and bathymetry of the survey area; the plunging occurs in area where contractions exist laterally and where the bathymetry shoals and then deepens.

Observations of the density, velocity, and acoustic volume backscatter made for the spring tidal (see Figure 6.20, 6.21) cycle, show similar characteristics to the neap tidal cycle (see Figure 6.4). The main difference between the neap and spring tidal cycles is that at neap tides the pycnocline is at 6m to 8m depth, whilst at spring tides the pycnocline is at 8m to 10m depth. The fall in pycnocline may be due to the fact that at spring tides there was an increase in the river discharge which may have caused an increase in the thickness of the freshwater layer and therefore an increase in the water level (see section 2.4, Figure 2.12).

Figure 6.22 shows the presence of type 1 and type 2 waves at the interface at spring tides. The similarity in observations for both neap and spring tides suggests that under highly stratified conditions, the type 1 and type 2 waves are expected to be present.

To determine if the observations made at the interface are associated with possible turbulent mixing events, a dynamical approach is performed using the gradient Richardson number ( $Ri$ ) and a linear stability analysis.

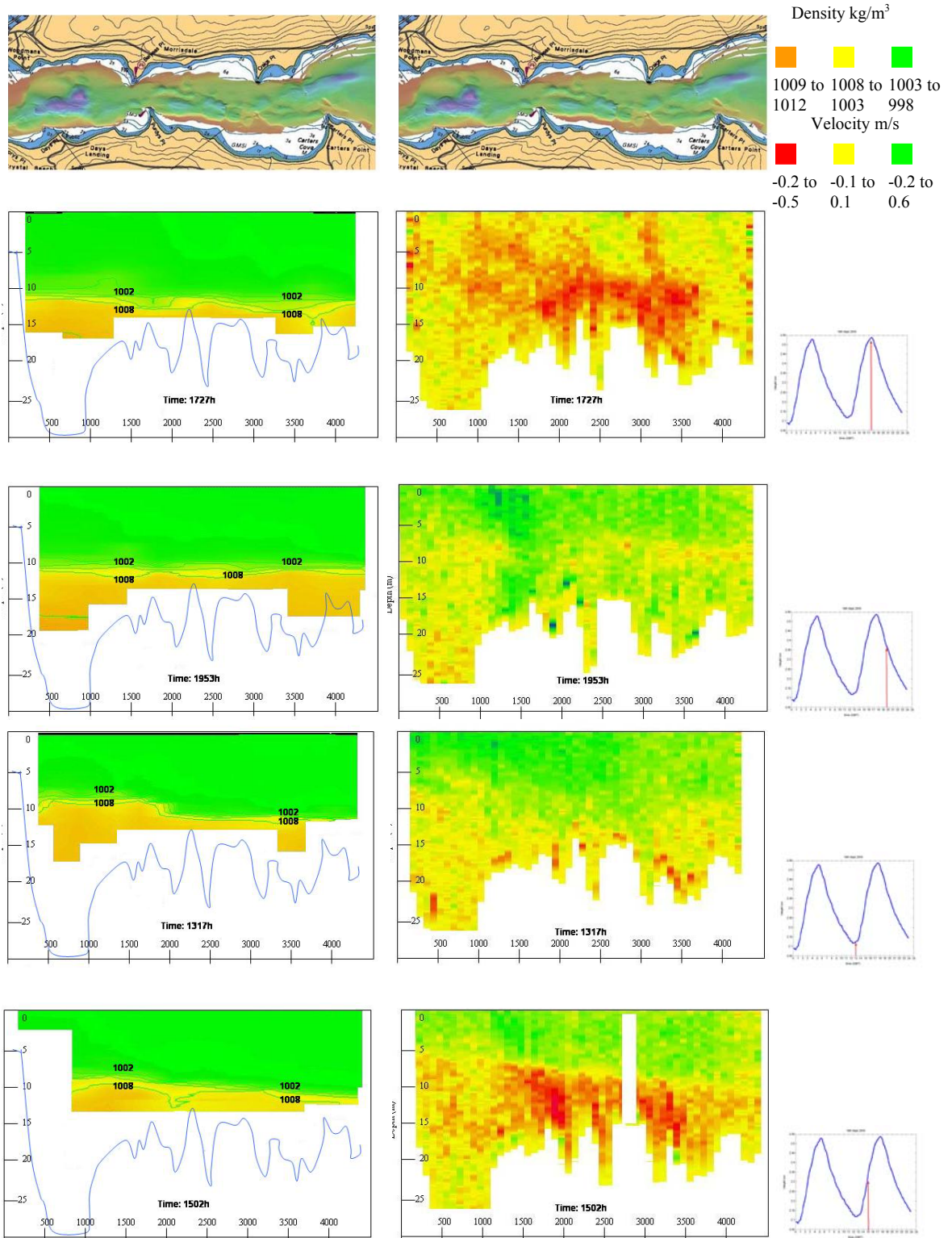


Figure 6.20: Longitudinal density (left) and velocity profile (right) for the spring tidal cycle.

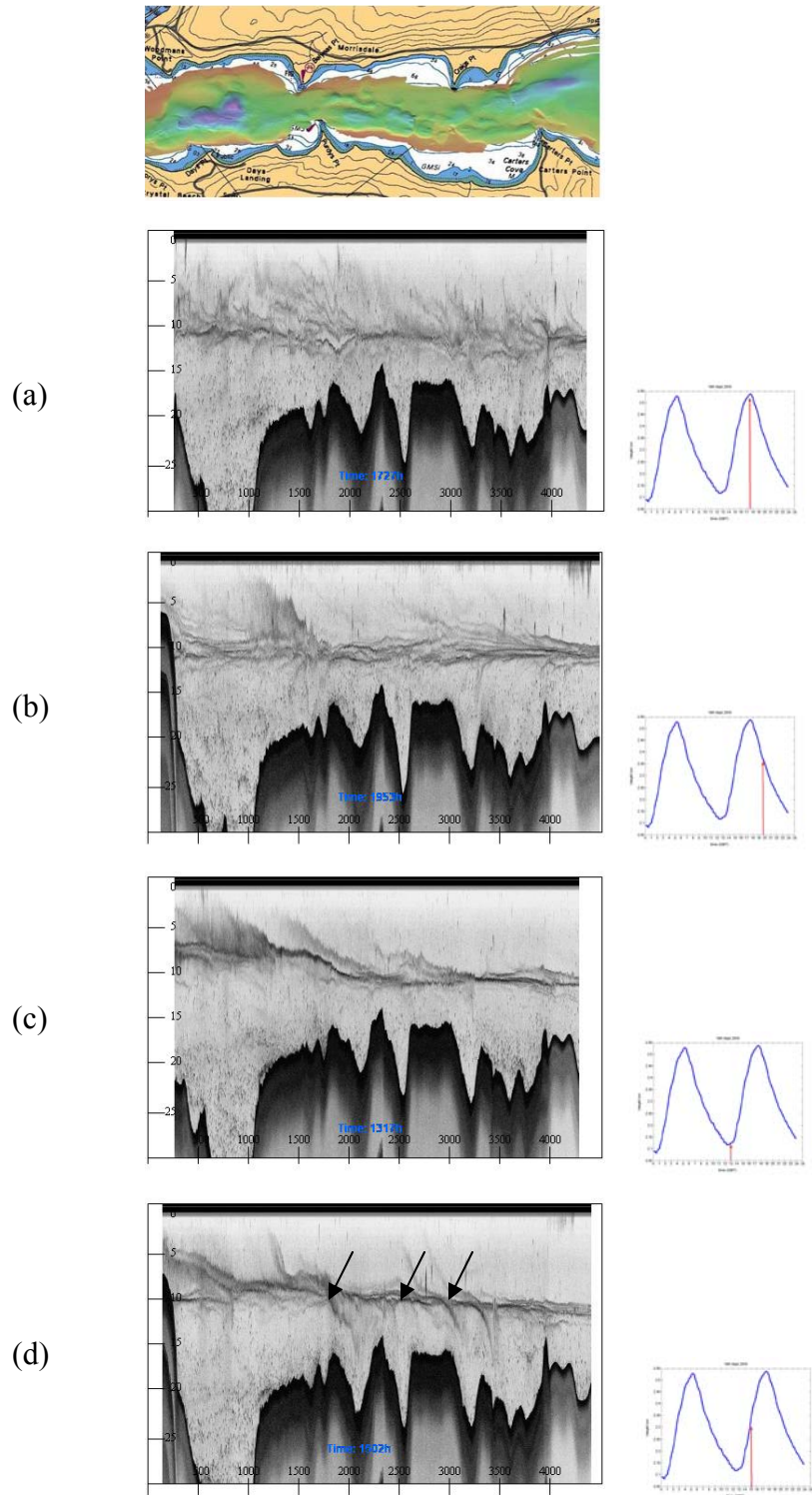


Figure 6.21: Acoustic volume backscatter images for the spring tidal cycle. The tilt of the pycnocline at low tide (c) and the plunging of the pycnocline (d) are observed from the images.



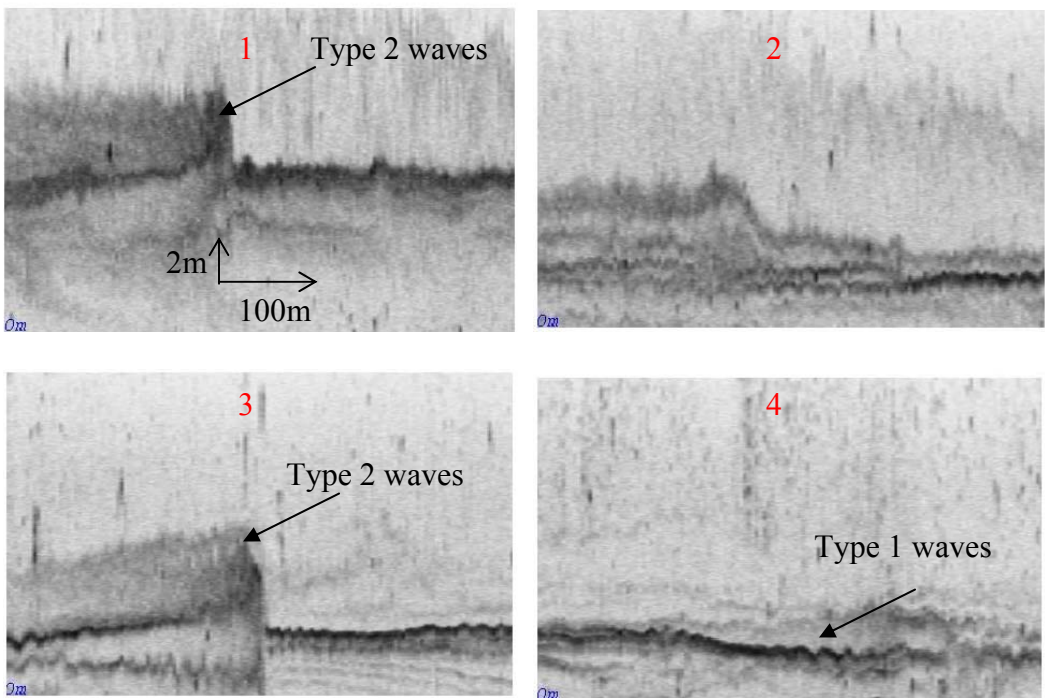
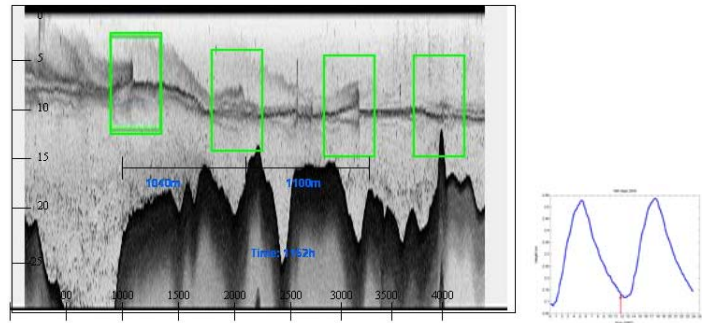


Figure 6.22: Identification of type 1 and type 2 wave for the spring tidal cycle.

### **6.3 Dynamic Investigation: Linear Stability Analysis**

Interfacial variations in the density and acoustic volume backscatter longitudinal profiles may have originated from either interfacial mixing or mixing occurring elsewhere which is horizontally advected into the region.

A classical approach that investigates mixing at interfaces is a linear stability analysis. This approach predicts whether the interface is unstable and if so, the type of instability which one expects to occur (KH or Holmboe waves). Either of these waves, when influenced by enough velocity shear, may break in a turbulent manner that causes mixing to occur.

Two methods of distinguishing between the KH and Holmboe are: (1) the Gradient Richardson number and (2) a linear stability analysis using the normal mode approach. In this research both methods are implemented. The theory for the gradient Richardson number is referenced from Richardson [1920], Miles [1961] and Dyer [1991]. The normal mode approach to the linear stability analysis is sourced from Lawrence et al. [1991] and Haigh [1995]. The theory of both the gradient Richardson number and the linear stability analysis was described in Chapter 3.

The linear stability analysis used in this study shall only indicate theoretically if the KH or Holmboe waves exist and provide a possible identification of the instability. To better understand the processes which are observed, it may be necessary in the future to perform a nonlinear analysis which considers the evolution of the waves.

### 6.3.1 Interfacial Mixing and the Gradient Richardson Number

The gradient Richardson number ( $Ri$ ) is used to determine whether interfacial mixing is occurring and the source of the mixing. It compares, at a particular location, the density stratification against the velocity shear. The theory of the  $Ri$  was discussed in Section 3.2.1. To recapture the essential theory:

1. Dyer [1995] states that for  $0 < Ri < 0.25$  Kelvin Helmholtz (KH) waves are likely to be present and turbulent mixing takes place.
2. If  $Ri > 0.4$  Holmboe waves are likely to be present and the mixing is negligible.
3.  $Ri > 1.0$  represents conditions unamenable for mixing (Richardson [1920])

In the theoretical studies of Miles [1961], Mile et al. [1964] and Dyer [1997] there is no mention of the vertical resolution required in calculating the  $Ri$  which in turn controls the critical value of  $0 < R < 0.25$  to determine the possibility of mixing. There has been field confirmation by Geyer et al. [1989], [1987] that when  $0 < R < 0.3$  KH instabilities were observed. There are also studies where the critical value has had to be increased to 0.4 to agree with the observations. An example of this is in Nepf et al. [1996] where the resolution of the survey sensors affects the calculations and in Chant et al. [2000] where the spatial distribution of the lowest  $Ri$  was used to determine mixing.

In this study of Long Reach was limited by: the vertical resolution of the ADCP which is 0.5m. The vertical resolution of the CTD is 0.1m. The CTD data were averaged to conform to the resolution of the ADCP (see Section 5.4.1 for procedure). The ADCP data were also averaged with all the pings within a 200m radius of the CTD dips, thus the velocity used was not the measured velocity at that particular location but the averaged



velocity. Bearing in mind these limitations, setting a critical value for the KH and Holmboe waves proved to be unreliable and subject to errors.

Based on the limitations of the Ri with respect to the resolution of the equipment available, a critical value of  $0 < Ri < 1$  was used to determine all mixing events in this study. The main purpose of employing the Ri in this study is to possibly determine if interfacial mixing is occurring in the survey area.

### **6.3.1.1 Results**

The Ri is calculated for all the CTD profiles cast throughout the tidal cycle. An assessment is then made on the results to determine when a velocity shear existed within the pycnocline and  $0 < Ri < 1$ . This was performed for both the neap and spring tidal cycles.

The results show that  $0 < Ri < 1$  occurred at group1, group2 and group3 at rising tide (see Figure 6.23). For all of these observations the critical value occurred at the base of the pycnocline (see Figure 6.24 and 6.25).

The results of the Ri showed that the critical value of the Ri occurred at the base of the pycnocline. This observation is also similar to the observations made of the longitudinal density profiles where: (1) the density profile shows a decrease in density gradient at the lower pycnocline region (see Figure 6.9) and (2) the acoustic backscatter profiles shows the plunging of the pycnocline at the lower interface layer (see Figure 6.4, time 2128h). It can be deduced, based on these observations, that interfacial mixing is occurring at the base of the pycnocline, at group1, group2 and group3 during rising tide.

Mixing was not observed to occur within the vicinity of Carters Pt, yet in Section 6.2.1 a decrease in bottom density was observed in this region at rising to high tide. Thus the mixing events occurring in the groups may have advected to Carters Pt at rising to high tide or it may be due to bottom boundary layer shear rather than interfacial mixing.

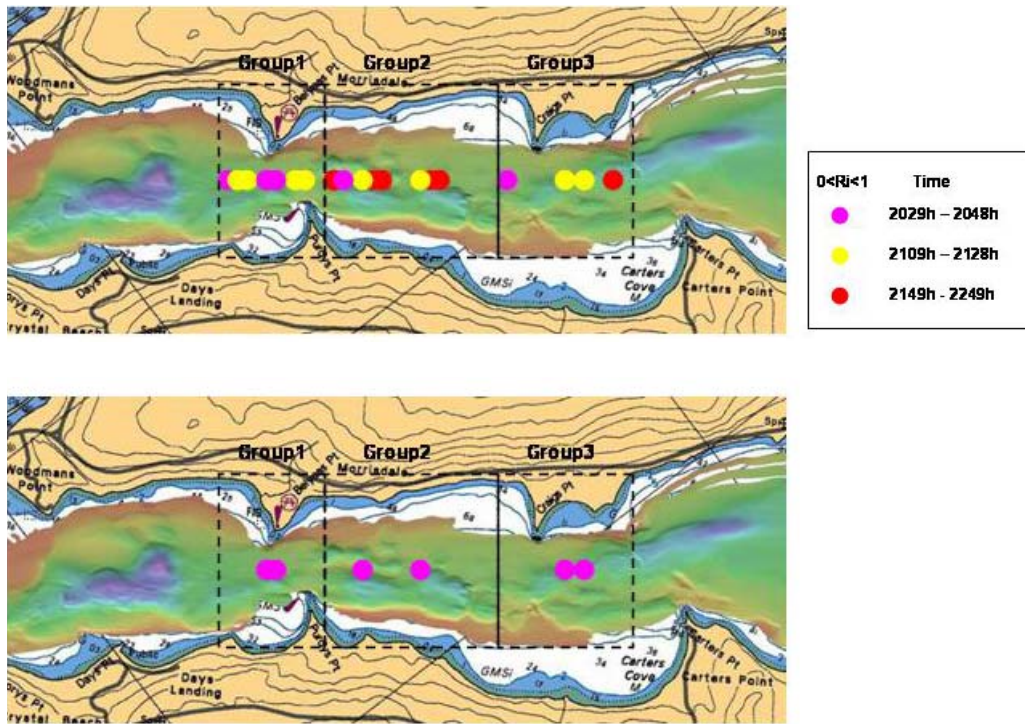
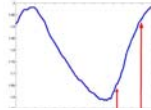


Figure 6.23: Gradient Richardson number from rising into high tide at neap (top) and spring tides (bottom).

7<sup>th</sup> September Gradient Richardson Number: Group1

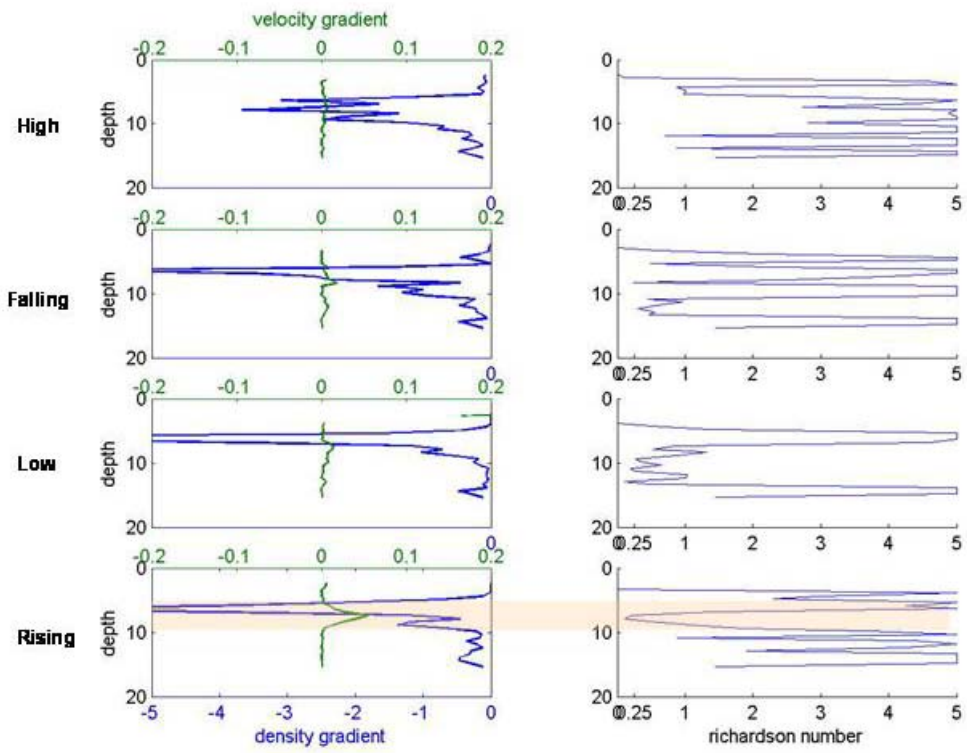


Figure 6.24 (a): The Ri for Group 1 at neap tides. Shaded regions represent mixing.

7<sup>th</sup> September Gradient Richardson Number: Group2

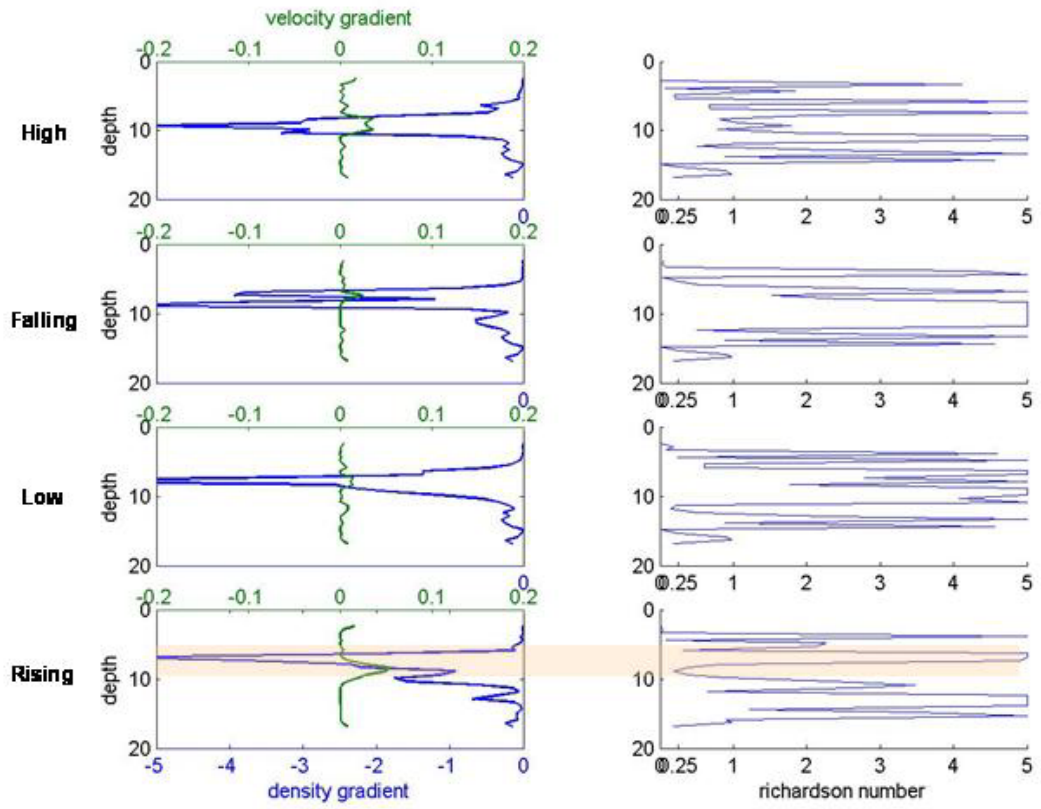


Figure 6.24 (b): The Ri for Group 2 at neap tides. Shaded regions represent mixing.

7<sup>th</sup> September Gradient Richardson Number: Group3

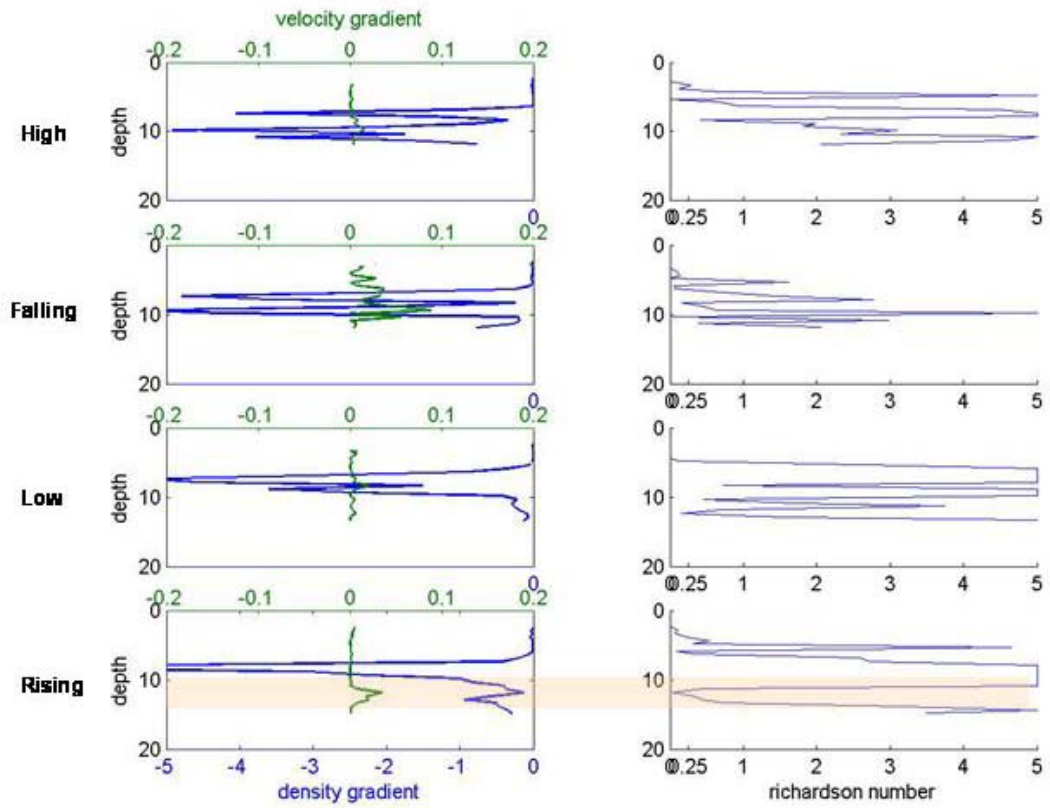


Figure 6.24 (c): The Ri for Group 3 at neap tides. Shaded regions represent mixing.

14<sup>th</sup> September Gradient Richardson number: Group 1

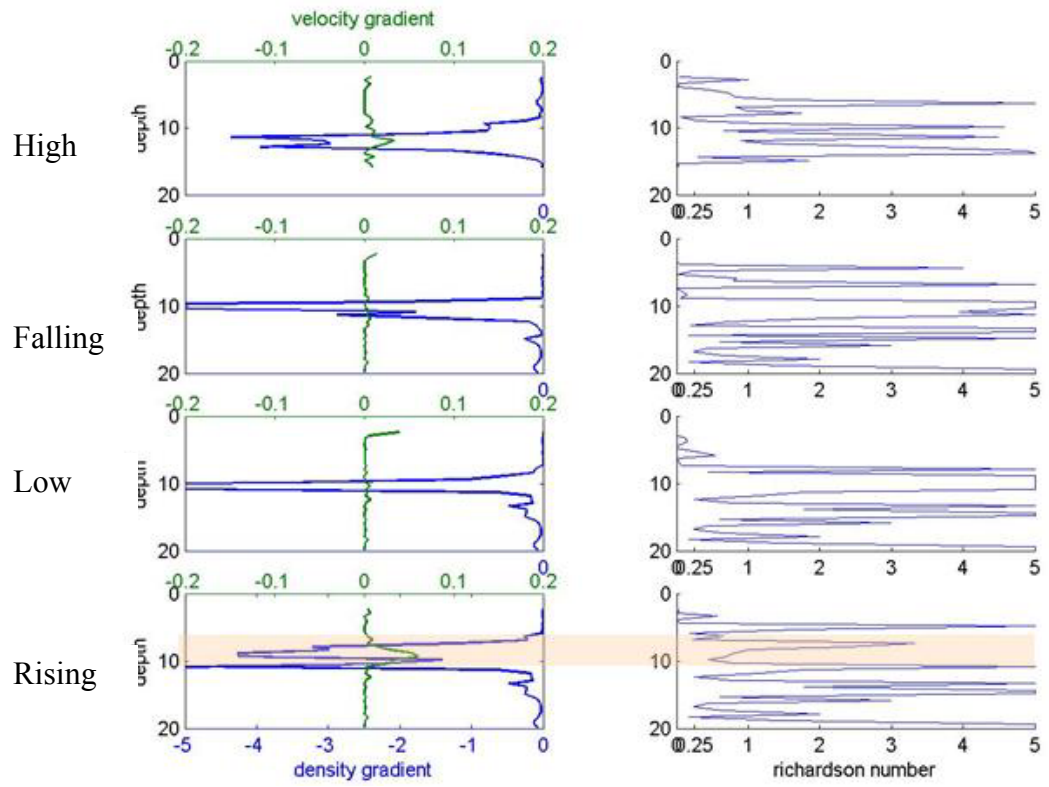


Figure 6.25 (a): Ri for Group 1 at spring tides. Shaded regions represent mixing.

14<sup>th</sup> September Gradient Richardson number: Group2

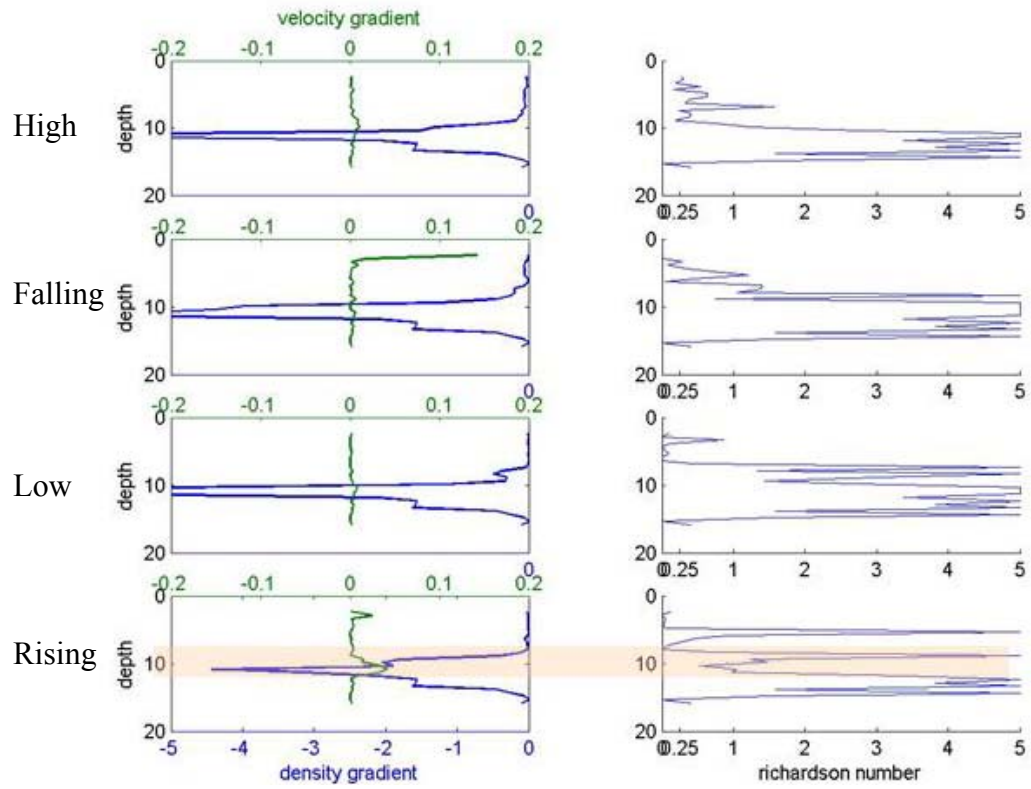


Figure 6.25 (b): Ri for Group 2 at spring tides. Shaded regions represent mixing.



14<sup>th</sup> September Gradient Richardson number: Group3

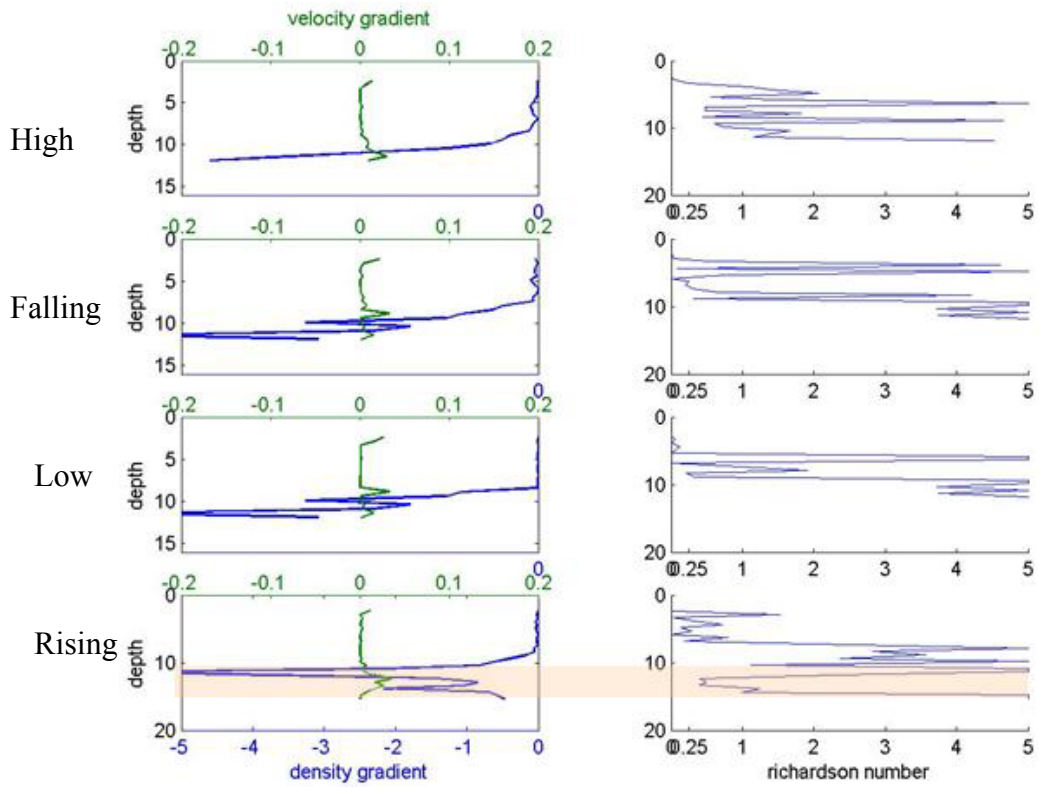


Figure 6.25 (c): Ri for Group 3 at spring tides. Shaded regions represent mixing.

Studies performed in the Fraser River estuary by Geyer and Farmer [1989] observed that, on the ebb tide, KH waves existed (see section 3.4 Figure 3.11), followed by the upward movement of the pycnocline at particular locations. This was then followed by the collapse of the salt wedge (see Figure 6.26a).

Studies in the Knight Inlet Sill by Farmer and Smith [1980] observed that, within the vicinity of the sill, the pycnocline plunges downwards into the bottom layer (see Figure 6.26 b). Solitons wave packets were observed at the interface.

In this study of Long Reach the opposite occurs to that of Geyer and Farmer [1989]. In Long Reach at rising tide the pycnocline plunges downwards and the whole salt wedge does not collapse (see Figure 6.26c). KH waves were not observed. The difference in the layer that mixing appears to be taking place, may be attributed to the phase of the tide. In Geyer et al.[1989] studies, the mixing occurred at ebb tide and thus the most active layer was the surface layer. In Long Reach the mixing is observed to occur at rising tide thus the most active layer is the bottom layer. Interestingly, in both studies the mixing is first initiated where constrictions exist laterally.

The observations in Long Reach are similar to those made by Farmer and Smith [1980] in the Knight Inlet Sill. However in Long Reach the plunging of the pycnocline occurs soon after the disappearance of the soliton wave packets. It is after the disappearance of the solitons that mixing is determined to occur, within the vicinity of the plunges. Thus it appears that one of the following scenarios is occurring: (1) the solitons cause the mixing to take place, (2) at rising tide when maximum shear occurs, KH or Holmboe waves may have initiated the mixing process or (3) the plunges are the main source of mixing.

To determine the possible source of mixing in Long Reach, a linear stability analysis using the normal mode approach is performed. It should be cautioned that the linear stability analysis can only identify if the KH or/and Holmboe waves are possible. To identify the other types of interfacial waves that may exist (solitons) a non linear analysis needs to be performed. A non linear analysis is beyond the scope of this research.

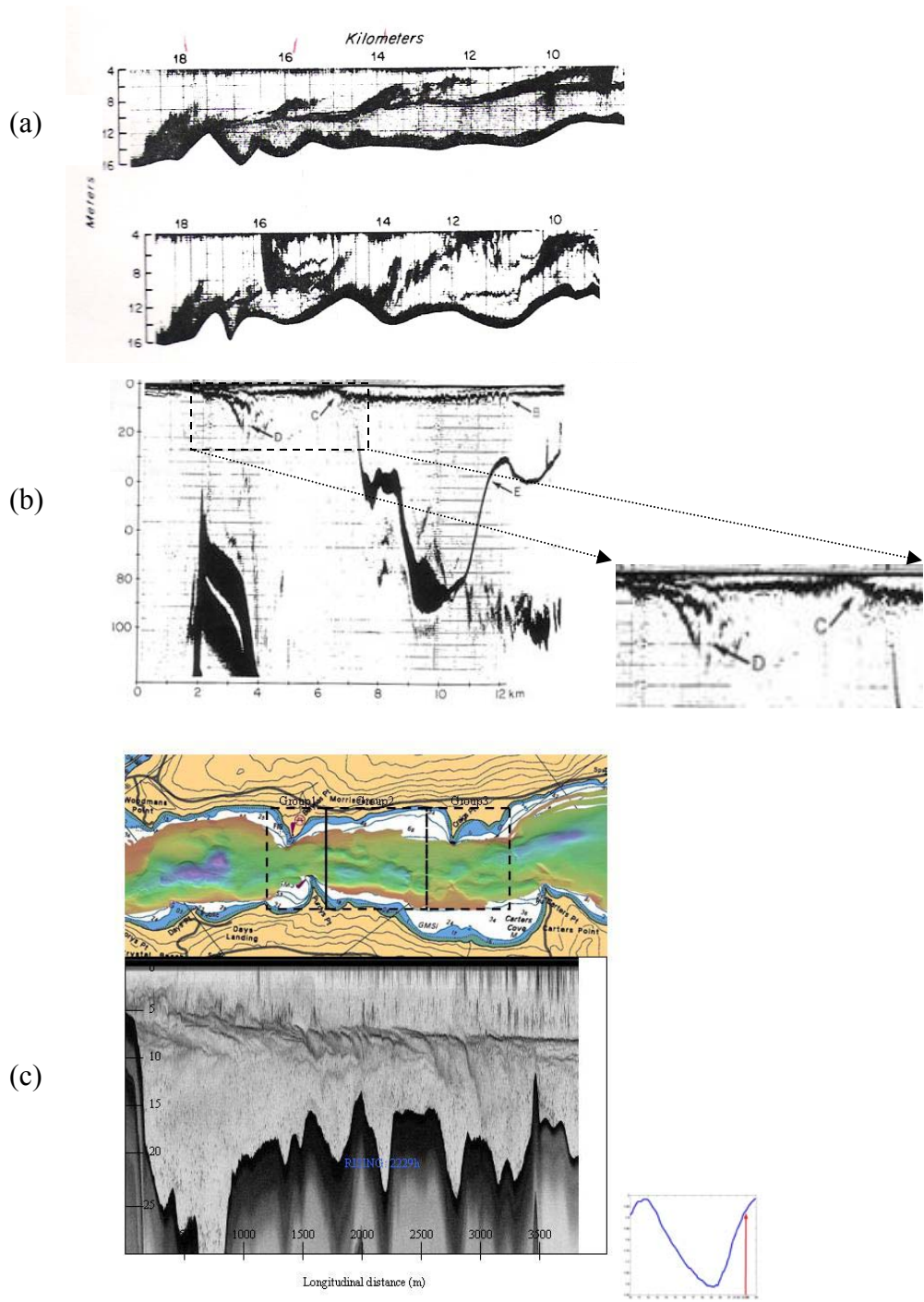


Figure 6.26: Echosounder images (a) Geyer et al.[1989] at ebb tide (top)at the start of mixing and the collapse of the salt wedge; (b) plunging of pycnocline in the Knight Inlet Sill;(c) plunging of the pycnocline in Long Reach at rising tide.

### **6.3.2 Linear Stability Analysis**

Visual observations of the density and echosounder profiles suggest that mixing processes may be occurring at the pycnocline for group1, group2 and group3 at rising tide. Calculations of the gradient Richardson number confirmed that mixing is occurring since  $0 < Ri < 1$  for these three groups. To identify the source of the instability that is initiating the mixing process (Kelvin-Helmholtz or Holmboe) a linear stability analysis is performed using a normal mode approach. The theory and calculations used in this section are discussed in Section 3.3.1. Due to similarity of observations of the neap and spring tides the stability analysis is performed using only the neap tides velocity and density data.

#### **6.3.2.4 Application of Theory to Observations in Long Reach**

Variations in the density and the plunging of the pycnocline are observed within the 1500m to 4000m marker (see Figure 6.8). In section 6.2.4.2 this region was divided into three groups (see Figure 6.11). To determine the type of instability that may contribute to the mixing process, a piecewise approximation and smooth profile fit are performed for the profiles (see Sec 3.3.1.1 Figure 3.6). For the smooth profile fit a hyperbolic tangent approximation is used in this study.

The linear stability analysis is first performed using the piecewise approximation because of its simplicity. Examination of the individual velocity and density profiles indicate that only some of the profiles fit the pattern of the linear piecewise approximation as depicted in Section 3.3 Figure 3.6a. Figure 6.27 illustrates the different typical density and velocity profiles that are observed and those which are used in the

theory. The piecewise approximation is only applicable for those profiles that are well represented by this approximation. It is observed that in group 3 the profiles do not match the theory. Therefore the linear stability analysis is performed for only group1 and group2.

To calculate the wave number which is used to calculate the wavelength the following were calculated: the density interface thickness, the shear layer thickness, the asymmetry  $\varepsilon$ , and the bulk Richardson number ( $J$ ).

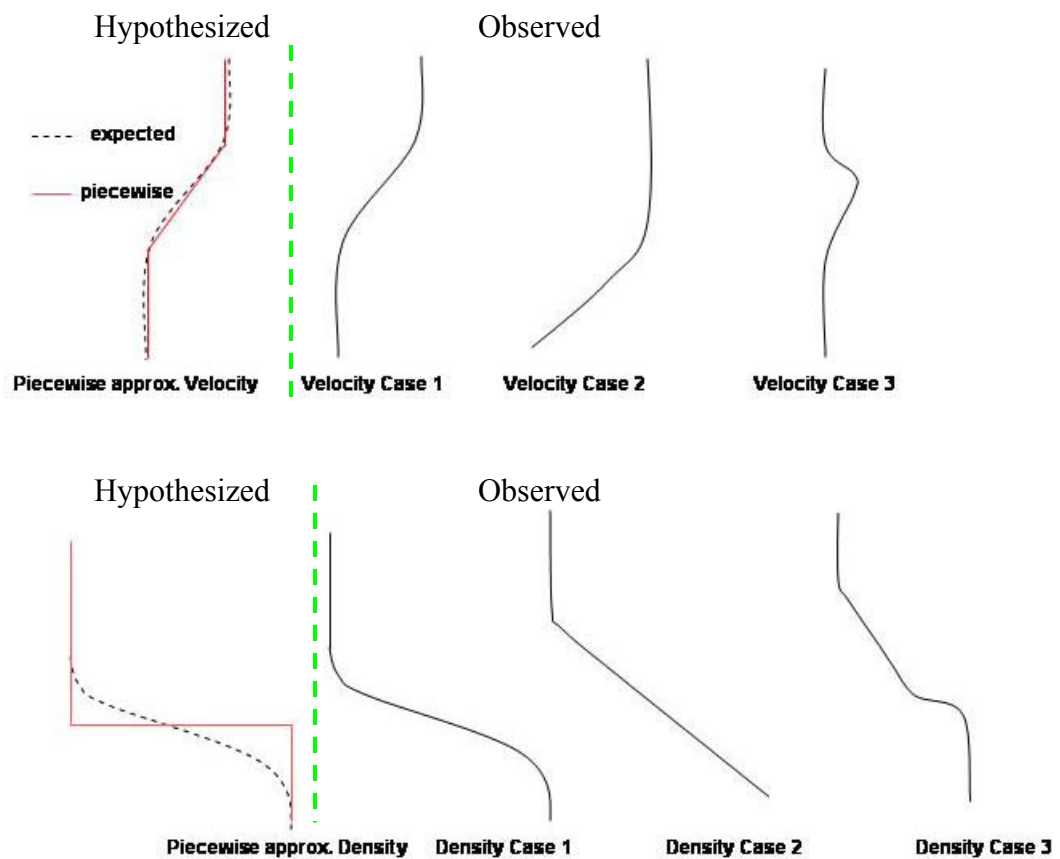


Figure 6.27: Typical velocity (top) and density (bottom) profiles observed at rising tide.

### 6.3.2.5 Results of Linear Stability Analysis

The results of the piecewise approximation of the linear stability analysis show that  $\varepsilon$  varied from -0.5 to -1.0 (which indicates that shear was below the pycnocline) and  $0.93 < (J) < 1.43$  (see Table 6.3). The asymmetry of  $\varepsilon$  indicates that either the flow is stable or Holmboe waves are present.

$\varepsilon < 0$  indicates that the left wave has the largest growing amplitude. The left wave is the mode that is closer to the  $J$  axis whilst the right wave is closer to the wave number axis (see Figure 6.28). The graphs in Figure 6.28 show that as  $\varepsilon$  decreases the left wave has the largest growing rate and that at  $\varepsilon = -0.7$  the right wave solution has vanished.  $J$  interpolated on the stability diagram shows that the Holmboe wave can be present with a wave number ( $w$ ) varying between 1.75 to 2.2 (see Table 6.3 and Figure 6.29). Calculations of the wavelength ( $k$ ) where  $k = 2\pi h/w$  gives a wavelength of between 8.56m to 10.47m.

The results of the piecewise approximation method suggests that, since the left wave has the largest growth rate, that mixing occurs in the bottom layer. This result is also confirmed both theoretically and descriptively. Theoretically the Gradient Richardson number shows mixing occurring at the base of the pycnocline. Descriptively the density profiles show at rising tide a decrease in density at the lower pycnocline region and the acoustic backscatter images also show at rising tide the plunging of the pycnocline into the bottom salty layer.

The potential Holmboe waves (type 1 waves) are visually identified from the acoustic backscatter images at time 2029h, 2049h and 2149h. Table 6.3 shows the values

of the measured wavelength. Figure 6.30 shows the image of the Holmboe waves. The Holmboe wave is the type 1 wave observed in section 6.2.

Table 6.3 shows that a difference exists between the observed and calculated wavelength. This difference can be attributed to two factors: (1) in the piecewise stability analysis the approximations of the velocity and density profile are a poor fit to the data (see Appendix 3) and (2) the flow is considered to be unbounded. Thus this approximation may not be good enough to give a good prediction of the wavelength.

The piecewise approximation identifies the type of wave that may possibly contribute to the mixing. However it did not accurately predict the wavelength of the waves that are observed in the acoustic backscatter images.



Table 6.3: Results of the linear stability analysis using the piecewise approximation.

<b>DIP#</b>	<b><math>\varepsilon</math></b>	<b>J</b>	<b>w</b>	<b>k (m)</b>	<b>Observed k(m)</b>
<b>415</b>	-0.7	1.43	2.2	10.47	12
<b>421</b>	-0.5	1.23	2.2	8.56	20
<b>422</b>	-0.88	0.93	1.75	9.68	15
<b>465</b>	-0.66	0.996	1.8	10.46	14

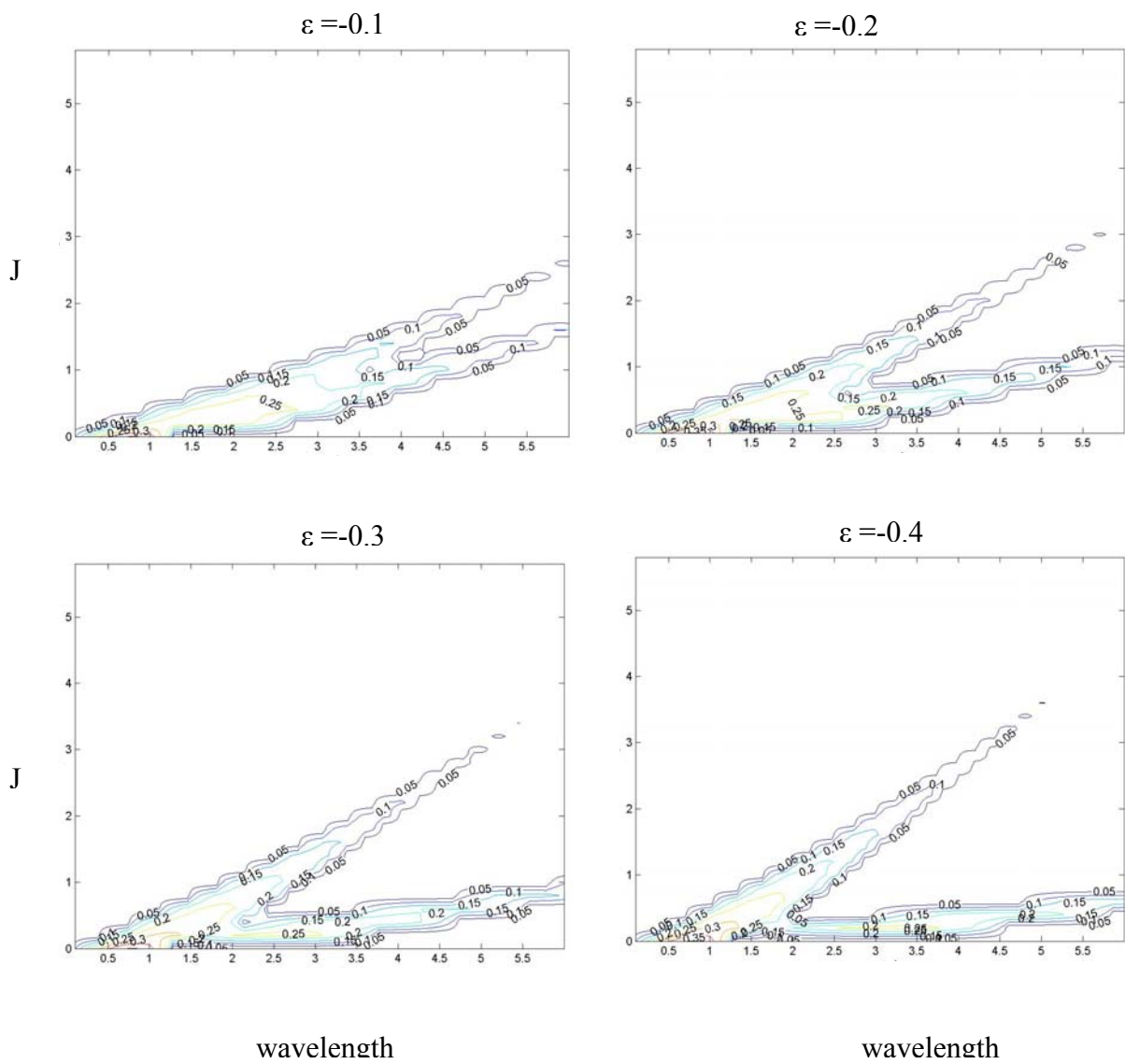


Figure 6.28: Stability diagrams of the wave amplitude derived from the piecewise approximation

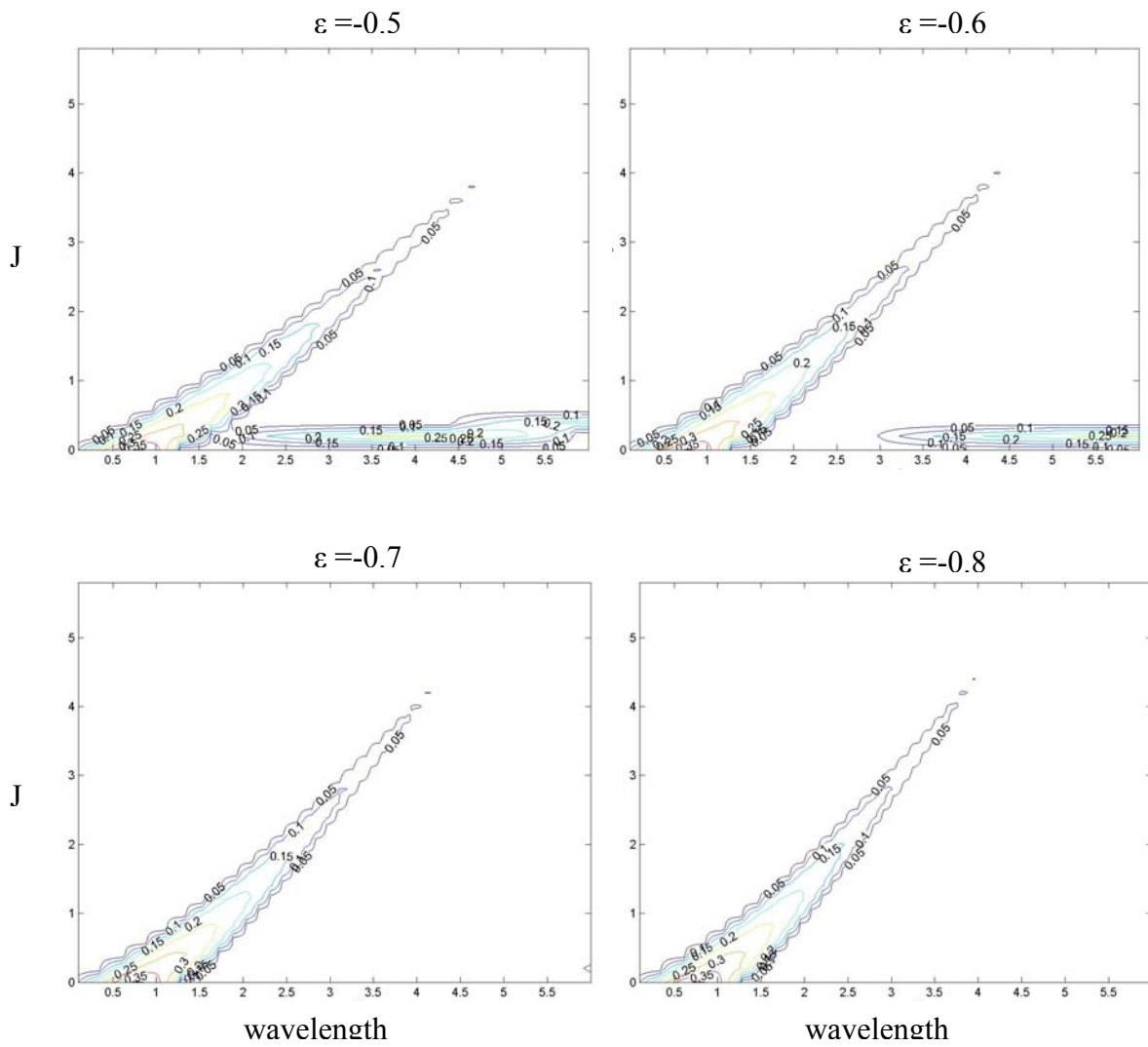


Figure 6.28 (continued): Stability diagrams of the growth rate derived from the linear stability analysis (piecewise approximation).

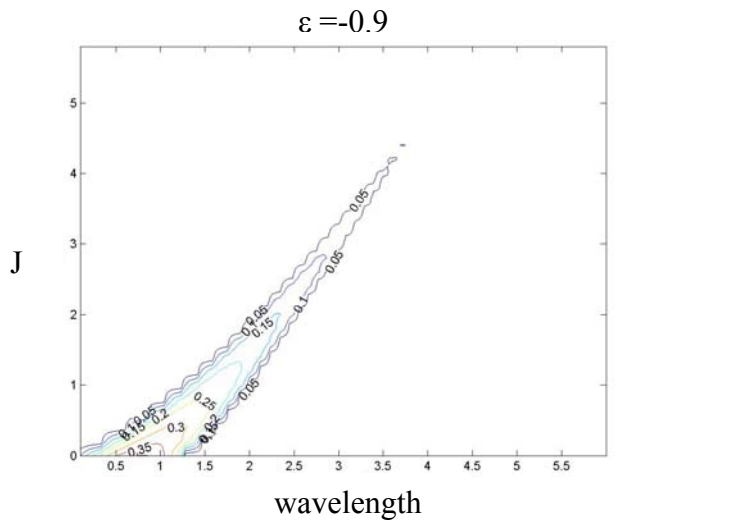


Figure 6.28 (continued): Stability diagrams of the growth rate derived from the linear stability analysis (piecewise approximation).

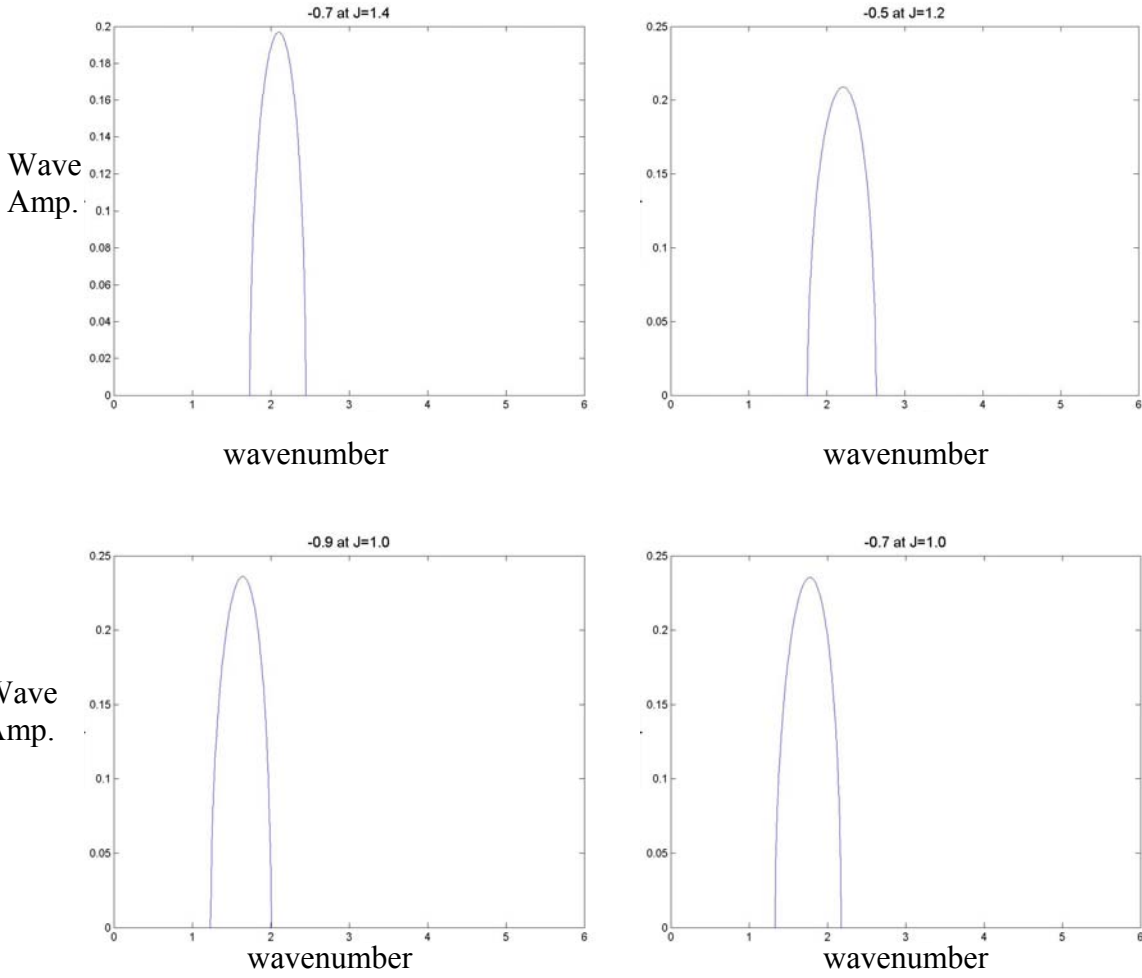


Figure 6.29: The interpolation of the J (see table 6.3) on the growth rate for the piecewise approximation method.

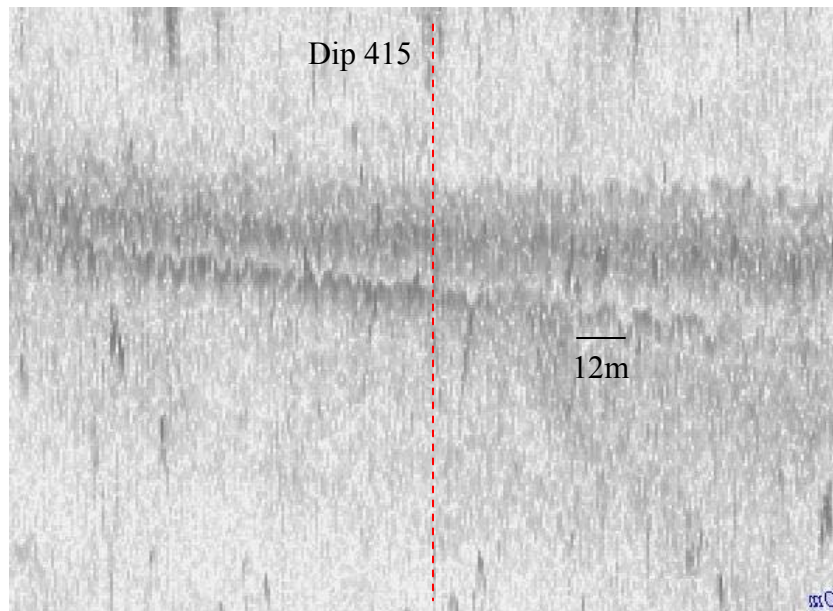
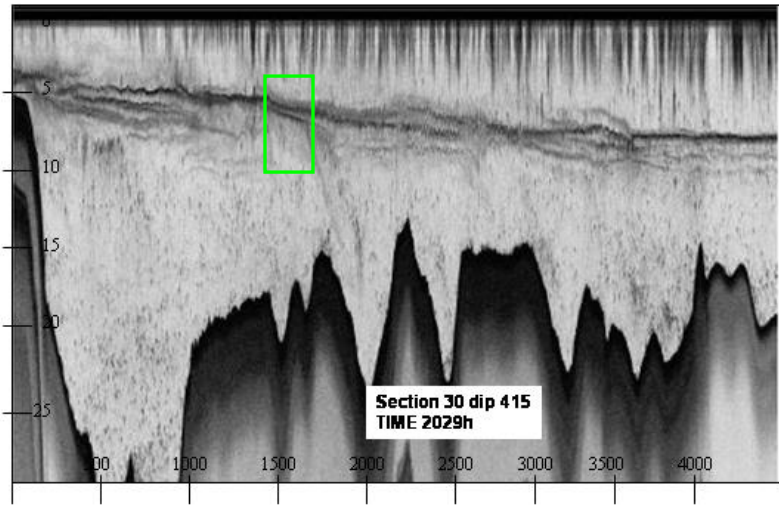
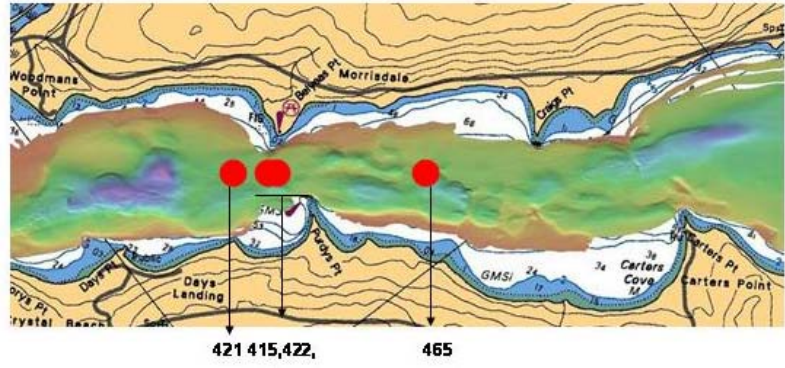


Figure 6.30 (a): Holmboe wave identification for CTD dip 415.

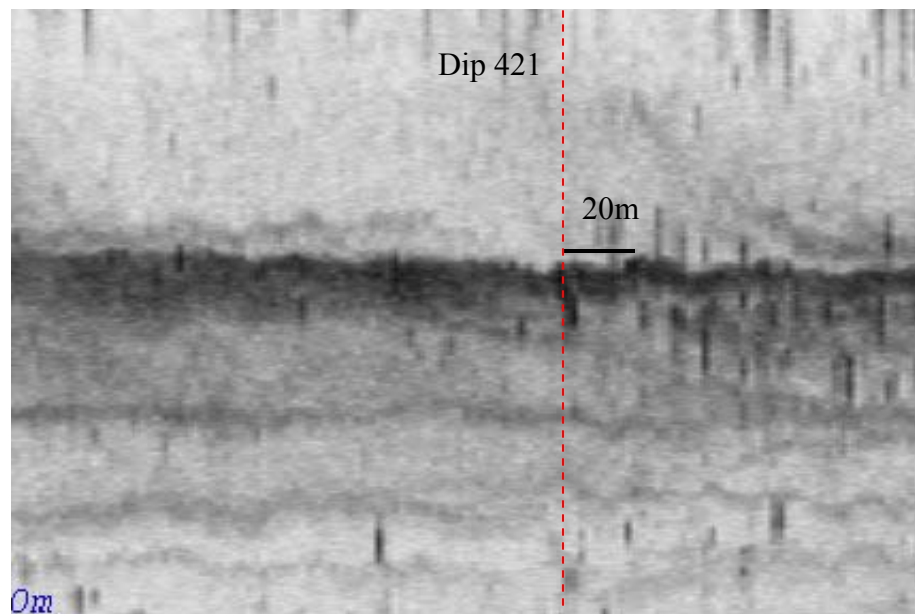
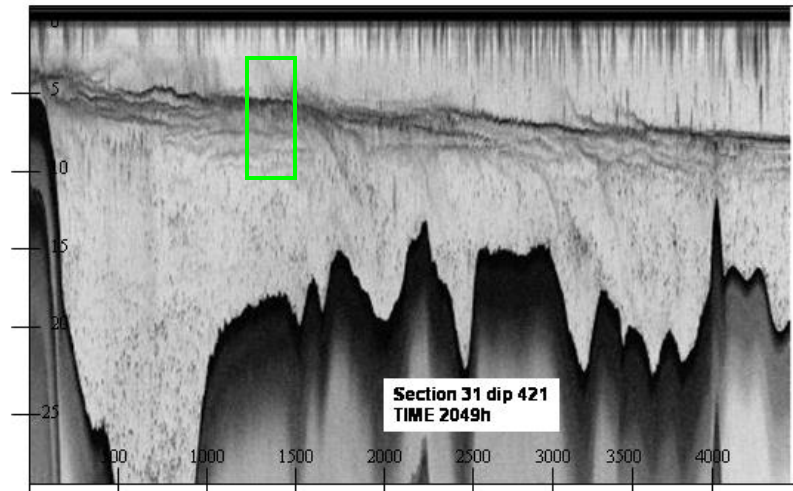
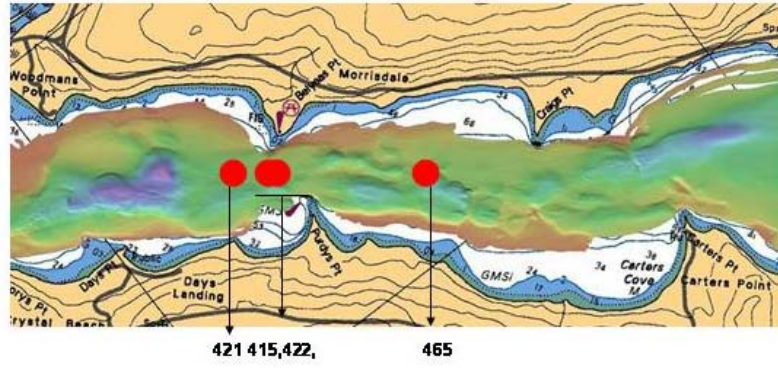


Figure 6.30 (b): Holmboe wave identification for CTD dip 421.



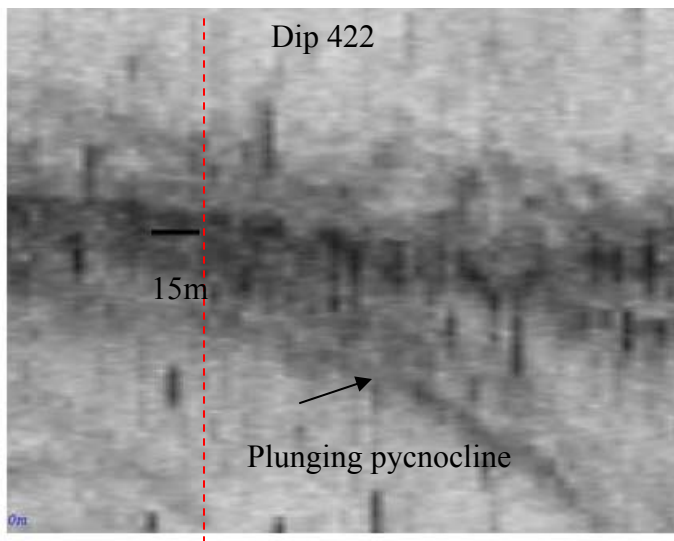
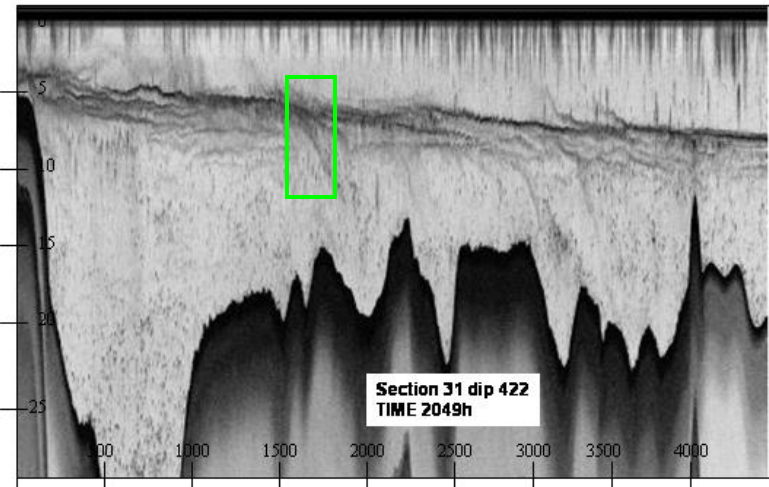
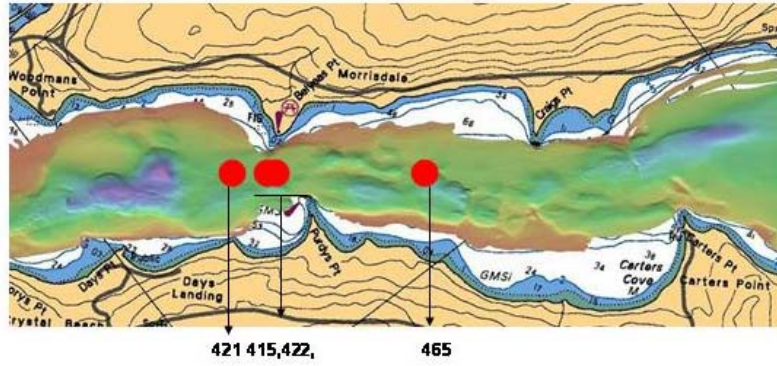


Figure 6.30 (c): plunging of the pycnocline (top) and Holmboe wave identification (bottom) for CTD dip 422.



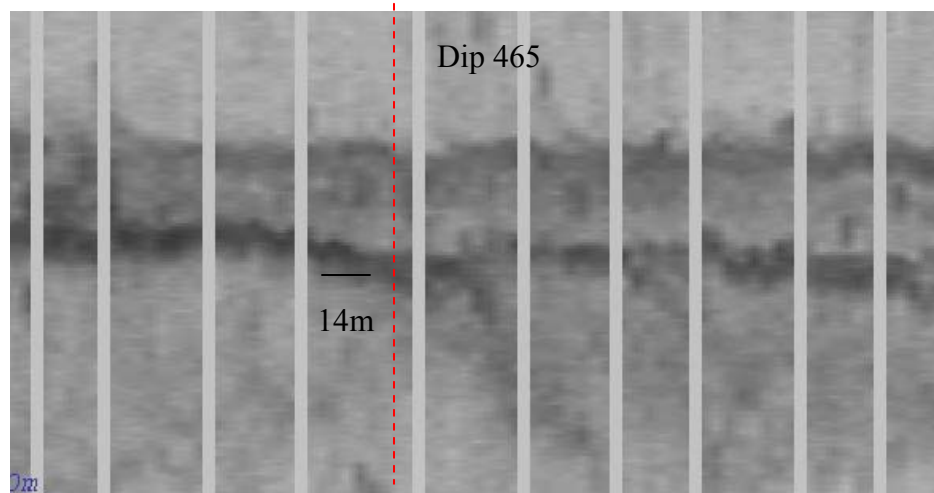
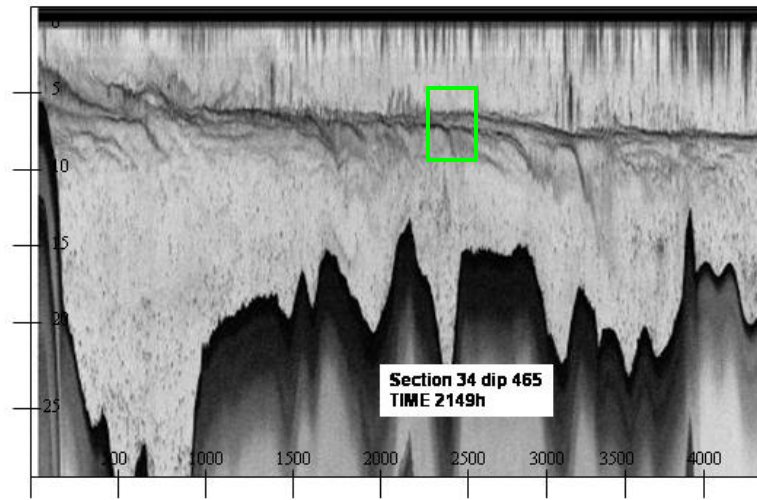
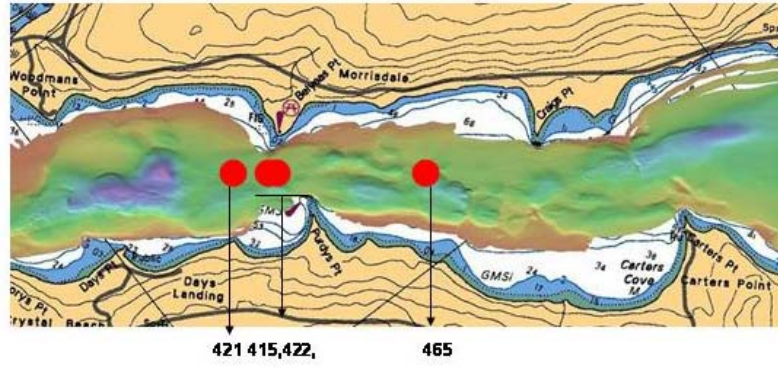


Figure 6.30 (d): Holmboe wave identification at CTD dip 465.

As a result of the difference between the predictions of the piecewise theory and observations, the smooth profile method is employed. This method models the velocity and density profiles more accurately. The smooth profile approximation is solved numerically using software provided by S. Haigh (see Haigh [1995] or Smyth et al. [1989] for a description of the numerical method used).

Appendix II shows the approximation of the smooth profiles using the hyperbolic function. Fitting the smooth profiles showed that  $\varepsilon < 0$  with a range of -0.46 to -0.92 (shear below the pycnocline). This indicates that the left moving wave is the most unstable.  $J$  varied between 0.9 and 1.48 and the wavenumber varied from 0.9 to 1.3. The predicted wavelengths are illustrated in Table 6.4.

Linear stability analysis predicts that Holmboe waves are only possible for  $R > 2$  (for the symmetric case of  $\varepsilon = 0$ ). In this study the range of  $R$  values is from 1.58 to 3.5. Thus these results show that for the non-symmetric case (where  $\varepsilon$  is large) Holmboe waves can exist when  $R < 2$  (see dip 422).

Examination of the results of the piecewise approximation and the smooth profile method with the observed wavelength is performed (see Table 6.3 and 6.4). The results show that in general the smooth profile method agrees with the observed wavelength better than that of the piecewise method. The exception was dip 415 which agreed with the piecewise approximation method better than that of the smooth method. However both the piecewise approximation and smooth profile method results indicate that Holmboe waves are present in the estuary and may be a potential source of mixing.

The theory of the stability analysis has been verified by laboratory experiments. This research has applied this theory to field observations. In the field different

conditions exist that affects the characteristics of the wave such as the geometry and bathymetry of the area and possibly secondary flow.

Field observations performed by Yoshida et al. [1998] in the Ishikari River, Japan used the piecewise approximation to determine the mixing mechanism at the interface. Their results, using the piecewise approximation, identified the wave as the Holmboe wave and accurately predicted a wavelength of 4.96m.

The results of the linear stability analysis indicate that Holmboe waves can exist in Long Reach. From the acoustic backscatter images the type 1 waves have a wavelength comparable to that predicted for the Holmboe waves identified at the interface. Thus Holmboe waves may be the source of mixing observed in Long Reach. The Holmboe waves may have been created by the shear which was enhanced at rising tide in the region where constrictions exist both laterally and vertically.

#### **6.3.2.6 Other Sources of Mixing**

The descriptive analysis has shown that the soliton wave packets disappear at early rising tide followed by the plunging of the pycnocline during which turbulent mixing occurs. These observations suggest that one or all of the following are the main causes of the turbulent mixing observed in Long Reach:

1. The soliton wave packets disappears and this is followed by mixing
2. The Holmboe waves, influenced by the stratification and shear at rising tide, causes mixing to occur
3. At rising tide the pycnocline is influenced by the flow of the upper and lower layer. Thus as it passes over the shoal and deep areas of Long Reach it causes the

pycnocline to plunge downwards thus causing turbulent mixing to occur. The scale of the plunges suggests that they may contribute the most to the exchange of water for upward entrainment.

Table 6.4: Results of the linear stability analysis using the smooth profile method

<b>DIP#</b>	$\epsilon$	<b>J</b>	<b>w</b>	<b>Prandtl</b>	<b>Reynolds</b>	<b>R(m)</b>	<b>H</b>	<b>k(m)</b>	<b>Observed</b>
<b>415</b>	-0.7	1.44	1.3	697	300	3.5	5.25	16.9	12
<b>421</b>	- 0.46	1.3	1.3	697	300	3.0	6.5	14.5	20
<b>422</b>	- 0.88	0.9	0.9	697	300	1.58	5.65	18.85	15
<b>465</b>	- 0.92	1.48	1	697	300	2.25	4.65	16.9	14

## 6.4 Summary of Section One

An oceanographic survey performed in Long Reach in September 2004 shows the estuary to be highly stratified with surface and bottom waters of near constant density. From rising tide into falling tide (during which the maximum upstream flow and boundary shear occurs) a thickening of the pycnocline was observed at an area in the estuary where constrictions exist both laterally and vertically.

To determine if, at rising tide, the decrease in density at the lower pycnocline region is due to turbulent mixing occurring at the interface, calculations of the gradient Richardson number were performed searching for evidence of  $0 < Ri < 1$ . Calculations of the gradient Richardson number indicate that interfacial mixing is taking place in a region where the bathymetry is irregular and constrictions exist laterally.

To identify if either the KH or Holmboe waves may have initiated the mixing events, a linear stability analysis was performed using both piecewise linear and hyperbolic tangent approximations of the velocity and density profiles. Both methods predicted that Holmboe waves are a potential source of mixing.

Observations of interfacial waves from the echosounder images show two possible types of waves. Type 1 waves with a wavelength of 15m to 30m; type 2 waves with packet spacing of 450m to 710m.

The wavelength of the type 1 wave observed from the echosounder images is accurately predicted by the linear stability analysis using the smooth profile approximations for the velocity and density profiles with linear stability analysis.

The type 2 waves observed is not a type of wave predicted by linear stability analysis. However it resembles soliton wave packets described by Apel [2002] and

observed in the field by Farmer and Smith [1980]. To theoretically confirm if the type 2 wave is actually a soliton wave packet, a non linear analysis would have to be performed which was beyond the scope of this research. However the coincidence of its departure just before mixing takes place and its existence at the interface at the constrictions suggests that it is also a potential source of mixing.

The plunging of the pycnocline into the bottom layer is observed to occur just after the disappearance of the soliton wave packets. In the areas of the plunges, mixing was observed to occur. These observations and calculations ( $Ri$ ) suggest that either the plunges are the result of the disappearance of the soliton wave packets or the plunges are a different phenomena altogether. These phenomena may be the result of the flow pattern of the upper and lower layers as it passes over the shoals and deep areas of Long Reach.

## CHAPTER 7

### ANALYSIS: SECTION TWO

In this section the surface layer refers to the 0m to 10m depth whilst the bottom layer refers to the 10m to 25m depth. The observations of this section are described in a similar style as those described in Chapter 6 for section one. The velocity and density shall first be described followed by the acoustic volume backscatter images. Mention is made of particular locations along the estuary. These locations are referenced with respect to the beginning of the survey area, which is represented by the 0m marker.

#### 7.1 Bathymetry

The extent of this section is from Carters Pt. to Victoria Shoals. The width is ~1200m and the depth varies from 5m to 30m (see Figure 7.1).

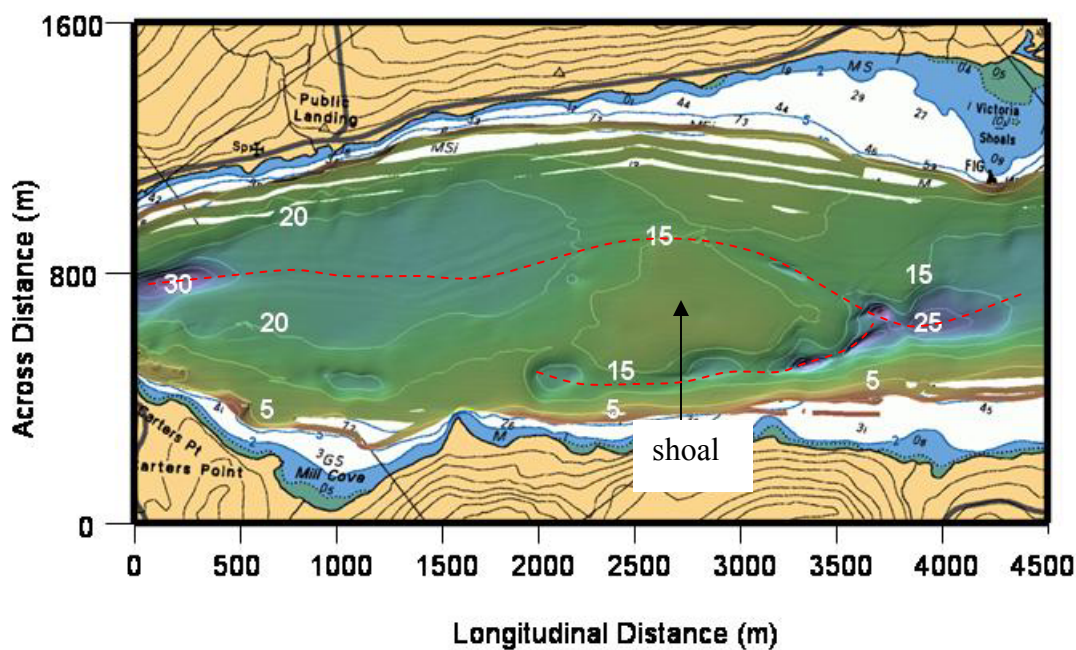


Figure 7.1: Plan View map of section two.

This bathymetry of this area is almost regular apart from a few exceptions. They are:

- A 30m channel that exist north of Carters Pt.
- In the middle of the survey area a 15m shoal exists
- To the south and north of the shoal a deep channel exists

## 7.2 Density Structure

The surface and bottom layers are almost homogenous throughout the tidal cycle with a surface density of  $\sim 999 \text{ kg/m}^3$  and a bottom density of  $1011 \text{ kg/m}^3$ . These two layers are separated by a  $\sim 1.5 \text{ m}$  thick pycnocline (see Figure 7.2). This density structure resembles a highly stratified estuary which was also observed in section one.

Figure 7.3 shows that a variation in bottom density occurs at two locations: (1) at falling tide (7.3(b)) within the vicinity of the downstream side of the sill (at the  $\sim 2000 \text{ m}$  marker) and at rising tide into high tide (7.3(a, d)) on the upstream side of the sill ( $\sim 3000 \text{ m}$  marker). In these two locations a decrease in density from  $1010 \text{ kg/m}^3$  to  $1009 \text{ kg/m}^3$  occurs.

The pycnocline remains at an almost constant level for the duration of the tidal cycle except for two occasions when a displacement of the pycnocline occurs. (see Figure 7.4). This displacement is first sighted at high tide at  $\sim 500 \text{ m}$  marker (referred to as location A) and mid falling tide at the sill at the  $\sim 3000 \text{ m}$  marker (referred to as location B). The displacement of the pycnocline at location A appears to move to the  $\sim 1500 \text{ m}$  marker from high tide to falling tide. At location B the displacement moves to the  $\sim 3500 \text{ m}$  marker at low tide. In section one a similar displacement of the pycnocline was associated with internal waves, thus this may also be the case in section two. At the



1700m marker to the 3000m marker there also appears to be a decrease in density at the upper portion of the pycnocline.

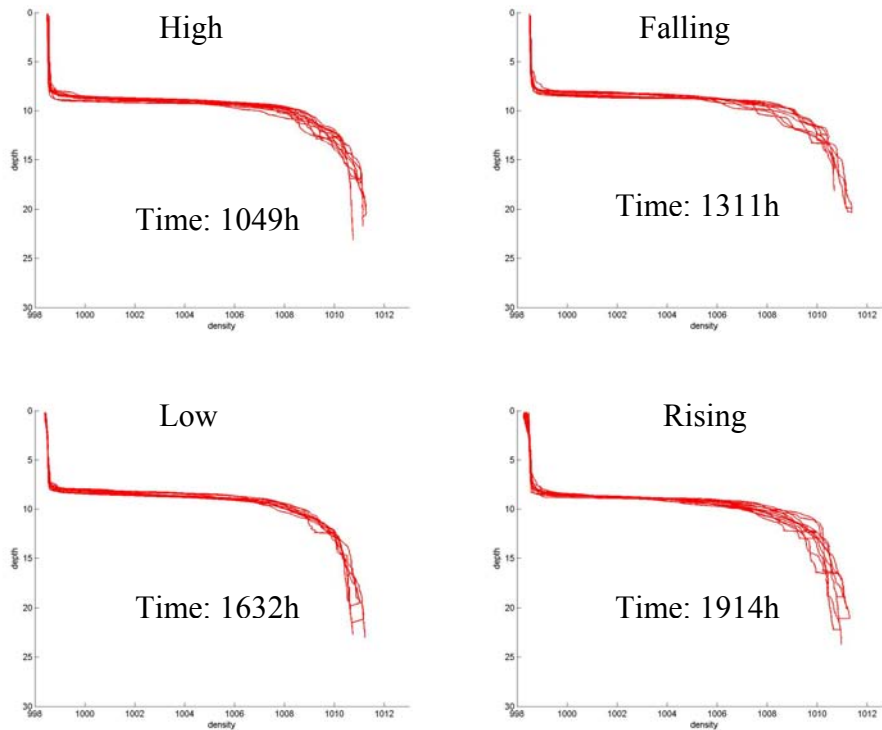


Figure 7.2: Individual density profiles. For all the CTD dips made at high, falling, low and rising tide

The pycnocline remains at an almost constant level for the duration of the tidal cycle except for two occasions when a displacement of the pycnocline occurs. (see Figure 7.4). This displacement is first sighted at high tide at ~500m marker (referred to as location A) and mid falling tide at the sill at the ~3000m marker (referred to as location B). The displacement of the pycnocline at location A appears to move to the ~1500m marker from high tide to falling tide. At location B the displacement moves to the ~3500m marker at low tide. In section one a similar displacement of the pycnocline was

associated with internal waves, thus this may also be the case in section two. At the 1700m marker to the 3000m marker there also appears to be a decrease in density at the upper portion of the pycnocline.

Individual density profile plots of locations A and B at the different phases of the tides confirm a decrease in the density gradient (see Figure 7.5). The profiles at these locations show that the stratification is maintained at the interface for the duration of the tidal cycle. However at both locations A and B the 1007 isopycnal is at the 8m depth. At falling tide (location A) falls to the 9m depth whilst at rising tide and high tide (location B) it falls to the 9m depth.

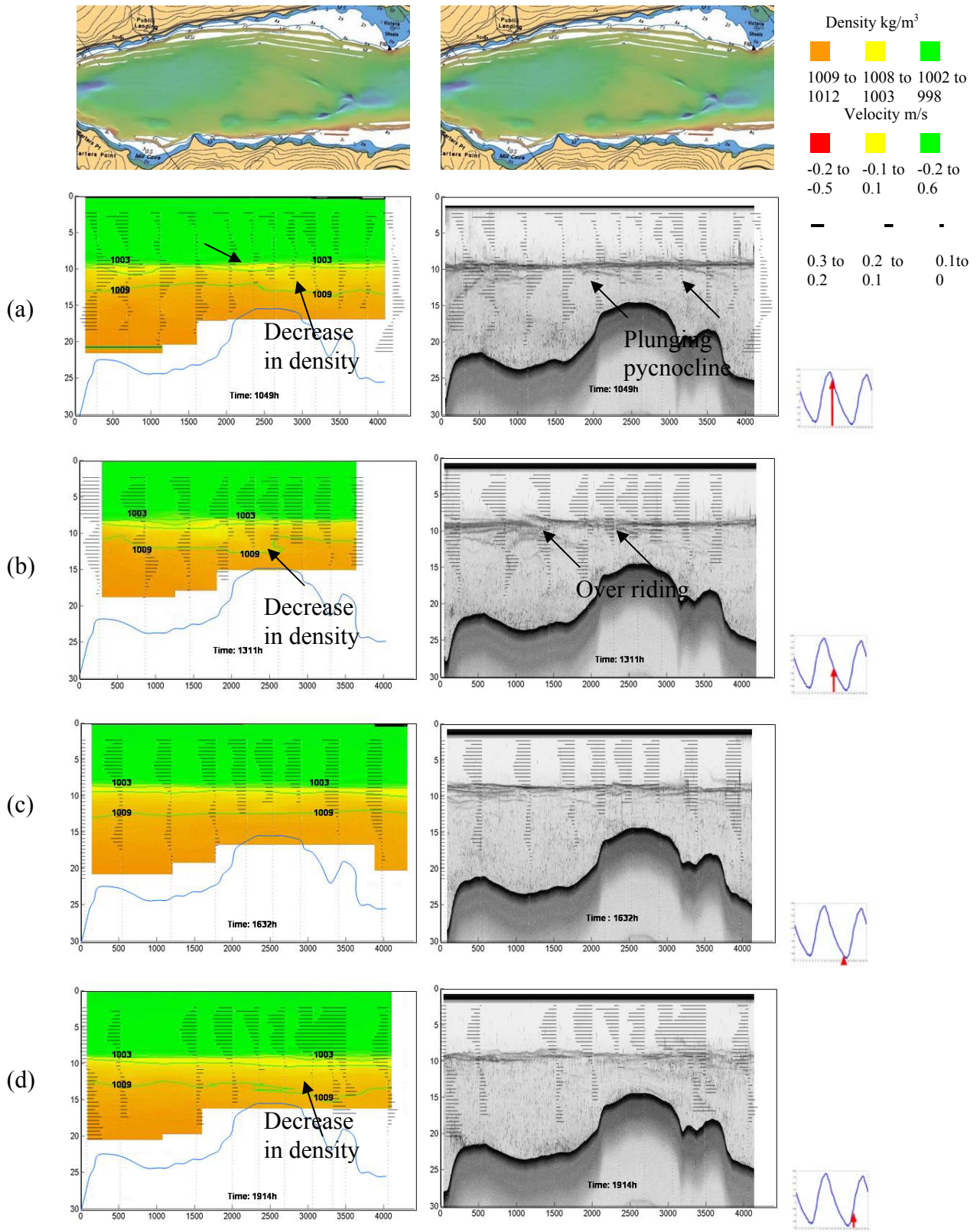


Figure 7.3: Profiles of density (left) and acoustic volume backscatter (right) for neap tides at section two. The arrows indicate areas where a decrease in density occurs.

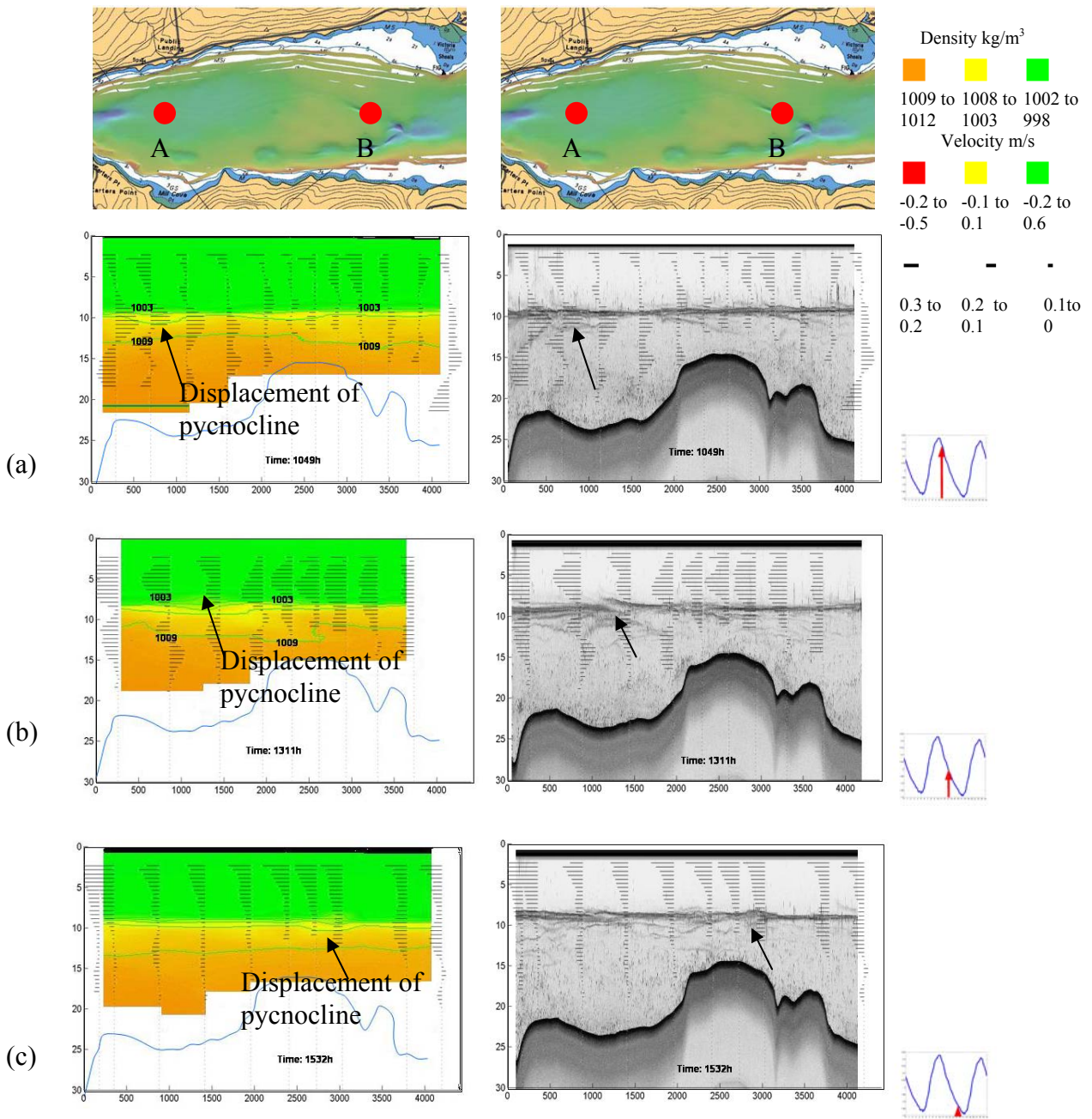


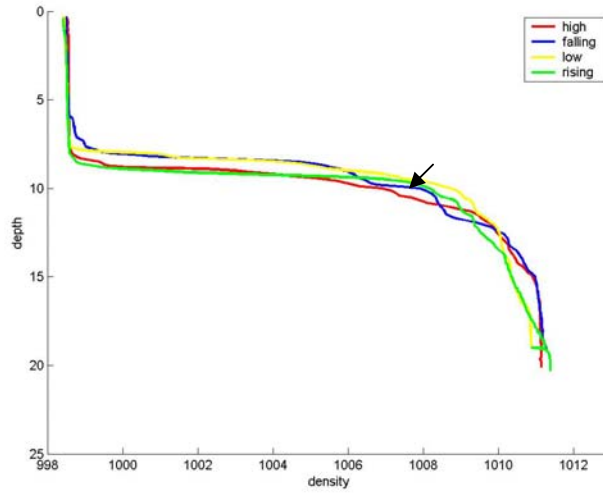
Figure 7.4: Longitudinal profiles showing the displacement of the pycnocline. These illustrations are for neap tide at section two. The arrows indicate the locations where the displacements were observed.

A comparison of the density contours with the echosounder images is performed (see Figure 7.6). The results show that the pycnocline corresponds to the high intensity acoustic backscatter strength observed at the interface.

Sequential observations (w.r.t time) of the acoustic volume backscatter images illustrate that from falling tide into low tide a possible internal wave develops that moves upstream. Interestingly the sighting of the wave from the acoustic backscatter images corresponds to the spatial and temporal location of the displacement of the pycnocline observed at location B (see Figure 7.7). This wave is calculated to have a speed of approximately  $-0.4\text{m/s}$ .

It can be argued that if the displacement of the pycnocline represents an internal wave, then the density contour images should show the displacement progress upstream. However on examination of the longitudinal density profiles, the displacement of the pycnocline is only observed on some of the density contour images. This difference may be influenced by the fact that the CTD data are  $\sim 400\text{m}$  apart, whilst the horizontal resolution of the echosounder is  $\sim 1\text{m}$ . The greater resolution of the acoustic volume backscatter images allows more detail to be observed at the pycnocline. This implies that the resolution of the CTD casts is not great enough to capture all of the wave movement. It is also observed that the wave appears to be moving upstream whilst the flow at the interface is moving downstream (see Section 7.4 for more details on the internal wave).

5<sup>th</sup> September 2004 Density Profiles at location A



5<sup>th</sup> September 2004 Density Profiles at location B

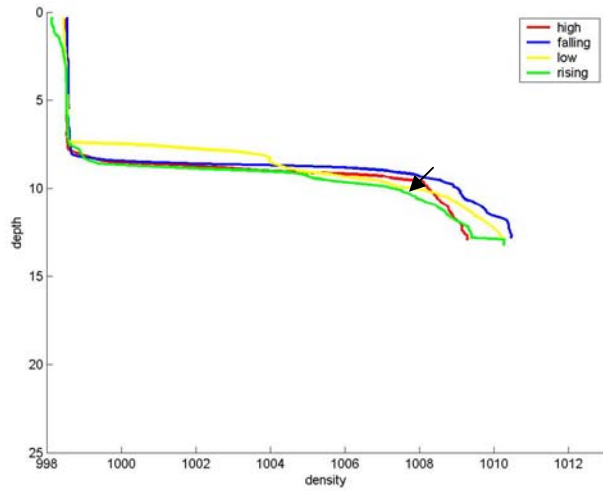


Figure 7.5: Individual density profiles at location (A) top and location B (bottom)



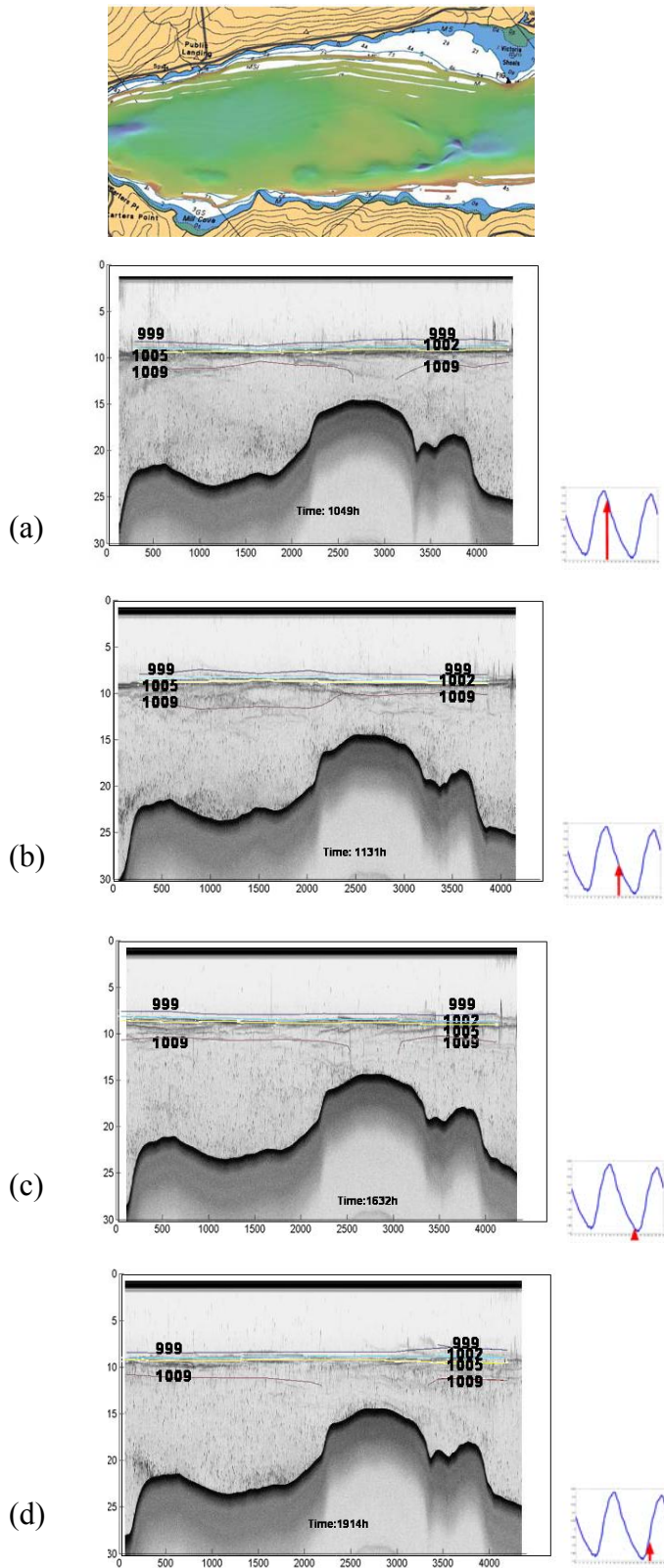


Figure 7.6: Acoustic volume backscatter profiles overlaid with density contours. The profiles are for neap tides at section two.

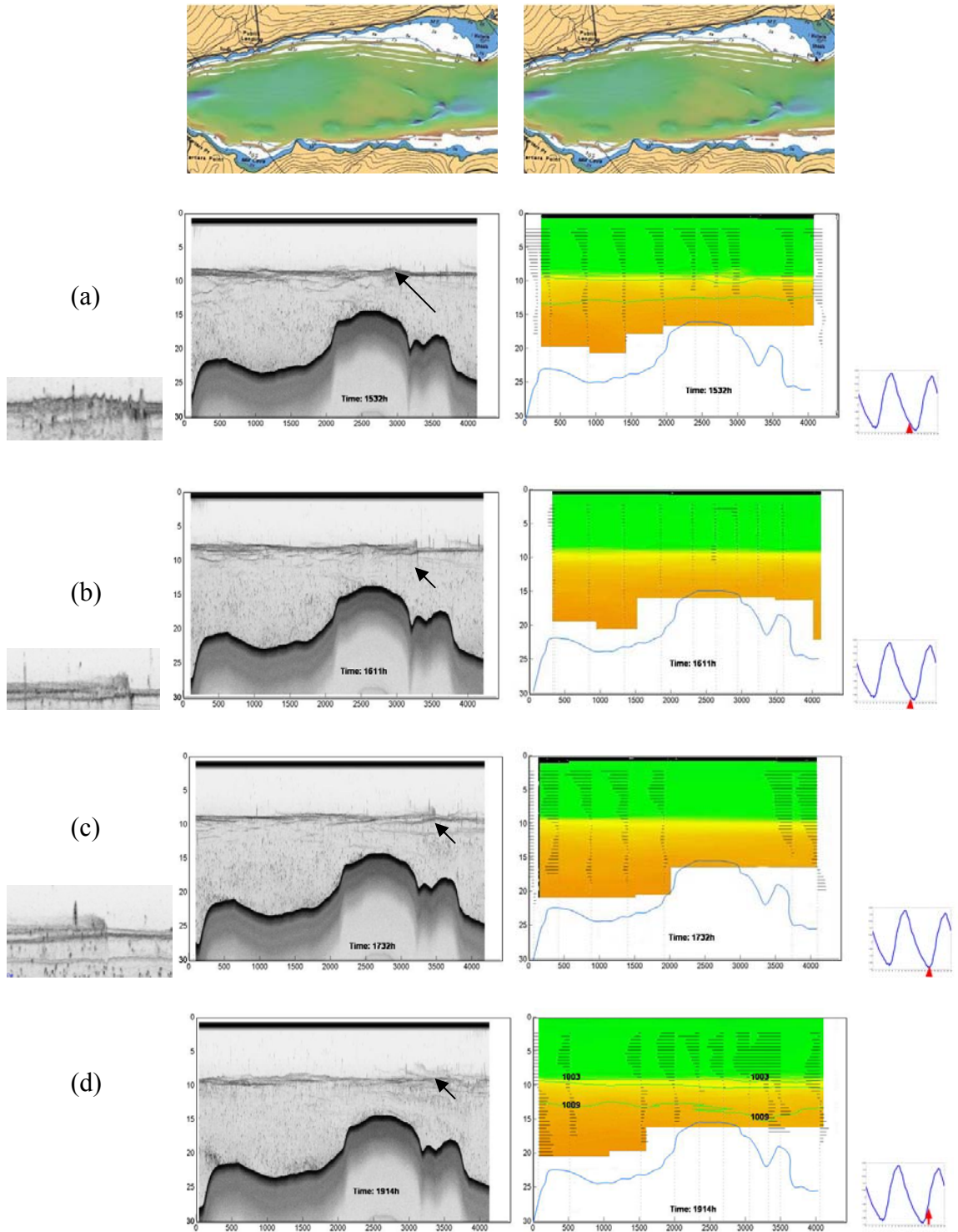


Figure 7.7: The progression of an internal wave (a, b, c) and its possible collapse (d) during neap tide at section two



### 7.3 Velocity Structure

For the duration of the tidal cycle the surface velocity flows downstream whilst the bottom velocities are observed to vary (see Figure 7.8). The variation in the bottom velocities appears to be influenced by a combination of the tides and the bathymetry of the area.

#### High Tide

Figure 7.8 shows that at high tide the surface velocities ebb with a magnitude of 0.05m/s to 0.1m/s. The exception being at the ~2000m marker where the velocities flood upstream at -0.1 m/s to -0.2m/s. At the pycnocline the velocities also flow upstream with velocity of -0.1m/s to -0.2m/s but this upstream flow discontinues at the sill (~2300m marker). On the north eastern side of the sill (2700m upstream) the pycnocline velocities ebb at 0.05 to 0.1m/s.

Similar observations are made for the bottom layer. However within the vicinity of the sill (1500m to 3000m) the velocities are basically stationary.

The acoustic backscatter images show at high tide the plunging of the pycnocline at the 1700m and 3000m markers. In section one it was suggested that the plunging of the pycnocline occurs due to one or more of the following : (1) mixing events associated with soliton wave packets; (2) mixing events created by Holmboe waves; (3) an undulatory bore or (4) the difference in flow of the upper and lower layer as it passes over irregular bathymetry. Thus it is possible that the plunges observed in this section are also due to one of the above mentioned mechanisms.

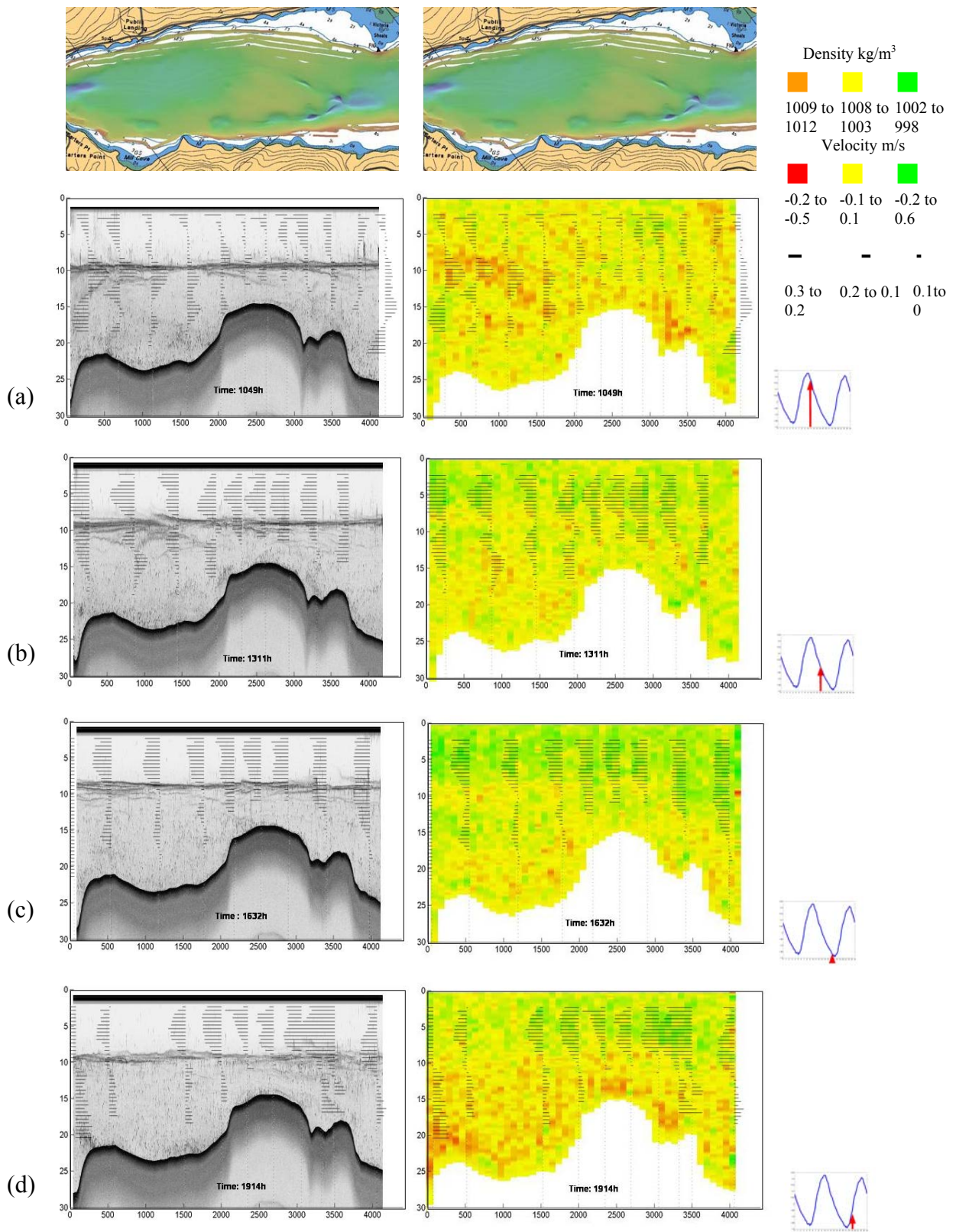


Figure 7.8: Longitudinal profiles of the acoustic backscatter (left) and velocity (right) for section two during neap tides.

On the upriver side of the sill, the velocities are flooding at  $-0.05$  to  $-0.1\text{m/s}$ . At the  $15\text{m}$  to  $25\text{m}$  depth it is observed that at the  $0\text{m}$  to  $500\text{m}$  (the downriver side of the sill) the velocities ebb at  $0.05\text{m/s}$  to  $0.1\text{m/s}$ . A similar situation is observed to occur at the  $4000\text{m}$  marker.

The variations in the velocity observed (both spatially and with depth) appears to be influenced by the flow as it interacts with the sill. It is observed that two circulation patterns exist on the downriver and upriver side of the sill. Three scenarios (referred to as case 1, case 2 and case 3) may explain the flow pattern observed at high tide:

Case 1: At high tide, salty water advects upstream. On approaching the sill the flood waters are weakened. This causes the magnitude of the velocities to decrease at the sill. The flood velocities on interaction with the sill cause the circulation of water to be redirected downstream. This causes the bottom  $15\text{m}$  to  $25\text{m}$  depth on the downriver side of the sill, to flow downstream at high tide.

Case 2: The decrease in density and increased flood velocity observed at location A at the pycnocline is due to an internal wave. This wave may have originated from further downstream, possibly in section one. The wave on approaching the sill cannot propagate further upstream and causes mixing to occur.

Case 3: Downriver of the sill the bottom layer ebbs whilst on the upriver side the bottom velocities floods. This difference may be due to the fact that the illustrations of the density and velocity profile are all profile views along the axis of the estuary. To the southeast and northwest of the sill deep channels exist. It is possible that at flood tide the water flows upstream and diverts around and on either side of the sill. This may explain the increased flood velocities observed at the  $4000\text{m}$  marker. However on approaching

the sill (to the north of the channel) the velocities are ebbing. It may be necessary in future work to observe at this location cross-section profiles of the velocity structure of the sill at high tide.

## **Falling Tide**

At falling tide the surface layer ebbs with velocities from 0.1m/s to 0.2m/s whilst the bottom velocities ebbs with velocities of 0.05 to 0.1m/s. At ~700m it is observed that the bottom layer floods upstream at ~-0.1m/s. This local variability strongly suggests a cross-channel flow.

From high tide to falling tide the velocities at the pycnocline changes direction and ebb at ~ 0.05m/s. However at the ~1800m marker the pycnocline velocities are flooding at 0m/s to -0.1m/s whilst the surface and bottom layers ebb. This also suggests cross channel flow.

At high tide the plunging of the pycnocline was observed to occur within the vicinity of the 1700m and 3000m markers. Within these areas a decrease in density was observed. At falling tide at the ~1200m marker an over-riding phenomena occurs. The flow upstream of the 1200m marker appears to be riding on top of the flow downstream of this marker. The 1200m marker is within the vicinity of the sill where a decrease in bottom density was observed at falling tide.

To the right of the ~1200m marker the pycnocline waters are less dense than the waters to the left of the marker. A possible explanation of the over riding follows. At high tide, a decrease in density was observed at the ~1700m marker at which time the water flowed upstream. At falling tide there is a change in direction of the flow from upstream

to downstream. Thus the less dense water to the right of the 1200m marker is advected downstream. As it is less dense than the surrounding bottom waters it flows on top (overrides) of the surrounding bottom waters.

At the sill and on the upriver side of the sill upstream (2000m upstream) the pycnocline ebbs at 0.1m/s. This indicates that the downstream flow on the upriver side of the sill ebbs faster than the downriver side.

It was mentioned in section 7.1 that, at the sill, a decrease in the bottom density occurs at falling tide. This decrease in density at the sill may be due to one of the following: (1) mixing events occurring at the interface, (2) mixing events occurring at the bottom, (3) or advection of less dense water from further upstream. For the latter to be plausible, less dense water should be observed moving downstream earlier in the tidal cycle. This was not observed. Instead the less dense water was observed to evolve within the vicinity of the sill, thus suggesting in-situ mixing.

It is also possible that an internal wave exists (as was mentioned at high tide) that propagates upstream. However on approaching the strong ebb flow at the sill the internal wave is forced to diminish. This collapse of the internal wave may have caused mixing to occur which may have created the decrease in density observed at falling tide at the sill.

## **Low Tide**

Low tide velocities have similar characteristics to falling tide. However the surface velocities increase to 0.25m/s whilst the bottom velocities ebb at 0.1m/s. The pycnocline also ebbs at ~0.15m/s to ~0.2m/s. The decrease in density that was observed at the sill at falling tide is no longer present.

## **Rising Tide**

At rising tide, the surface velocities continue to ebb but have slowed to 0.15m/s. The bottom velocity changes direction and begins to flood upstream with velocities of -0.15m/s to -0.2m/s. At the pycnocline the velocities ebb at  $\sim 0.05\text{m/s}$ .

A decrease in density was observed at rising tide on the upriver side of the sill. This decrease in density occurs at the same location that the internal waves are observed from the acoustic volume backscatter images (see Figure 7.3, time 1914h and Section 7.3). From this observation it can be assumed that either the internal wave causes mixing events to occur at this time period or mixing is occurring due to the bottom boundary.

## **7.4 Acoustic Backscatter Images**

The echosounder images of the pycnocline show the existence of the type 1 and type 2 waves that are observed in section one (see section 6.2.5.4 figure 6.15). In section 6.2.5.4 the type 1 waves are identified as possibly being Holmboe waves and the type 2 waves as being soliton wave packets.

Figure 7.9 shows illustrations of the pycnocline at high tide. At high tide type 1 waves are observed at the  $\sim 500\text{m}$  to the  $\sim 1000\text{m}$  marker on the south western side of the sill. These waves are observed at the same location that a displacement of the pycnocline occurs at location A. The waves are first observed during late rising tide with a wavelength of 25m. These waves disappear at falling tide.

Figure 7.10 shows the development of the type 2 wave within the vicinity of the sill, mentioned in section 7.1. This wave first develops at falling tide when the water

within the pycnocline moves downstream with velocities of 0 to 0.1m/s (see Figure 7.7). The wave is observed to move upstream with a velocity of  $\sim -0.4$ m/s. The wave continues upstream on the upriver side of the sill until it enters the area of the deep channel. When the wave approaches the channel it is low tide and the waters on the north eastern side of the sill are ebbing at  $\sim 0.2$ m/s. Thus the wave appears to dissipate since it cannot move upstream any further.

In Apel [2002] it was suggested that, due to the nonlinearity of the wave, the propagation speed of the soliton wave packets exceeds the fluid speed and the wave packets move against the current. This is observed from figure 7.7 and 7.10.

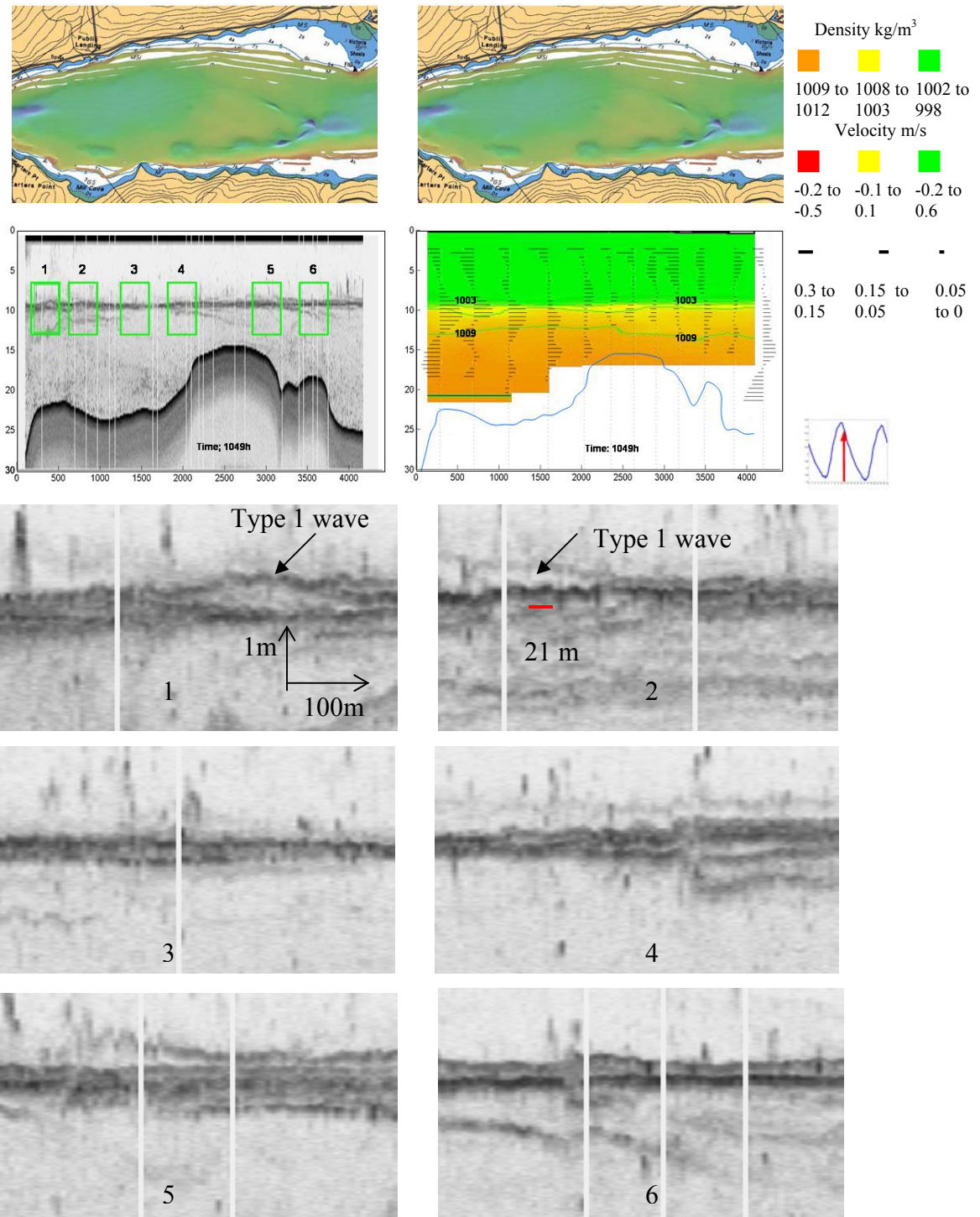


Figure 7.9: Type 1 wave (1, 2) at the interface developed just after high tide neaps for section two. (3, 4, 5, 6) show areas of the pycnocline where type 1 waves are not present.



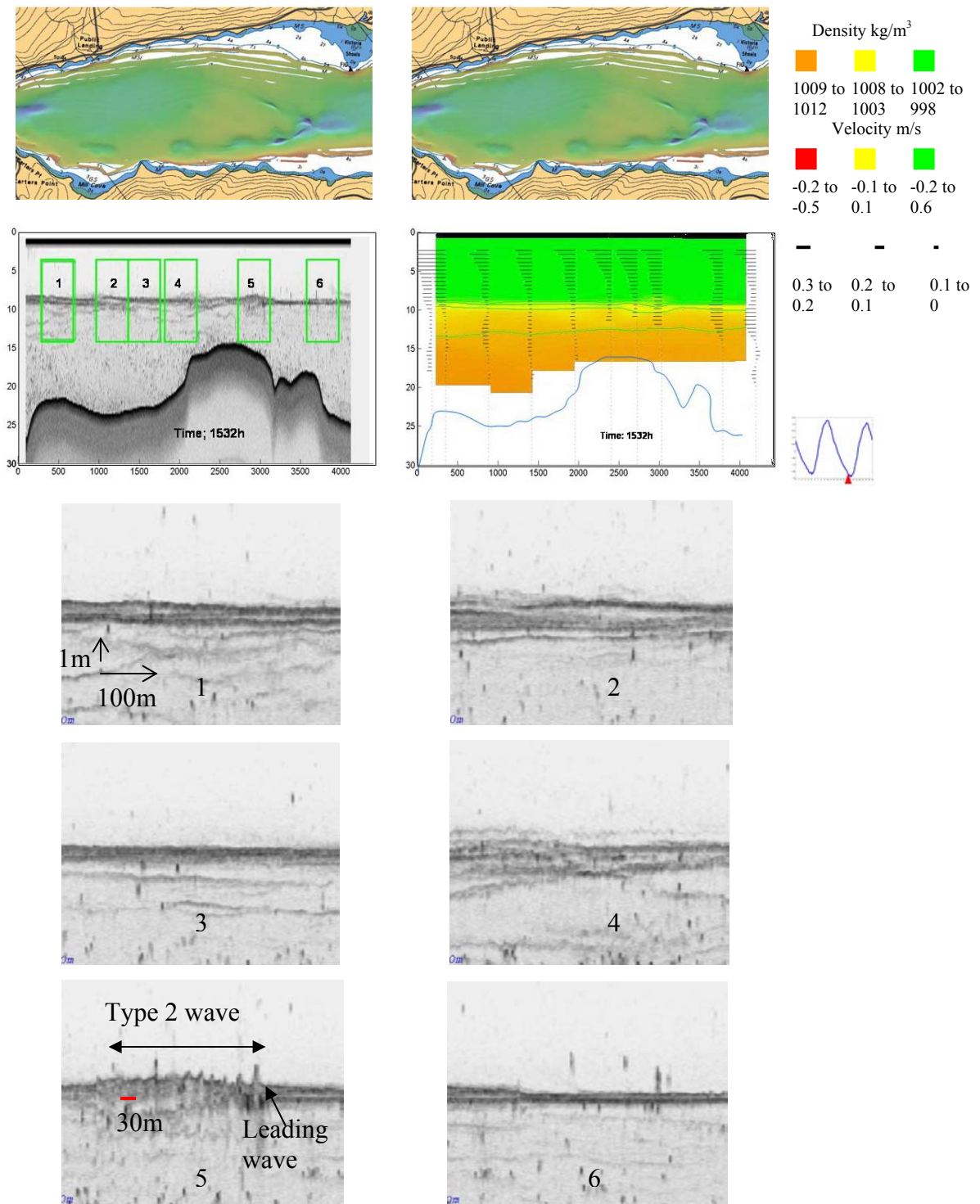


Figure 7.10: Type 2 wave (5) at the interface developed around low tide. 1, 2,3,4,6 shows the pycnocline where the type 2 is not present. These illustrations are for neap tides at section two.

Of interest is that, in the initial development of this wave, a leading wave is observed at time 1532h within the vicinity of the ~2600m marker (see Figure 7.9(5)). The wavelength of this wave appears to decrease as the leading front progresses upstream.

## **7.5 Summary of Density and Velocity Observations**

For the duration of the tidal cycle, the density structure resembles that of a highly stratified estuary. The sill appears to create two circulation patterns on either side of it. At high tide on the downriver side of the pycnocline velocities are flooding, whilst on the north eastern side the pycnocline velocities are ebbing. At falling and low tide the ebb velocities are much stronger at the pycnocline on the upriver side than on the downriver side.

Throughout the tidal cycle there are variations in the velocity and density structures. At high tide, within the vicinity of the sill there is a decrease in density and the greatest flood velocity occurs at the interface. In addition there is a plunging of the pycnocline at the ~1700m and ~3000m markers. The surface and bottom layers (15m to 25m depth) are ebbing at this time. It is suggested that either a bottom boundary layer develops or an internal wave exists that progresses upstream and on approaching the sill causes mixing to take place. This mixing may have caused the decrease in bottom density observed at the sill at falling tide.

The decrease in bottom density at the sill is also not far from the location of the over riding event of the pycnocline. Thus the decrease in density observed at the sill at falling tide may be due to: (1) advection of mixed waters from further downstream; (2)

bottom boundary mixing; (3) mixing caused by an internal wave or; (4) mixing caused by the over riding phenomena.

From mid falling tide into low tide a soliton wave packet appears to develop in the vicinity of the sill. This has been confirmed by the echosounder images. The wave appears to move upstream whilst the flow moves downstream. A decrease in bottom density is also observed from early rising tide to late rising tide.

The solitary wave packet, on encountering the high velocities on the north eastern side of the sill at low tide, could not maintain its progression upstream. Thus it disappears. These observations of the wave may indicate that: (1) the wave in stopping causes mixing to take place within this vicinity (~3500m); (2) the less dense water observed are due to bottom boundary mixing or (3) less dense water from further upstream is advected to location B.

## 7.6 Spring Tidal Cycle

The spring tidal cycle is observed to have similar characteristics to the neap tidal cycle. One of the main features observed is that the estuary maintains a salt wedge appearance, with a surface layer, density of  $998\text{kg/m}^3$  and a bottom waters density of  $1010\text{kg/m}^3$ . These two layers were separated by a ~1.5m thick pycnocline (see Figure 7.11).

The main differences between the neap and spring tidal cycle are as follows:

- At spring tides there was an increase in the river water level which causes the pycnocline to fall from the 8m depth at neap tides to the 10m depth at spring tides

- For the neap tidal cycle at high tide the surface layer still flows downstream never reversing. In the spring tidal cycle the surface layer reverses and flows upstream with velocities between  $-0.05\text{m/s}$  to  $0.1\text{m/s}$ . (see Figure 7.11, time 1902h).
- For the neap tidal cycle, at high tide the flow at the pycnocline moves upstream (see Figure 7.3(b)) whilst at spring tides the flow upstream occurs just below the pycnocline (see Figure 7.11, time 1902h)
- At neap tides a type 2 wave (solitary wave packet) wave develops at the sill at falling tide. This wave is observed to progress upstream as the flow moves downstream. In the spring tidal cycle this is not observed to take place (see Figure 7.11, time 2123h). Whilst observations of the acoustic backscatter profiles show possible development of the type 2 wave (see Figure 7.13 (4)). This type of wave was not observed to fully develop.
- A decrease in bottom density occurs at two locations in the neap tidal cycle: (1) at the sill at falling tide and; (2) on the upstream side of the sill at rising tide. In the spring tidal cycle a decrease in bottom density is observed to occur only at the sill at falling tide (see Figure 7.11, time 2123h)

## 7.7 Summary of Neap and Spring Tidal Cycle

Similar observations made for both the neap and spring tidal cycles include the displacement of the pycnocline at the  $\sim 500\text{m}$  marker at high tide. The temporal and spatial progression of this displacement results in a decrease in the bottom density at the sill at falling tide. At this location the acoustic volume backscatter images shows the over riding of the pycnocline of the surface layer on top of the bottom salty layer. This may be due to

less dense water from upstream advected on top of the more dense water that exists downstream.

The major difference between the neap and spring tidal cycle is the appearance of a soliton wave packet at the sill at falling tide on the neap. This solitary wave packet is observed to progress upstream whilst the flow flows downstream. The solitary wave packet disappears at low tide and is followed by a decrease in the bottom density on the eastern side of the sill.

This soliton wave packet is not observed to develop at spring tides and the decrease in density observed at location B at neap tides does not occur. This implies that this interfacial wave may have contributed to the decrease in density observed at neap tides on the eastern side of the sill.

The stratification pattern of both the neap and spring tides are basically the same resembling that of a highly stratified estuary. The main differences that occur between the neap and spring tides are due to increased river discharge. These differences show the importance of the flow conditions to the development of the internal waves and possible mixing events.

To determine if the decrease in density observed within the vicinity of location A and B are due to possible mixing events occurring at the interface, the gradient Richardson number and a linear stability analysis are now employed.

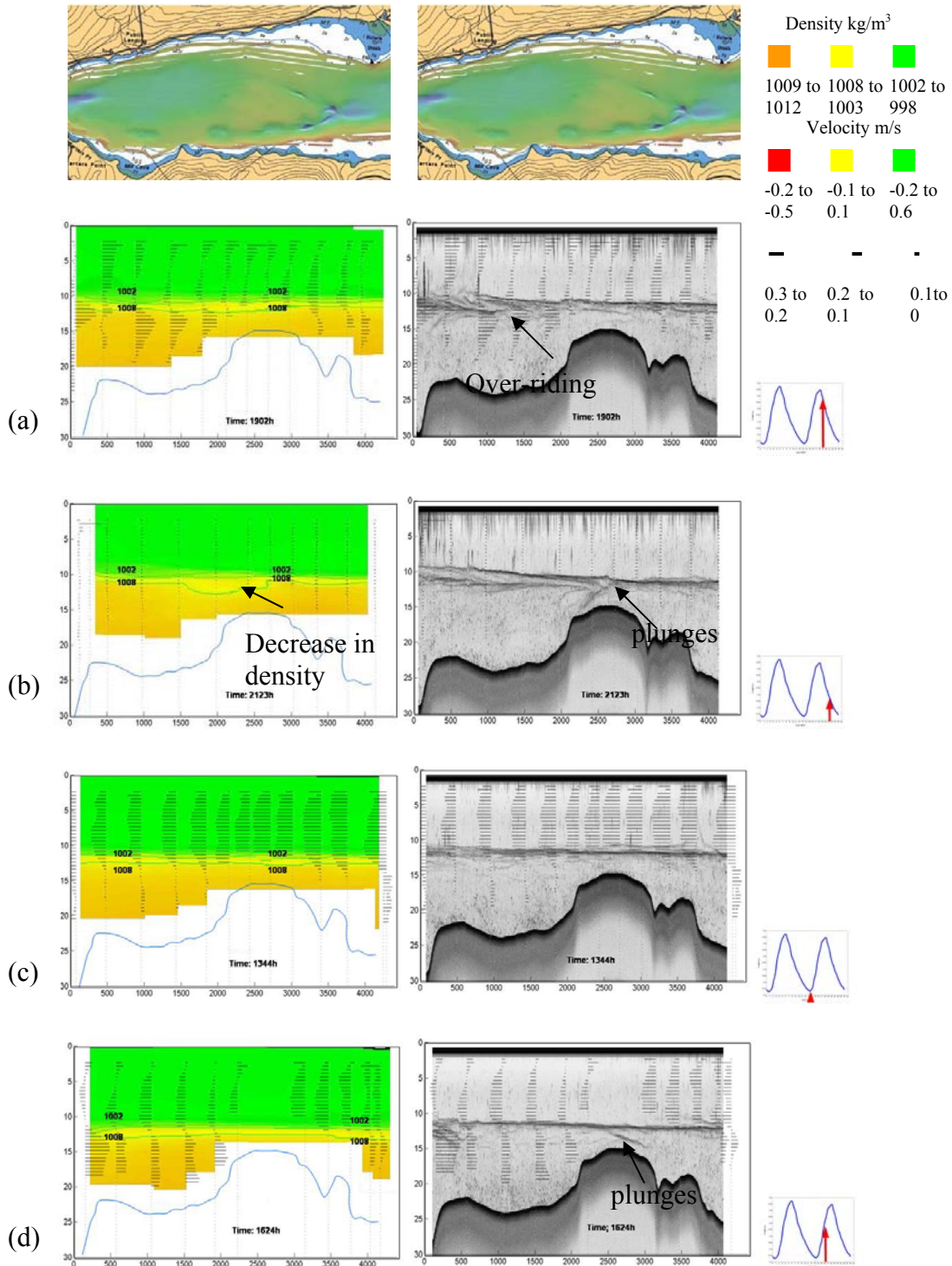


Figure 7.11: Longitudinal profiles of density (left) and acoustic volume backscatter (right) at section two during spring tide.

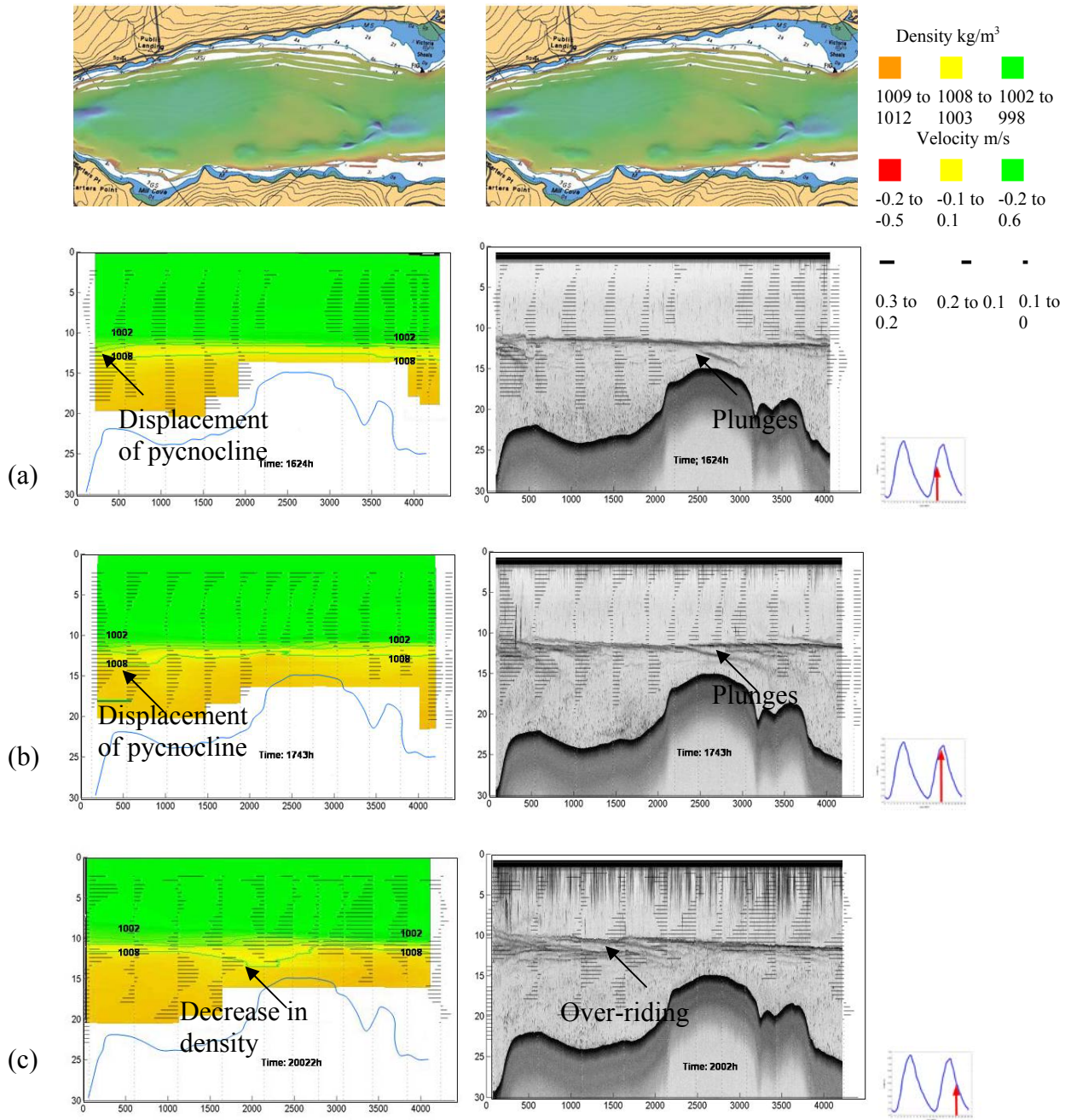


Figure 7.12: Longitudinal profiles of density (left) and acoustic volume backscatter (right) for spring tide at section two. The density profiles show the displacement of the pycnocline which leads to a decrease in the bottom density



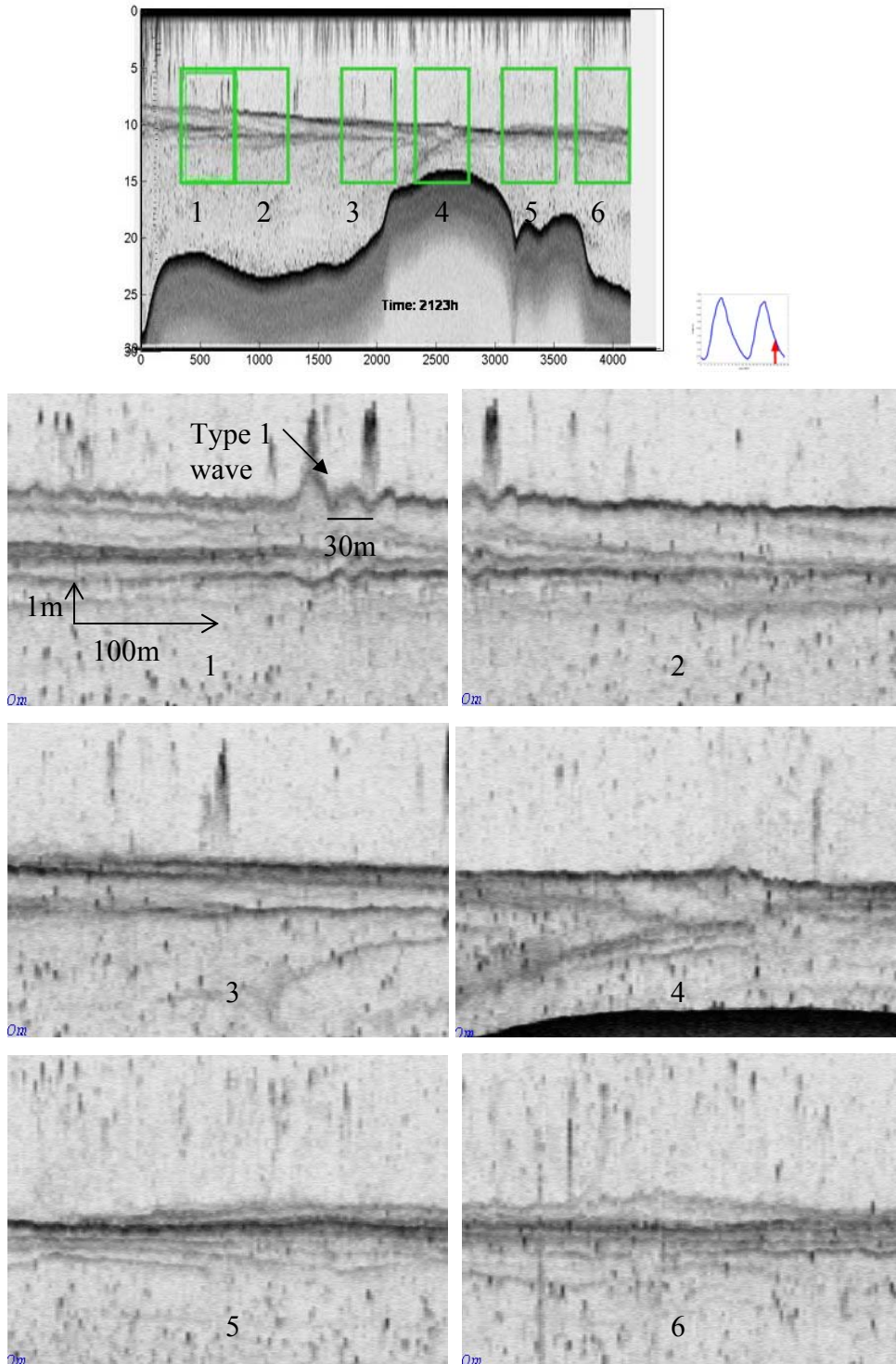


Figure 7.13: Type 1 wave at the pycnocline (1) during falling tide. These illustrations are for spring tide at section two.



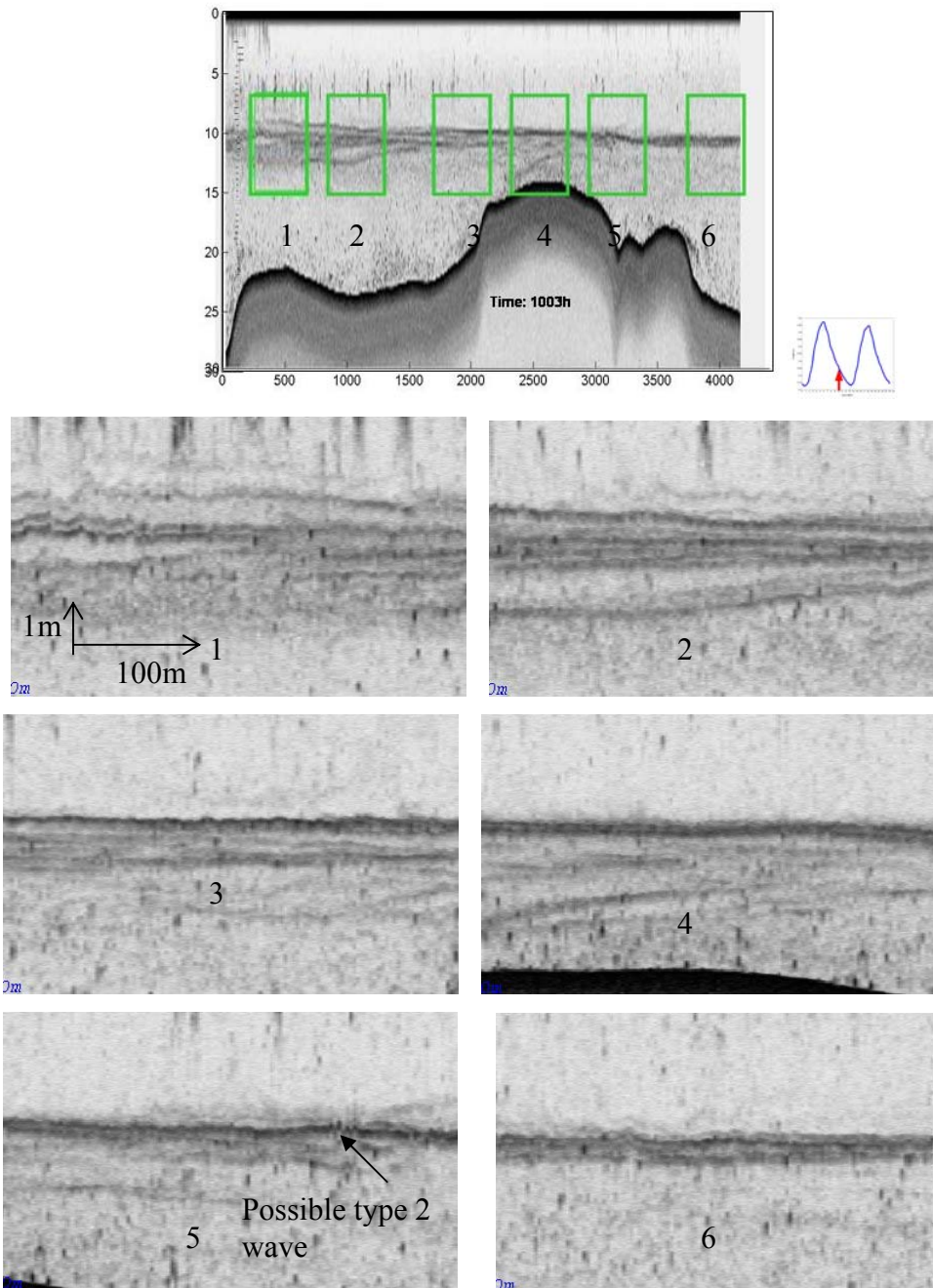


Figure 7.14: Type 2 wave at the pycnocline (5) for spring tide at section two. 1, 2, 3,4,6 show areas of the pycnocline where the type 2 waves are not present

## 7.8 The Gradient Richardson Number

The gradient Richardson number is calculated for all of the CTD casts made throughout the tidal cycle for both the neap and spring tidal cycles. A critical value is used to determine if interfacial mixing is taking place. The critical value of  $0 < Ri < 1$  is the same as employed for section one.

Figure 7.15 illustrates the location of  $Ri < 1$ . The results indicate that mixing at the interface is only possibly occurring at ~500m marker. Figure 7.16 shows that, for location A, the mixing is taking place at the base of the pycnocline at high tide. This location also coincides with the area that the displacement of the pycnocline was observed together with a decrease in the bottom density. Thus mixing at the interface appears to be taking place at location A at high tide.

Location B has similar characteristics with respect to the density structure. However no mixing is inferred from the Ri value. This possibly suggests that the wave observed at the interface does not contribute to mixing and that the less dense waters observed at the disappearance of the wave is most likely advected at low tide from further upstream of location B. Another possibility is that mixing from the bottom layer may have caused the less dense waters observed at location B.

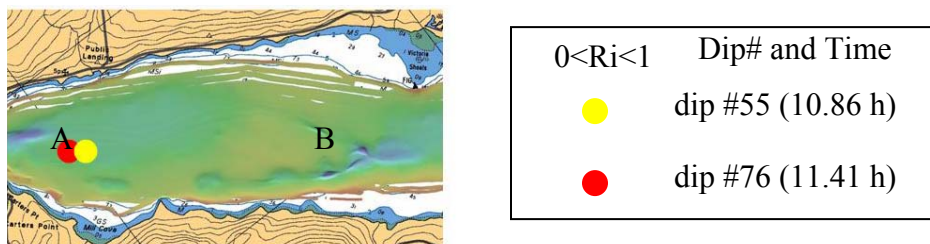


Figure 7.15: Section two location of A and B of mixing events for neap tide.

5<sup>th</sup> September Gradient Richardson at Location A

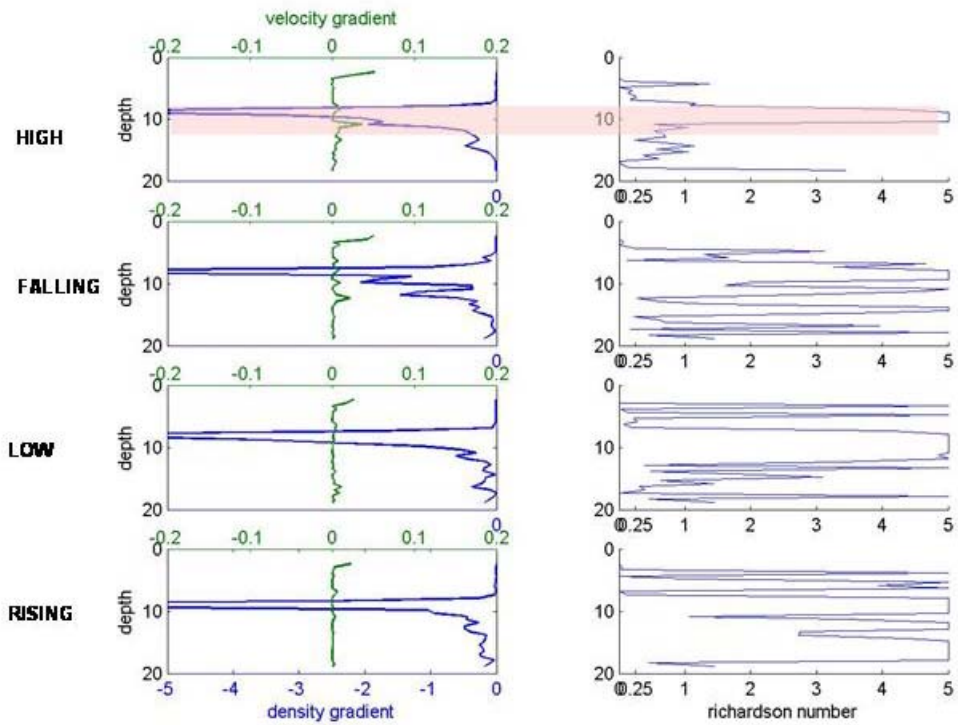


Figure 7.16: Graphs of the density and velocity gradient (left) and the gradient Richardson number (right) during neap tides at locations A in section two. The shaded region represents mixing

## 7.9 Linear Stability Analysis

To perform a linear stability analysis requires a similarity of the theoretical density and velocity profiles to that of the observed. At location A, where mixing was calculated to be occurring at the interface, the density profiles reasonably match the theory. However most of the velocity profiles differ from the approximations used in the theory (see Figure 7.17).

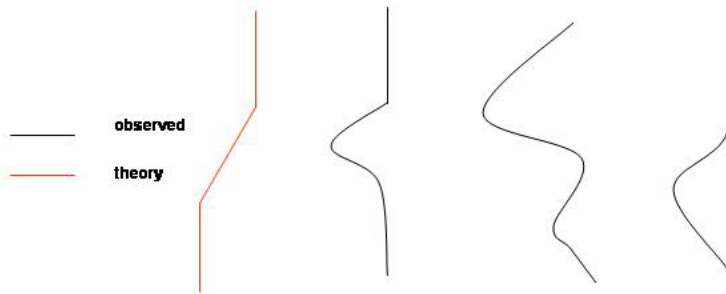
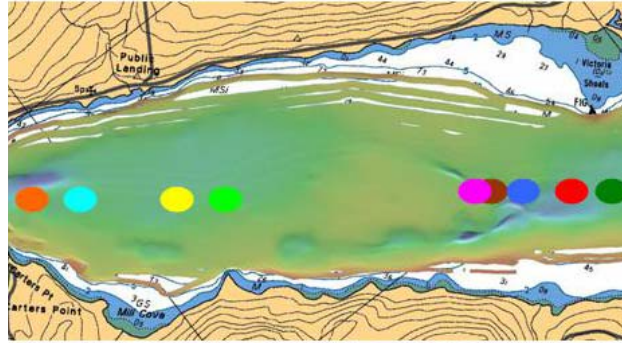


Figure 7.17: Velocity profiles used in linear stability analysis (red) and observed velocity profiles (black).

Most of the velocity profiles did not fit the theoretical velocity profile and this proved to be a limitation in applying the theory at location A. Nevertheless the linear piecewise approximation is still applied for the profiles that reasonably matched the theory. It should be noted that the profiles used occurred at different locations and times than the mixing event predicted by the Ri method occurred. Figure 7.18 shows the locations of the profiles that matched the theory. Appendix III shows the piecewise approximation used for the velocity and density profiles.

The results of the linear stability analysis show that instabilities would not exist at these locations at the specific times. In this study the velocity profiles were calculated by averaging all the pings within a particular location of the CTD profile. This process assumes that the velocities within the area defined are similar. This is not, however, always the case. Therefore the velocities profiles calculated represent the average conditions of the area and not the exact velocity at that particular location.

Though for most of the profiles the linear stability analysis could not be performed at location A, at time 20.2h at dip #347, the density and velocity profiles reasonably match the theory. However at this time period, the piecewise theory does not indicate an instability existing. The waves observed at the interface at location A have a close resemblance to that of the type 1 wave in section one. The results of the linear stability analysis in section one identified this wave as possibly the Holmboe wave.












Dip#	Symbol	Time	J	$\epsilon$	d	h	w	k
63		11.06h	17.47	0.73	0.55	1.5	-	-
191		15.21h	17.97	-2.2	-5.74	5	-	-
233		16.6h	7.76	-5.33	-1.5	1.5	-	-
292		18.48h	6.6	-2.6	-3.25	2.5	-	-
342		20.08h	20.67	-0.5	-0.75	3	-	-
347		20.2h	12.9	-0.5	-1	4	-	-
354		20.4h	23.29	0	0	2	-	-
365		20.8h	15.32	-0.8	-2.4	5.7	-	-
369		20.9h	8.09	-1.25	-2.5	4	-	-

Figure 7.18: Results of the linear stability analysis for section two during neap tides.

## 7.10 Summary

Longitudinal profiles of observed density, velocity and acoustic volume backscatter have shown section two to be basically stable, for both the neap and spring tidal cycle. Two possible instances were observed when the flow may become unstable: at falling tide at the sill and at rising tide on the downriver side of the sill (observed only for the neap tides).

The gradient Richardson number calculated that mixing is only occurring at the interface within the vicinity of ~500m longitudinal distance (location A). Investigations of the acoustic backscatter images at this location show the existence of small amplitude waves with wavelength of ~21m. This wave resembles that of the type 1 wave observed in section one.

A normal mode approach to the linear stability analysis is attempted. However due to the complexity of most of the observed velocity profiles the stability analysis could not be applied at this location accurately. Nevertheless the normal mode approach is performed for all the profiles in the study area that fitted the theory. The results suggest that an instability should not exist. It should be noted that the profiles used were not at location A and were not at the same time that the type 1 waves were observed.

During the neap tidal cycles when the tide is falling, the acoustic volume backscatter images show the existence of an internal wave at the upriver side of the sill. The characteristics of the wave include: a leading wave, varying amplitude and travelling in the opposite direction of the flow. This waves resembles that of the type 2 wave described in section one. The waves in both these sections resemble the soliton wave packets described by Apel [2002].

Calculations of the  $Ri$  show that mixing is not taking place at the interface within the vicinity of this type 2 wave. However at spring tides the interfacial wave was not present and the decrease in density observed on the north eastern side of the sill at rising tide was not observed. This implies that this interfacial wave most likely influences the decrease in density that is observed.

It can be concluded that internal waves play a major role in the mixing events occurring in this study area. The linear stability analysis was not successfully performed, due to the velocity profiles not fitting the approximations used to model the background flow. However the waves resemble those of section one which were identified as Holmboe waves. A soliton wave packet was also observed. To further understand the development of these waves it may be necessary to: (1) perform a nonlinear analysis for both the type 1 and type 2 waves, (2) perform more detailed observations (Eulerian type) for a longer time period at the locations of the locations A, B and the sill.

In section one it is suggested that the plunging of the pycnocline is related to: (1) mixing caused by solitary wave packets; (2) mixing caused by Holmboe waves; (3) an undulatory bore or (4) the flow of the upper and lower layers passing over irregular bathymetry. In section two, there were two instances where the plunges were observed at high tide neaps: (1) at the 1700m marker and (2) at the 3000m marker. At the 1700m marker solitary wave packets are not observed to be present throughout the whole tidal cycle. Whilst at the 3700m marker a solitary wave packet is observed to disappear within the vicinity. Thus the possible causes for the plunging of the pycnocline is still inconclusive and the suggestions listed above are still all valid.



The main difference between the plunges in section one and section two is that the plunges in section one remained stationary where they occurred whereas in section two the plunges appear to be advected with the flow as it moves downstream. Within the vicinity of the plunges less dense bottom water are present than further downstream. Thus as this less dense water is advected downstream it rides over the more dense bottom water. This creates the over riding phenomena observed at falling tide.

## CHAPTER 8

### CONCLUSIONS AND RECOMMENDATIONS

Our understanding of stratified environments and mixing processes originates from laboratory experiments, theory, numerical simulations and field observations. Based on these sources it has been found that interfacial mixing initiates in the form of a wave. The Kelvin-Helmholtz (KH), Holmboe and solitons waves are the three known internal waves that contribute to turbulent mixing in stratified fluids. These waves have all been observed in the field, thus verifying the theory and experiments.

In this study of Long Reach all three types of internal waves have been observed. The field observations have shown the generation and evolution of mixing in Long Reach. The results have also enhanced our understanding of the importance of internal waves in the mixing process and possibly the contribution of other mechanisms to the mixing process.

Each environment is known to be unique. In Long Reach new observations have shown mechanisms that experiments and theory have not yet captured. These observations have allowed us to better understand our environment. The existing theory on internal waves and the new observations made in Long Reach are now described.

#### **8.1 Internal waves and Mixing**

Linear stability analysis states that for either the KH or Holmboe waves to develop in stratified fluids a velocity shear and density gradient must be present. The difference between the development of the KH and Holmboe waves is due to the

thickness of the density interface. For a thick density interface only the KH waves may develop, whilst for a thin density interface both the KH and Holmboe waves may develop. The KH waves tend to grow faster than the Holmboe wave and occur only when the mean velocity shear and mean density interface coincides with each other. When the density and velocity shear are off set from each other, only Holmboe waves may be present. Solitons tends to develop where tides, stratification and irregular bathymetry are present.

There are two methods that can be used to identify internal waves: (1) visually (descriptively) by the characteristics of their shape and form or (2) mathematically (dynamically) based on their velocity and density structure.

KH waves have been described as the rolling up of the density interface that resembles a cats eyes feature; Holmboe waves as a train of small amplitude periodic waves and solitons as groups of waves with varying amplitude and wavelength (see diagram 8.1).

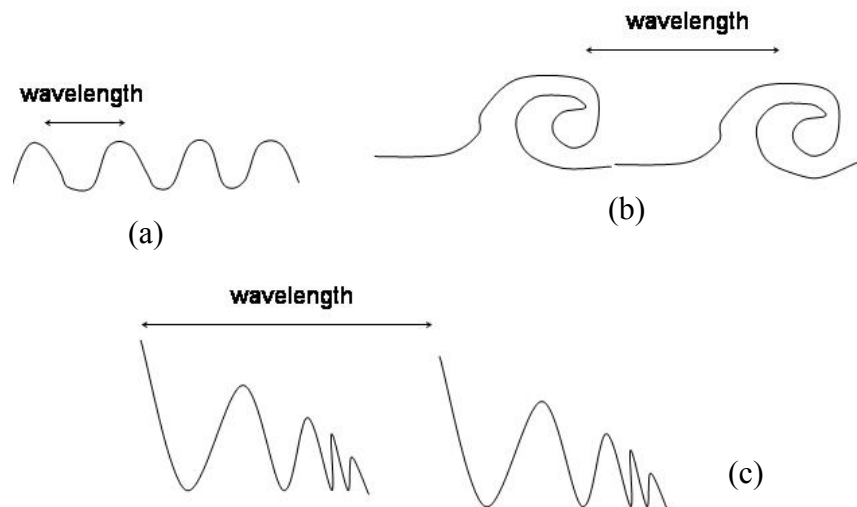


Figure 8.1: The three types of interfacial waves. (a) Holmboe waves, (b) Kelvin-Helmholtz waves and (c) soliton wave packets.

To visualize the shape and form of these waves in the water column an echosounder is usually employed. The echosounder measures the acoustic backscatter from the water column. The main sources of acoustic backscatter in the water column are zooplankton, the density interface, internal waves and suspended sediments. The echosounder is utilized in this study to identify the pycnocline and internal waves.

The two common dynamical approaches that are used to differentiate between the KH and Holmboe waves are the gradient Richardson number ( $Ri$ ) and a linear stability analysis. The  $Ri$  compares the magnitude of the velocity shear to the strength of the stratification in order to determine if turbulent mixing is occurring. Mixing tends to occur within the range  $0 < Ri < 1$ . Based on laboratory experiments and theoretical studies it has been found that the KH waves occur for  $0 < Ri < 0.25$  and Holmboe waves for  $Ri > 0.4$ .

A linear stability analysis assumes that the background flow (defined by the density and velocity profiles) when perturbed will create internal waves and that these internal waves grows exponentially. These waves only grow exponentially for a very short time and most observations occur in the nonlinear form.

The background flow may be approximated by a piecewise linear profile or a smooth profile. In the piecewise method the density is approximated by an abrupt step. Whilst in the smooth profile method the density and velocity profiles can be represented by any functions that fit the profiles. Results of a linear stability analysis predict a wave length and wave speed which may be confirmed from the echosounder images.

It should be noted that the  $Ri$  and linear stability analysis only distinguish between the KH and Holmboe wave. To dynamically identify the soliton wave packet a non linear analysis using KDV equations are normally employed. For this research both a

descriptive and dynamical analysis is employed. However the dynamical analysis is restricted to only identifying the KH and Holmboe waves. The methodology used to map the oceanographic processes occurring in Long Reach is summarized below.

## **8.2 Methodology**

The survey sensors used to map the oceanographic processes occurring in Long Reach were: (1) the Acoustic Doppler Current Profiler (ADCP) which measures current magnitude and direction, (2) a Moving Vessel Profiler (MVP) with a Conductivity Temperature Depth (CTD) sensor from which density is derived and (3) an echosounder which measures acoustic backscatter from the water column. To interpret the data, longitudinal profiles of density, along velocity and acoustic backscatter are used. These images were all produced using software produced by the OMG.

The echosounder had the greatest resolution both horizontally and vertically and is used in this research to identify the pycnocline and internal waves. However the data of this sensor can only be interpreted qualitatively. In order to identify the source of the backscatter additional measurements are required. In this study confirmation of the pycnocline from the acoustic backscatter is made by using the CTD data.

To reconfirm the observations of Trites [1965] and Metcalfe et al. [1979] a seasonal oceanographic survey was performed in 2003. The 2003 observations confirmed that a seasonal variation in stratification still exists. In addition it was observed that during the summer and autumn seasons processes were occurring at the interface of Long Reach. These processes appear to be prominent in the areas that irregular bathymetry occurs.

Investigations of the acoustic backscatter images at the interface show the presence of internal waves. The KH wave was identified on ebb tide within the vicinity of the Oak Pt sill in the late summer (September) of 2004. The observed wavelength of the KH varied between 15m to 30m. In the region of the area of study small amplitude periodic waves with wavelength of 15m to 30m were observed at various sections of the estuary. This wave was referred to as type 1.

The implementation of the echosounder and the increased resolution of the CTD data suggest that interfacial turbulent mixing may be one of the main processes occurring in Long Reach. It should be noted that the data collected for the seasonal survey were performed at random phases of the tide. Thus these surveys only illustrate a glimpse of the possible processes. To confirm and understand the possible interfacial mixing processes occurring in Long Reach required more detailed observations within the specific areas.

Two areas were chosen based on the processes observed and the bathymetry of the area (see Figure 8.2). Section one is the area at the entrance of the estuary. Section one is ~4.5km in length and the bathymetry of this area is irregular with several lateral constrictions existing. This results in an estuary width that varies from 800m to 300m. There exists a ~42m deep hole on entrance to this section. Section two is located adjacent to section one and is ~4.5km in length. The bathymetry is basically regular with a depth range of 22m to 25m. In the middle of section two there exists a 15m shoal. To south west and north east of this shoal, several deep channels exist.

To understand in detail the processes occurring in section one and section two of Long Reach a survey line along the centre of the survey area was traversed back and forth

for the duration of a tidal cycle. These surveys were performed to coincide with both neap and spring tides.

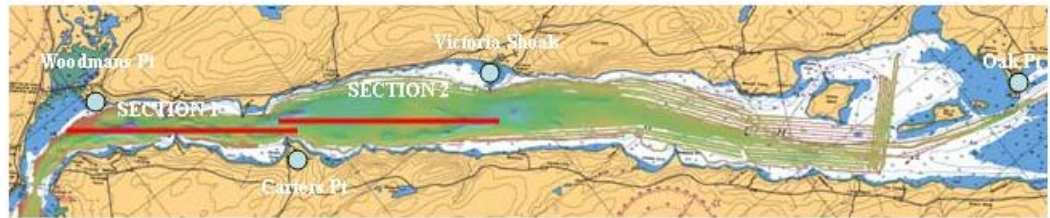


Figure 8.2: Map of Long Reach illustrating sections one and sections two.

### 8.3 Observations of Section One

For both neap and spring tides the estuary is highly stratified with warm fresh water overlying salty colder water (see Figure 8.3). A pycnocline thickness of ~2m separates the layers.

The surface and bottom layers remain basically homogenous throughout the section, apart for the deep hole area that contains saltier water than the rest of the survey area. It was also observed that at high tide a decrease in bottom density occurred at ~4000m marker. Using the acoustic backscatter images two types of internal waves are observed at the interface: (1) soliton wave packets and (2) small amplitude periodic waves referred to as type 1. The solitons are observed within the vicinity of the shoals. The following characteristics are observed during the tidal cycle:

1. A decrease in density and increase in pycnocline thickness occurs within the vicinity of the irregular bathymetry at rising tide into high tide.
2. Within the vicinity of the soliton wave packets a periodic oscillation of the pycnocline occurs.

3. At early rising tide the soliton wave packet disappears followed by the downward dip of the pycnocline. This occurred at the locations where the bathymetry shoaled then deepened.



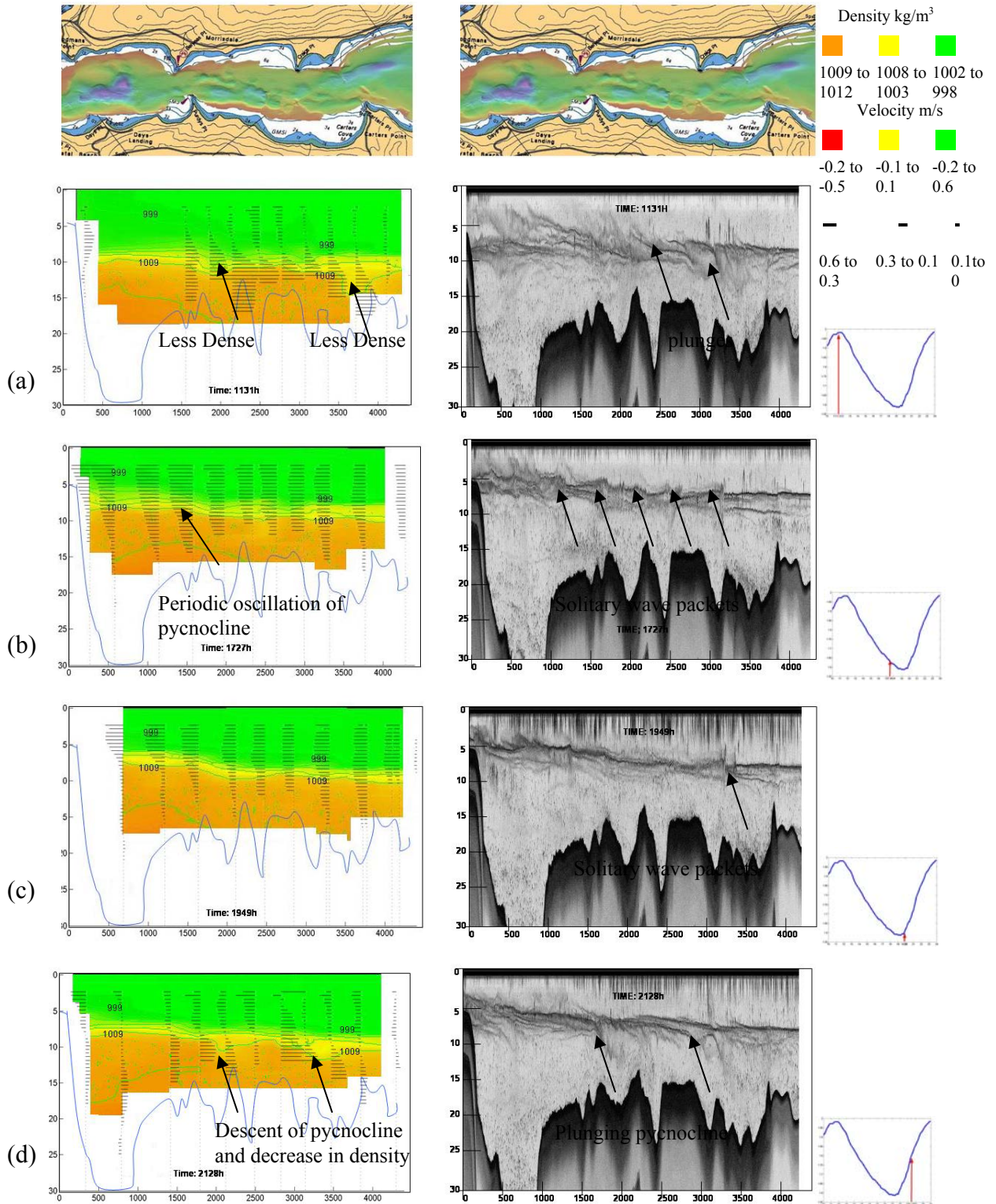


Figure 8.3: Density (left) and acoustic backscatter (middle) at the different phases of the tide (right) for section one neap tide.

The downward dip of the pycnocline is referred to in Apel [2002] as the plunging of the pycnocline. It was suggested in Apel [2002] that this plunging of the pycnocline was associated with (1) lee wave down current caused by a sharp change in bathymetry or (2) an undulatory bore. In this study the decrease in density and solitary wave packets are basically stationary. This implies that it is most likely not an undulatory bore. In fact it appears that the solitary wave packets are trapped in the bathymetry.

The plunges referred to in Apel [2002] do not possess the exact form as the plunges observed in Long Reach (see Figure 8.4). In Apel [2002] a periodic oscillation of the pycnocline still exists in front of the plunge. In Long Reach the pycnocline is level in front of the plunge. Thus this study suggests that the plunging of the pycnocline is associated with (1) possible mixing events associated with the soliton wave packets; (2) the flow pattern of the upper and lower layer, as it passes over the irregular bathymetry.

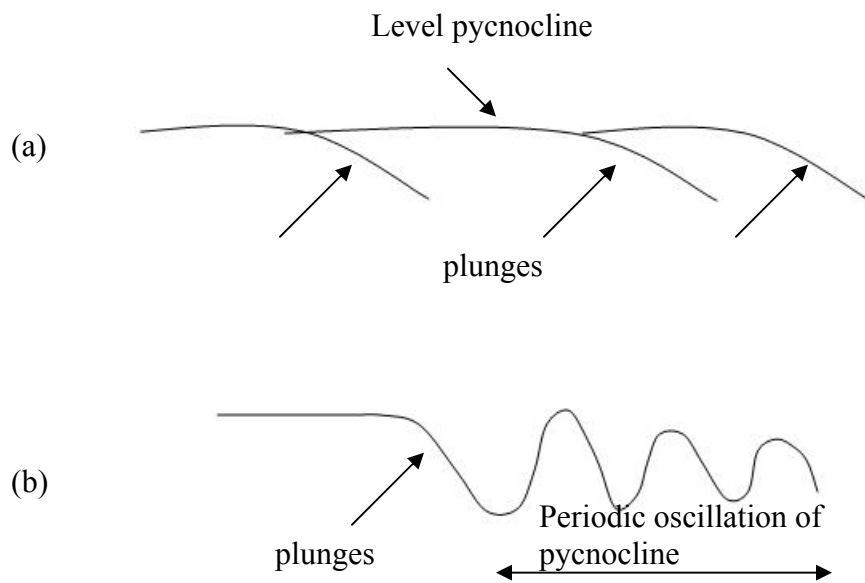


Figure 8.4: (a) schematic of the plunges observed in Long Reach and (b) those described by Apel [2002].

To confirm whether the decrease in density observed at the interface is due to possible mixing events occurring, a critical gradient Richardson number of  $0 < Ri < 1$  is sought. The results for both neap and spring tides confirm that mixing is occurring within the vicinity of the irregular section of the estuary at rising tide.

The disappearance of the soliton wave packets just before mixing occurs and the plunging of the pycnocline suggests that the solitons are a possible source of the mixing events occurring.

To dynamically identify the source of internal waves that may contribute to the mixing process a linear stability analysis is employed. The results found that Holmboe waves are a possible source of mixing in Long Reach. These waves were identified as the type 1 waves observed.

Thus in Long Reach Holmboe waves, soliton wave packets and the plunging of the pycnocline are present. It is possible that either one or all of these mechanisms contributes to the mixing process observed

## **8.4 Observations of Section Two**

For both neap and spring tides the surface fresh layer overlies a salty bottom layer. A pycnocline thickness of  $\sim 1.5\text{m}$  is observed (slightly less than in section one). Observations of longitudinal profiles of density, along velocity and acoustic backscatter showed that:

1. A displacement of the pycnocline at  $\sim 500\text{m}$  marker (referred to as location A) at high tide. This displacement was observed to be progressing upstream. At the shoal the echosounder images show the plunging of the pycnocline. This

was followed by a decrease in density within the vicinity of the shoal at falling tide. Inspection of the acoustic backscatter profiles at this time and within this vicinity shows type 1 waves present.

2. At falling tide there appears to be an over riding of the pycnocline where the waters originating from the shoal side rides on top of the waters downstream.
3. At falling tide at ~3000m marker (referred to as location B) (on the north eastern side of the shoal) the echosounder images show a soliton wave packet progressing upstream, whilst the flow of water moves downstream. The soliton travels a further 500m upstream until it diminishes. Within this vicinity a decrease in density occurs. The soliton wave packet and the decrease in density are not observed at spring tides.
4. At high tide the shoal appears to create two types of circulation pattern on either side of it. At flood tides the pycnocline waters are flowing upstream however at the shoal and on the upriver side of the shoal the waters are ebbing. The bottom 20m to 25m waters are also observed to be ebbing. Three possible explanation for this circulation pattern are :

Case 1: At high tide salty water advects upstream in the lower layer, however on approaching the shoal the velocities decrease and a bottom boundary layer flow develops

Case 2: The flow upstream is created by an internal wave on approaching the shoal it cannot propagate any further, thus it diminishes.

Case 3: At the shoal the bottom layer ebbs whilst on the upriver side the bottom velocities floods. This may be due to the shoal blocking the flow of

flood waters upstream. It is assumed that some of the flood waters flow through the deep channels located on either side of the shoal.

Calculations of the  $Ri$  confirm that mixing is occurring only at location A, thus a linear stability analysis is attempted. However due to the fact that the velocity profiles at location A were not similar to the theorized profiles it could not be performed for the observed profiles. However the type 1 waves observed in section two are similar to the Holmboe waves identified in section one by the linear stability analysis and the acoustic backscatter images.

Mixing was not calculated to be occurring at location B, but the presence of a soliton followed by its disappearance and then a decrease in density suggests that possible mixing process is occurring even though it was not calculated.

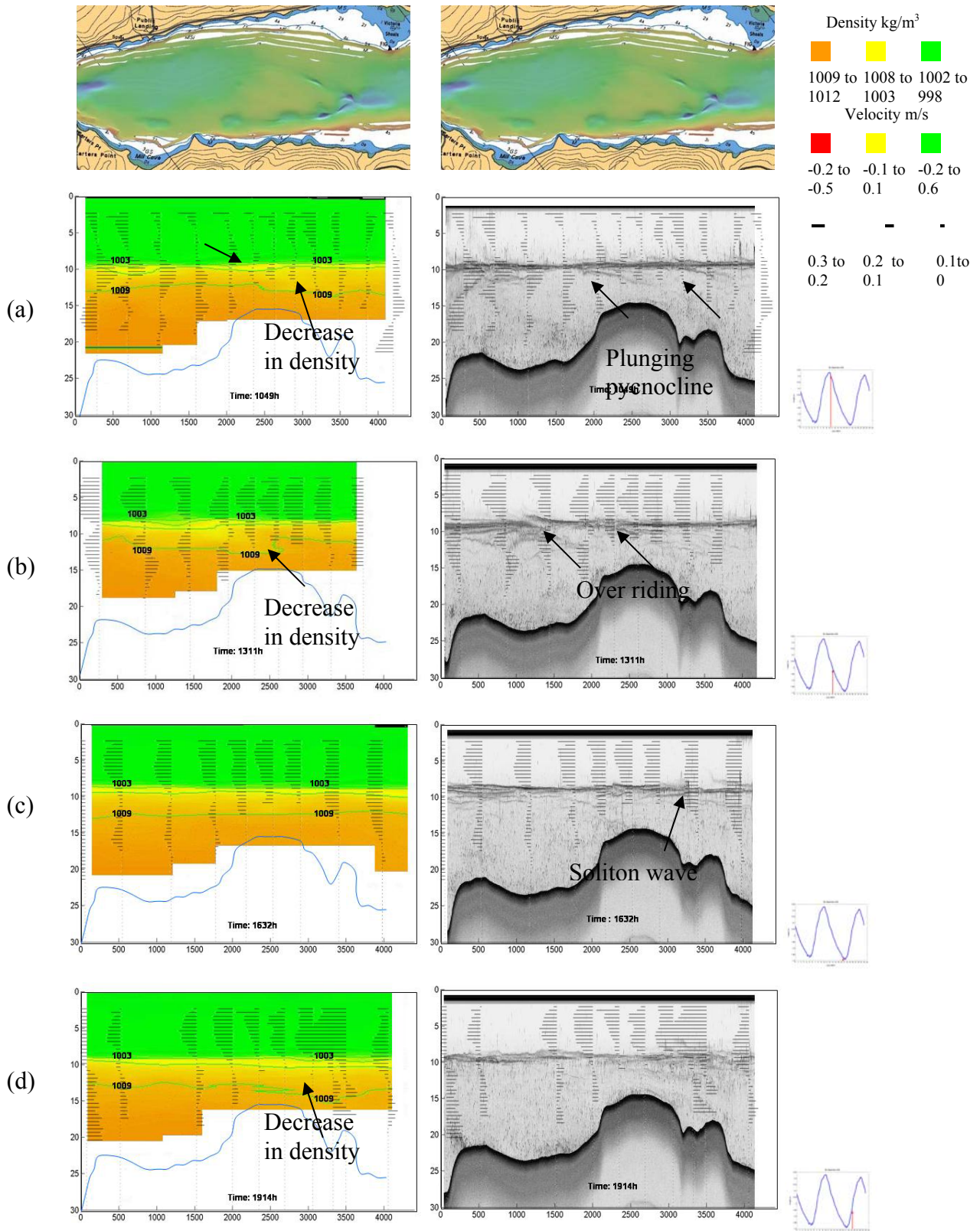


Figure 8.5: Profiles of density (left) and acoustic backscatter (right) for section two. The arrows in the density profiles indicate areas where a decrease in density occurs.

## 8.5 Conclusions

Results of the Ri analysis conclude that in both section one and section two interfacial mixing is occurring in Long Reach. This mixing occurs from the pycnocline into the bottom salty layer. Observations of the echosounder images show that both Holmboe waves and soliton wave packets are present and can possibly be the sources of this mixing.

The echosounder images also show that, in section one just after the disappearance of the soliton wave packets, the plunging of the pycnocline occurs. It is at these instances of the plunges that the mixing was calculated to occur. These plunges were also observed in section two within the vicinity of the 15m shoal. However the soliton wave packets were not present. Thus it is very possible that the plunging of the pycnocline in section two is a different mixing process than that caused by the plunging of the pycnocline in section one.

The existing theory on interfacial mixing suggests that internal waves are a source of mixing in stratified environments. The observations made of the plunging pycnocline in Long Reach suggest that the form of the mixing is dependant on the bathymetry and pattern flow and may not always take the form of the three known internal waves.

In section two the plunging of the pycnocline is observed to occur at high tide within the vicinity of the 15m shoal. Less dense water was observed at the pycnocline at this time. At falling tide the less dense water at the pycnocline advects downstream and, on interaction with the more dense water at the pycnocline downstream, rides on top of the denser water. This event is visualized in the echosounder images as the over - riding phenomena.



Implementation of a linear stability analysis proved successful in identifying the type 1 wave as the Holmboe wave in section one. However using piecewise linear approximations of density and velocity profiles did not accurately predict the observed wavelength of the Holmboe wave. When smooth profile approximations were used more accurate estimates of the wavelength were obtained.

In section one the piecewise method may not have accurately predicted the observed wavelength due to the fact that this method assumes an abrupt step for the density profile. The piecewise linear velocity and density approximations were a poor fit to the observed profiles and hence gave a poor prediction of the wavelength.

In section two of Long Reach another example of the application of theory to field observations was presented. In section two the velocity profiles are very different from the theory, resulting in inaccurate approximations of the flow field and yielding inaccurate results. The identification of the type 1 wave as the Holmboe in section two depended on the results of the linear stability in section one and its identification from the acoustic backscatter images.

This research has shown that the bathymetry and geometry of Long Reach plays a major role in the development of internal waves, plunging of the pycnocline and interfacial mixing. In section one and section two the soliton waves develop within the vicinity of the shoals. In section one mixing was observed in the areas where the greatest shear occurred and was enhanced by the areas where contractions existed both laterally and vertically.

Mixing occurs mainly at rising tide and high tide as it is at this time that greatest shear occurs. The effect of the neap and spring tides on mixing varies for each section. In



section one the same pattern of processes were observed to occur for both neap and spring tides. In section two a solitary wave packet was observed at neap tides however at spring tides it was not observed. It appears from this observation that the change in river discharge was more important than the change in spring/neap tides.

In conclusion the results of both section one and section two has illustrated that both advection and turbulent mixing is occurring in Long Reach and the potential sources that may have contributed to the mixing process is that of the Holmboe waves, soliton wave packets or the plunges.

## **8.6 Recommendations**

These surveys have concentrated on the occurrence of along estuary processes. It possible that secondary circulation patterns also influence the mixing processes observed. Thus it may be necessary in future work to consider secondary circulation.

In section two within the vicinity of the shoal, there appears to be a number of processes occurring during the tidal cycle. To obtain a better understanding of these processes more observation may be needed within the vicinity of the sill both across and along stream.

This research has performed detailed surveys in both section one and section two. The results have concluded that interfacial mixing created by soliton wave packets and/or Holmboe waves and/or the plunges is one of the major processes occurring in Long Reach. In addition the seasonal surveys have shown that, in the summer, KH waves exist at ebb tide within the vicinity of the Oak Point sill (upstream of section one and two).

Thus to obtain a better understanding of all the major processes occurring in Long Reach more detailed observations is required in the other survey area.

This study has concentrated on the processes occurring under highly stratified conditions. It will be interesting to observe the processes that occur when Long Reach is partially mixed.

## References

- Alexakis, A. (2005). "On Holmboe instability for smooth shear and density profiles." *Physics of Fluids*, Vol. 17, Issue8, pp. 084103-084103(8).
- Apel, J.R. (2002). "Oceanic Internal Waves and Solitons." Global Ocean Associates prepared for Office of Naval Research.
- Betteridge, K.F.E., J.J. Williams., P.D.Thorne., and P.S. Bell. (2003). "Acoustic Instrumentation for measuring near-bed sediment processes and hydrodynamics." *Journal of Experimental Marine Biology and Ecology*, No. 285-286, pp. 105-118.
- Browand, F and C. Winant., (1973). "Laboratory observations of shear instability in a stratified fluid." *Boundary Layer Meteorology*, Vol. 5, pp. 67-77.
- Chant, R.J., and R.E Wilson (2000). " Internal hydraulics and mixing in a highly stratified estuary." *Journal of Geophysical Research*, Vol. 105, No.C6, pp. 14,215 -14222.
- Canadian Hydrographic Survey. (2005).Tidal harmonic constituents for the Bay of Fundy and the Saint John River. Personal communication by email: [guay@meds-sdmm.dfo-mpo.gc.ca](mailto:guay@meds-sdmm.dfo-mpo.gc.ca), contact: Claude Guay
- Dyer, K.R (1973). *Estuaries a Physical Introduction*. 1st ed., John Wiley & Sons Ltd, New York
- Dyer, K.R (1997). *Estuaries a Physical Introduction* 2nd ed., John Wiley & Sons Ltd, New York.
- Environment Canada. (2005). Climate data online and Climate data Normal and Averages for New Brunswick at Saint John A, [On-line] 23 January 2006, [http://www.climate.weatheroffice.ec.gc.ca/climateData/canada\\_e.html](http://www.climate.weatheroffice.ec.gc.ca/climateData/canada_e.html)
- Farmer, D.M., and J.D. Smith (1980). "Tidal interaction of stratified flow with a sill in Knight Inlet." *Deep Sea Research*, Vol. 27A. pp. 239 to 254.
- Farmer, D and Armi L (1999). " The Generation and Trapping of Internal Solitary Waves over Topography." *Science*, Vol. 283, no. 5398, pp. 188-190.
- Fisheries and Oceans Canada (2002). "The Saint John River Basin and its Fishery Resources." [On-line] 10 November 2005. <http://www.mar.dfo-mpo.gc.ca/science/mactaquac/stjohn.html>
- Geyer, W.R., and D.M Farmer (1989). " Tide-Induced Variation of the Dynamics of a Salt Wedge Estuary." *Journal of Physical Oceanography*, pp. 1060-1072.

- Godin, G. (1985). "Modification of River Tides by the Discharge." *Journal of Waterway, Port, Coastal and Ocean Engineering*, Vol. 111, No. 1, pp 257-274.
- Godin, G. (1991). "Tidal Hydraulics of Saint John River." *Journal of Waterway, Port, Coastal and Ocean Engineering*, Vol. 117, No. 1, pp 19-28.
- Goodman, L., J. Oeschger and D. Szargowicz (1992). "Ocean acoustics turbulence study: Acoustic scattering from a axisymmetric plume." *Journal of Acoustic Society of America*, Vol. 91, pp. 3212-3227.
- Greenlaw, C.F (1979). "Acoustical estimation of zooplankton populations." *Limnology of Oceanography*, Vol. 24, pp. 226-242.
- Haigh, S.P (1995). "Non Symmetric Holmboe waves." Ph.D. thesis, Department of Mathematics, University of British Columbia, Vancouver, BC., Canada, 179pp.
- Hansen, P.H. (1977). Hydraulic Model Study Of The Reversing Falls At Saint John New Brunswick. M.Sc.E. thesis, Department of Civil Engineering, University of New Brunswick, N.B., Canada, 116pp.
- Hazel, P. (1972). "Numerical studies of the stability of inviscid parallel shear flows." *Journal of Fluid Mechanics*, Vol. 51, pp 39-62.
- Holmboe, J (1962). "On the Behaviour of Symmetric Waves in stratified shear layers" *Geofys Publ.*, Vol. 24, pp. 67-113.
- Hughes Clarke, J.E. (2004). Personal communication. Chair of Ocean Mapping Group, University of New Brunswick, December.
- Hughes Clarke, J.E and S.P. Haigh (2005). "Observations and Interpretation of Mixing and Exchange Over A Sill At the Mouth of the Saint John River Estuary." 2<sup>nd</sup> CSCE Speciality Conference on Coastal, Estuary and Offshore Engineering.
- Ingham, A.E (1994). *Hydrography For The Surveyor and Engineer* 3<sup>rd</sup> ed., Blackwell
- Jay, D.A., and J.D Smith (1990). "Residual Circulation in Shallow Estuaries, Weakly Stratified and Partially Mixed Estuaries." *Journal of Geophysical Research* , Vol. 95, No. C1, pp. 733-748.
- Klymak, J.M., and M.C Gregg (2001). "Three-dimensional nature of a flow near a sill." *Journal of Geophysical Research*, Vol. 106, No. C10, pp22295-22311.
- Klymak, J.M., and J.N Moum (2003). "Internal solitary waves of elevation advancing on a shoaling shelf." *Geophysical Research Letters*, Vol. 30, No. 20.

- Klymak, J.M., and M.C. Gregg (2003). "The Role of upstream waves and a downstream density pool in the growth of lee waves: Stratified Flow over the Knight Inlet Sill." *Journal of Physical Oceanography*, Vol. 33, pp. 1446-1461.
- Koop, C. and F. Browand (1979). "Instability and turbulence in a stratified layer with shear." *Journal of Fluid Mechanics*, Vol. 93, pp. 135-159.
- Korteweg, D.J and G. de Vries. (1895) "On the change of form of long waves advancing in a rectangular canal, and on a new type of long stationary wave." *Phil Mag.* Vol 39 Ser.5, pp 422-443.
- Lawrence, G.A., F.K. Browand and L.G. Redekopp. (1991) "The stability of a sheared density interface." *Physics of Fluids A*, Vol. 3, No. 10, pp. 2360-2370.
- Lurton, X (2002). *An Introduction to Underwater Acoustics*. Praxis, Chichester, U.K.
- Mann, R., B.M Campos and M.W. Luckenbach (1991). "Swimming rate and responses of larvae of three mactrid bivalves to salinity discontinuities." *Marine Ecology Progress Series*, Vol. 68, pp. 257-269.
- Martin, L.V, T.K Stanton, P.H Weibe and J.F Lynch (1996). "Acoustic classification of zooplankton." *ICES Journal of Marine Sciences*, Vol. 53, pp. 217-224.
- Metcalf, C., C., M.J Dadswell, G.F. Gillis, M.L.H Thomas (1976). "Physical, chemical and biological parameters of the Saint John River Estuary, New Brunswick, Canada" Department of the Environment Fisheries and Marine Service. Technical Report No 686.
- Miles, J. (1991). "On the stability of heterogeneous shear flows." *Fluid Mechanics*, Vol. 10, pp. 496-508.
- Miles, J. and L.N Howard (1964): "Note on heterogeneous shear flow." *Journal of Fluid Mechanics*, Vol. 20, pp. 331-336.
- Nepf, H.M., and W.R Geyer (1996). "Intratidal variations in stratification and mixing in the Hudson estuary." *Journal of Geophysical Research*, Vol. 101. No.C5 pp. 12,079-12086
- Peters, H. (1997). "Observations of Stratified Turbulent Mixing in an Estuary: Neap to Spring Variation During High River Flow." *Estuarine, Coastal and Shelf Science*, Vol. 45, pp. 68-88.
- RD Instruments. (1996). *Acoustic Doppler Current Profiler: Principles of Operation*. 2<sup>nd</sup> Edition.
- Richardson, L.F (1920) "The Supply of Energy from and to Atmospheric Eddies." *Proceedings of the Royal Society of London. Series A, Containing Papers of a Mathematical and Physical Character*. Vol. 97, No. 686, pp. 354-373.

- Russell, J.S. (1838) "Report on waves." Report of the 7<sup>th</sup> Meeting of British Association for the Advancement of Science., London John Murray, pp. 417-496.
- Russell, J.S. (1844) "Report on waves." Report of the 14<sup>th</sup> Meeting of British Association for the Advancement of Science., London John Murray, pp. 311-390.
- Seaman, A.A. (2004) "Late Pleistocene history of New Brunswick, Canada." In Quaternary Glaciation –Extent and Chronology Part II, Ed. J.Ehlers and P.L. Gibbard. Developments in Quaternary Science, Elsevier, Amsterdam., Vol. 2b, pp. 151-167.
- Seim, H.E., M.C Gregg and R.T. Miyamoto (1995). "Acoustic Backscatter from Turbulent Microstructure." Journal of Atmosphere Oceanic Technology, Vol. 12, pp. 367-380.
- Smyth, W.D., and W.R Peltier (1989). " The Transition between Kelvin-Helmholtz and Holmboe Instability: An Investigation of the Overreflection Hypothesis." Journal of Atmospheric Sciences, Vol. 46, No. 24, pp. 3698 – 3721.
- Stanton, T.K., J.D. Warren., P.H. Weibe., M.C. Benfield and C.H. Greene. (1998). " Contributions Of The Turbulence Field and Zooplankton to Acoustic Backscattering by an Internal Wave." Presented at the IOS//WHOI/ONR Internal Solitary Wave Workshop B.C. Canada 1998, On-line 8 August 2006, <http://www.whoi.edu/science/AOPE/people/tduda/isww/text/tkstanton/tkstanton.htm>
- Thorp., S (1973). "Turbulence in stably stratified fluids: a review of laboratory experiments." Boundary Layer Meteorology, Vol. 5, NO. 95
- Thorp., S (1985). " Laboratory observations of secondary structures in Kelvin-Helmholtz billows and consequences for ocean mixing." Geophysics Astrophysics Fluid Dynamics, Vol. 92, pp. 5231-5245.
- Traykovski, L.V., R.L O'Driscoll and D.E. Mc Gehee (1998). "Effect of orientation on broadband acoustic scattering of Antarctic Krill *Euphausia superba*: Implications for inverting zooplankton spectral acoustic signatures for angle of orientation." Journal of Acoustical Society of America, Vol. 104(4), pp. 2121-2135.
- Trites, R.W. (1959). " An Oceanographic and Biological Reconnaissance of Kennebecasis Bay and the Saint John River Estuary." Journal of Fisheries Research Board Canada. Vol(17)3.
- Water Survey of Canada (2004). Data Products and Services [CD-ROM] River Discharge data at Mactaquac [On-line] 23 January 2006,[On-line] 10 November 2005. [http://www.wsc.ec.gc.ca/products/hydat/main\\_e.cfm?cname=hydat\\_e.cfm](http://www.wsc.ec.gc.ca/products/hydat/main_e.cfm?cname=hydat_e.cfm)

Warren, J.D, T.K Stanton, M.C Benfield, P.H. Wiebe and D. Chu. (1999). "In Situ Measurements of Acoustic Target Strength of Siphonophores." Proceedings of the 2<sup>nd</sup> EAA International Symposium of Hydroacoustics June 1999 [On-line] 31<sup>st</sup> July 2005, [http://www.oal.who.edu/tstanton/pubs/EAA\\_proc.html](http://www.oal.who.edu/tstanton/pubs/EAA_proc.html)

Yoshida, S.M., Ohtani, S.Nishida and P.F. Linden. (1998) "Mixing Processes in a Highly Stratified River." Physical Processes in Lakes and Oceans: Coastal and Estuarine Studies, Vol. 54, pp. 389-400.

Zhu, D.Z and G..A. Lawrence. (2001) "Holmboe instability in exchange flows." Journal of Fluid Mechanics, Vol. 429, pp. 391-409.

# Appendix I



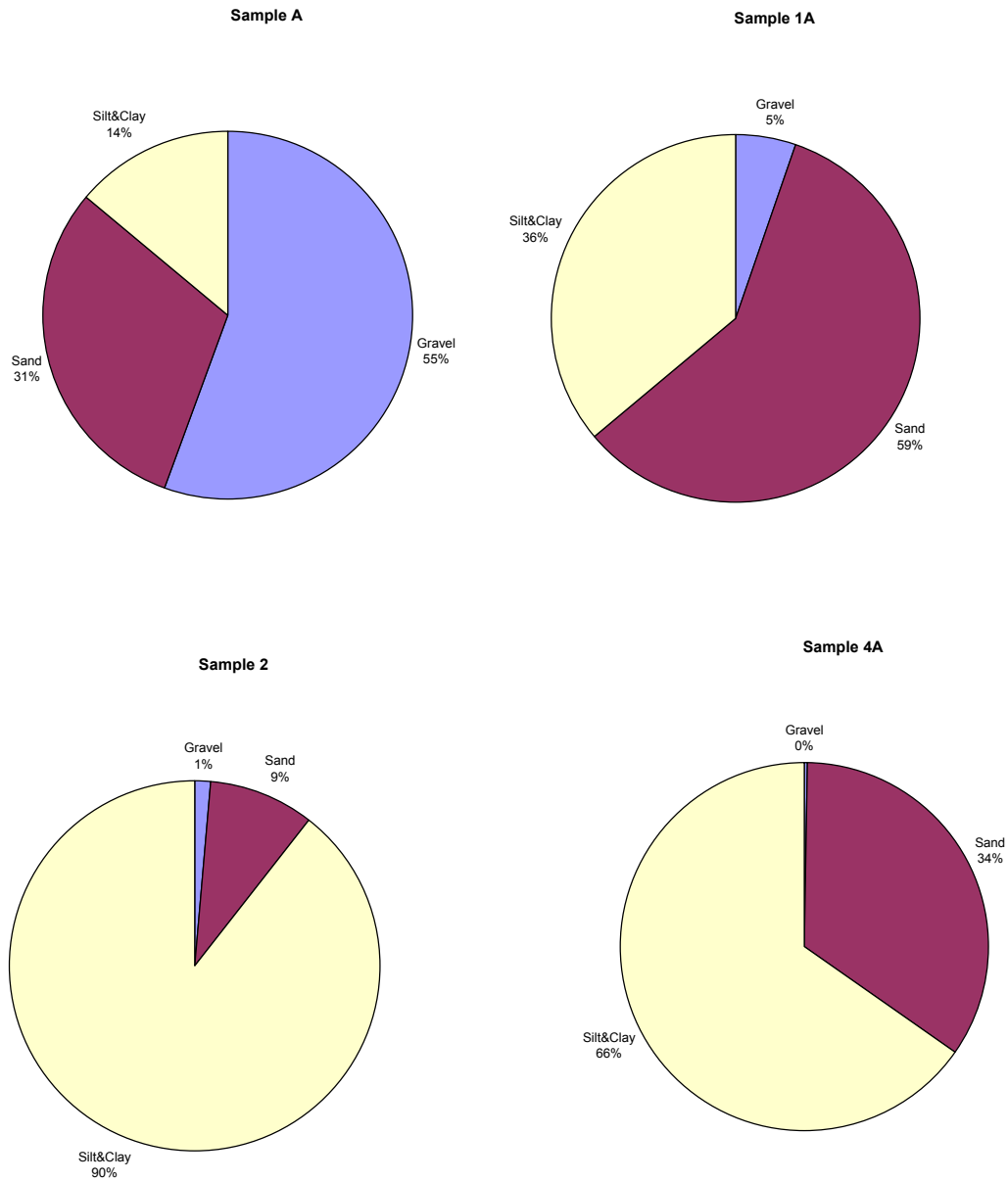


Figure I.1: Sediments graphs of Long Reach

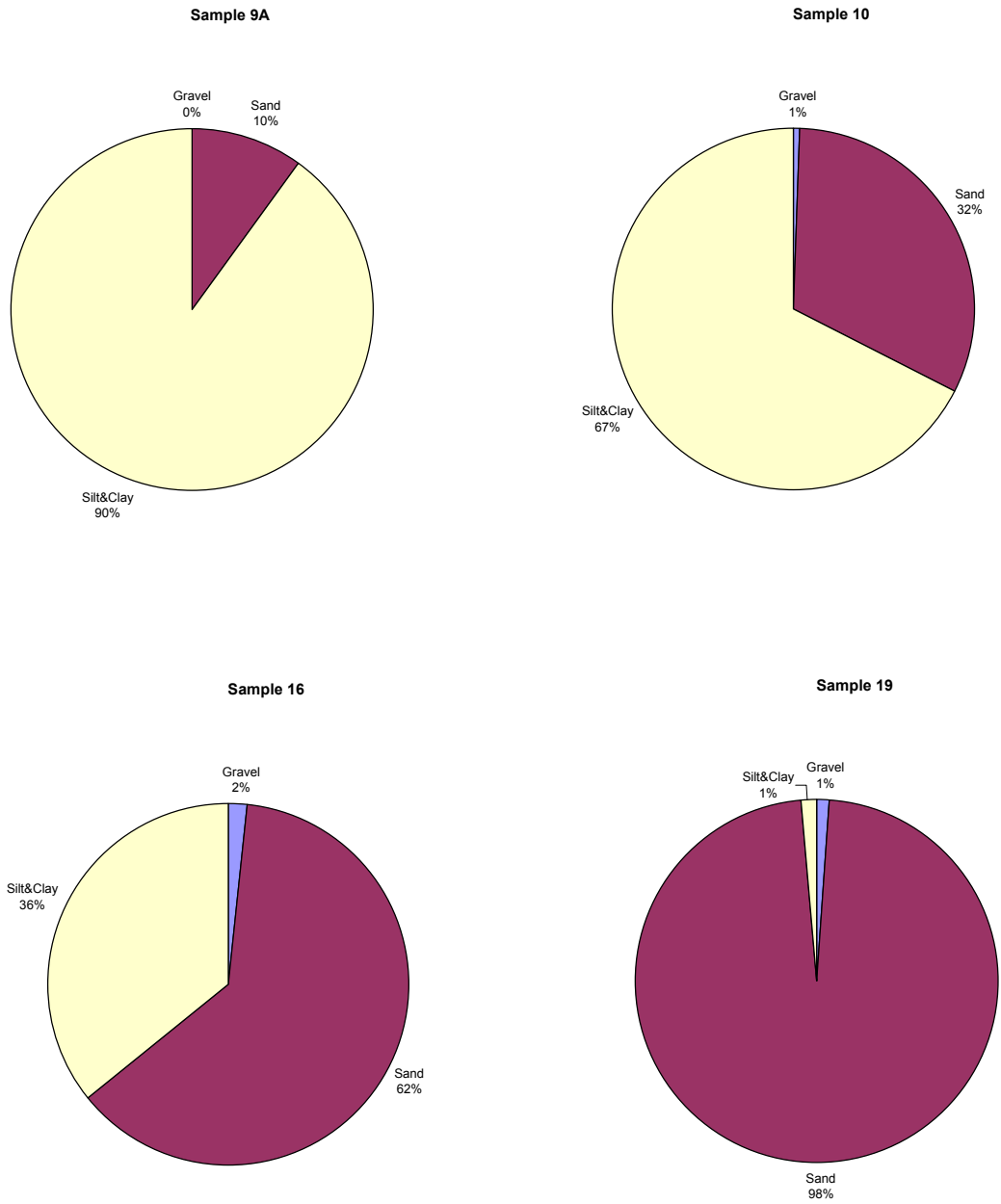


Figure I.1 (continued): Sediments graphs of Long Reach

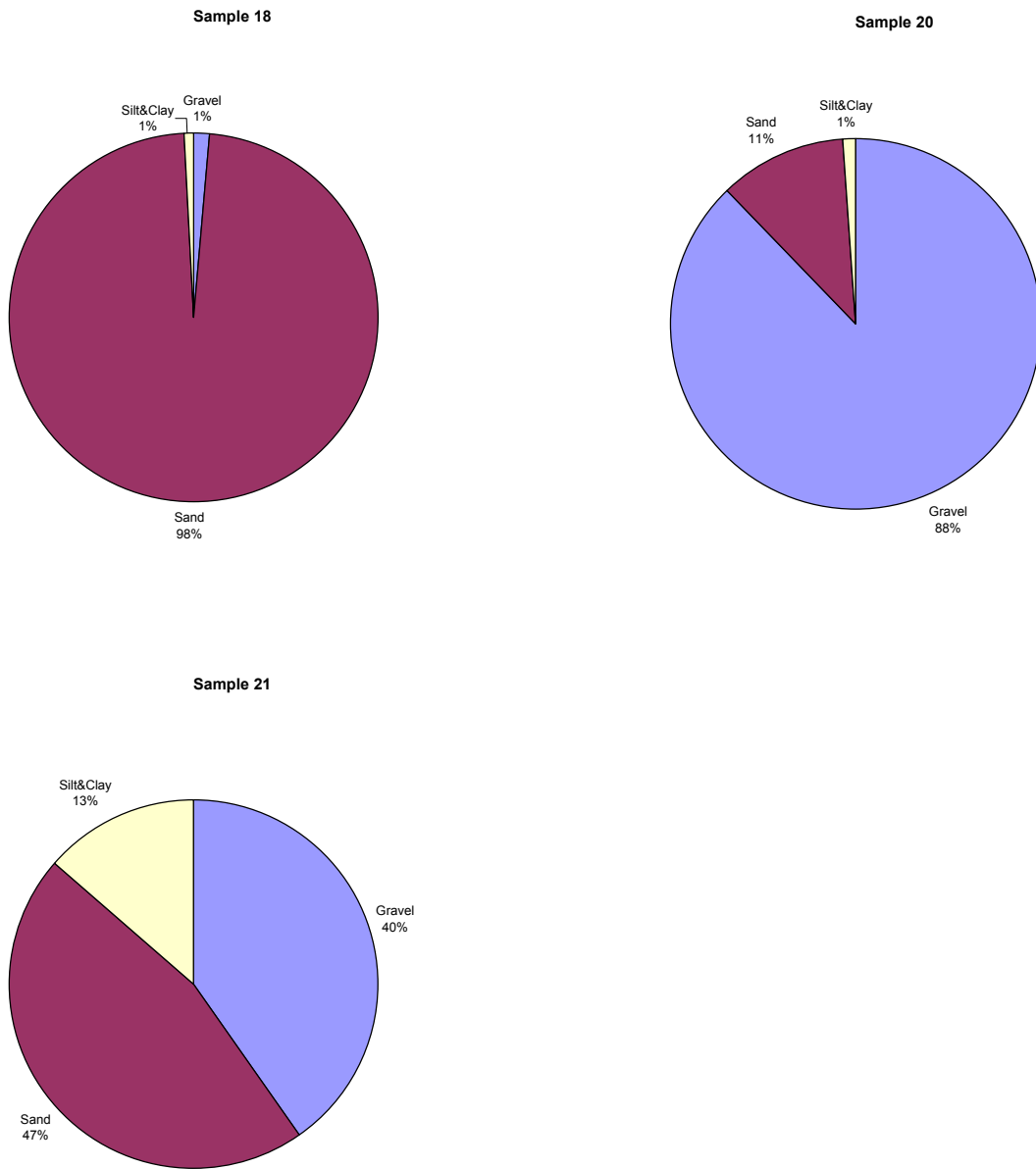


Figure I.1 (continued): Sediments graphs of Long Reach

## APPENDIX II

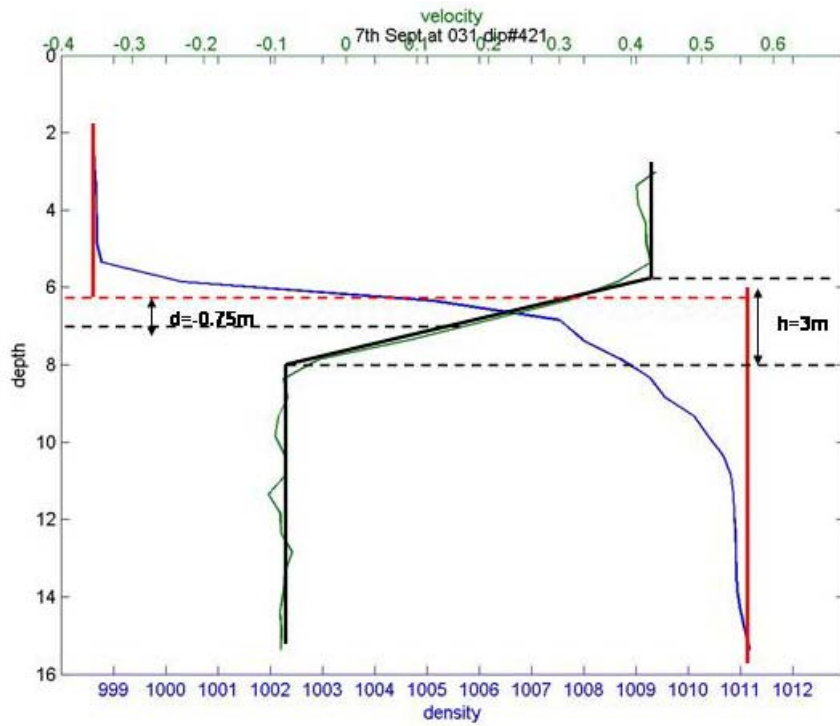
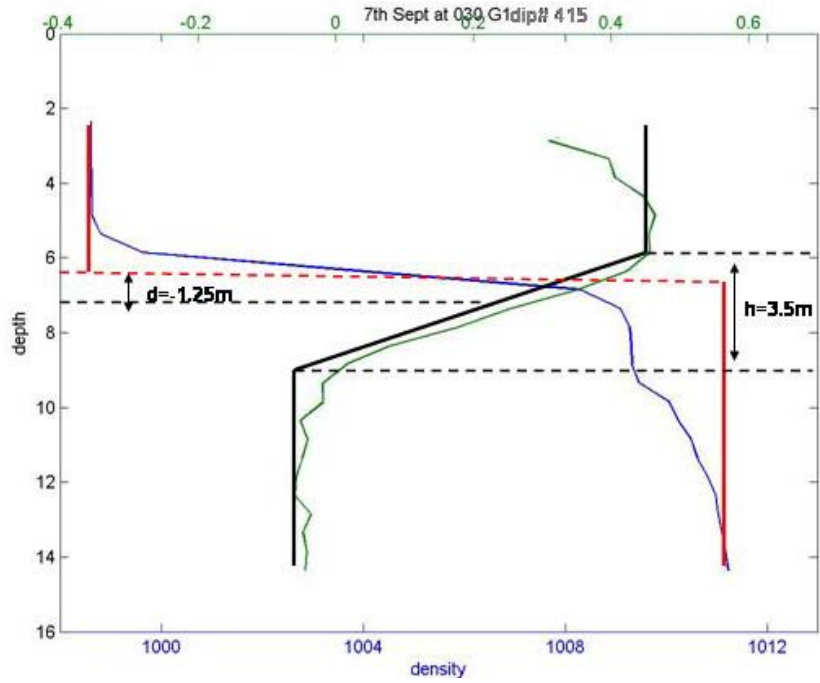


Figure II.1: Piecewise approximations for section one

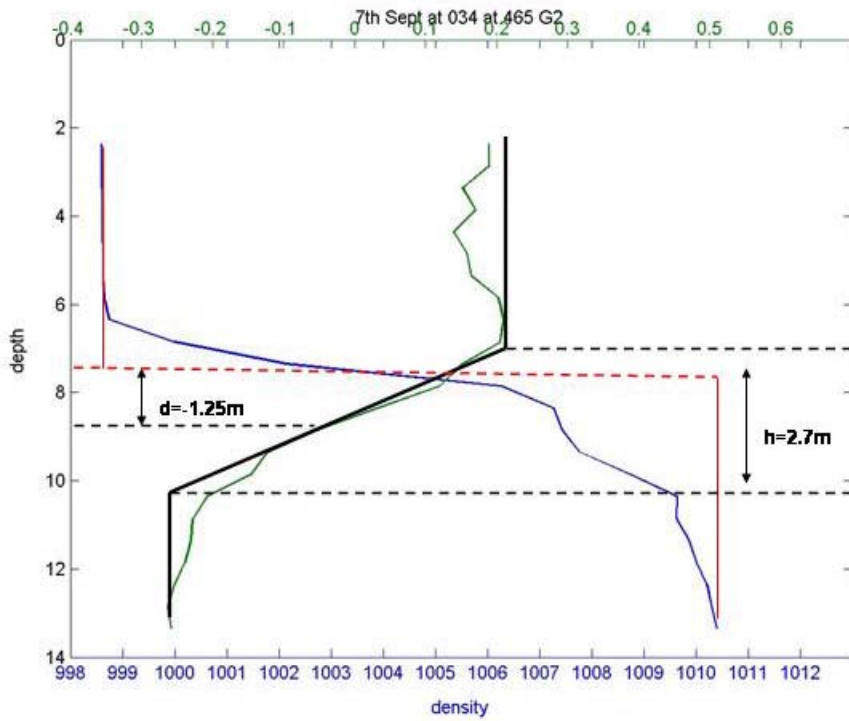
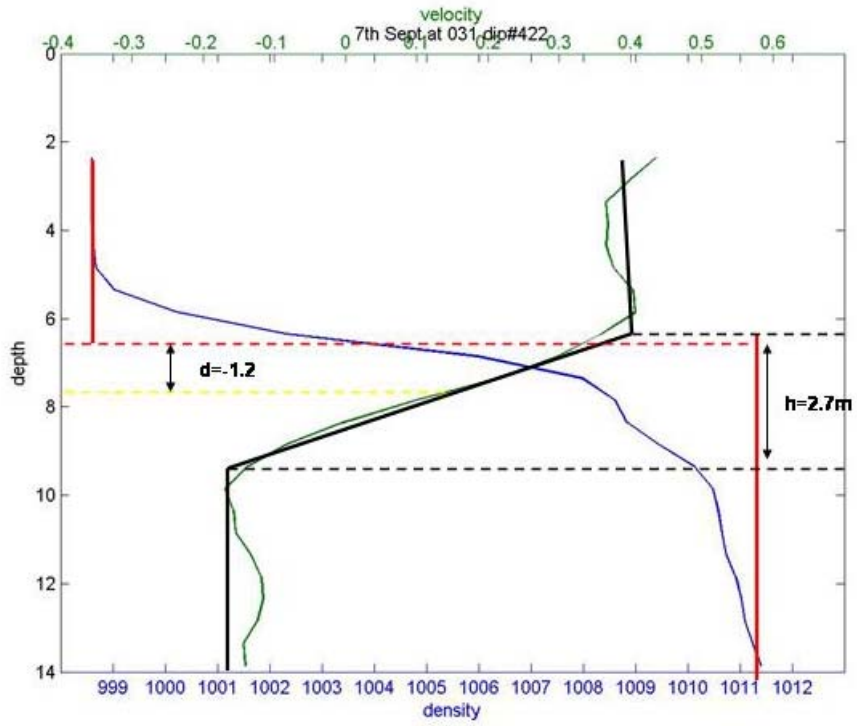


Figure II.1 (continued): Piecewise approximations for section one

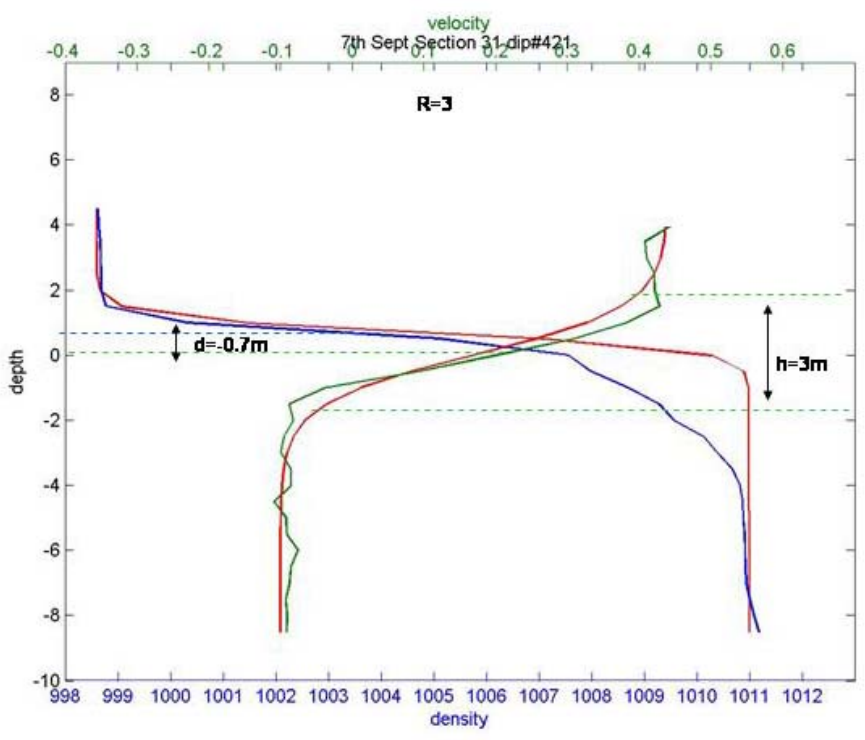
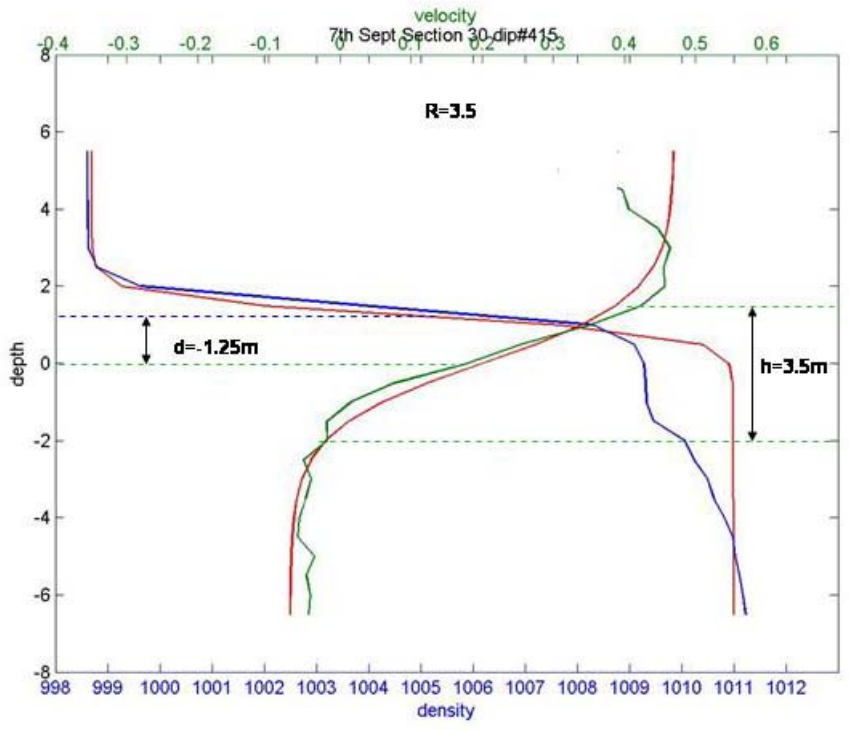


Figure 11.2: Smooth profile approximations for section one

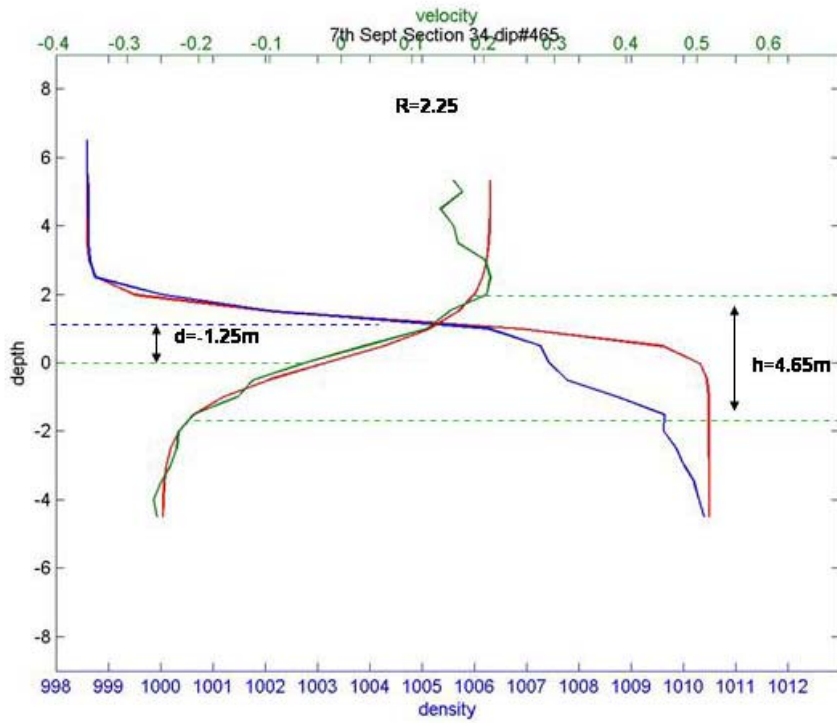
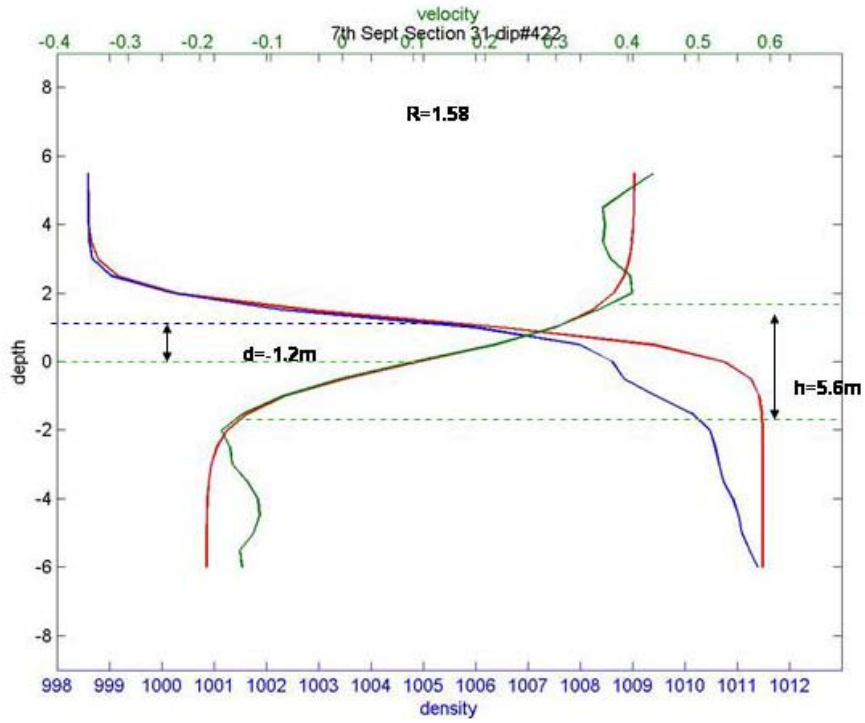


Figure 11.2 (continued): Smooth profile approximations for section one



## APPENDIX III

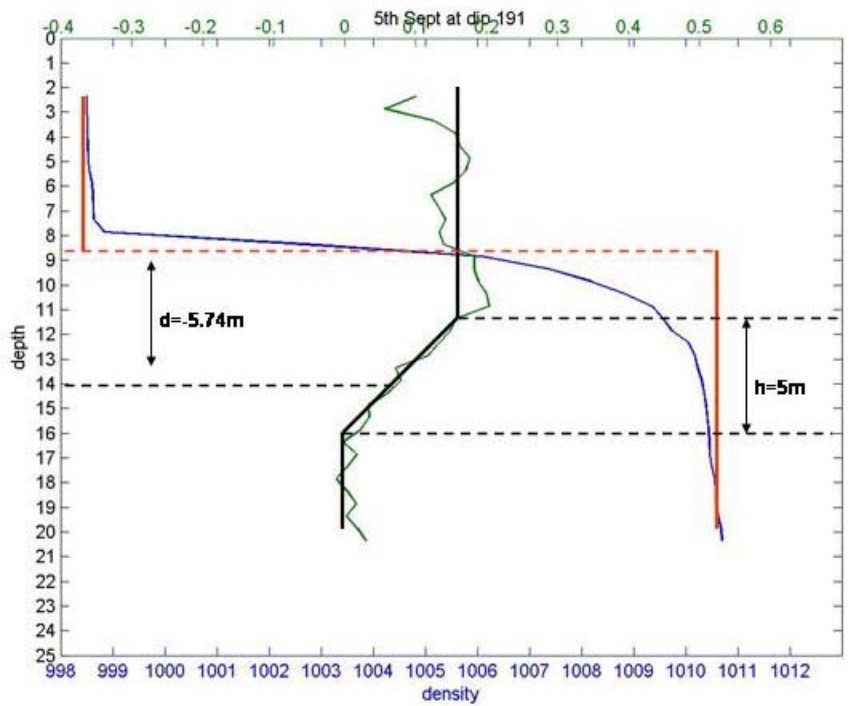
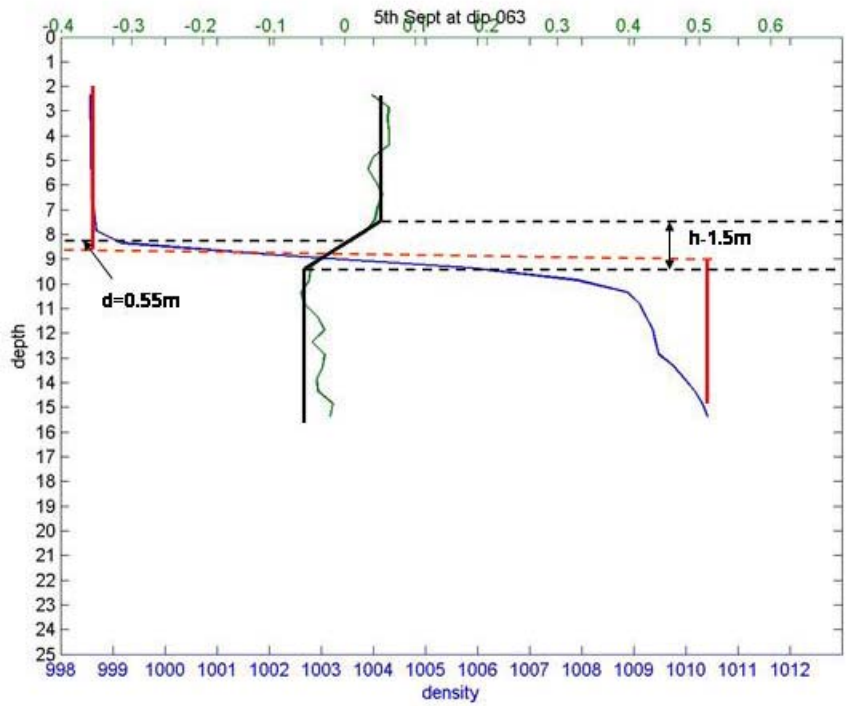


Figure III.1: Piecewise approximation for section two

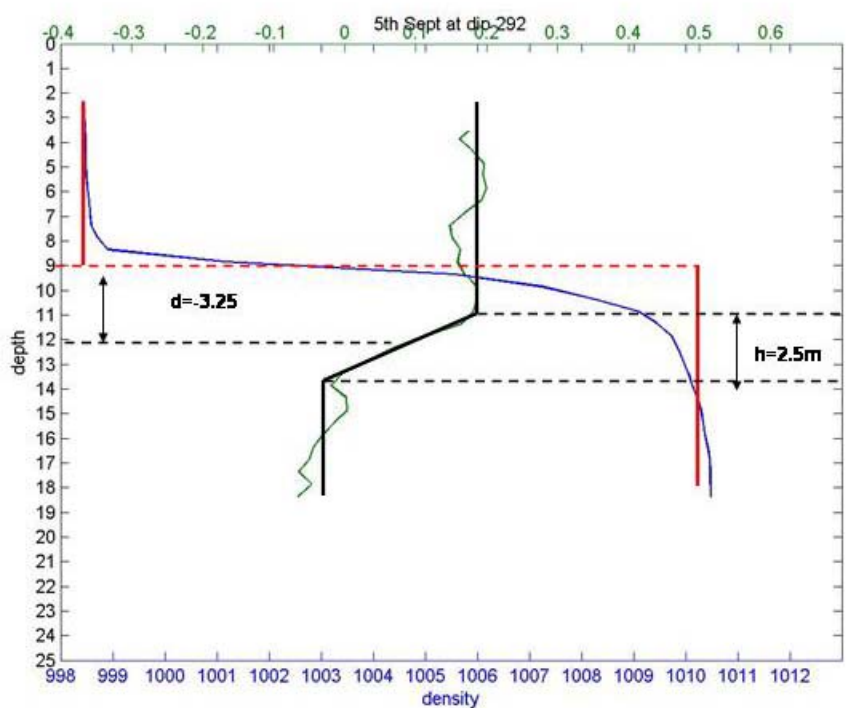
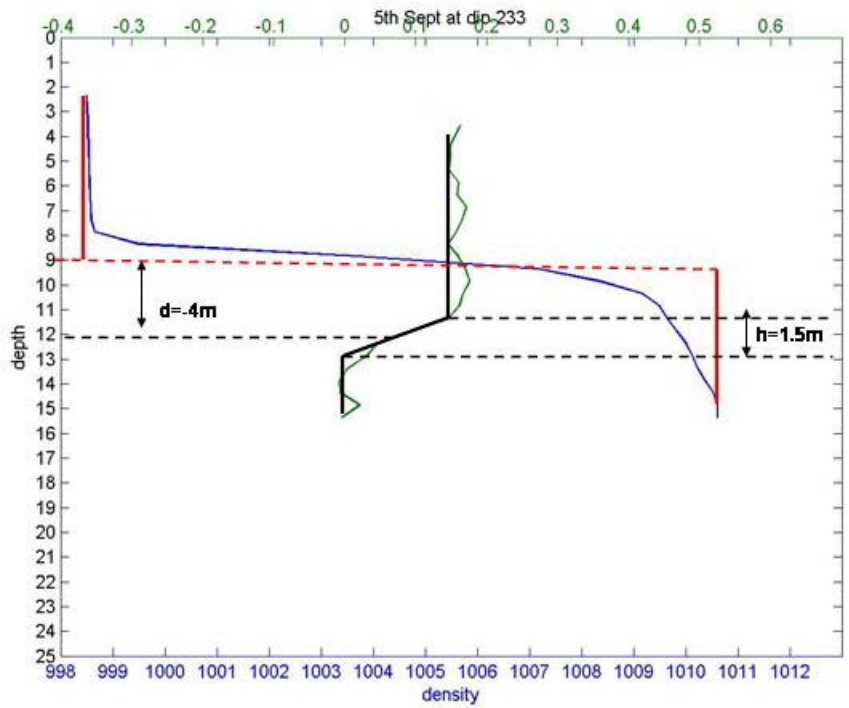


Figure III.1: Piecewise approximation for section two

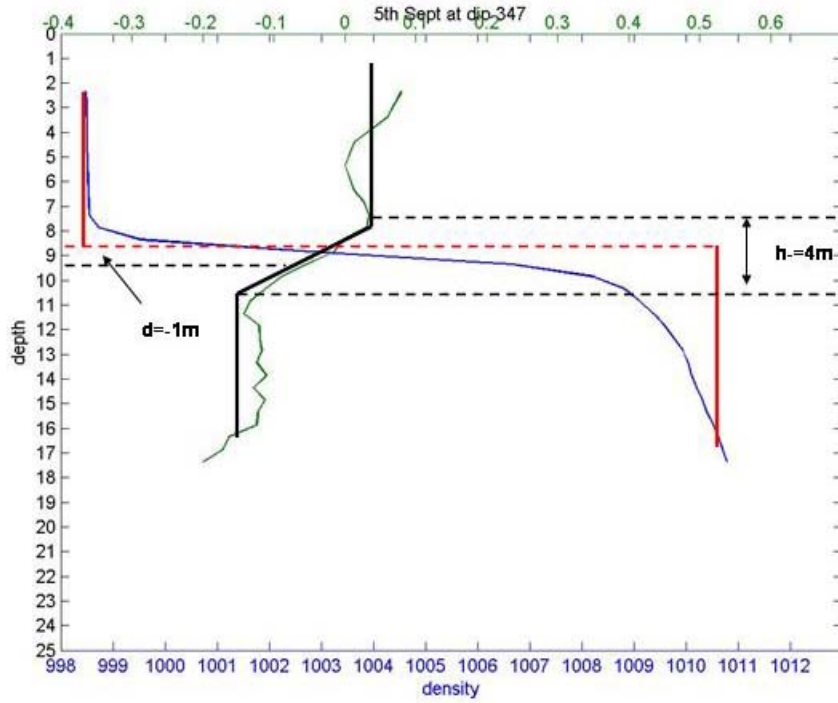
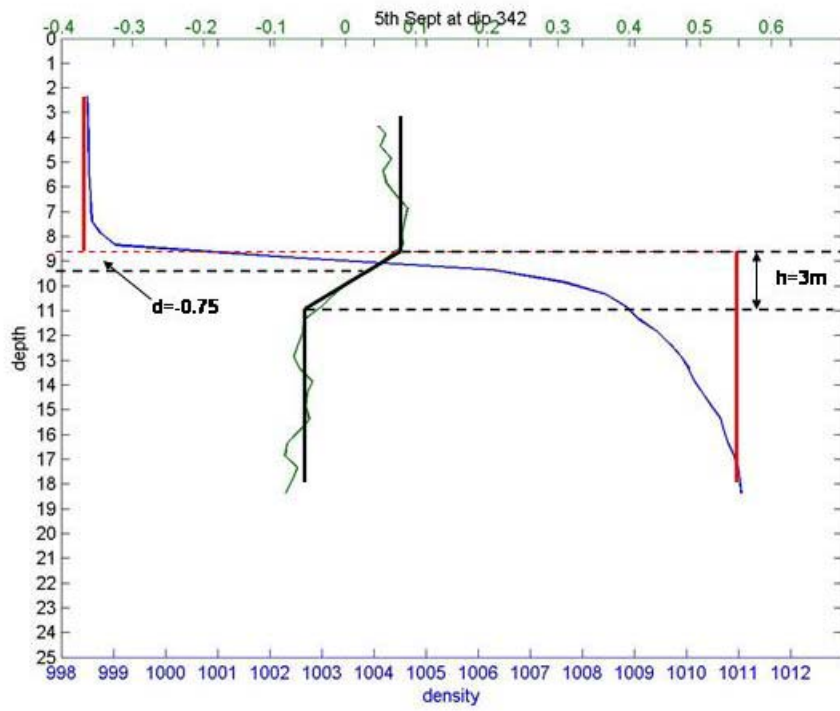


Figure III.1: Piecewise approximation for section two

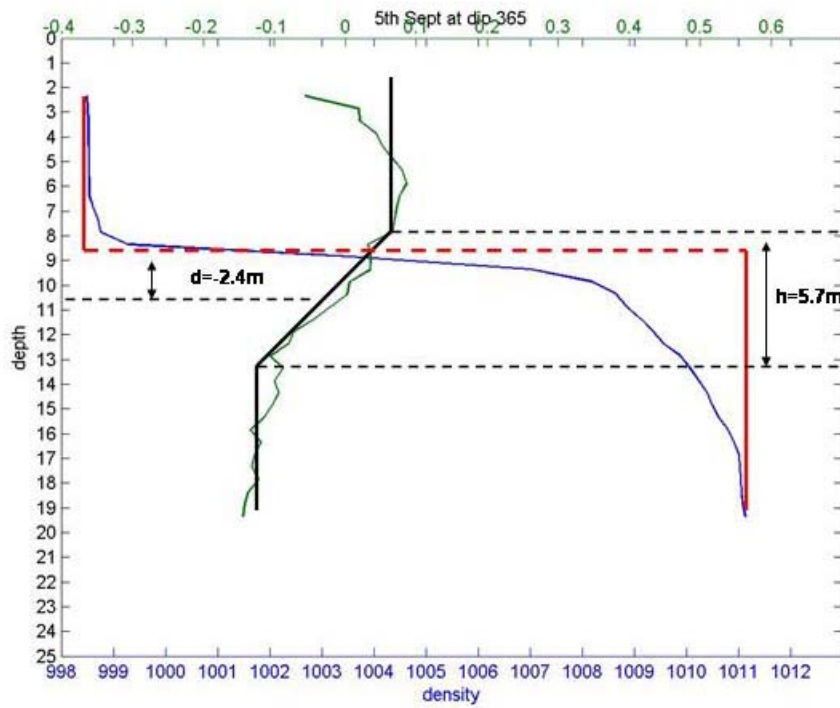
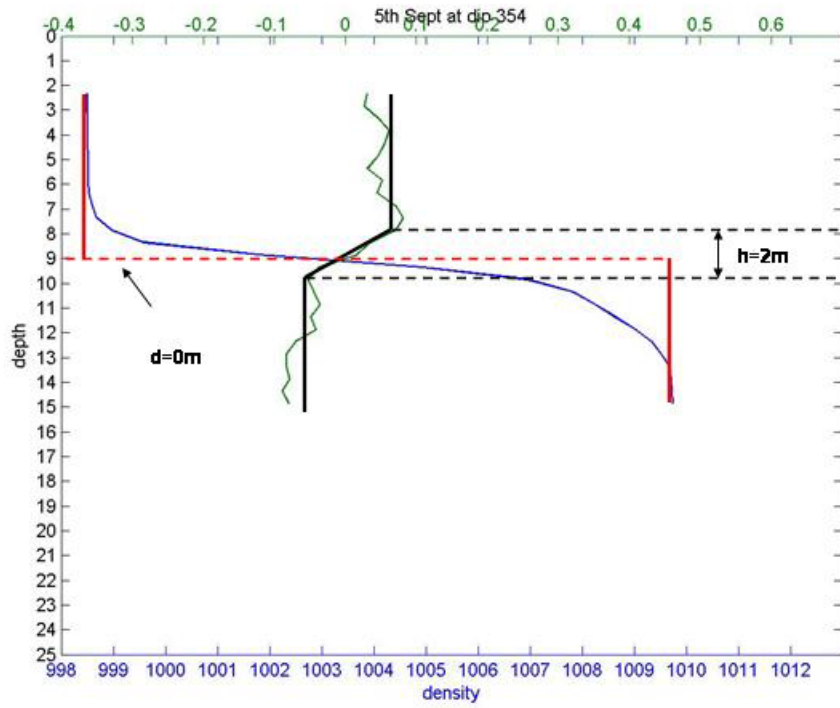


Figure III.1: Piecewise approximation for section two

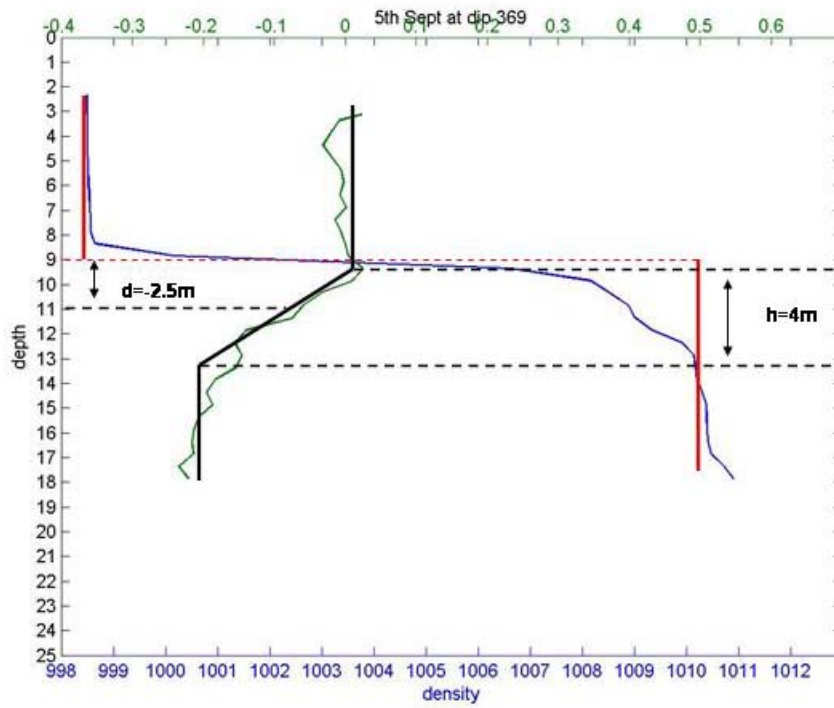


Figure III.1: Piecewise approximation for section two

## VITA

Candidate full name:

Nicole Delpeche

Universities attended:

B.Sc. Surveying and Land Information (2001)

University of the West Indies

Conference presentations:

Identification of Instabilities in the Saint John River Estuary, New Brunswick

Atlantic Canada Coastal and Estuarine Science Society (ACCESS)

Moncton, 2005